INVESTIGATIONS INTO INTERMEDIATE TEMPERATURE POLYMER ELECTROLYTE FUEL CELL GAS DIFFUSION LAYERS: WHEN SCIENCE MEETS ART

BY

AMRIT SINGH CHANDAN

A thesis submitted to the

University of Birmingham

for the degree of

DOCTOR OF PHILOSOPHY

Centre for Hydrogen and Fuel Cell Research

School of Chemical Engineering

University of Birmingham

2015

Declaration

I, Amrit Singh Chandan, hereby declare that the work presented in this thesis is my own with no help of more than the cited literature and auxiliary means.

I also confirm that this work has not been submitted to another examination office, neither in content nor in shape.

_____

Signature (Amrit Singh Chandan)

Date: _____

DEDICATION

I dedicate this thesis to hydrogen. There's so much of it in the universe – some would say it's elemental… Who knew you could combine it with oxygen to make water? Without hydrogen this thesis would not have been possible!

I would also like to dedicate this work to the particle of inspiration which travelled across the galaxy, riding the aether to impart ground breaking knowledge of fuel cells unto me. It's a shame you got lost along the way!

ACKNOWLEDGEMENTS

This thesis represents the culmination of my PhD journey which began on a cold autumn day in October 2010 at the Centre for Hydrogen and Fuel Cell Research in the School of Chemical Engineering at the University of Birmingham. The completion of this work has only been possible through the support and encouragement of family, friends, colleagues and supervisors. Above all, I thank God for giving me the strength, stubbornness and a head strong enough to break through the wall I was constantly smashing it against.

I would like to thank Prof. Dr. Robert Steinberger-Wilckens for his support, guidance and allowing me to get away with a lot more than any other supervisor would! I would also like to thank the numerous other supervisors I have had over the years, including; the late Dr. Waldemar Bujalski, Dr. Andrew Ingram & Dr. Neil Rees. I would like to also thank Dr. Shangfeng Du for his guidance. Special mention should also be made of the most eminent Prof. Dr. Ahmad el-Kharouf.

Thanks must also be given to Tata Motors European Technical Centre for their funding for this project. In particular, thanks to Dr. Valerie Self and Dr. John Richmond for their support.

I would like to thank Bob and Bill in the mechanical engineering workshop for always being on hand to help! The Chemical Engineering administration staff were of vital assistance during this time, with special thanks to John Hooper and Lynn Draper. Without the many procrastination breaks with John, this work would not have been possible!

Special mention should be made to the “Chandan Research Group”, which comprised the 11 MSc/MEng/MPhil students that I was responsible for supervising during my tenure; Tom Kaminski, Matthew Spraggs, John Ramsay, Joe Bode, Tom Slater, Mandeep Sangha, Pritpal Singh, Chris Harding, Manveer Hayre, Haitao Yu and Meng Sun.

I am grateful for the help and support of my friends in the completion of work. This includes all members of the Hydrogen and Fuel Cell Research CDT. Special mention should be made to my friend & partner in crime, Suleman Khan. Furthermore, I would like to thank my fellow members of the Coffee Club; Mariska Hattenberger, Scott Hardman, John Geoffrey Maillard VI, Paul Jennings, Nikkia McDonald, Arvin Mossadegh Pour, Lydia Gurley, Anwar Sattar, Fatima Zia, Peter Haldane Robbs, Lois Milner, Laura Allerston, James Walker and Aimee Jackson.

I would finally like to thank my mother Arvinder Chandan, father Gurcharan Chandan and brothers, Gurmukh and Gurpreet Chandan for always keeping me sane. I must also thank my Grandparents Pita Ji, Mama Ji, Nana Ji and Nani Ji for all of their blessings. Thank God this is finally over!

ABSTRACT

Polymer Electrolyte Fuel Cells (PEFCs) are a key technology to secure the future of the automotive sector. PEFCs are advantageous due to their low operating temperature (60-80 ^{o}C), quick start up times and responsiveness to load change. However, the requirement for expensive platinum, difficulty of water management and heat dissipation means that further improvements are required. One way of reducing the impact of these challenges is to increase the cell operating temperature to above 100 ^{o}C. In particular by operating the cell at 120 ^{o}C, labelled as the Intermediate Temperature (IT)-PEFC, it becomes theoretically possible to simplify water and thermal management. In order to realise these benefits, further research is required into components of the Membrane Electrode Assemblies (MEAs).

In this work, fundamental properties of the GDL have been investigated such as the influence of porosity on electronic conductivity, the influence of the microporous layer, the influence of hydrophobicity and the influence of GDL thickness. This has been done using a mixed methods approach consisting of simulation and experimental work. MEAs were simulated and hand-painted to test the GDL material properties. From this, recommendations for an ideal GDL for intermediate temperature conditions are suggested, for example, using a GDL with; a porosity of 40%, a permeability greater than 10^{-10} m^2, an MPL, hydrophobic treatment and as thin as possible. The possibility of using metallic GDLs was also investigated using simulation and experimental work. It was found that metallic GDLs do show better mass transport properties however further work is required to overcome the higher contact resistance.

LIST OF PUBLICATIONS

1. Symes, D., Maillard, J. G., Courtney, J., Watton, J., Meadowcroft, A., Chandan, A. S., Gurley. L., Priestly, R., Serdaroglu, G. (2014). Development of a Hydrogen Fuelling Infrastructure in the Northeast U.S.A., *International Journal of Hydrogen Energy*, 1-7
2. Hardman, S., Chandan, A., Steinberger-Wilckens, R., (2015) Fuel Cell Vehicles: Value Added Niche Marketing, *Journal of Power Sources,* 287, 297-306
3. Hardman, S., Chandan, A., Steinberger-Wilckens, R., (2014) Fuel Cell Added Value, *5th European Fuel Cell Forum Conference Proceedings*.
4. Chandan, A., Pour, M. A., McDonald, N., Maillard, J. G., Steinberger-Wilckens, Numerical Analysis of an SOFC Single Cell: A Multiphysics Approach, *5th European Fuel Cell Forum Conference Proceedings*.
5. El-Kharouf, A., Chandan, A., Sharma, S., Rees, V. N., Steinberger-Wilckens, R., R., Duraman, N., Taechakijviboon, T., Chan S. L.I., (2013). The Use of Carbon Nanotube Thin Films as a Microporous Layer for GDLs in Polymer Electrolyte Fuel Cells. *5th FDFC conference proceedings*.
6. Chandan, A., Hattenberger, M., El-kharouf, A., Du, S., Dhir, A., Self, V., Bujalski, W. (2013). High temperature (HT) polymer electrolyte membrane fuel cells (PEMFC) – A review. *Journal of Power Sources*, *231*, 264–278. doi:10.1016/j.jpowsour.2012.11.126
7. Chandan, A., Harding, C., Singh, P., Du, S., Rees, N. V., Ingram, A., Steinberger-Wilckens, R., Self, V., Richmond, J., (2013) The Use of a Microwave Assisted Polyol Process as a Production Tool for Finely Controlled Fuel Cell Catalysts, *4th European Fuel Cell Forum Conference Proceedings*.
8. El-kharouf, A, Chandan, A, Hattenberger, M., & Pollet, B. G. (2012). Proton exchange membrane fuel cell degradation and testing: review. *Journal of the Energy Institute*, *85*(4), 188–200. doi:10.1179/1743967112Z.00000000036

CONTENTS

LIST OF ILLUSTRATIONS

LIST OF TABLES

LIST OF DEFINITIONS AND ABBREVIATIONS

Abbreviation	Definition
ε_{anode}	Anode GDL porosity
κ_{anode} **(m^2)**	Anode GDL permeability
σ_{anode} **(S m^{-1})**	Anode GDL conductivity
$D_{H_2-H_2O}$ **(m^2 s^{-1})**	Binary Diffusion Coefficients H_2-H_2O
$D_{N_2-H_2O}$ **(m^2 s^{-1})**	Binary Diffusion Coefficients N_2-H_2O
$D_{O_2-H_2O}$ **(m^2 s^{-1})**	Binary Diffusion Coefficients O_2- H_2O
$D_{O_2-N_2}$ **(m^2 s^{-1})**	Binary Diffusion Coefficients O_2-N_2
S_m	Mass flux source term
β_C **(mV/dec)**	Tafel slope
η_{act} **(V)**	Activation Overpotential
η_{ohmic} **(V)**	Ohmic Overpotential
η_{trans} **(V)**	Mass Transport Overpotential
σ_l **(S m^{-1})**	Ionic conductivity of the membrane
σ_s **(S m^{-1})**	Electronic conductivity of the electrode
φ_l **(V)**	Ionic potential in the membrane
φ_s **(V)**	Electronic potential in the electrode
ΔG **(J mol^{-1})**	Gibbs Free Energy
ΔH **(J mol^{-1})**	Enthalpy
ΔS **(J K^{-1} mol^{-1})**	Entropy
μ_{anode} **(Pa s)**	Anode gas viscosity
$\mu_{cathode}$ **(Pa s)**	Cathode gas viscosity
ASR	Area Specific Resistance
BoP	Balance of Plant
BPP	Bipolar plate
CCM	Catalyst Coated Membrane
CFD	Computational Fluid Dynamics
$C_{H2,ref}$ **(mol m^{-3})**	Hydrogen reference concentration
CHP	Combined Heat and Power
$C_{O2,ref}$ **(mol m^{-3})**	Oxygen reference concentration

$C_{p,GDL}$ (J kg^{-1} K^{-1})	GDL specific heat capacity
$C_{p,H2}$ (J kg^{-1} K^{-1})	Oxygen specific heat capacity
$C_{p,H2O}$ (J kg^{-1} K^{-1})	Water specific heat capacity
$C_{p,membrane}$ (J kg^{-1} K^{-1})	Membrane specific heat capacity
$C_{p,N2}$ (J kg^{-1} K^{-1})	Nitrogen specific heat capacity
DOE	US Department of Energy
E (V)	Cell potential
EIS	Electrochemical Impedance Scpectroscopy
E_{thoery} (V)	ORR equilibrium reaction potential at 120 ^{o}C
F (C mol^{-1})	Faraday Constant
FEP	Flourinated Ethylene Propylene
FFP	Flow Field Plate
GDE	Gas Diffusion Electrode
GDL	Gas Diffusion Layer
GHG	Green House Gasses
H_{C_ch} (mm)	Cathode flow channel height (Z axis)
H_{C_GDL} (mm)	Cathode GDL height (Z axis)
H_{cool} (mm)	Cooling channel height (Z axis)
H_{FFP} (mm)	Flow field plate height (Z axis)
HOR	Hydrogen Oxidation Reaction
H_{tot} (mm)	Total height of model (Z axis)
HT-PEFC	High Temperature PEFC
I (A)	Current
ICR	Interfacial Contact Resistance
i_{local} (A m^{-2})	Local current density
i_{o_a} (A m^{-2})	Anode exchange current density
IT-PEFC	Intermediate Temperature PEFC
JM	Johnson Matthey
K_{GDL} (W m^{-1} K^{-1})	GDL thermal conductivity
$K_{membrane}$ (W m^{-1} K^{-1})	Membrane thermal conductivity
L_{A_ch} (mm)	Anode flow channel length (Y axis)
L_{A_GDL} (mm)	Anode GDL length (Y axis)
L_{C_ch} (mm)	Cathode flow channel length (Y axis)

L_{C_GDL} (mm)	Cathode GDL length (Y axis)
L_{cool} (mm)	Cooling channel length (Y axis)
L_{FFP} (mm)	Flow field plate length (Y axis)
L_{mem} (mm)	Membrane length (Y axis)
L_{MPL} (mm)	Anode and cathode MPL length (Y axis)
L_{tot} (mm)	Total length of model (Y axis)
LT-PEFC	Low Temperature PEFC
MEA	Membrane Electrode Assembly
MEMS	Microelectromechanical System
MPL	Microporous Layer
OCV	Open Circuit Voltage
ORR	Oxygen Reduction Reaction
PBI	Polybenzimidazole
PDMS	Poly(dimethysiloxane)
PEFC	Polymer Electrolyte Fuel Cell
PEM	Polymer Electrolyte Membrane
PFSA	Perfluorosulfonic Acid (Nafion)
PTFE	Polytetrafluoroethylene (Teflon)
PVDF	Polyvinylidene Flouride
R ($J\ K^{-1}\ mol^{-1}$)	Universal Gas Constant
SEM	Scanning Electron Microscopy
T_{inlet} (K)	Inlet Temperature
TMETC	Tata Motors European Technical Centre
U ($mL\ min^{-1}$)	Flow Rate
URFC	Unitized Regenerative Fuel Cell
V (V)	Voltage
W_{A_ch} (mm)	Anode flow channel width (X axis)
W_{A_GDL} (mm)	Anode GDL width (X axis)
W_{C_ch} (mm)	Cathode flow channel width (X axis)
W_{C_GDL} (mm)	Cathode GDL width (X axis)
W_{cool} (mm)	Cooling channel width (X axis)
W_{FFP} (mm)	Flow field plate width (X axis)
W_{mem} (µm)	Membrane width (X axis)

W_{MPL} (µm)	Anode and cathode MPL width (X axis)
W_{tot} (mm)	Total width of model (X axis)
η (V)	Overpotential
ρ_{matrix} (kg m^{-3})	MEA density
P (Pa)	Pressure
T (K)	Temperature
u (m s^{-1})	velocity
∇	$\nabla = \hat{x}\frac{\partial}{\partial x} + \hat{y}\frac{\partial}{\partial y} + \hat{z}\frac{\partial}{\partial z}$
κ (m^2)	Permeability
λ	Stoichiometry
µ (Pa s)	Viscosity
ρ (kg m^{-3})	Density

CHAPTER 1

Introduction

"…we are entitled to assert that the current in question is caused by the combination of hydrogen with (the) oxygen (contained dissolved in water) and not by contact"

Christian Friedrich Schoenbein, 1839 [1]

Chapter 1 Introduction

1.1 Fuel Cell Principles

By definition, a fuel cell is an electrochemical device that convserts the chemical energy of the supplied fuel without combustion. There are several different types of fuel cells, all of which have their own advantages and disadvantages. The classification system of fuel cells is based on the choice of electrolyte and fuel, which in turn determine the ion type that travels across the electrolyte and the electrode reactions [2]. Of all the different types of fuel cells, Polymer Electrolyte Fuel Cells (PEFCs) have been identified as the best type of fuel cell for the automotive industry due to their quick start up times, excellent load change response and the possibility for simple system design [3]. The most common fuels that are used in fuel cells include hydrogen, methanol and ethanol. All of these fuels react in the same way (Figure 1.1). The fuel, for example hydrogen, will first come into contact with the anode where it is split into its component protons and electrons

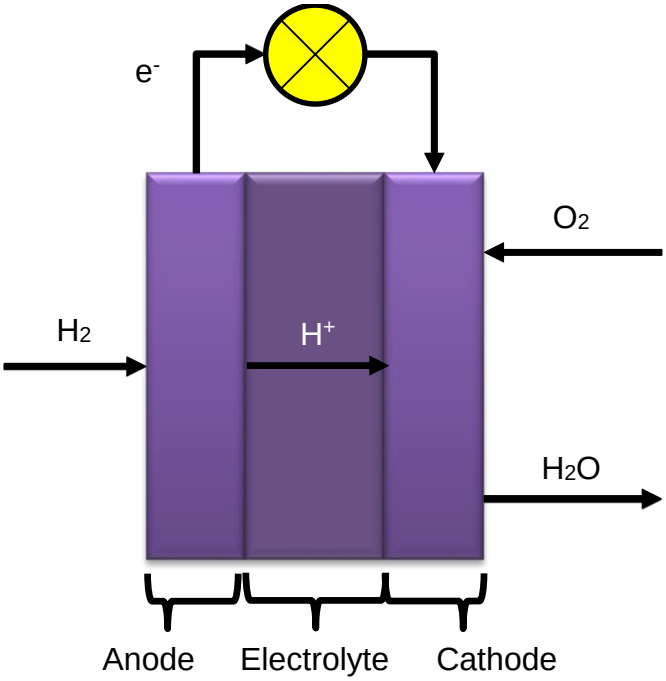

Figure 1.1: Fuel Cell Schematic

At this point, the protons will travel through the proton conducting electrolyte which will not conduct electrons. The electrons will travel through the circuit where it will recombine with the hydrogen and oxygen at the cathode giving out water as the sole product. When alternative fuels are used, such as ethanol and methanol then some carbon dioxide will be produced also. The reactions that occur can be summarised as follows:

Anode Electrode:	$H_2 \rightarrow 2H^+ + 2e^-$	Equation 1.1
Cathode Electrode:	$O_2 + 4H^+ + 4e^- \rightarrow 2H_2O$	Equation 1.2
General Fuel Cell Reaction:	$2H_2 + O_2 \rightarrow 2H_2O$	Equation 1.3

Just like other fuel cell types, the PEFC is made up of an anode, cathode and an electrolyte and these, along with the bipolar plates, make up the membrane electrode assembly (MEA) (see Figure 1.2). The heart of the MEA is made up of a multi-layered membrane that consists of a polymeric membrane sandwiched between catalyst layers and gas diffusion layers (GDLs) [3]. These can be combined together to make up the stack. The PEFC differs from other fuel cells in that it has a solid phase polymer membrane that is used in the capacity of the electrolyte. This polymeric nature of the electrolyte ensures that issues which plague other types of fuel cell, such as cell sealing assembly and handling are less of a problem in the PEFC system.

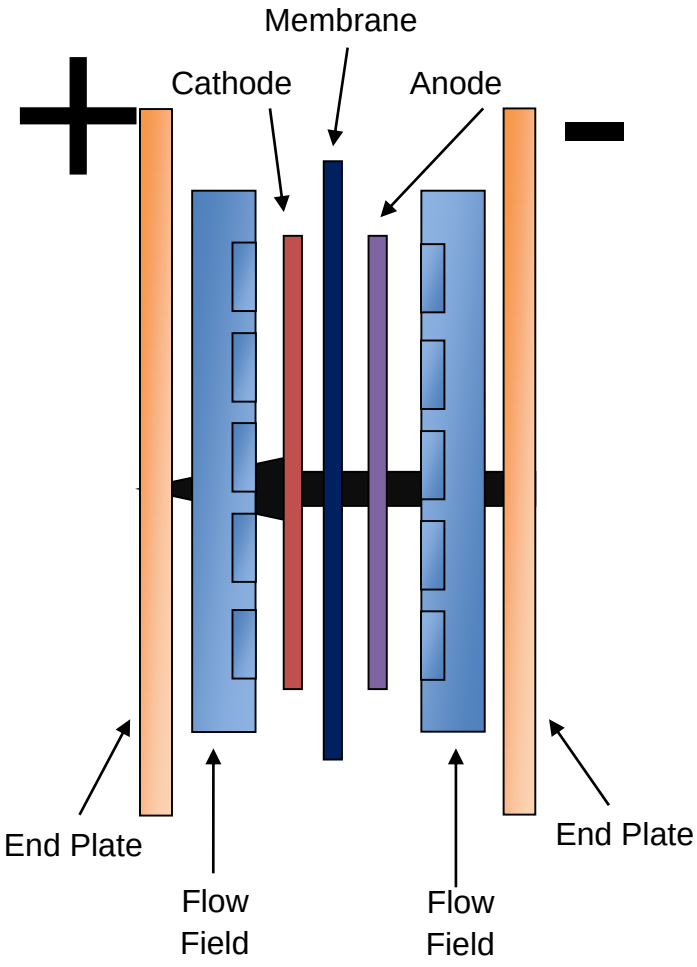

Figure 1.2: PEFC Single Cell

The main advantages of the fuel cell over other equipment that produces energy is that fuel cells have a much higher efficiency (45-55% electrical efficiency compared to internal combustion engines) so less fuel is required, there are no moving parts so less can go wrong with the fuel cell and also there is no noise pollution or emission of greenhouse gasses. The main disadvantages of fuel cells are that currently they have a high cost and they do not have a high durability as well as public acceptance of the technology. This can be addressed by the application of new technologies, for example through the development of novel membrane materials. However, the advantages put the fuel cell as a technology ahead of competitive technology, such as the internal combustion engine.

1.1.1 Polarisation Principles

The overall fuel cell reaction (Equation 1.3) are exothermic by nature [4] which means that the overall reversible energy from the reaction will be equal to the Gibbs Free Energy (ΔG). However, as there are irreversible losses in the cells, there is deviation from the theoretically obtained values ($\Delta G = \Delta H - T\Delta S$). From this, the open circuit voltage (OCV) can be determined using Equation 1.4.

$$E_0 = \frac{-\Delta G}{2F} \qquad \text{Equation 1.4}$$

However, this theoretical value will be higher than the values obtained experimentally due to irreversible losses based on materials, for example the electrical conductivity of the electrolyte, gas cross over, mixed potentials and sealing issues. Furthermore, as the OCV represents the fuel cell reactions in equilibrium, when a current is drawn from the cell, the voltage drops as this equilibrium is forced in the forward direction.

Therefore as the current drawn increases, the voltage of the cell decreases. This is represented in the polarisation curve or I-V curve as shown in Figure 1.3.

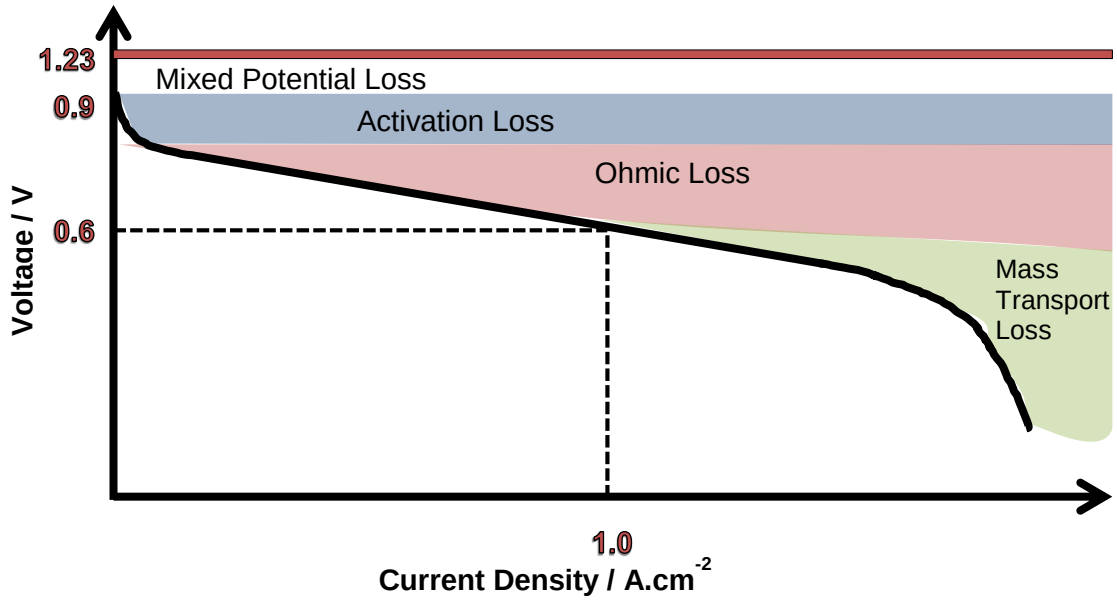

Figure 1.3: Fuel Cell Polarisation Curve

Figure 1.3 also highlights the three main mechanisms by which energy is lost within the fuel cell; (i) activation losses, (ii) ohmic losses and (iii) mass transport losses. The activation losses, or activation overpotential (η_{act}) is related to the energy required to overcome the barrier to the Oxygen Reduction Reaction (ORR). The Hydrogen Oxidation Reaction (HOR) is often considered negligible as the kinetics are significantly faster than for the ORR. The ohmic overpotential (η_{ohmic}) results from the flow of electrons through electrically conductive materials and the flow of protons through protonically conductive materials. The mass transport overpotential (η_{trans}) results from the inability of fuel to be supplied at a sufficient rate to the electrode surfaces.

1.2 PEFC Types

As mentioned previously, since the invention of the fuel cell, many different types of fuel cells have been discovered. They are categorised by their electrolyte which in turn determines their operating temperature.

Of particular interest is the sub variants of the PEFC, for example the Intermediate Temperature Polymer Electrolyte Fuel Cell (IT-PEFC) and the High Temperature Polymer Electrolyte Fuel Cell (HT-PEFC) (Table 1.1) [5].

Table 1.1: Variants of the PEFC

Fuel Cell Type	**Low Temperature**		
	Polymer Electrolyte Fuel Cell (PEFC)	**Intermediate Temperature (IT) PEFC**	**High Temperature (HT) PEFC**
Electrolyte	Nafion (PFSA) Polymer	Nafion (PFSA) Polymer	H_3PO_4 based Polybenzimidazole (PBI)
Catalyst	Pt	Pt	Pt or cheaper metal
Electrodes	Carbon	Carbon	carbon
Operating Temperature / ^oC	60-80	100-140	140-180
Fuel	H_2	H_2	H_2 (CO)
Oxidant	O_2/(air)	O_2/air	O_2/air

One option with the PEFC is to increase the operating temperature above 100 ^oC, the so called intermediate and high temperature PEFCs. The drive for higher temperature PEFCs will be discussed in Section 1.3.

Generally, the low temperature fuel cells are more suited to mobile applications whereas the high temperature fuel cells are suited for stationary power applications. The efficiency of all of the fuel cells can be further enhanced if the waste heat is utilised

in a given application, for example Combined Heat and Power (CHP). The main advantage high temperature fuel cells have over low temperature fuel cells is in the fuel requirements in that they possess a much higher tolerance to impurities than the low temperature fuel cells.

1.3 The Drive for Higher Temperature PEFCs

The most important drive for the development of HT-PEFCs is provided by the automotive industry. The automotive sector has the largest volume potential but is currently very demanding, for example concerning operating temperatures and responses to rapid load changes. The following table summarises the main advantages and disadvantages of the HT PEFC and the conventional PEFC (Table 1.2).

Table 1.2: Advantages and Disadvantages of Conventional and Higher Temperature PEFCs

Conventional PEFC		**HT PEFCs**	
Advantages	***Disadvantages***	***Advantages***	***Disadvantages***
High current densities achievable	High Platinum loading levels required	Can use alternative metals to Platinum	PBI requires phosphoric dopant
Fast start capability	Nafion® is an expensive material	Improved tolerance to contaminants	Increased degradation speed of materials
Rapid response to load changes	Requires very pure Hydrogen	Higher quality heat for use in CHP systems	Longer start-up times
No corrosive fluid hazard	Easily susceptible to Carbon Monoxide poisoning	Does not require humid environment	A loss of mechanical stability

Lower sensitivity to orientation	Requires a humid environment	Improved water management	Failure mechanisms not well understood [6]
Can start from ambient conditions	Very difficult heat/ water management	Improved electrolyte and electrode kinetics	
	Requires purging of the stack using a dry gas	Improved heat management	
		Improved stability and durability at sub zero temperatures [7]	
		No need to purge stack after use	

1.4 Conventional PEFC challenges

There have been many advances in the development of conventional PEFCs, for example power densities increased significantly. Also the catalyst loadings have been significantly reduced by 10 and even 100-fold since the 1980s and thus the overall cost of the PEFC has decreased [5,8]. However, there remain several issues that need to be addressed before the PEFC can be commercialised. The low operating temperature of the PEFC is in many ways both a blessing and a curse. On the one hand it allows for a very rapid start-up of the fuel cell which allows the fuel cell to start from ambient conditions. On the other hand there are several associated disadvantages:

i. Slow electrode kinetics due to the low temperature which means that high catalyst loading levels are required to counter this.

ii. Low operating temperature means that little to no heat available for extraction and use with other processes, for example endothermic heat reforming.

iii. 40% - 50% of the energy produced is heat which, due to the low operating temperature of the PEFC is difficult to manage. This is because there will exist a low thermal gradient between the PEFC and the ambient environment due to the low operating temperature which means that complex cooling architectures must be used to maintain cell temperature.

iv. The water produced from the reaction can cause ‘flooding’ at the cathode. This adversely affects oxygen diffusion and therefore will adversely affect the fuel cell performance.

Due to the nature of industry accepted Nafion®, a humid environment is required for the cell to work. This causes problems when the ambient temperature drops below zero as the fuel cell must be thawed before the cell can work. As a result the reliability of the fuel cell is compromised.

Another challenge that remains with the PEFC is the durability. The US Department of Energy (DOE) has placed a target of at least 5000 hours for a PEFC operating at/below 80 ^{o}C. These targets can only be met, currently, under the most stringent laboratory conditions although some companies, for example Daimler, claim to have achieved a life time of 2000 hours without performance degradation [9].

1.4.1 Gas Diffusion Layers (GDLs)

A vital component of the fuel cell is the GDL. The GDL must fulfil several requirements [10]:

I. The GDL must possess excellent reactant transport properties in order to ensure even distribution of gasses across the catalyst layer active sites. This also applies to the removal of product water from the catalyst layer to the flow channel.

II. The GDL must have low contact and bulk resistance to conduct electrons between the electrode and flow field plate.

III. The GDL must have a good mechanical strength and physical durability to ensure that there is good contact between the catalyst layer and the membrane.

IV. The GDL must have good thermal conductivity properties to aid in the removal of excess heat generated mainly by the fuel cell reactions.

Of particular importance is point (i). In low temperature PEFC systems, water is a liquid (depending on the operational relative humidity and thus the saturation pressure) and so water management is key to avoid “flooding” and to achieve good cell performance, especially when operating at higher current densities. At higher temperatures the product water will be a vapour and therefore mass transport limitations should be reduced. However, it is still vitally important to have a GDL that allows good diffusion in order to remove the water vapour. The GDL also plays a very vital role in the improvement of fuel cell performance by improving the diffusion characteristics of the reactant gases and the water vapour [11]. Whilst providing sufficient pathways for

reactants to diffuse through, the GDL must also have sufficient electronic conducting material to transfer electrons to and from the flow channel and catalyst layer.

With respect to the materials that are used in the GDL, the same materials, for example Teflon® treated carbon paper, which are used for low temperature PEFC are also used in the higher temperature PEFCs.

GDLs for higher temperature PEFCs will be discussed in the literature review.

1.4.2 Flow Fields

One of the many key elements for the operating and performance of the PEFC is the flow field design [12]. The flow fields provide channels (Figure 1.4 [3]) that are responsible for the transportation of water vapour, reactant gasses and liquid water. As such flow channel dimensions such as the ratio of channel width or height and channel configuration of the flow fields can have a huge impact on the PEFC performance.

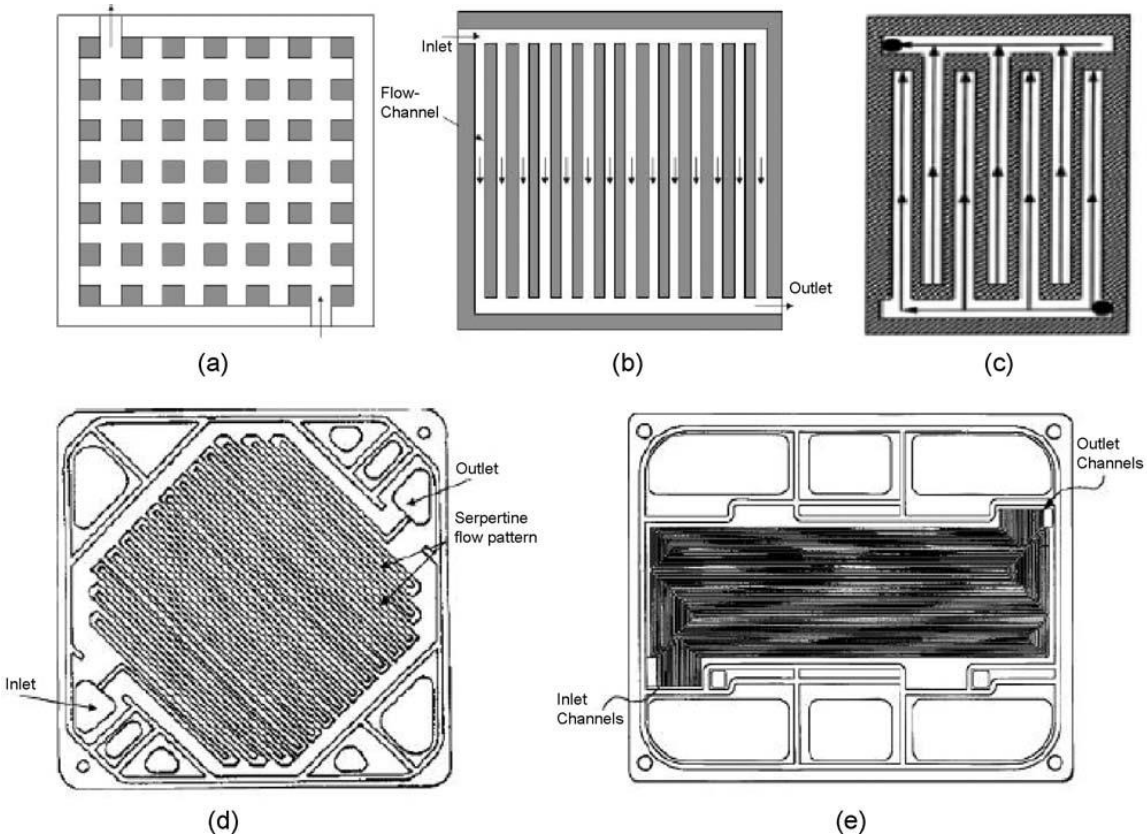

Figure 1.4: Different Flow Field Plate Designs [12].

By optimising the design of the flow field, it should be possible to prevent the build-up of waste product water in the channels. It is important to have a larger pressure drop across the flow field pattern as this improves the removal of liquid waste water from the channels through the physical “pushing” of droplets. However, for high temperature operation, water will exist in the vapour phase and therefore flooding should be reduced. As a result, for high temperature operation, there is less of a need for this high pressure drop across the flow field and so the focus of flow field design should be on reducing inefficiency due to mass transport concerns.

Another challenge that is faced with flow fields is the non-uniformity of the distribution of reactants along a channel. The concentration of reactants and products changes locally based on the distance to the active site from the closest flow channel, leading to large reactant gradients as you move further from the channel. Another complication

is the increase of product water concentration along the channel. Towards the end of the flow channel, there will be a lower concentration of reactants, which means that there is a smaller concentration gradient between the flow channel and the catalyst sites thus decreasing the rate of diffusion and increasing the mass transport resistance. This also occurs for the waste water products, which can quickly saturate the catalyst active sites and reduce cell performance. Therefore, flow field design is important to ensure good transport of reactants and removal of waste water.

1.5 Automotive Fuel Cell Challenges

There are several factors that must be considered when engineering a fuel cell for automotive applications. Namely these are:

I. The life and reliability of the fuel cell system must be improved.
II. The fuel cell system must be made more robust so as to handle operating conditions that are out of the norm, i.e. sub-zero temperatures in the UK.
III. The volume and the weight of the fuel cell needs to be reduced.
IV. There needs to be further material development to achieve cost reduction.
V. There needs to be a hydrogen infrastructure in place, with accompanying peripherals, for example road tax, car insurance, health and safety.
VI. Some sort of platform needs to be designed for the fuel cell as most PEFCs are not designed for the vibrations that it will undoubtedly receive while in the car.

1.6 Availability of HT-PEFCs

The following companies are involved with HT-PEFC (Table 1.3) (adapted from www.Fuelcellmarkets.com accessed 9/12/2010 [13] and www.fuelcelltoday.com accessed 9/12/2010 [14])

Table 1.3: Companies involved with HT-PEFC Development

Company	Involvement	Location
EnerFuel (A subsidiary of Ener1)	In March 2009, President Obama pledged 1 million plug in hybrid electric vehicles on US roads by 2015. EnerFuel has been developing electric vehicle range extenders using a HT PEFC system. The range extender can act as an onboard battery charger that can be used when the vehicle is parked or idling, or used together with the vehicle batteries to provide the power necessary for long range journeys. *Sales unknown.*	USA
Advent Technologies S.A	Advent is focused on the systematic development and production of polymer membranes that can be used as an electrolyte for HT PEFC. *Sales unknown.*	Greece
SerEnergy A/S	SerEnergy offers a range of HT PEFC stack solutions as well as custom built cells. In 2010, SerEnergy supplied 10 of their “Serenus” 3 kW HT PEFCs for use in Microcab’s next generation of prototype hybrid vehicles. *10 confirmed sales*.	Denmark
Dynergy	Dynergy are a UK based manufacturer of fuel cell systems that includes high HT PEFC. *Sales unknown.*	UK
BASF	BASF are a large multinational company that produces both HT MEAs and important pre products such as electrodes. *Sales unknown.*	Germany
Cidetec	In 2006, Cidetec unveiled a working HT PEFC for the first time using PBI and operating over 150 degrees. *Sales unkown.*	Spain

1.7 Intellectual Property

To date, approximately 350,000 patents have been applied for within the fuel cell field with the number of issued patents at approximately 37,700 patents worldwide. The first

patent was filed by Hitachi Ltd in 1983 and was granted in 1985 [15]. Currently Plug Power Inc. hold the most granted patents, followed by Umicore however very little of this tech is currently being exploited. Several car companies including Toyota, Honda, Daimler & VW have shown interest in HT-PEFC technology however only VW has made any serious public statements on HT-PEFC. However, VW recently has stopped all research into HT-PEFC systems [16]. This was due to the lack of a consortium of OEMs through which the development costs could be reduced as is the case for conventional PEFCs. There are several other companies that are not publically associated with HT-PEFC technology but hold patents in the field, for example companies such as LG, Plug Power and Advent. The ownership of the patents may indicate that these companies wish to move into this sector over the coming years.

Table 1.4: Owners of Patents in the HT-PEFC Field

Assignee	**Number of Patents Filed (Year)**							**Area of Interest**	**Still Operational in HT-PEFC?**
	10	**11**	**12**	**13**	**14**	**Total Filed**	**Total Granted**		
Plug Power Inc.	0	0	0	0	0	90	51	CHP	N
Umicore Ag & Co. Kg	1	2	2	0	0	69	38	Catalysts and membranes	Y
Toyota Jidosha Kabushiki Kaisha	2	3	2	0	0	102	33	Membranes /catalysts /MEAs /stack /systems	Y
Pemeas Gmbh	0	0	0	0	0	193	27	Mmebranes	N
Basf Fuel Cell Gmbh	2	1	0	0	0	99	27	Mmebranes /MEAs	N

Samsung Sdi Co., Ltd.	2	1	1	1	0	42	26	Membranes /catalysts /MEAs /systems	Y
Daimlerchrysler Ag	0	0	0	0	0	105	25	Stack /systems	N
University Of California	1	1	1	1	0	61	25	Membranes	Y
Honda Motor Co., Ltd.	1	1	0	2	0	100	23	Membranes /catalysts /MEAs /Stack /System	unknown
Advent Technologies	1	1	1	0	0	45	9	membranes	Y
California Institute Of Technology	1	0	3	1	0	23	9	Membranes	unknown
Celanese Ventures Gmbh	0	0	0	0	0	102	3	Membranes	unknown
Lg Chem, Ltd.	0	0	0	0	0	6	3	Catalyst layers	unknown
Volkswagen Ag	3	0	0	0	0	64	1	Membranes /catalyst layers	N
Enerfuel, Inc.	13	3	9	0	0	44	1	MEAs /Bipolar plates	N
Sartorius Ag	0	0	0	0	0	6	1	Membranes	N
SerEnergy A/S	0	0	0	0	0	4	1	Stacks	Y
Universität Stuttgart	0	0	0	0	0	1	1	Membranes	unknown
Cidetec	1	0	0	0	0	1	0	Membrane materials	unknown
Dynergy	0	0	0	0	0	0	0	n.a.	N

1.8 Thesis Objective and Outline

As has been shown in this chapter, there are clear benefits to shifting from a conventional PEFC operating at 70 ^{o}C to one operating above 100 ^{o}C. As this work is sponsored by Tata Motors European Technical Centre (TMETC), the focus of this work should therefore be on the development of a higher temperature PEFC that operates with 50 % relative humidity anode/cathode which is suitable for use in an automotive application. With this in mind, the best “sub variant” of the PEFC would be the IT-PEFC operating between 100 ^{o}C and 140 ^{o}C. This is because the IT-PEFC has the benefits of the higher temperature PEFC, namely simplified water and thermal management, whilst being able to avoid the other challenges of long start up times faced by cells operating above 140 ^{o}C. Thus far, a majority of work conducted within the field has been conducted on development of novel membrane materials which is an important consideration. However, in this case, the membrane development for our IT-PEFC is being conducted by my colleague, Mariska Hattenberger.

Of particular interest to the development of IT-PEFC is that of the GDL. The GDL is an integral component of the MEA however there is very little understanding understanding of GDL design, especially for intermediate temperature operation. As the water should exist in the vapour phase, it is important to understand what the different parameters of the GDL mean for MEA performance and if techniques that are used to improve cell performance at lower temperature operation are even necessary.

Therefore, the following objectives were identified for this study:

I. To develop an understanding of what the different GDL parameters mean for the processes occurring within the cell and therefore the impact this has on the

MEA performance. Of interest is the GDL porosity, permeability, electrical conductivity and thermal conductivity.

II. To predict if the MEA design could be changed to take advantage of the higher operating temperature based on the understanding gained of the GDL.

III. To develop an understanding of the necessity for manufacturing techniques used for conventional GDLs. Of particular interest is the influence of the micro porous layer, hydrophobicity and the GDL thickness.

IV. To build the proposed cell design and to see how the GDL design can be improved to achieve better MEA performance.

Through these objectives, this study offers insights into the roles of the GDL material properties and manufacturing techniques on the cell performance using a combination of theoretical simulation study as well as in-situ testing. This will lead to the development of an MEA design which will be able to take advantage of the intermediate temperature operating temperature which in turn should increase the system efficiency.

Chapter 2 reviews the research that has been conducted on the GDLs at intermediate/high temperature. Chapter 3 looks at understanding the GDL material properties of porosity, permeability, electrical conductivity and thermal conductivity using simulation study. From this a new MEA design will be proposed. Using in-situ testing methods, a baseline is established in Chapter 4. Chapter 5 goes on to understand the influence of the microporous layer on the cell performance. Chapter 6 looks at the influence of teflonation on MEA performance and Chapter 7 looks at the influence of GDL thickness on MEA performance. Chapter 8 then goes on to build and

test using metallic based GDLs at intermediate temperature. Finally, Chapter 9 summarises the findings and conclusions from this study and provides recommendations for future work.

CHAPTER 2

Literature Review

“I think that in the discussion of natural problems we ought to begin not with the scriptures, but with experiments, and demonstrations.”

Galileo Galilei, 1615

Chapter 2 Literature Review

2.1 State of the Art: Higher Temperature PEFCs.

This review discusses the High Temperature Polymer Electrolyte Fuel Cell (PEFC) technology (100-200 ^{o}C) with a particular focus on intermediate temperature (IT-PEFC) (100-120 ^{o}C) PEFCs and the development of the Gas Diffusion Layer (GDL). PEFCs are ideally suited for automotive applications [17] as well as stationary Combined Heat and Power (CHP) and mobile auxiliary power units. Among the many attractive features, the high power density, rapid start up and high efficiency makes the PEFC the system of choice for the automotive manufacturers. The aforementioned features are further enhanced when combined with their simple modular design [18], low weight and the stationary electrolyte in the form of a solid polymer membrane [19].

There have been many advances in the development of conventional PEFCs, for example power densities have increased when varying the electrode assembly methodology. Power densities increased from approximately 93 mW cm^{-2} at 0.6 V when using the PTFE bound method to 147 mW cm^{-2} at 0.6V when using a thin film transfer method [20]. Higher power densities of 233 mW cm^{-2} have been achieved by using commercially available, mass manufactured, standardised electrodes [21]. Recent studies show power densities of 680 mW cm^{-2} can be achieved [22] for conventional PEFCs. A power density of 100 mW cm^{-2} when tested at 160 ^{o}C was obtained when using a commercial HT-PEFC CELTEC-P1000 MEA produced by BASF [23]. This is a much lower power density than that found for the conventional

PEFC electrodes because of the large activation and ohmic losses found with the use of acid based membranes. Therefore considerable work still needs to be invested into improved performance of HT-PEFC systems. Also the catalyst loadings have been significantly reduced by 10 and even 100-fold since the 1980's and thus the overall cost of the conventional PEFC has decreased. However, there are disadvantages to using this system. For example, the conventional PEFC has a very low tolerance to impurities in fuel, thus requiring 99.999% pure hydrogen which is costly to supply. The heat produced from the conventional PEFC is of a low temperature and thus is difficult to transfer away for use in other processes for instance heating water for use in houses. Due to the nature of the membrane, a complex water management system is needed to prevent flooding/drying out of the MEA, both of which lead to a loss in performance. High performance PEFC systems can therefore become complex.

The HT-PEFC (100^{o}C – 200^{o}C) variant is able to overcome all of these issues as current systems are able to operate without the addition of water (depending on the membrane system used), tolerate higher impurity fuel streams and the high temperature waste heat can be easily utilised for other processes (e.g. cogeneration of heat and power or on-board reforming). These factors potentially result in increased efficiency and simplification of the HT-PEFC system as compared to the PEFC variant.

This review focuses on recent advances in the field of GDLs for high temperature operation, specifically for intermediate temperature operation. R&D into HT-PEFCs has increased in the last few years, with around 3,850 papers published on the topic in 2013 and 3,130 in 2014 (between Jan and Sept). The IT-PEFC field is a lot younger and so only 1,390 and 1,070 papers have been published in 2013 and 2014 (between Jan and Sept) respectively, with a majority of the papers on membrane research.

So far, on either side of the temperature scale, Nafion® and polybenzimidazole doped polymeric membranes with phosphoric acid (PBI/H_3PO_4) are the most efficient proton conducting membranes as shown in Figure 2.1 [17].

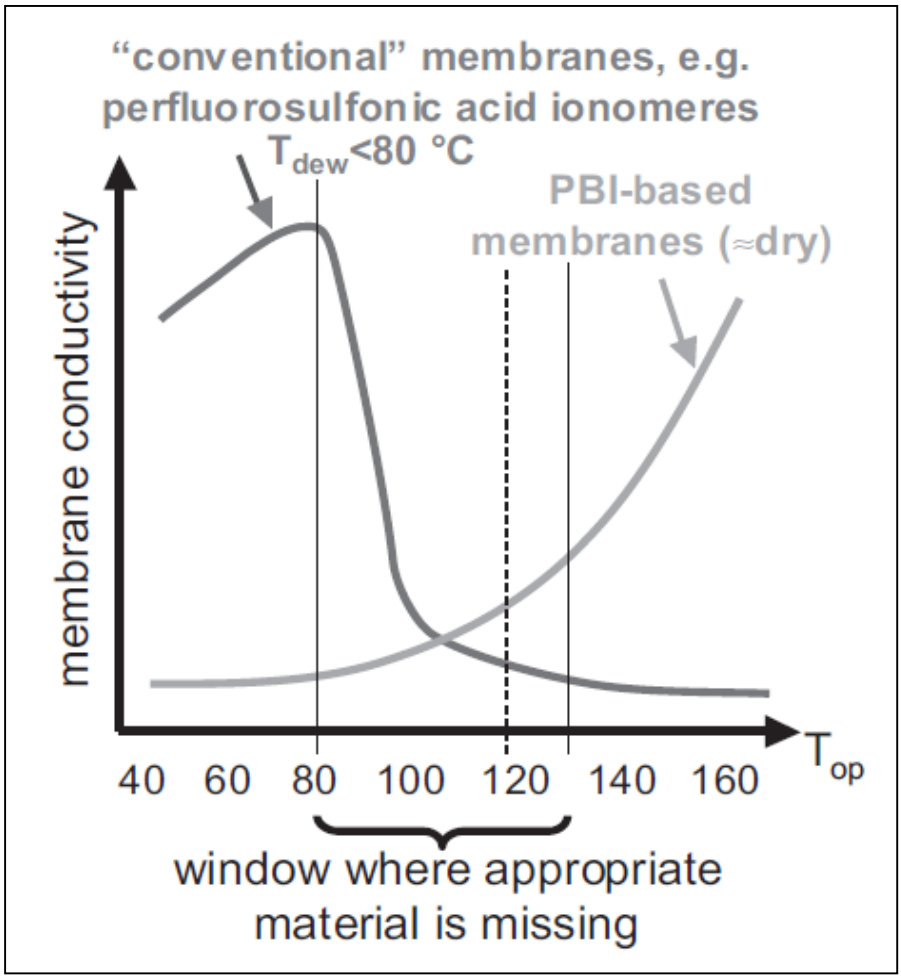

Figure 2.1: 80°C - 130°C Conductivity window [17]

The temperature range of 80–130°C is the domain of many novel materials including composites and blends of conventional materials. The greatly varied class of polyaromatic hydrocarbons span the conventional temperature and intermediate temperature ranges.

As such, the HT-PEFC is unsuitable for automotive applications where quick start-up times are a requirement. These disadvantages can be reduced by lowering the operating temperature slightly. In particular, by operating the cell at 120 ^{o}C, as we label it, an IT-PEFC, it becomes possible to simplify heat and water management as higher temperature heat is produced alongside water that exists in the vapour phase. This in turn should lead to a more efficient system as the balance of plant required can be simplified

The next two sections briefly discuss the benefits and disadvantages of IT-PEFCs. Following that, progress in GDLs at both conventional temperatures and intermediate temperatures are reviewed.

2.2 Advantages and Disadvantages of HT-PEFCs

By switching to high temperature operation, theoretical and experimental analyses [24] have shown the following benefits:

2.2.1 Electrode Reaction Kinetics

In the conventional PEFC, the Oxygen Reduction Reaction (ORR) has the slowest electrochemical kinetics and thus is the limiting factor in the overall reaction rate. As a result of the slow reaction kinetics, the overpotential at the cathode is responsible for a major part of the cell voltage losses of the conventional PEFC. By switching to higher temperatures, the ORR reaction rate is significantly increased [24], thus improving the performance of the PEFC as a whole.

2.2.2 CO tolerance

The primary catalyst in conventional PEFCs is platinum, which has a significant affinity for carbon monoxide (CO) which is a by-product of reformation of hydrocarbon fuels [25]. As a result, trace levels of carbon monoxide can cause a large decrease in the performance of the conventional PEFC due to poisoning effects. HT-PEFCs avoid this problem. At operating temperatures above 150 °C, the Pt affinity for carbon monoxide is reduced and so CO tolerance is increased from sub 300ppm to several percent. For example, below 80 °C CO adsorbs onto the platinum catalyst in the electrode and severely affects the performance [18,26–29]. Above 160 °C up to 3 % CO can be tolerated in the fuel stream [30–32]. The membrane system that is chosen for the HT-PEFC is one of the main factors in the use of impure fuels as the membrane system will dictate the optimum temperature chosen. This offers a significant advantage as many stages of fuel processing and gas cleaning can be removed thus allowing for cost-effective fuel, which is especially useful for stationary applications of the PEFCs where natural gas supplies may be used.

2.2.3 Heat and water management

In the conventional PEFC, 40-50% of the energy is produced as heat which must be removed quickly to avoid overheating causing increased degradation of the materials. As the operating temperature of the PEFC is increased, the heat transfer rate should increase as there is a larger temperature gradient between the fuel cell and the external environment. For a conventional PEFC system, the heat removal using existing radiator technology found in automotive vehicles can become insufficient in temperate environments. As a result, specialised cooling methodologies are required, all of which

adds to the Balance of Plant (BoP) costs associated with the PEFC. Increasing the temperature of the PEFC will allow for existing cooling architectures present in automotive vehicles to be used thus increasing the weight and mass specific energy densities and the overall energy efficiency. The efficiency can be further increased when cogeneration [33] and on- board reforming [24,30] are considered through the utilisation of the higher temperature waste heat in these endothermic processes.

When operating at lower temperature (80 ^{o}C or less) under atmospheric pressure a dual phase water system is present in the fuel cell. This dual phase water system must be kept in tight control due to the stringent humidification requirements of the membrane, which makes water management difficult. This is an issue for conventional PEFCs as the membrane system requires a certain level of water to be present to ensure high electrolytic conductivity however too much water will cause flooding of the electrodes which causes a loss in MEA performance.

Higher operating temperatures mean that water management is simplified significantly as there is only a single (gaseous) phase present. This means that the transport of water in the membrane, electrodes and diffusion layer is easier and flow field plate design can be greatly simplified [26,27,29]. Another effect of the higher temperatures is that the reactant and product gasses are expected to have increased diffusion rates [25] and with no liquid water present to block the electrochemically active surface area, a higher reaction rate is expected.

Both the simplified heat and water management means that much simpler flow field designs can be used which should help decrease the overall cost of the stack as machining plates should be cheaper.

2.2.4 Alternative catalysts

Due to the increased electrode kinetics at higher temperatures, it becomes possible to utilise alternative catalysts [28] at the electrodes, thus significantly reducing the cost of the PEFC. For example, iron (Fe) may be used as a catalyst [34]. Other work has been performed with the use of cobalt (Co) [35].

2.3 Disadvantages

Many years have been spent devoted to optimising the low temperature technology and each component within the PEFC. For example the gas diffusion electrode (GDE), MEA, gaskets, bipolar plates and the rest of the stack have been optimised for operation up to 80^{o}C; however many issues remain. When the operating temperature exceeds 100 °C, dehydration of conventional membranes occurs. This yields large ohmic losses, lower operating cell voltages and power densities [36]. Acid-based HT membranes, for example phosphoric acid doped PBI type materials, are thought to be a way of addressing dehydration issues; however, acid leaching from these materials leads to serious degradation of the fuel cell components. This in turn affects the power density and the performance of the fuel cell. The other concern which could affect commercial viability is the increased start- up time. The HT-PEFC must slowly be brought up to its operating temperature which could mean waiting for half an hour after start-up before any current can be drawn. As the average driving range is only around 23 miles per day in the UK (based on 2009 data), this would rule out HT-PEFC use in vehicles as far as short distance driving is concerned [37].

2.4 Industrial Employment of HT-PEFC technology

In the recent history of HT-PEFC technology, there are few companies that are actively working on HT-PEFC technology, with none working on IT-PEFCs. Companies such as Sartorius AG [38], Seremergy A/S [39], Elcomax [39], EnerFuel [39], Samsung [39] are all focused on acid based PBI membrane MEAs operating at approximately 180 ^{o}C. Insight gained from the 3rd Carisma Conference (2013), the world leading conference in HT-PEFC technology, the focus seemed to be on using the technology for stationary applications in a combined heat and power (CHP) aspect.

The only company known to work on IT-PEFC technology was Volkswagen AG (VW), in particular looking at applying IT-PEFC for automotive applications. Indeed, they are the only known automotive manufacturer who was looking at HT-PEFC technology for use in vehicles. From a search of patents filed by VW [40–45], it appears that VW were interested in areas ranging from the bipolar plates, the membrane materials, gas diffusion electrodes, cell assembly, stack design and system design. As noted in the Introduction chapter, VW have since ceased activities in this area. In a private communication with Professor Frederick Panik [16], who was the head of the fuel cell R&D program at Daimler, potential reasons for this stoppage were discussed. In particular, a majority of the automotive OEMs created consortiums to develop the automotive fuel cell systems. This was done to reduce the development costs for the systems significantly. This was an issue for VW as they were trying to develop a HT-PEFC system by themselves which would have meant large costs of development. Furthermore, from the patent search, VW filed 64 patents and were only granted 1.

This may have contributed to the decision to cease developing HT-PEFC systems as it would be difficult for them to protect their inventions.

2.5 The Gas Diffusion Layer (GDL)

The GDL is one of the key components within the MEA of the PEFC. The GDL must be both thermally and electronically conductive and connects the flow field plate (FFP) and the catalyst layer. Furthermore, it must allow for the transport of both reactants and waste products to and from the catalyst layer and the flow channel. Indeed, it should enhance the diffusion of the fuel in such a way that good coverage across the MEA active area is achieved. With regards to water management, the GDL must be capable of allowing water vapour to diffuse into the MEA to allow for sufficient humidification while also being capable of removing excess water to prevent flooding of the catalyst layers [8,46]. The GDL is also responsible for offering mechanical stability to the catalyst layer as well as the MEA as a whole. Finally, through its connection with both the catalyst layer and the flow field plate, the GDL offers a conduction pathway for the removal of waste heat generated from the exothermic fuel cell reactions.

From this, an ideal GDL will have a sufficient porosity to allow for the transport of reactants and waste products whilst also providing mechanical support for the catalyst layer. The pore structure should be optimised in terms of hydrophobic treatment to allow for good water management. High thermal and electrical conductivities are also key properties.

With respect to IT-PEFC MEAs, to the authors' knowledge there is no information within the literature on the development of GDLs specifically for this application.

Therefore this review will investigate carbon based GDLs developed for conventional PEFCs whilst highlighting where potential differences may lie. Furthermore, this review will also look at the development of metallic based GDLs for conventional PEFCs.

Current studies within the GDL field include; (i) conventional GDL materials [22,47,48], (ii) GDL processing [49–56] and (iii) metallic GDLs/flow distributors [57–61]. In the following section previous work conducted within this field will be reviewed.

2.6 Conventional GDL materials

The typical material used for the GDL is carbon. This is because it has; (i) good electrical conductivity, (ii) good relative stability in an acidic environment, (iii) elastic properties with respect to compressibility and (iv) high permeability for both liquids and gases [47]. The GDL will always contain a substrate layer (macroporous layer) and may contain a microporous layer. This leads to the GDL being classified as either a single layer or a dual layer GDL (Figure 2.2).

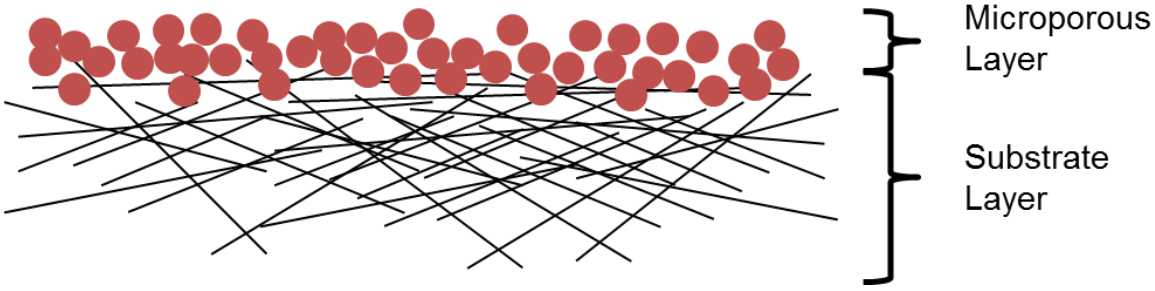

Figure 2.2: GDL Schematic; Single Layer – substrate layer only, Dual Layer – Microporous layer and substrate

2.6.1 Single Layer GDLs

The carbon material used in the GDL is commonly in the form of carbon-fibres. These fibres are either formed into carbon papers or cloths. During the manufacture processes, graphitization of the fibres occurs at high temperature (>2000 ^{o}C) which enhances both the mechanical strength as well as the electrical conductivity. The last step of the process to manufacture the carbon paper is to impregnate the fibres using thermoset resins. On the other hand, carbon cloths are made using yarns of carbon fibre that are spun and weaved which is then graphitized [62,63]. This process allows for modifications to be made to the manufacturing method in a simple fashion. For example, phenolic resin was added to a carbon-fibre cloth prior to graphitisation [64] in order to improve the structure of the carbon cloth. It was thought that the phenolic resin would help the carbon cloth retain some of its softness. It was found that this improved fuel cell polarisation characteristics without increasing the ohmic or mass transport. Another test was conducted by Liu et al [65] where different weights of carbon-fiber paper (70-320 g m^{-2}) were used. It was found that using the thinner paper with a lower permeability showed greater performance despite lower electric conductivity.

A less common material structure is that of expanded graphite which is manufactured by perforation of flexible graphite [66]. The observed performance from this has been comparable to dual-layer structured GDLs (see below).

A lot of work has been conducted to test whether carbon paper or carbon cloth enhance the performance of the MEA. Ralph et al. [67] used commercially available carbon cloth (Panex PWB-3, Zoltek) and carbon paper (Toray TGP-090). They found that when

operating at higher current densities, better performance was obtained by using a carbon cloth as compared to the carbon paper. This was attributed to the carbon cloth having a higher porosity than the carbon paper which led to a faster oxygen diffusion rate and an increased rate of water removal. This result was replicated by Frey and Linardi [68] who showed that by using a carbon cloth, improved performance could be gained even though their carbon cloth was thicker than the carbon paper. Simulation study by Wang et al [69] showed that the carbon cloth aided water removal as it has a lower tortuosity and a rougher surface than the carbon paper. This also allowed for better oxygen transport towards catalytic sites.

Further simulation studies [70] showed that in-plane water saturation is much more limiting to GDL performance compared to through-plane saturation. Gerteisen et al [71,72] used laser perforation to drill holes in the carbon paper along the flow channel (80 µm diameter). From their results, it was shown that there is better water management for both single cell and stack testing as the load was changed when comparing with an untreated GDL. One of the reasons that carbon cloth is superior to carbon paper is because of the dual pore size distribution and the relatively low tortuosity which results from spaces forming between the carbon fibres and yarns [73]. Therefore the improvement in water management seen with the laser perforation in the carbon paper is attributed to the formation of a dual pore size distribution which provides an easy pathway for water to leave the GDL. This means that local flooding is mitigated.

2.6.2 Dual-Layer GDL

Of the many strategies to reduce the mass transfer resistance of the PEFC, the usage of a dual-layer GDL has proven to be one of the most effective. This is commonly formed of; (i) a carbon fibre paper or fibre cloth macrostructure which provides mechanical stability and support for the electrode and functions as the gas diffuser, and (ii) a microporous layer (MPL) that is typically a mixture of hydrophobic agent and amorphous carbon black [11,54,74–91]. The main function of the MPL is to increase the contact between the catalyst layer and the substrate layer of the GDL through the formation of a uniform, flat layer that doesn't let the catalyst layer fall "within" the GDL. Furthermore, the MPL has been shown to enhance the water management properties of the GDL thus improving MEA performance.

Simulation studies were performed by Nam et al [85] on the MPL. In particular the study focussed on rate of formation of water, capillary forces in a hydrophobic MPL and the condensation/evaporation kinetics. From their study, they found that the interfacial saturation of liquid water between the MPL and the GDL substrate is lowered. This had the effect of suppressing the flooding of the cathode by liquid water. Another study by Weber et al [87] found that the MPL acts like a valve that keeps the water away from the catalyst layer and pushes the liquid water towards the flow field in order to control the amount of liquid water present. When increasing the penetration of the MPL into the GDL substrate, the power volume is changed along with the GDL substrate wettability [74]. Park et al [92] found that the amount of hydrophilic surfaces is changed due to the more hydrophobic MPL. This allows for increased removal of liquid water from the cathode catalyst layer.

One of the key methods by which water is removed from the catalyst layer is by capillary driven flow. This is due to the difference between the pressures of the vapour phase and the liquid phase [93,94]. As it is assumed that the vapour pressure will not change significantly at the operating temperature of the PEFC, it is the liquid pressure which builds up between the catalyst layer and the MPL which acts as the driving force for the flow of water from the catalyst layer [75,87,95–97]. It is suspected that high capillary pressure between the catalyst layer and the MPL would reduce the cell performance through the reduction of active area of the catalyst particles. This is due to the high partial pressure of water within the catalyst layer blocking active sites. However, it was found that the oxygen diffusion rate within the GDL substrate dominated the polarisation curve in the mass transport resistance region [96].

In general, the method by which the MPL is applied to the GDL substrate is as follows; (I) carbon powder is mixed into an ink along with PTFE, water and other solvents/surfactants, (ii) This ink is deposited onto the GDL substrate and (iii) the GDL is then heated up in order to remove all solvents/substrates. Many studies have investigated the MPL physical properties; (i) carbon material [80,83,89,90,98–102], (ii) wettability [75,78,79,87,95–97,103], (iii) MPL Thickness [54,75,77,82,85,87,95,98,104–106] and (iv) microstructure [83,107–111].

2.7 GDL processing

2.7.1 Hydrophobic treatment of the GDL Substrate

One aspect of the GDL that is very important to consider is its propensity to retain water. This is particularly a problem at low temperature where liquid water is formed at the cathode. Liquid water is notorious for being adhesive due to the potential for

hydrogen bonds to form with the substrate it is on. Therefore control of the substrate hydrophobicity is of paramount importance. Hydrophobic treatment of the carbon paper or cloth is used to control the wettability in order to aid in the removal of the saturating water within the cathode [75,95].

The hydrophobicity is controlled using treatment with various agents. For example, Teflon® (Polytetrafluoroethylene PTFE) [11,112,113], fluorinated ethylene propylene (FEP) [114,115] and polyvinylidene fluoride (PVDF) [116]. Application of this hydrophobic treatment is done using all of the usual methods, for example, spray coating, dip coating, brushing etc. The trade-off for this control in the hydrophobicity is that the porosity is decreased, tortuosity is increased and the pore size is decreased which all reduce the ability for the GDL to transport reactants to the catalyst layer thus affecting mass transport.

The influence of PTFE content on GDL performance for conventional PEFCs was studied by Bevers et al [113]. They loaded carbon papers with different amounts of PTFE before sintering the GDL at different temperatures. These treated papers were then characterised for different properties, in particular; (i) permeability to gasses, (ii) wettability and (iii) electronic conductivity were all measured. From their results, it was shown that as the PTFE content of the GDL increased, the water saturation of the GDL decreased. However, they also found that as the PTFE content increased, the ability for the GDL to transport gas was reduced as well as the electronic conductivity. A study conducted by Park et al [11] looked at the influence of PTFE concentration in the carbon paper on the cathode polarisation performance at different relative humidities. They found that when 15 wt % PTFE was used on carbon paper, it resulted in a higher performance due to the increased water removal and high gas permeability.

Different loadings of PTFE (10-40 wt %) on commercial carbon papers were studied by Prasanna et al [117]. The different PTFE loadings were characterised using different techniques. These included; (i) scanning electron microscopy (SEM), (ii) electrochemical impedance spectroscopy (EIS), (iii) gas permeability measurements and (iv) in-situ fuel cell testing. The poor porosity at higher PTFE loading (30 wt %) led to the in-situ fuel cell performance being poor as reactant transport was severely limited. This was confirmed by the gas permeability measurement and the EIS measurements. From their study, the optimum PTFE content in the GDL was 20 wt % as this optimised the balance between oxygen diffusion, liquid water transport and electronic conductivity.

A further study conducted by Lim et al [115] looked at treating commercially available GDLs (Toray TGP-H-090) that contain no hydrophobic agent. They used FEP to load the GDL with either 10 or 30 wt %. The influence of the FEP loading on the MEA performance was then examined. They found that using just 10 wt % FEP was sufficient to provide enough hydrophobic characteristic to avoid the issue of flooding of the electrode thus increasing the MEA performance. This effect was found to increase as the operating temperature increased (up to 90 ^{o}C in their study). Further, the performance increase was attributed to the better transport of reactants through the GDL as the pores were not blocked by the water saturation.

Benziger et al [118] studied the impact of hydrophobic treatment on liquid water transport by using a membrane filtration cell to measure the GDL liquid-water interface through measurements of pressure penetration. For samples that had been hydrophobically treated, they found that the hydrophobic treatment does indeed make the removal of water easier. However, they also found that higher pressure is required

to force the water into the hydrophobic channels to begin with. The study found that the PTFE treatment increases the number of pores within the GDL that are free of any water. This factor increased with higher PTFE content thus improving gas diffusion characteristics. The authors attributed this to the increase in surface energy of the water/carbon fibres with the hydrophobic treatment interface.

Park et al [119] also characterised commercially available carbon cloths (E-TEK) with different applied PTFE content on the cathode GDL. The intention of this study was to investigate the effect that the hydrophobic treatment has on the mass transfer resistance of the PEFC. Using a combination of porosity experiments and in-situ MEA testing, they found that by using the derived limiting current from the polarisation curve, there exists a relationship between the saturation of the GDL by product water, the water contact angle and the water permeability of the GDL. Furthermore, it was found that the water contact angle and water permeability actually governed the limiting current of the MEA. They also used an analytical model [92] to quantify the effect of the level of hydrophobicity and pore geometry on the MEA performance and the water management of the cathode.

Another issue that may arise is centred on phase change of water within the GDL as a result of temperature gradients with the MEA. Typically, the catalyst layer will generate heat due to the exothermic nature of the fuel cell reactions which means that the local temperature within the catalyst layer is usually higher than that of the temperature within the gas channel. As a result, at a given temperature, water vapour moving from the catalyst layer though the GDL substrate towards the gas channel will condense within the GDL substrate due to the lower vapour pressure. To alleviate this issue, hydrophilic channels within the GDL substrate could aid with the transport of

condensed water. This is known as Phase Change Induced Flow [120–126], and has been studied by various research groups. Different hydrophilic materials were added to a primarily hydrophobic GDL substrate as a method to reduce the amount of water saturating the GDL and catalyst layer. For example, inorganic oxides (e.g. Al_2O_3+SiO_2, Aerosil®, TiO_2, Al_2O_3 and SiO_2) were introduced into a GDL [127] by Cindrella et al [128] with a comparison of polarisation curves from different operating conditions. It was found that the GDL coated with TiO_2 led to a greater performance at higher operating relative humidities (70-100 %) whereas when a layer of Al_2O_3 or SiO_2 was coated on the GDL, better performance was observed at lower operating relative humidities (50-70 %). Another study conducted by Wang et al [129] aimed to insert a layer comprised of both poly(dimethysiloxane) (PDMS) and superhydrophobic silica nanoparticles in-between the GDL substrate and the catalyst layer. The layer that formed was interesting as it was indeed superhydrophobic ($\theta_{c,app}$= 162º). This was attributed to hydroxyl groups on the silica surface of hydrophilic pores [130,131]. From their study, the presence of a super hydrophobic surface of the inserted layer aids in the removal of water droplets at the catalyst layer/GDL interface whilst the hydrophilic pores prevent the saturation of other pores within the GDL which allows for better diffusion of oxygen through the GDL pores.

In summary, the hydrophobic treatment of GDLs has been found to be key to the improvement of MEA performance. The reasons for this improvement are that the hydrophobic treatment changes the interfacial energy between the water droplets and the GDL. This means that water is less likely to saturate the GDL and is easier to remove from the pores, which in turn increases the rate of diffusion for the reactant gases. However, the disadvantage of this process is that the mass transport limitations

of the MEA increases as more treatment is applied and this causes a decrease in the porosity and permeability for gases. Thus a fine balance is required.

With respect to intermediate temperature operation, it is unknown whether this hydrophobic treatment is necessary. This is because the water that is generated will be in the vapour phase and therefore there should not be the issue of the water saturating the GDL and blocking pores. This will be investigated in this thesis because if the hydrophobic treatment is unnecessary, it may be possible to cut out a potentially expensive manufacturing step.

2.7.2 Hydrophobic Treatment of the MPL

In order to improve the water management characteristics of the GDL by capitalising on the capillary driven flow of water (as described in Section 2.6.2), treatment of the MPL has been studied extensively.

An investigation into the PTFE loading of the MPL and how it influences the MEA performance was conducted by Girogi et al [78]. They found that a 10 wt % loading of PTFE improved the gas transport properties of the cathode whilst more effectively managing the water within the electrode. Lufrano et al [79] conducted another study which showed that, in a pressurised system, 20 wt % is the optimum PTFE loading. The influence of the hydrophobic chemical concentration with respect to the MPL was studied by Popov et al [103] using a number of techniques including; (i) water permeation, (ii) in-situ MEA testing and (iii) mercury porosimetry. As expected, the porosity experiments showed that as the PTFE content of the MPL increased, the pore volume decreased. The average GDL porosity values decreased from 80.8 % at 10 wt % PTFE to 77.9 % at 40 wt % (with the average pore diameter decreasing from

1.1 µm to 0.6 µm for 10 wt% and 40 wt%, respectively). However, upon microstructural analysis of these MPLs, it was difficult to ascertain the individual properties of the MPL as it was intruding into the GDL substrate which was attributed to the method by which the MPL was applied. From the water permeability tests conducted, it was found that water flow resistance through the MPL was found to increase with the increasing MPL PTFE content. This was attributed to the decreasing porosity of the MPL with increasing PTFE content. From the in-situ MEA testing (Figure 2.3), the polarisation curves were empirically fitted to determine the limiting current density as well as the Tafel slope, of which both were used to determine the concentration losses occurring due to the oxygen diffusion limitation within the catalyst layer and the GDL, respectively. When air was used at the cathode, it was found that the 20 wt % PTFE loading showed the highest improvement on MEA performance. In this case, intermediate current densities were used to determine the Tafel slope. This is different from the usually thought of kinetic Tafel slope, which is related to the oxygen reduction reaction (ORR) kinetics and is determined from low current densities when there is no limitation with respect to oxygen concentration within the catalyst layer. On the other hand, the Tafel slope derived from the intermediate current density is strongly affected by the oxygen concentration within the catalyst layer and therefore becomes much larger [132–135]. As shown in Figure 2.3 (b), the 20 wt % PTFE loading led to a much lower empirical Tafel slope, which indicates that there is more effective oxygen transport within the catalyst layer. Further it is shown that this PTFE loading gives a higher current density which shows that there is more effective transport of oxygen within the GDL [132–135] .

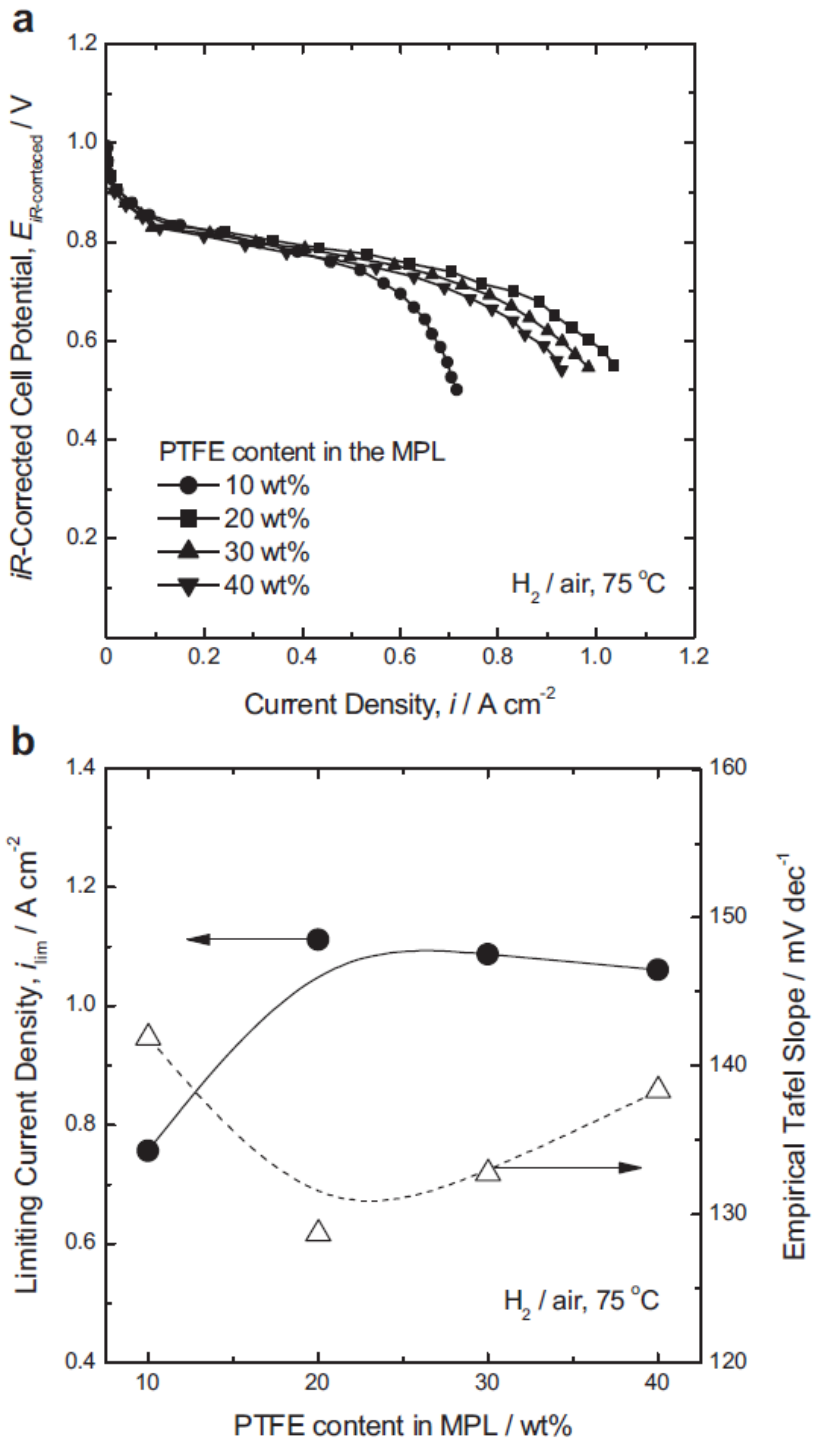

Figure 2.3: (a) in-situ polarisation curves showing the change in performance with respect to the PTFE loading of the MPL and (b) the influence of PTFE loading on the empirically derived Tafel slope and the limiting current. [103]

From the limiting current that was empirically measured, it was also possible to derive the pore volume fraction that is open to oxygen with the GDL, i.e. the effective GDL porosity. The effective porosity was determined to be 19 % which indicated that a majority of the pores were saturated with liquid water. It is important to note that these measurements for effective porosity and oxygen diffusion are for the whole GDL and not just the GDL substrate/MPL independently. Indeed, it is not practically possible to empirically obtain the discrete limiting currents due to the GDL and the MPL respectively. This is because the transport mechanisms change with the addition of the MPL. Therefore, in order to help work out the mechanism and profile of water saturation within the GDL, simulation studies will be important. This will help to determine the effective porosities of the GDL macrostructure and the MPL.

Returning to the mechanism of Phase Change Induced Flow, as described in section 2.7.1, whereby water changes phase within the GDL substrate due to the temperature gradients present within the MEA, a study was conducted by Schweiss et al.[136] to add hydrophilic channels to the MPL. This is because previous studies [123,137] showed that within the catalyst layer, the product water exists mainly within the vapour phase. As it moves towards the gas flow channel, the waste water changes phase with the MPL/CL interface often being the site at which this nucleation of water condensate usually appears. Therefore, Schweiss et al [136] used cylindrical hydrophilic aluminosilicate fibres by adding them to the hydrophobic MPL ink prior to application in order to reduce the condensate found at the catalyst layer/MPL interface. Using a water permeation test, they found that the thickness is the primary factor which affects the diffusion rate of water vapour through the GDL irrespective of the GDL wettability. However, when testing how liquid water permeability was affected on a GDL (SGL

25BL) treated with inorganic fibres, it was found that the liquid water permeability was approximately five times greater than the permeability through a standard hydrophobic GDL (SGL 25BC). This was attributed to the wicking effect created by the generation of liquid water flow channels through the GDL. A similar study by Ahn et al [138] found that by adding different amounts of perflourosulfonated acid monomer to a carbon black slurry, the resulting MPL led to much faster water removal from the catalyst layer.

It remains to be seen whether these effects will be important at higher temperature operation of the PEFC as the water generated should exist in the vapour phase and therefore water saturation of the GDL should not be such a big problem. It will also be important to see if condensation within the GDL still occurs at high temperature. Indeed it may be that the hydrophobic treatment of the MPL is not necessary at high temperature and therefore may be an unnecessary cost.

2.8 Metallic GDLs and Flow Distributors

Metallic materials, particularly in the form of meshes or foams offer an interesting avenue of research for the GDL of the PEFC. Specifically, metals such as stainless steel mesh [139], nickel mesh [61], titanium mesh [57–59,140–143], or Nickel-Chromium alloy foam [144] work well as a good diffusion facilitator for liquid fuel (i.e. in a direct methanol fuel cell) as well as in the cathode of the PEFC. Another major advantage of the metallic based GDLs is that they provide excellent mechanical strength which allows for very thin diffusion layers and thus mass transport limitations are reduced. Furthermore, unlike their carbon counterparts, meshes/foams possess a very uniform structure with a controllable pore size. Indeed, they also have excellent

electrical and thermal conductivities which means that they appear ideal for use as GDLs.

Stainless steel wire mesh (Filtertechnik GmbH Willy Spee), carbon paper (Toray TGP-H-090) and carbon cloth (E-TEK) were compared using their polarisation characteristics when used as GDLs by Oedegaard et al [139]. They found that, due to the higher electronic conductivity, the stainless steel wire mesh gave better performance when employed as the anodic diffusion medium for a DMFC. They also found that there was improved dual phase transport dynamic between the carbon dioxide waste and the methanol when using the stainless steel mesh. Another study conducted by Wittstadt et al [145] and Ioroi et al [146] tested a titanium based GDL which was treated using a PTFE emulsion prior to heat treatment. This titanium GDL was then tested within a unitized regenerative fuel cell (URFC) as the bifunctional oxygen electrode. The titanium GDL showed excellent performance whilst displaying reduced saturation of the electrode with water when the URFC was used in fuel cell mode.

Microfabricated metallic GDLs have also been developed using micro machining techniques [60,147]. This process consists of a combination of chemical etching and photochemical processing of a base metallic material. Fushinobu et al [147] used this technique to gain very fine control of various GDL design parameters using a thin titanium sheet. GDL parameters such as the diameter of the microholes, the thickness of the GDL and the pattern of the current collection were tested. Their results showed that the relative humidity as well as the operating temperature played a large role in the performance of the cell. At low operating temperatures (40 ^{o}C), the titanium GDL was unable to manage the water adequately which lead to flooding of the electrode.

However, at higher operating temperatures (80 ^{o}C), the titanium GDL improved performance due to increases in the membrane conductivity. It was also found that the thinner titanium GDL, as well as smaller diameter microholes at a constant porosity, gave better performance. From their study, when compared with commercial carbon paper, the titanium GDL gave similar performance at low current densities (< 0.2 A cm^{-2}).

Using microelectromechanical system technology (MEMS), Zhang et al [60] made a thin copper based GDL. They compared carbon paper (Toray TGP-H060) with their copper GDL both as cathode GDLs. They found that at low stoichiometries ($\lambda_{H_2} = 2$ and $\lambda_{air} = 2$), the copper GDL showed better management of the water within the electrode which led to better diffusion characteristics for oxygen moving into the electrode. However, when tested at stoichiometries ($\lambda_{H_2} = 4$ and $\lambda_{air} = 4$), the carbon paper showed better MEA performance.

However, there are drawbacks to using the metallic materials. Metallic materials are commonly used as the main material for the flow field plates and studies have shown that corrosion is a big issue [3,148–150]. These studies have shown that the metals corrode in both an anodic and cathodic environment. Indeed this corrosion leads to an enhancement of other degradation processes, in particular of the polymer electrolyte membrane [5,151]. One way around this issue is to coat the metallic material with a protective, corrosion resistant material [152–157].

Currently there is very little work done within the literature on the usage of metallic materials as GDLs in a hydrogen powered PEFC. A majority of work reviewed is on using the GDL in a DMFC. There is especially no work on the use of a metallic GDL in

a higher temperature PEFC where the benefits of higher temperature operation offer good synergy with the properties of the metallic materials. This is an interesting area for further study, as well as investigating the use of corrosion resistant materials or coatings. Furthermore, long term degradation or accelerated corrosion conditions must be tested with these materials.

2.9 Simulation Studies of IT-PEFC

One method for the development of HT-PEFCs is to employ *ab initio* simulation studies as this allows for further information to be gained on what is happening within the MEA that would be difficult to ascertain empirically.

The first PEFC models were published in the early 1990s by Springer et al [158,159] and Bernardi and Verbrugge [160,161] and were one dimensional models. These models were based on experimental studies carried out on phosphoric acid fuel cells. In these models, species transport, water balance and influence of relative humidity of reactant gases were investigated. Recently, the influence of several parameters were studied by Song et al [162] using a dynamic two phase model that was non-isothermal in order to describe the multiphase dynamics within the GDL.

Current modelling work has focused on conventional low temperature PEFCs, see for example [163–168]. For HT-PEFCs in particular, research has been devoted to modelling of the membrane in order to understand and improve membrane design [169–173].However, a study of membrane materials at intermediate temperatures is still lacking. For low temperature PEFC, a large focus has been on the transport phenomena within the cell [163–168] through to modelling of the stack [174–176]. However, little work has been conducted on either the IT-PEFC.

With respect to simulating higher operating temperature PEFCs, Baschuk et al [177] produced a comprehensive model for use within CFD software which included all elements of the PEFC, including mass, momentum and heat conservation as well as the fuel cell electrochemical reactions. The study showed the influence of various operating parameters on the MEA performance. However, the model was a generalised 2D case which was not experimentally validated. Another study by Kulikovsky et al [178] produced a model where the typical 10 parameter models were reduced to a 4 parameter model in order to create a simple representation. Isothermal behaviour is assumed and the ORR is modelled using the Tafel Law. However, this model does not allow for the prediction of component parameters, for example GDL porosity, and therefore is not useful as a predictive tool.

More recent work has been conducted into the expansion of the analytical and empirical models to include the behaviour of the fluids in the flow channels. Several studies have shown that the behaviour of the gas within the flow channel can significantly affect the MEA performance and so work has been undertaken to expand this understanding of the MEA design. Cheddie et al have been strong contributors to simulating PEFCs. Their study [171] was the first to simulate an IT-PEFC. However, their definition of an IT-PEFC is synonymous with contemporary HT-PEFC, i.e. an acid based membrane with an operating temperature between 130-180 ^{o}C. The model developed was a 1D parametric model to describe MEA performance [170]. However, the model failed to predict mass transport limitations of the cell, and displayed that potential areas for improvement were in the field of membrane development and cathode catalyst activity. A further study focussed on the mathematical modelling of a

1D cell, and incorporated non-isothermal effects [169]. A separate study looked into the use of analytical correlations for performance in 1D geometries (i.e. along a flow channel), which accurately predicted cell performance [171]. They also presented a three-dimensional model based on a HT-PEFC with a polybenzimidazole (PBI) membrane, and correctly estimated the effects of ohmic resistance in the ribs in the catalyst layer [169] which was validated experimentally. The model could be further improved by accounting for gas solubility, which was investigated in a later two-phase model to account for aqueous electrochemical reactions in the catalyst layers [171]. The work highlighted the importance of including gas solution in the electrolyte prior to reaction, though only a two-dimensional domain was investigated.

The work of Sharmadina et al. [179] investigates the properties of a HT-PEFC using a model based on physical and mathematical principles. The work accurately accounts for H_2 and air crossover through the membrane, though is limited to dry gases and isothermal conditions. The work of Cheng et al. [180] also investigates the effects of hydrogen crossover, highlighting the importance of reducing this to minimise cathode potential depression, fuel inefficiency and peroxide formation. The work focussed on the determination of crossover, and discovered that hydrogen permeation through the PEM was the limiting step in the crossover process.

Several papers have been written with regard to modelling varying cell geometry and design, with a view to optimising performance. Kumar & Reddy [181] have worked to produce a three-dimensional model to investigate the effect of flow field design in steady-state operation of conventional PEFCs, and also to observe the transient response of these flow field designs. The key benefit of the work is the observation of

transient behaviour, with interdigitated flow fields faring the worst out of all possible field designs. This indicates that for automotive applications where transient operation is to be expected, serpentine or multi-parallel flow field designs should be implemented. The work includes a number of assumptions about water transport within the cell, which may limit its utility in HT-PEFC modelling.

Ferng & Su [182] have produced a full-cell CFD model in three dimensions to investigate different channel designs. The work found that a parallel flow channel design with a stepped depth presents the greatest performance, which disagrees with other authors who suggest a serpentine flow field is superior. Henriques et al [183] recently performed a simulation investigating the effect of varying channel depth on cathode performance, finding that a trivial straight channel design with enough width proved to be sufficiently effective at increasing cell efficiency. However, the research does not investigate the use of different flow channel geometries, such as serpentine designs.

Dutta et al [184] created a three-dimensional model to determine mass flow following a serpentine flow path, assuming isothermal behaviour and modelling the electrochemical reactions as mass sources and sinks, i.e. ignoring reaction kinetics. Their work discovered that the pressure drop within serpentine flow channels was lower than expected for a straight channel flow, which is in disagreement with other authors. This discrepancy is believed to be due to significant flow through the porous diffusion layers. The research also concluded that flow patterns are significantly dependent on mass consumption patterns on the MEA. Another study by Guvelioglu et al [185] produced a two-dimensional isothermal model, with a particular focus on

modelling the water balance in the membrane. The work pays particular attention to channel and bipolar plate shoulders, allowing for optimisation of the size of these components, however does not include concentration effects along the length of the channel.

As can be seen, little to no simulation work has been conducted at intermediate temperature, with a majority of modelling studies focused on either higher temperature PEFC or conventional PEFC. Studies on GDL material parameters are focussed on water transport effects within the GDL which may not be an issue at intermediate temperature due to the higher operating temperature.

2.10 Outlook for Intermediate Temperature PEFC

There is a lot of scope for research to be carried out at intermediate temperature operation of PEFCs. As has been shown, a large majority of work conducted has been focused on membrane material development. Little to no work has been conducted on the GDL at these operating conditions, neither by simulation study nor by experiments.

Understanding the influence of fundamental GDL parameters is of particular interest, such as the porosity and permeability, which have not been studied in depth. Furthermore, the advantages of intermediate operation will not be exploited fully if a conventional PEFC cell design is used, such as the possibility of single phase flow which could mean high pressure drop flow field designs are not necessary. Further study is required to see if further enhancements can be gained.

CHAPTER 3

Investigating and Designing Gas Diffusion Layers Using a Sensitivity Analysis

"In theory, there is no difference between theory and practice. But in practice, there is"

Jan L. A. van de Snepscheut, n.d.

Chapter 3 Investigating and Designing Gas Diffusion Layers Using a Sensitivity Analysis

3.1 Introduction

In this study, several multiphysics models have been built which all take an ab initio approach. Material properties were taken from literature and the models generated results which were then compared with experimental data. Several aspects of the IT-PEFC are then investigated in order to gain further insight into IT-PEFC operation. Aspects of thermal management and water management are also investigated. Due to the lack of information about intermediate temperature membranes, a short sensitivity analysis on membrane material properties was also included.

In addition, the fundamental properties of the GDL (electrical conductivity, porosity, permeability and thermal conductivity) have been investigated in detail. Furthermore, the feasibility of changing the MEA design in order to allow for new materials as the GDL, for example metallic foams and meshes, has been investigated. This work has been conducted to improve the design and performance of IT-PEFCs while providing insight into the role of electrical conductivity, porosity, permeability and thermal conductivity and optimising MEA component properties.

Current modelling work has focused on conventional low temperature PEFCs, see for example [163–168].For high temperature PEFCs in particular, research has been devoted to modelling of the membrane in order to understand and improve membrane design [169–173].However, a study of membrane materials at intermediate

temperatures is still lacking. For low temperature PEFC, a large focus has been on the transport phenomena within the cell [163–168] through to modelling of the stack [174–176]. However, little work has been conducted on IT-PEFC.

3.2 Theoretical Model

3.2.1 Numerical Procedure

Comsol Multiphysics 4.4 was used to build the models described. A free triangular mesh was used to mesh the flow channels with a quad element based mesh to describe the GDLs and membrane in order to minimise solution time. In addition, boundary layers were added to the free triangular mesh so that effects at the boundaries of channels could be observed. A mesh convergence study was carried out and the final mesh contained 41744 elements (see Figure 3.1). A fully coupled, parametric solver was used (MUMPS) to solve the simulation with a convergence criteria of 0.00001 used to ensure accuracy of the simulation.

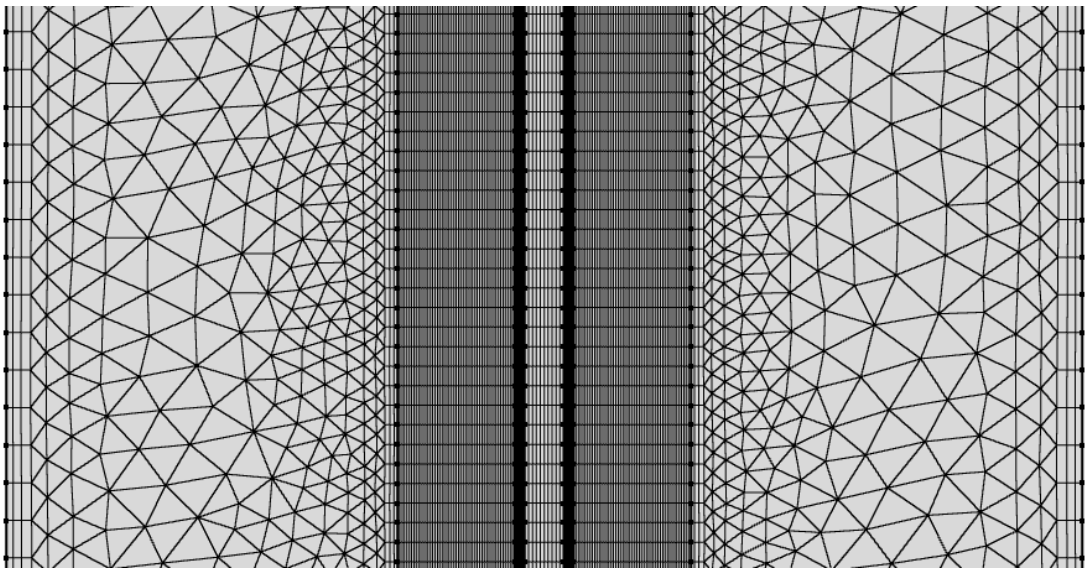

Figure 3.1: Mesh distribution

3.2.2 Model Geometries

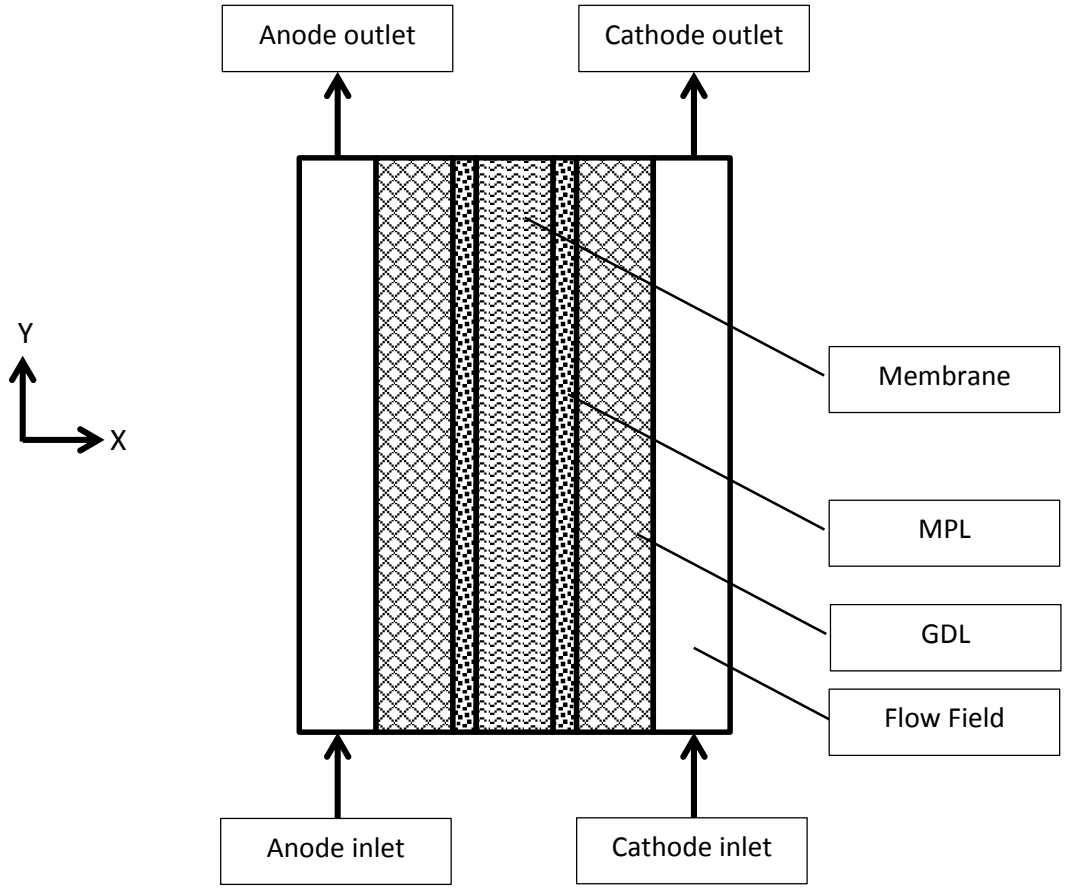

Figure 3.2: Model Geometry for Case 1 and Case 2

The model represents a cross section through the MEA along a gas flow channel. It is used to calculate the MEA performance under varying operating conditions, e.g. relative humidity in the gas influx, and polarisation curves. We use these models to analyse gas, heat and water distribution on the air side with the anode conditions remaining constant. Charge, energy mass and momentum conservation are all modelled in order to investigate the influence of GDL properties.

Two cases were taken:

Case 1 – where a typical carbon GDL is modelled as the cathode GDL

Case 2 – where a metallic foam is modelled as the cathode GDL

Following from this 2D simulation, a 3D model (Figure 3.3 & Figure 3.4) was built to describe the cathode GDL in order to compare flow, pressure and heat transfer profiles when a conventional GDL and a metallic GDL were used. We use this model to analyse gas, heat and water distribution on the air side with the anode conditions remaining constant. For this model, two further cases were taken:

Case 3 – where a typical carbon GDL and serpentine flow field design are used on the cathode.

Case 4 – where an integrated metallic flow field/GDL is modelled on the cathode.

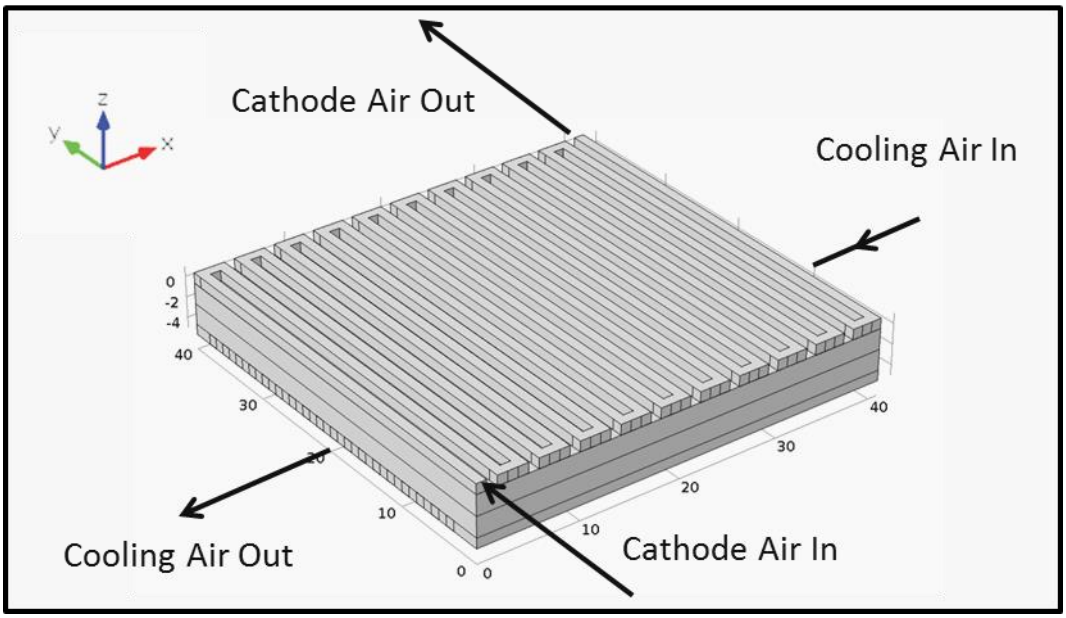

Figure 3.3: Model Geometry for Case 3

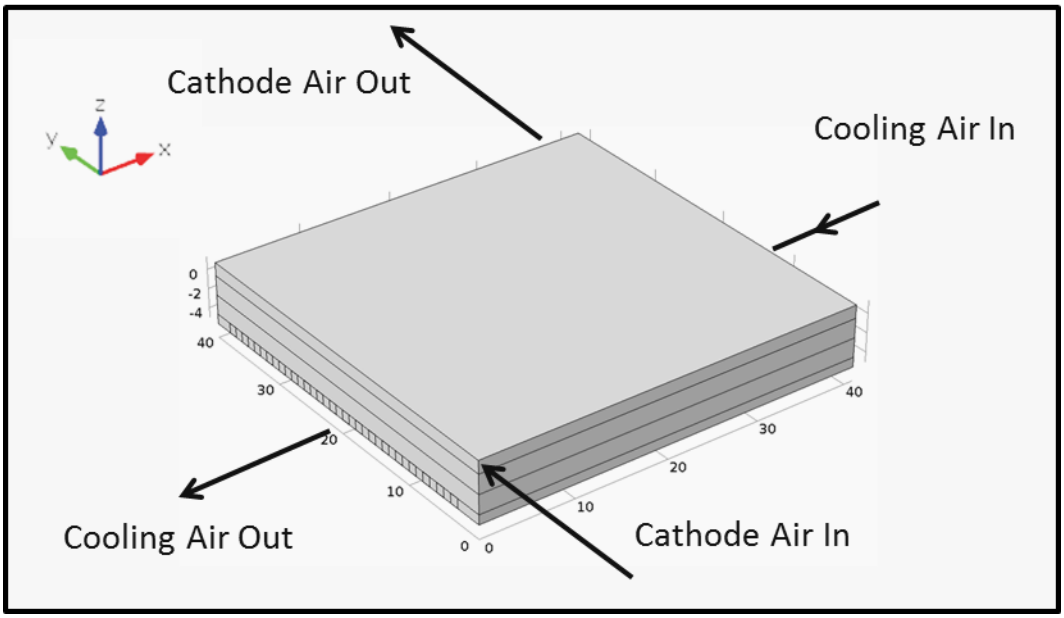

Figure 3.4: Model Geometry for Case 4

As this is high temperature, single phase flow is assumed. Laminar gas flow is assumed and thus is governed by the standard Navier-Stokes equations. Within the porous regions (GDLs and electrodes), the fluid is modelled using the Brinkman-Stokes equation which takes into account continuity between free and porous materials

[186]. All physical properties of the MEA are considered to be constant and temperature and pressure invariant within the variables spaces used (0-120 ^{o}C and 1-1.8 bar). In all of the calculations where the anode is modelled (Case 1 and 2), the anode side parameters are considered to be operating under the same conditions, with identical GDL properties and constant electrochemical performance. Interfacial contact resistance was not included in this model as this is a proof of concept model. Whilst it is known that the interfacial contact resistance can have a large impact on cell performance, interfacial resistance is difficult to measure independently of bulk material resistance (for example, the contact resistance of the MPL and GDL surface) and therefore, rather than adding parameters to obtain a better fit, it was decided to assume that interfacial contact resistance is negligible. All of the models built are stationary models.

Several conservation equations are utilised to account for mass, momentum, transport of the various species within the system (namely hydrogen, oxygen and water), electric potential and energy, as displayed by the equations shown below.

In all of the studies where an MPL is present, the MPL parameters remain unchanged (as shown in Table 3.1). An average of the MPL and the GDL substrate porosity was used in this study when considering the model on commercially available GDLs in the model.

3.2.3 Parameters

Table 3.1 shows the physical parameters used for the models in this study as well as other parameters that were kept constant. Other parameters, such as the flow rates,

electrochemical parameters (e.g. exchange current density, Tafel slope) etc. will be presented with each particular study.

Table 3.1: Physical parameters used in the models; dashes denote parameters not applicable to the individual models.

Parameter	Case 1	Case 2	Case 3	Case 4
Total Length (Y axis), L_{tot} / mm	22	22	40	40
Total Width (X axis), W_{tot} / mm	2.68	3.43	40	40
Total Height (Z axis), H_{tot} / mm	-	-	6.35	6.35
Flow Field Plate Length (Y axis), L_{FFP} / mm	-	-	40	40
Flow Field Plate Width (X axis), W_{FFP} / mm	-	-	40	40
Flow Field Plate Height (Z axis), H_{FFP} / mm	-	-	3	3
Anode Flow channel length (Y axis), L_{A_Ch} / mm	22	22	-	-
Anode Flow channel width (X axis), W_{A_Ch} / mm	1	1	-	-
Cathode Flow channel length (Y axis), L_{C_Ch} / mm	22	-	40	-
Cathode Flow channel width (X axis), W_{C_Ch} / mm	1	-	1	-
Cathode Flow channel Height (Z axis), H_{C_Ch} / mm	-	-	1	-

Parameter	Case 1	Case 2	Case 3	Case 4
Anode GDL Length (Y axis), L_{A_GDL} / mm	22	22	-	-
Anode GDL Width (X axis), W_{A_GDL} / µm	275	275	-	-
Cathode GDL length (Y axis), L_{C_GDL} / mm	22	22	40	40
Cathode GDL Width (X axis), W_{C_GDL} / mm	0.275	1.975	40	40
Cathode GDL Height (Z axis), H_{C_GDL} / mm	-	-	0.35	1.35
Anode and Cathode MPL length (Y axis), L_{MPL} / mm	22	22	-	-
Anode and Cathode MPL Width (X axis), W_{MPL} / µm	40	40	-	-
Membrane Length (Y axis), L_{mem} / mm	22	22	-	-
Membrane Width (X axis), W_{mem} / µm	50	50	-	-
Cooling Channel Length (X axis), L_{cool}/ mm	-	-	40	40
Cooling Channel Width (Y axis), W_{cool}/ mm	-	-	1	1
Cooling Channel Thickness (Z axis), H_{cool}/ mm	-	-	1	1
Anode exchange current density, i_0 / A m^{-2}	1×10^5	1×10^5		

Parameter	Case 1	Case 2	Case 3	Case 4
ORR equilibrium reaction potential at 120 ^{o}C, E_{thoery}/ V	1.15	1.15	-	-
Oxygen reference concentration, $c_{O2,ref}$/ mol m^{-3}	40.88 [187]	40.88 [187]	-	-
Hydrogen reference concentration, $c_{H2,ref}$/ mol m^{-3}	40.88 [187]	40.88 [187]		
Anode gas viscosity, μ_{anode} / Pa s	1.19 x 10^{-5}	1.19 x 10^{-5}	-	-
Anode GDL permeability, κ_{anode} / m^2	8.9 x 10^{-12}	8.9 x 10^{-12}	-	-
Anode GDL porosity, ε_{anode}	0.4	0.4	-	-
Anode GDL conductivity, σ_{anode} / S m^{-1}	253	253	-	-
Cathode gas viscosity, $\mu_{cathode}$ / Pa s	2.46x 10^{-5}	2.46x 10^{-5}	2.46x 10^{-5}	2.46x 10^{-5}
Hydrogen specific heat capacity, $C_{p,H2}$ / J kg^{-1} K^{-1}	14283	14283	-	-
Oxygen specific heat capacity, $C_{p,O2}$/ J kg^{-1} K^{-1}	919.31	919.31	919.31	919.31
Water specific heat capacity, $C_{p,H2O}$/ J kg^{-1} K^{-1}	4186	4186	-	-
Nitrogen specific heat capacity, $C_{p,N2}$/ J kg^{-1} K^{-1}	1040	1040	1040	1040
Membrane thermal conductivity, $k_{membrane}$/ W m^{-1} K^{-1}	0.95 [188]	0.95 [188]	-	-

Parameter	Case 1	Case 2	Case 3	Case 4
Gas diffusion layer thermal conductivity, k_{GDL}/ W m^{-1} K^{-1}	0.3[189]	13[190]	0.3[189]	13[190]
MEA density, ρ_{matrix}/ kg m^{-3}	1000 [187]	1000 [187]	-	-
Membrane specific heat capacity, $C_{p,membrane}$/ J kg^{-1} K^{-1}	1650 [187]	1650 [187]	-	-
Gas diffusion layer specific heat capacity, $C_{p,GDL}$/ J kg^{-1} K^{-1}	568 [187]	450 [190]	568 [187]	450[190]
Binary Diffusion Coefficients H_2-H_2O, $D_{H_2-H_2O}$ / m^2 s^{-1}	9.15 x 10^{-5} *(T_{local}/307 K)$^{1.75}$ [191]	9.15 x 10^{-5} *(T_{local}/307 K)$^{1.75}$ [191]	-	-
Binary Diffusion Coefficients N_2-H_2O, $D_{N_2-H_2O}$ / m^2 s^{-1}	2.56 x 10^{-5} *(T_{local}/307 K)$^{1.75}$ [191]	2.56 x 10^{-5} *(T_{local}/307 K)$^{1.75}$ [191]	-	-
Binary Diffusion Coefficients O_2-N_2, $D_{O_2-N_2}$ / m^2 s^{-1}	2.2 x 10^{-5} *(T_{local}/293 K)$^{1.75}$ [191]	2.2 x 10^{-5} *(T_{local}/293 K)$^{1.75}$ [191]	-	-
Binary Diffusion Coefficients O_2- H_2O, $D_{O_2-H_2O}$ / m^2 s^{-1}	2.82 x 10^{-5} *(T_{local}/308 K)$^{1.75}$ [191]	2.82 x 10^{-5} *(T_{local}/308 K)$^{1.75}$[191]	-	-
GDL - Binary Diffusion Coefficients H_2-H_2O, $D_{H_2-H_2O\_GDL}$ / m^2 s^{-1}	$D_{H_2-H_2O}$*$\varepsilon_{GDL}^{1.5}$	$D_{H_2-H_2O}$*$\varepsilon_{GDL}^{1.5}$	-	-
GDL - Binary Diffusion Coefficients N_2-H_2O, $D_{N_2-H_2O\_GDL}$ / m^2 s^{-1}	$D_{N_2-H_2O}$*$\varepsilon_{GDL}^{1.5}$	$D_{N_2-H_2O}$*$\varepsilon_{GDL}^{1.5}$	-	-

Parameter	Case 1	Case 2	Case 3	Case 4
GDL - Binary Diffusion Coefficients O_2-N_2, $D_{O_2-N_2\_GDL}$ / $m^2 s^{-1}$	$D_{O_2-N_2} * \varepsilon_{GDL}^{1.5}$	$D_{O_2-N_2} * \varepsilon_{GDL}^{1.5}$	-	-
GDL - Binary Diffusion Coefficients O_2- H_2O, $D_{O_2-H_2O\_GDL}$ / $m^2 s^{-1}$	$D_{O_2-H_2O} * \varepsilon_{GDL}^{1.5}$	$D_{O_2-H_2O} * \varepsilon_{GDL}^{1.5}$	-	-
MPL - Binary Diffusion Coefficients H_2-H_2O, $D_{H_2-H_2O\_MPL}$ / $m^2 s^{-1}$	$D_{H_2-H_2O} * \varepsilon_{MPL}^{1.5}$	$D_{H_2-H_2O} * \varepsilon_{MPL}^{1.5}$	-	-
MPL - Binary Diffusion Coefficients N_2-H_2O, $D_{N_2-H_2O\_MPL}$ / $m^2 s^{-1}$	$D_{N_2-H_2O} * \varepsilon_{MPL}^{1.5}$	$D_{N_2-H_2O} * \varepsilon_{MPL}^{1.5}$	-	-
MPL - Binary Diffusion Coefficients O_2-N_2, $D_{O_2-N_2\_MPL}$ / $m^2 s^{-1}$	$D_{O_2-N_2} * \varepsilon_{MPL}^{1.5}$	$D_{O_2-N_2} * \varepsilon_{MPL}^{1.5}$	-	-
MPL - Binary Diffusion Coefficients O_2- H_2O, $D_{O_2-H_2O\_MPL}$ / $m^2 s^{-1}$	$D_{O_2-H_2O} * \varepsilon_{MPL}^{1.5}$	$D_{O_2-H_2O} * \varepsilon_{MPL}^{1.5}$	-	-
Inlet Temperature, T_{inlet}/ K	393	393	393	393

3.2.4 Boundary Conditions

For Case 1 and 2:

Species Transport: Inlet mass fractions were specified for both the anode and cathode inlets. Outlet boundaries were specified and all other exterior boundaries were set such that there is no flux across them. The membrane was assumed to be impermeable to all species except for protons.

Momentum Transport: The air and hydrogen were assigned uniform gas inlet volumetric flow rates. The outlets were set such that the simulation calculated the exit pressure.

Heat Transfer: The exterior walls of the channels were set at a constant temperature which was taken as the operating temperature of the fuel cell. The temperature of the inlet gases was taken as a constant. The outlets were set such that the simulation calculated the exit temperature. All other boundaries were taken to be no-slip walls.

Charge Transport: The boundary between the anode flow channel and GDL was taken as the electric ground. The boundary between the cathode GDL and cathode flow channel was taken as the cell operating voltage.

For Case 3 and 4:

Momentum Transport: the flow channel inlet was assigned a uniform gas inlet volumetric flow rate. The outlet was set such that the simulation calculated the exit pressure.

Heat Transfer: The top surface of the cathode GDL was considered to be the cathode catalyst layer and was considered to be a constant heat source of power equal to the operating parameters of the fuel cell. The inlets for the cathode flow channel and cooling channels were kept at a constant value. The exterior walls of the cathode were considered thermally insulated such that heat transfer could only occur in the z-axis. The anode was not modelled.

3.2.5 Governing Equations

MASS

$$\nabla(\rho\,\vec{u}) = S_m \qquad \text{Equation 3.1}$$

where ρ is the density of the gas (kg m^{-3}), u is the velocity of the gas (m s^{-1}) and S_m is the mass flux source term, which accounts for the production and consumption of species by electrochemical reactions. In a three dimensional Cartesian co-ordinate system, the operator ∇ is defined in terms of partial derivates:

$$\nabla = \hat{x}\frac{\partial}{\partial x} + \hat{y}\frac{\partial}{\partial y} + \hat{z}\frac{\partial}{\partial z}$$

SPECIES CONSERVATION

$$\nabla(\rho\vec{u}Y_i) = \nabla\left(\rho D_i^{eff}\nabla Y_i\right) + S_i \qquad \text{Equation 3.2}$$

where Y_i is the mass fraction, D_i^{eff} is the effective diffusivity of species i (m^2 s^{-1}), and S_i is source term of species i, which accounts for the generation or consumption of a particular species.

MOMENTUM

$$\rho u\ \nabla \mathrm{u} = -\nabla p + \mu\nabla\left(\nabla \mathrm{u} + \nabla \mathrm{u}^T\right) + S_u \qquad \text{Equation 3.3}$$

where p is the local pressure of the gas (Pa), μ is the viscosity of the gas (Pa s) and S_u is a source term, which accounts for the viscous energy dissipation of the gas within the GDL and CL. In porous media, momentum conservation is described using the Brinkman equation:

$$\nabla\left(\mu/\kappa\right)\mathrm{u} = -\nabla p + \frac{\mu}{\varepsilon}\nabla\left(\nabla\mathrm{u} + \nabla\mathrm{u}^{T}\right) + S_u \qquad \text{Equation 3.4}$$

where κ is the material permeability (m^2) and ε is the material porosity.

ENERGY

$$\nabla\left(\rho C_p \vec{u} T\right) = \nabla\left(k_{g,s}^{eff} T\right) + S_T \qquad \text{Equation 3.5}$$

where C_p is the heat capacity of the gaseous mixture (J kg^{-1} K^{-1}), T is the local temperature, $k_{g,s}^{eff}$ is the effective thermal conductivity (W m^{-1} K^{-1}) of the gas mixture, membrane and electron conducting materials and S_T is the source term representing heat generation and dissipation.

CHARGE

Electronic potential: $\nabla(-\sigma_l \nabla\varphi_l) = S_l$ Equation 3.6

Protonic potential: $\nabla(-\sigma_s \nabla\varphi_s) = S_s$ Equation 3.7

where σ_l, σ_s, φ_l and $\varphi_s$are the ionic conductivity of the membrane (S m^{-1}) , electronic conductivity of the electrode (S m^{-1}), ionic potential in the membrane (V) and electronic potential in the electrode (V), respectively. The source terms, S_l and S_s (A m^{-2}), represent the production and consumption rate of hydrogen ions and electrons.

ELECTROCHEMICAL CONSERVATION PARAMETERS

The cathodic reactions are determined based on the Tafel equation, as shown in Equation 3.8.

$$i_{local} = i_0 \times 10^{\eta/\beta_C} \qquad \text{Equation 3.8}$$

Where i_{local} is the local current density (A m^{-2}), i_0 is the exchange current density (A m^{-2}), β_C is the cathodic Tafel slope (mV/dec) and η is the overpotential (V). The exchange

current density is defined by an Arrhenius-type expression, and corrected for with respect to the reactant species concentration [187]. The anodic reaction is determined using a linearised Butler-Volmer equation, as shown in Equation 3.9.

$$i_{local} = i_0 \left(\frac{(a_a + a_c)F}{RT} \right) \eta \qquad \text{Equation 3.9}$$

3.3 Experimental Verification

3.3.1 MEA production and testing

For the purpose of validating the model, a membrane electrode assembly (MEA) was produced and tested. Commercially available Johnson Matthey (JM) electrodes (Pt loading: 0.4 mg cm^{-2}, GDL: SGL 34BC, surface area: 5 cm^2), together with Nafion 212 (Ion Power Inc) were hot-pressed at 125 ^oC for 2 minutes at 1800 psi (124.1 bar). The MEA active area was 5 cm^2. While it is understood that current Nafion based membranes are not suitable for prolonged usage at intermediate temperature, the types of materials developed within our group for intermediate temperature are doped variants of Nafion. Therefore, it was felt that testing with commercial Nafion at intermediate temperature would be suitable for a simulation study. The MEA was then tested using a Scribner 850e Fuel Cell Test Station. Pure hydrogen (>99.999 %) and air were used for the anode and cathode gases respectively. All tests were conducted at 120 ^oC and a back pressure of 1.8 bar. The cell was heated and kept in an insulated chamber such that isothermal conditions could reasonably be assumed. The relative humidity was varied between 50 % and 100 % for both the anode and the cathode. The flow rates were kept constant at 200 mL min^{-1} and 500 mL min^{-1} for the anode and

cathode respectively. All flow rates quoted are related to standard temperatures and pressures. The cell consisted of a square shaped single serpentine flow field design, with co-current flow for the anode and cathode gases.

3.3.2 Model Verification

The MEA constructed was tested at an intermediate temperature of 120 ^{o}C at both 50% and 100% relative humidities in order to assess performance.

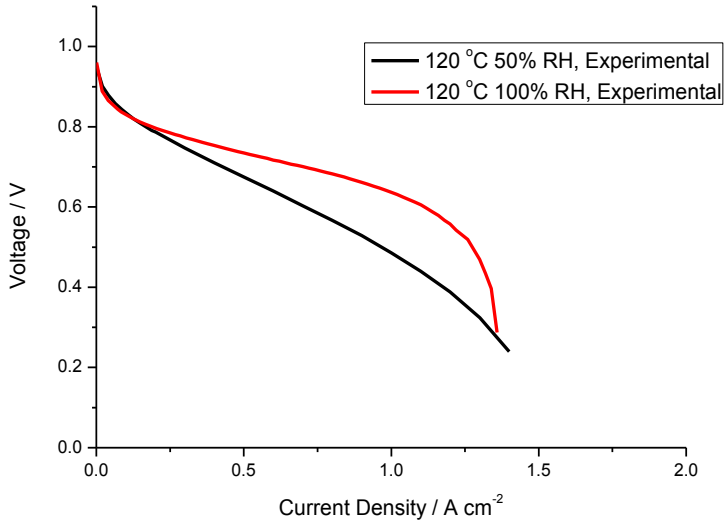

Figure 3.5: Polarisation Curves for the MEA at 120 ^{o}C 100% RH and 50% RH

Figure 3.5 shows the performance of the cell when operated at 120 ^{o}C, 50% and 100% RH. The cell performance at 50% RH is lower than expected when using commercial materials (a current density of 0.7 A cm^{-2} was achieved at 0.6 V) however this can be explained by the loss in conductivity of the membrane due to dehydration at this low RH value. When comparing the ohmic resistance measured by current interruption (at 0.5 A cm^{-2}) between the two operating conditions, it can be seen that the resistance at

100% RH (61 mΩ cm^2) is close to 4 times lower than that at 50% RH (232 mΩ cm^2). Assuming that the electrode electrical resistance should not change with humidity, the only factor of variation would be the membrane resistance. From empirical measurements conducted in our group using a four point probe conductivity analyser [192], at full hydration and 120 ^oC, the Nafion 212 membrane has a conductivity of 13 S m^{-1}. Therefore, based on the resistance measurement, the membrane conductivity can be taken as 2.7 S m^{-1} at 50% RH which is in good agreement with other empirical measurements taken (measured at 3.0 S m^{-1}).

In order to ensure that the water generated by the fuel cell reactions is taken up in the fuel stream and not condenses out at 100 % RH, a mass balance calculation was performed based on the polarisation curves in Figure 3.5. It was assumed that water flux through the membrane is negligible, therefore water coming into the MEA is the water from the inlet fuel streams. It was calculated that at the maximum current density of 1.36 A cm^{-2}, the rate of water generated would be 4.2 mol min^{-1}. The cell temperature increase across the MEA would need to be lower than 2 ^oC for this water to condense rather than being taken up in the cathode air stream. Thus, for the modelling study, it can be assumed that the water produced in the fuel cell reaction would completely exist in the vapour phase.

The model was then used to simulate the cell conditions in a cross-section of the MEA along the gas flow. A majority of the parameters used in the base case validation model were obtained from the experimental set up. In order to assess the accuracy of the model, both the 50% and 100% RH cases were modelled as well as changing the fuel inlet flow rate. The simulated results were then compared with the experimental data. It is important to note that for validation purposes, the cell was considered to be

isothermal since the “real” cell was temperature controlled and so the temperature difference across the cell could be considered negligible. The parameters for the two scenarios are shown in Table 3.2. Figure 3.6 shows the predicted cell performance and the real cell performance.

Table 3.2: Parameters used for base case validation

Parameter	**Value**	
Scenario	**120 ºC, 50% RH**	**120 ºC, 100% RH**
Exchange current density, i_0	0.99 A cm^{-2}	0.99 A cm^{-2}
Tafel Slope, β_c	79 mV/dec	79 mV/dec
Membrane Conductivity, σ_m	2.7 S m^{-1}	13 S m^{-1}
Average GDL porosity, ε_{GDL}	47.5 %[193]	47.5 %[193]
Average GDL permeability, κ_{GDL}	8.9 x 10^{-12} m^2 [193]	8.9 x 10^{-12} m^2 [193]
Anode Inlet Hydrogen Mass Fraction	0.25	0.1
Anode Inlet Water Mass Fraction	0.75	0.9
Cathode Inlet Oxygen Mass Fraction	0.186	0.143
Cathode Inlet Nitrogen Mass Fraction	0.639	0.473
Cathode Inlet Water Mass Fraction	0.175	0.384
Anode Flow Rate, U_a	5.5 mL min^{-1}	5.5 mL min^{-1}
Cathode Flow Rate, U_c	12.5 mL min^{-1}	16 mL min^{-1}

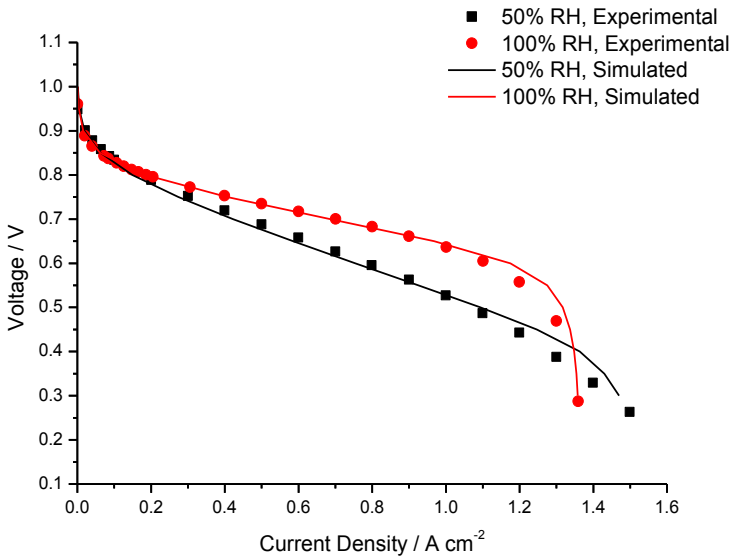

Figure 3.6: Predicted cell performance from (a) 120 ^{o}C 50% RH and (b) 120 ^{o}C 50% RH compared with the experimental cell data

The results predicted by the model correlate well with the experimental data. All aspects of the polarisation curve are well within an acceptable level of error (maximum error of 6 % in the mass transport region). The only discrepancy between the model and the experimental data was the cathode flow rates used. The experimental cathode flow rate was calculated such that for a 5 cm^2 cell, the cathode flow rate stoichiometry is equal to 5 at 1.5 A cm^{-2}. In the case of the model, the cathode flow rate was adjusted to a stoichiometry that is equal to 3 and 3.5 for 50% RH and 100% RH respectively at 1.5 A cm^{-2} for a single channel of area 0.22 cm^2. This difference in required stoichiometry is due to the catalyst layer being modelled as a 1D boundary rather than as a 2D domain which would lead to an under-prediction of the mass transport limitations of the cell. It was not possible to model the catalyst layer as a 2D domain due to the number of unknown parameters such as real catalyst surface area. Whilst

adding extra parameters would increase the agreement between experimental and simulated data, the results obtained from the model would not be meaningful.

3.4 Intermediate Temperature Membrane Materials

One of the key areas for IT-PEFC research is improvement of membrane conductivity at high cell temperatures, where membrane degradation reduces performance. A parametric study was performed in order to determine the effects of membrane conductivity on cell performance. This was done by varying the membrane conductivity at each separate voltage of the cell in order to give the polarisation plots seen in Figure 3.7.

The model was used to study this parameter independently of temperature and pressure effects. The parameters used in this study are summarised in Table 3.3. A range of σ_m= 1 S m^{-1} – 25 S m^{-1} was chosen because commercial Nafion has a conductivity of approximately 10 S m^{-1} [194] and there is a need to see if there was much use in increasing the conductivity beyond this point. Figure 3.7 shows the results from this study.

Table 3.3: Parameters used for studying the membrane; parameters not listed here can be found in Table 3.1

Parameter	Value
Exchange current density, i_0	0.99 A cm^{-2}
Tafel Slope, β_c	60 mV/dec
Membrane Conductivity, σ_m	Varied between 1 and 25 S m^{-1}
Average GDL porosity, ε_{GDL}	47.5 % [193]
Average GDL permeability, κ_{GDL}	8.9 x 10^{-12} m^2 [193]
Anode RH / %	50
Cathode RH / %	50

Parameter	Value
Anode Inlet Hydrogen Mass Fraction	0.25
Anode Inlet Water Mass Fraction	0.75
Cathode Inlet Oxygen Mass Fraction	0.186
Cathode Inlet Nitrogen Mass Fraction	0.639
Cathode Inlet Water Mass Fraction	0.175
Anode Flow Rate, U_a	5.5 mL min^{-1}
Cathode Flow Rate, U_c	13.5 mL min^{-1}

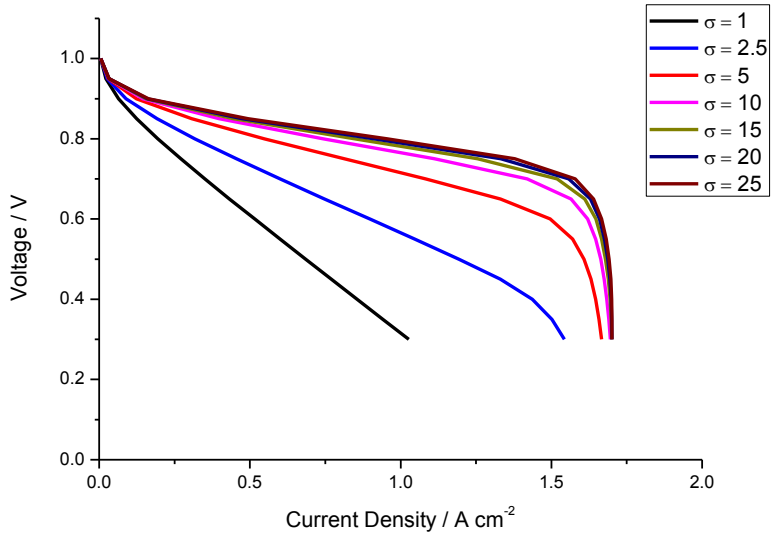

Figure 3.7: Predicted cell performance with respect to changing the membrane conductivity (S m^{-1})

Figure 3.7 shows that, as expected, the cell performance increases with increasing membrane conductivity. This is due to the decreasing resistance to transport of protons across the electrolyte membrane as conductivity increases, thus increasing the cell potential. For each unit of electrolyte conductivity increase, the corresponding performance increase becomes less apparent (see Figure 3.8). This indicates that beyond a certain value of membrane conductivity, other factors than proton conductivity limit the cell performance, such as the mass transport resistance. This can

be seen by the lack of change in current density at low cell potentials (0.5 and 0.3 V). Whilst operating at these cell potentials is not practical, they have been shown for completeness. This appears to occur at conductivities of approximately 10 S m^{-1}. This is particularly important to the field of membrane research, as current membranes cannot achieve such conductivity values at the temperatures found within IT-PEFCs and thus places an upper limit on further optimising of higher membrane conductivities.

(a)

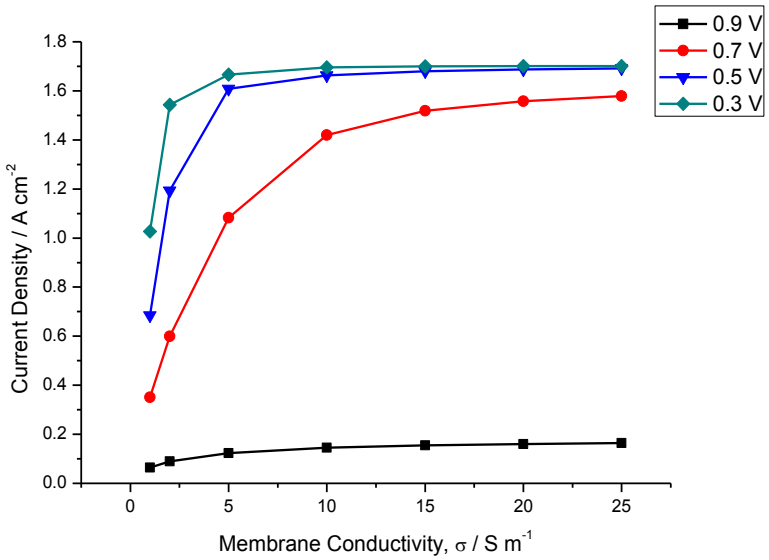

(b)

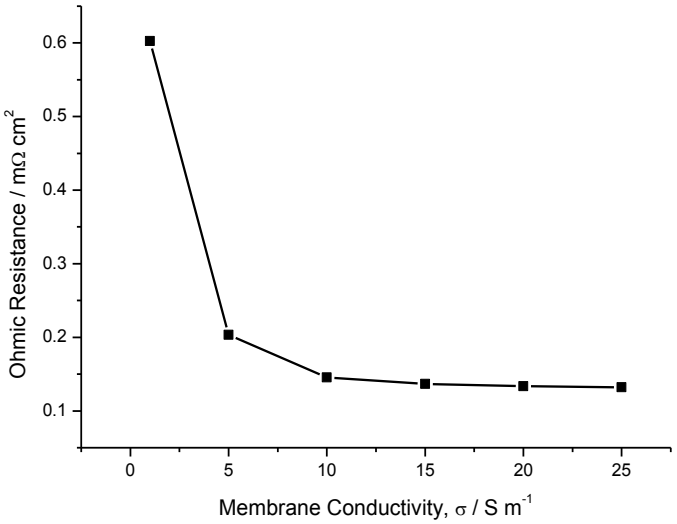

Figure 3.8: (a) Effect of membrane conductivity on the cell current density and (b) the ohmic resistance

3.5 GDL Properties

3.5.1 Influence of GDL Porosity on Electrical Conductivity and Mass Transport

The influence of porosity on the electrical conductivity of the cell can be described using a general equation (Equation 3.10).

$$\sigma_{GDL} = f(\varepsilon, compression, \sigma_c) \qquad \text{Equation 3.10}$$

Where σ_{GDL} is the electrical conductivity GDL (S m^{-1}), ε is the porosity and σ_c is the electrical conductivity of the base material. For the purpose of this study, it can be assumed that the compressive force acting on the GDL will not change with porosity and hence is negligible. Also, the base material, which in this case is assumed to be graphitic carbon, will not change its properties and therefore the conductivity of this material will not change. As the base material has a set electrical conductivity (at given operating parameters), it can be assumed that increasing the porosity of the material will cause a reduction of the GDL electrical conductivity (Equation 3.11). Following this inversely proportional relationship, a new coefficient, K, must be introduced into the equation which would describe intrinsic material properties such as its manufacturing processes, base material type etc.

$$\sigma_{GDL} \propto \frac{1}{\varepsilon} \qquad \text{Equation 3.11}$$

Similar theories have been developed in the literature when studying porous materials and their electrical conductivities. Equation 3.12 has been empirically developed using ex-situ testing techniques to describe the relationship of a materials property and its electrical conductivity [195]. This is done by taking into account the conductivity of the

compressed material and an intrinsic material coefficient. For this study, K of the 35BC GDL was found to be 2.2 x 10^{-2}.

$$\sigma_{GDL} = K\frac{1-\varepsilon}{3[(1-0.121)(1-\varepsilon)^{0.5}]}\sigma_c \qquad \text{Equation 3.12}$$

Using the model, the porosity of the cathodic GDL was then parametrically studied between 5 % and 95 % in order to assess its influence. The parameters used in this study are summarised in Table 3.4. At each porosity step, a polarisation curve was generated by the model as can be seen in Figure 3.9.

Table 3.4: Parameters used for studying the porosity of the GDL

Parameter	**Value**
Exchange current density, i_0	0.99 A cm^{-2}
Tafel Slope, β_c	60 mV/dec
Membrane Conductivity, σ_m	10 S m^{-1}
Average GDL porosity, ε_{GDL}	Varied using Equation 3.12
Average GDL permeability, κ_{GDL}	8.9 x 10^{-12} m^2 [193]
Anode RH / %	1
Cathode RH / %	1
GDL Thickness, W_{C_GDL}	275 µm
MPL Thickness, W_{C_MPL}	40 µm
Anode Inlet Hydrogen Mass Fraction	0.75
Anode Inlet Water Mass Fraction	0.25
Cathode Inlet Oxygen Mass Fraction	0.223
Cathode Inlet Nitrogen Mass Fraction	0.749
Cathode Inlet Water Mass Fraction	0.023
Anode Flow Rate, U_a	500 mL min^{-1}
Cathode Flow Rate, U_c	500 mL min^{-1}

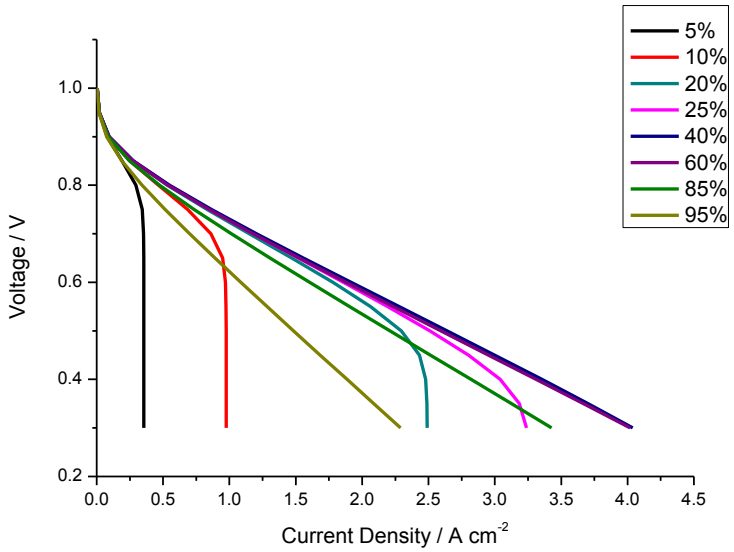

Figure 3.9: Polarisation curves changing as a function of porosity at 120 ^{o}C

As can be seen, the activation loss region of the polarisation curve (0.9 V to 0.8 V) does not appear to change much as the porosity of the GDL material is changed. This is as expected as the GDL plays a negligible role at these cell potentials. The ohmic loss region of the polarisation curve (0.8 V to 0.7-0.6 V) is where the porosity of the GDL makes a large difference. At lower porosities (5 % to 15 %), the conductivity of the material is higher as there is a greater amount of surface area for the current generated to flow through the GDL. However, mass transport limitations also occur at a higher voltage. Further confirmation of this can be seen by inspecting the mole fraction of oxygen within the GDL (Figure 3.10).

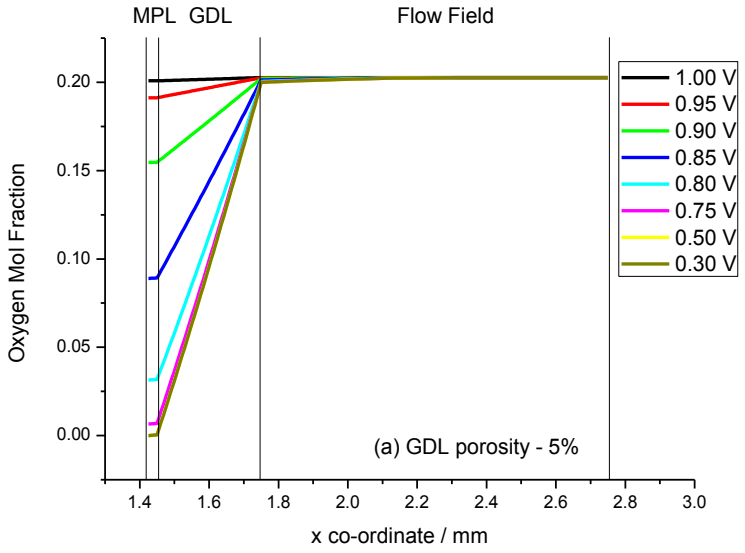
MPL
GDL
Flow Field
Oxygen Mol Fraction
0.20
0.15
0.10
0.05
0.00
1.4
1.6
1.8
2.0
2.2
2.4
2.6
2.8
3.0
x co-ordinate / mm
1.00 V
0.95 V
0.90 V
0.85 V
0.80 V
0.75 V
0.50 V
0.30 V
(a) GDL porosity - 5%

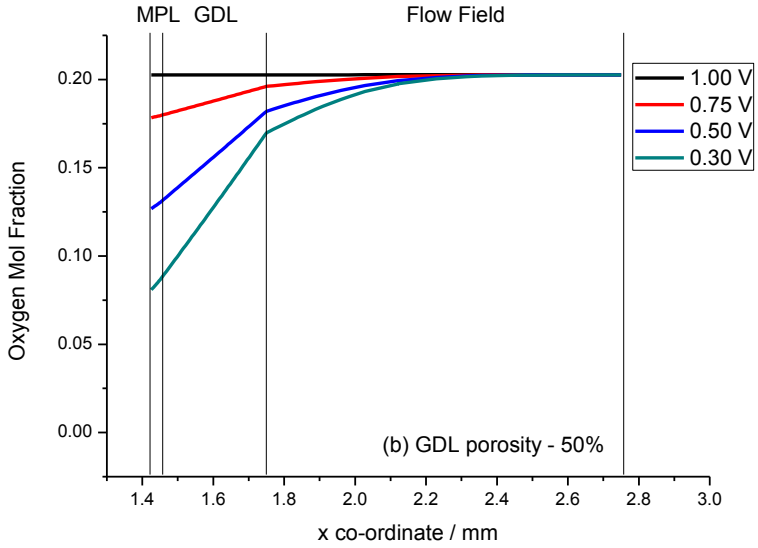
MPL
GDL
Flow Field
Oxygen Mol Fraction
0.20
0.15
0.10
0.05
0.00
1.4
1.6
1.8
2.0
2.2
2.4
2.6
2.8
3.0
x co-ordinate / mm
1.00 V
0.75 V
0.50 V
0.30 V
(b) GDL porosity - 50%

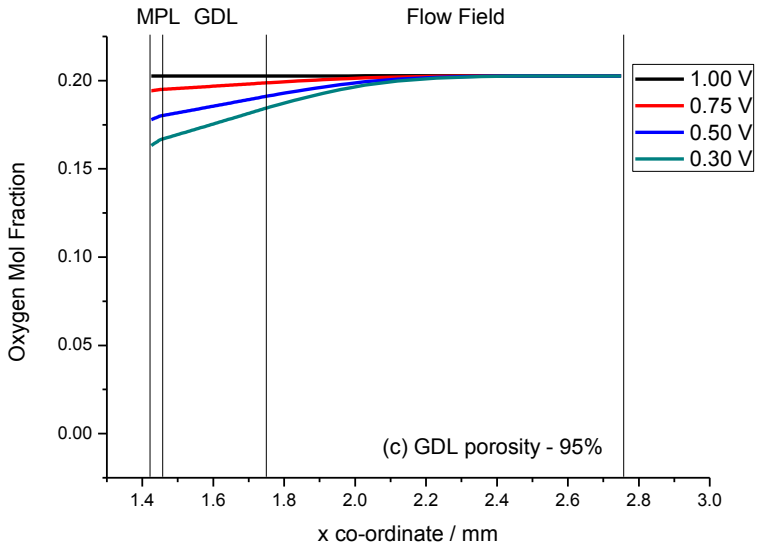

Figure 3.10: Oxygen mass fraction profiles for the cathode at y = 11mm; (a) GDL = 5% porosity, (b) GDL = 50% porosity and (c) GDL porosity = 95%

At higher porosities (20 % to 65 %), the conductivity of the material decreases however the added amount of reactants that is able to reach the catalyst layer is much higher and therefore the cell performance increases with mass transport losses occurring at lower voltages. At the highest porosities (70 % to 95 %), the lack of current pathways causes the electrical conductivity of the GDL to drop to such a level that the ohmic losses of the cell now dominate the polarisation curve. This resulting higher resistance is shown through the lower gradient of the ohmic resistance part of the polarisation curve (which is described by V = IR) (Figure 3.9). However, the mass transport limitations are now minimal as there is a much higher capability for the reactants to reach the catalyst layer. In all the cases shown in Figure 3.10, it appears that a concentration gradient is present within the MPL which can be explained by comparing the MPL porosity to the GDL porosity. When the GDL porosity is small (5 %) the MPL porosity is much larger and therefore the concentration gradient of oxygen within the MPL is small. When the GDL porosity is large (95 %), the MPL porosity is much lower

and therefore a more significant concentration gradient develops. These effects can be demonstrated more clearly by plotting the current density as a function of the porosity for each cell voltage (Figure 3.11).

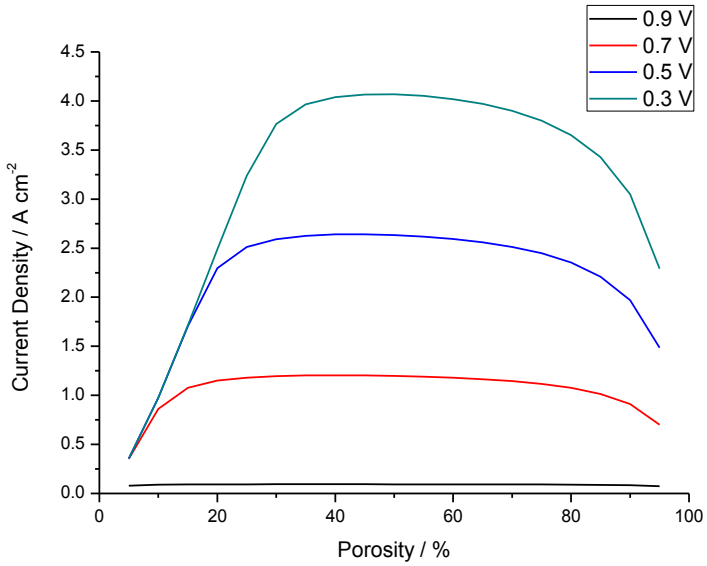

Figure 3.11: Current density as a function of GDL porosity for 0.9 V, 0.7 V, 0.5 V, and 0.3 V

From both Figure 3.9 and Figure 3.11, it can be seen that as the porosity of the GDL increases, the cell ohmic resistance increases. Furthermore, as the porosity of the GDL increases, the mass transport resistance decreases as more pathways are open to reactants. This culminates in a theoretical minimum resistance where both the ohmic and mass transport resistances are similar, thus allowing for a maximum current density to be achieved.

In order to ascertain which GDL material porosity is ideal for an intended application, it was decided to plot the porosity that generated the highest current density at each cell potential. A range of porosities that generated a current density within 1 % of the

maximum current density was then compared to elucidate the importance of porosity (Figure 3.12).

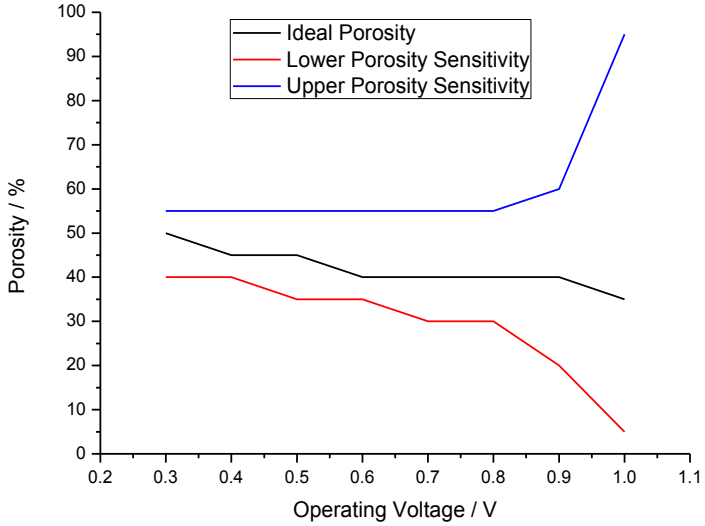

Figure 3.12: Ideal porosity of the GDL to be used at a given cell operating potential. Upper and lower porosity sensitivity indicates a current density within 1 % of the value at ideal porosity

Figure 3.12 illustrates the ideal porosity of the GDL material for a desired operating cell potential. The standard cell operating conditions of 0.7 V to 0.6 V is where the porosity of the GDL has the biggest impact. For a cell that is to spend a majority of operating time within this voltage window, a GDL of a porosity between 40-45 % would be ideal.

3.5.2 The Influence of GDL Permeability on MEA performance

The model was used to study the effect of the GDL permeability on the cell performance. The cathode GDL permeability was parametrically studied in order to see the sensitivity of the cell performance to this material property. The permeability was

changed independently of the porosity as it is possible to find materials which have a high porosity but a low permeability and vice versa for example materials with inaccessible air pockets [196]. Therefore it is not trivial to define the relationship between porosity and permeability. The permeability was varied between 5 x 10^{-6} and 5 x 10^{-12} m^2. The parameters used in this study are outlined in Table 3.5.

Table 3.5: Parameters used for studying the permeability of the GDL

Parameter	Value
Exchange current density, i_0	0.99 A cm^{-2}
Tafel Slope, β_c	60 mV/dec
Membrane Conductivity, σ_m	10 S m^{-1}
Average GDL porosity, ε_{GDL}	47.1 % [193]
Average GDL permeability, κ_{GDL}	Varied between 5 x 10^{-6} and 5 x 10^{-12} m^2
Anode RH / %	1
Cathode RH / %	1
Anode Inlet Hydrogen Mass Fraction	0.743
Anode Inlet Water Mass Fraction	0.257
Cathode Inlet Oxygen Mass Fraction	0.223
Cathode Inlet Nitrogen Mass Fraction	0.749
Cathode Inlet Water Mass Fraction	0.023
Anode Flow Rate, U_a	500 mL min^{-1}
Cathode Flow Rate, U_c	500 mL min^{-1}

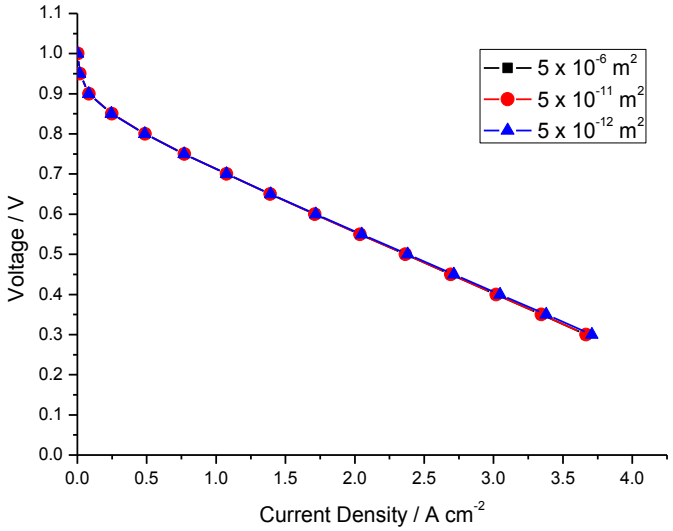

Figure 3.13: Effect of the GDL permeability on cell performance at 120 ^{o}C.

From Figure 3.13, the permeability of the GDL does not appear to have an effect on the performance of the PEFC. There are two reasons why this would be the case. Firstly, the permeability has a large impact at low temperatures, when liquid water is formed in the CL. This liquid water means that the velocity of the gas and thus convection effects have a larger impact on the removal of the water and thus a larger permeability is required [11,163]. However, at higher temperatures, the water exists in the vapour phase and thus is removed from the GDL through diffusion effects rather than convection. As the flow of the gas is modelled through the use of the Brinkman-Stokes equation, the permeability directly impacts the flow of the gas, however it has little impact on the diffusion of the reactants. This is in line with theories shown in the literature where it has been shown that gas diffusion is the dominant transport mechanism by more than four orders of magnitude than by convection forces [197,198]. Furthermore, it is found in conventional PEFCs that reducing the

permeability is generally effective at preventing membrane dehydration. However, as the water should exist in the vapour phase, changing the permeability should not affect whether water is retained within the MEA and therefore whether the membrane is dehydrated.

3.6 Novel MEA Design: Changing the GDL Material

The potential of novel GDL materials was studied by using the model. The main challenge at low temperature is with the water and thermal management of the cell. A conventional method for dealing with water management involves the optimisation of the flow field such that water droplet removal is improved[12]. The flow field is necessary at low temperatures as high pressure differences can be produced which help with the removal of the water droplets. This also has to be balanced with ensuring that gas distribution is as uniform as possible across the cell surface area. However, the drawback is the increased cost of manufacture of flow field plates as the design is made complex [3], as well as the increased balance of plant parasitic energy demand which decreases the system efficiency. Another method for dealing with is to treat the carbon based GDL to increase its hydrophobicity, commonly using teflonation of the carbon material. Hydrophobic treatment is important for a carbon based GDL as it reduces the tendency for water to stick to the walls of the GDL. This allows for easier removal of the water. This comes at the cost of reducing the GDL porosity and electrical conductivity, while also increasing the tortuosity of the GDL [10].

When considering IT-PEFCs, it is important to note that the operating temperature of the cell is such that water in the cell should mainly exist in the vapour phase. As such, some of these conventional methods for dealing with water are rendered unnecessary.

Therefore, it should be possible to change the GDL material from a carbon based material to a metal based material. Such materials would include both metallic meshes and foams. Metallic meshes would have the benefit of a very ordered structure which would ensure uniform gas diffusion through-plane. However, these meshes suffer from poor in-plane diffusion. The only material proposed would be metallic foams which would also have excellent in-plane conductivity. In particular, the use of metallic foams for IT-PEFC GDLs is very interesting as the lack of liquid water will mean that hydrophobic treatment is not necessary. Furthermore, the high conductivity of the material ensures that a thicker GDL can be used, potentially allowing for the elimination of a flow field. The flow of gas through the GDL would enable increased removal of water, however, it is limited by the thickness of the GDL and therefore the through-plane electrical conductivity of the GDL. As the metallic foam/mesh would have a higher electrical conductivity, the GDL can be made thicker so that the gas could flow directly through the GDL, therefore improving the water removal as long as the cell temperature is greater than 100 ^{o}C. The purpose of thickening the GDL would be to compensate for the removal of the flow field machined structure. This is what we call the “integrated flow field/GDL” design (Figure 3.14).

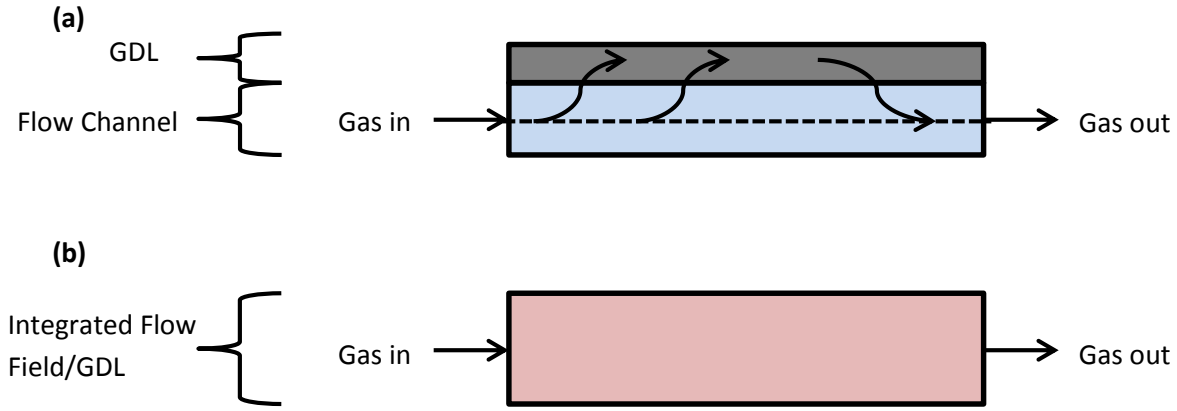

Figure 3.14: Cell schematic for; (a) a typical carbon based GDL and (b) an integrated flow field/GDL

An initial comparison of the conventional cell design with a flow field and the novel cell design without the flow channel was conducted. For the purpose of this study, the cell performance, the heat removal from the cell and the pressure drop across the cell were compared.

3.6.1 Cell Performance Using a Metallic Foam

The cell performance for both the conventional GDL/FFP and the integrated metallic GDL/flow field was simulated and predicted using the model. Parameters reported in Table 3.6 were used for the metallic foam which were obtained from literature and based on an INCOFOAM Ni Foam [190,199].

Table 3.6: Parameters used for the metallic foam

Parameter	**Value**
Exchange current density, i_0	0.99 A cm^{-2}
Tafel Slope, β_c	60 mV/dec
Membrane Conductivity, σ_m	10 S m^{-1}

Parameter	Value
Metallic Foam Thickness	1.35 mm
Metallic Foam Porosity, ε_{foam}	80 %[199]
Metallic Foam in-plane Permeability, κ_{foam}	1.13 x 10^{-8} m^2[190]
Metallic Foam Electrical Conductivity, σ_{foam}	1.3 x 10^6 S m^{-1}[190]
Metallic Foam Thermal Conductivity, K_{foam}	13 W m^{-1} K^{-1}[190]
Anode RH / %	1
Cathode RH / %	1
Anode Inlet Hydrogen Mass Fraction	0.743
Anode Inlet Water Mass Fraction	0.257
Cathode Inlet Oxygen Mass Fraction	0.228
Cathode Inlet Nitrogen Mass Fraction	0.749
Cathode Inlet Water Mass Fraction	0.023
Anode Flow Rate, U_a	500 mL min^{-1}
Cathode Pressure in, P_{inlet}	1.25 x 10^{-3} bar

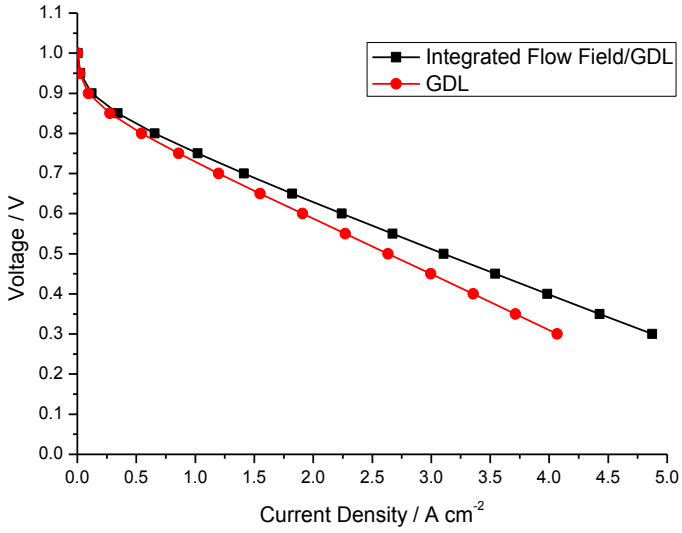

Figure 3.15: Cell performance when using a metallic foam and a conventional GDL at 120 ºC.

Figure 3.15 shows the comparison in the cell polarisation curves for the cells with the conventional GDL/FFP and the integrated metallic foam cell. Even though the metallic foam is much thicker (2 mm compared with 350 microns for the conventional GDL) and has a much higher porosity (80 % compared with 52 % for the conventional GDL), the conductivity of the metallic foam is much higher than the conventional GDL. This results in a lower cell ohmic resistance which in turn leads to a higher cell voltage. This is encouraging for the use of metallic foams within the IT-PEFC, especially as using a thicker GDL will allow for the removal of the flow field while improving contact with the electrode and providing good mechanical strength for the MEA.

3.6.2 Optimisation of the Porosity of the Metallic Foam

In order to optimise the porosity of the metallic foam with respect to the electronic conductivity, the same set of simulations were performed as described in section 3.5.1. The porosity of the foam was systematically increased from 5 % to 95 % in order to assess the cell performance. The parameters used in this study are identical to those listed in Table 3.6 with the exception of the foam porosity that was the parameter in this analysis, as shown in section 3.5.1.

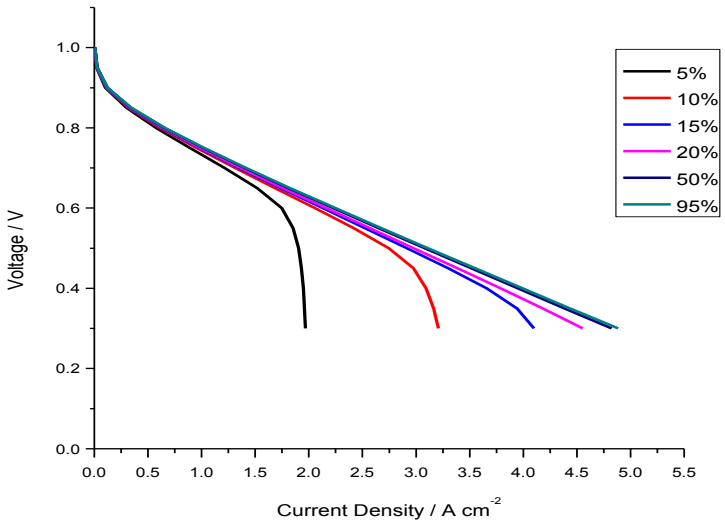

Figure 3.16: Effect of porosity on cell performance for the metallic meshes at 120 ^{o}C.

Figure 3.16 shows how the porosity of the metallic foam affects the cell performance. Only at low porosities (<20 %) mass transport limitations are observed within the MEAs. In fact, Figure 3.17 shows that the performance of the MEA continues to increase as the porosity increases even though the overall electrical conductivity is decreasing. This can be attributed to the very high electrical conductivity of the metallic foam which results in a conductivity that is still higher than that of a conventional GDL material even at the highest porosities. However, it is important to note that this may not be the case in a “real MEA” because as the porosity increases, the area of the GDL that is in contact with the catalyst layer decreases, resulting in a higher interfacial contact resistance. This is not accounted for in this study as the catalyst layers are modelled as 1D boundaries rather than 2D domains. As such, while the simulation suggests that a high porosity value is better for cell performance, it may be beneficial to use a material with a slightly lower porosity. It is clear from this study, however, that

a metallic foam with a porosity greater than 20 % will be sufficient to have excellent cell performance with minimal mass transport.

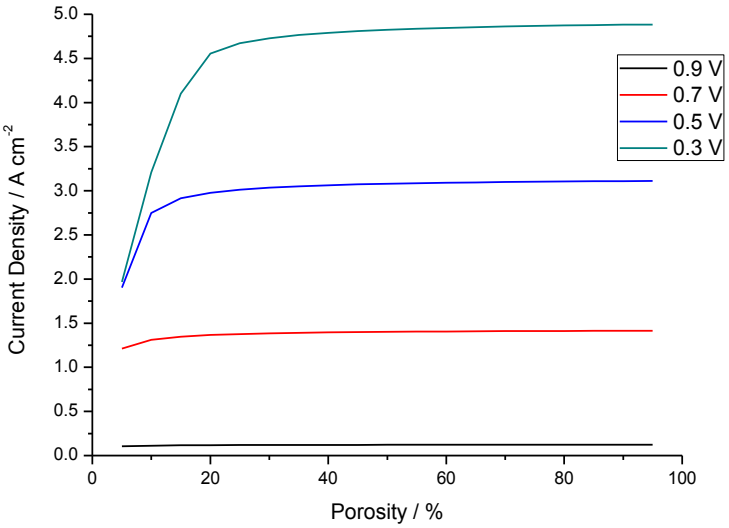

Figure 3.17: Current density as a function of porosity for 0.9 V, 0.7 V, 0.5 V, and 0.3 V at 120 ^{o}C.

3.6.3 Influence of permeability on the novel cells' performance

The permeability of the metallic foam is quite important for the cell performance as the flow of gasses will be directly through the metallic foam rather than through a free flow channel. As such it was decided to investigate the impact of the permeability of the metallic foam will have on the performance of this cell. The metallic foam would have an isotropic structure so it can be assumed that the permeability is also isotropic. The parameters used in this analysis are identical to those shown in Table 3.6 except for the metallic foam permeability which was varied between 7 x 10^{-9} and 7 x 10^{-16} m^2.

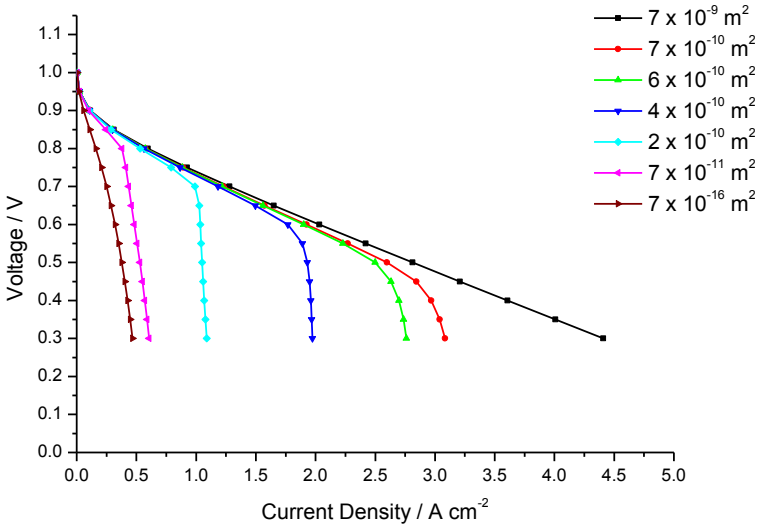

Figure 3.18: Effect of metallic foam permeability on cell performance

Figure 3.18 shows how the cell performance changes with respect to the foam permeability. As can be seen, the permeability of the metallic foam plays a much bigger role in the performance of the cell as compared with the conventional GDL. This is because the cathode gases are now flowing directly through the GDL and thus the higher the permeability, the greater the flow through the foam, the higher the performance of the cell. This is true up to a permeability of 10^{-9} m^2 after which the permeability is no longer the limiting factor in the cell performance. It appears that the permeability has the biggest effect on cell performance between 10^{-10} m^2 and 10^{-11} m^2 where the gas flow is reduced to such a level that the cathode air is severely limited in travelling through the cathode (Figure 3.19). As such, the metallic foam has a suitable permeability (1.13×10^{-8} m^2 [190]) that is high enough to not limit the MEA performance.

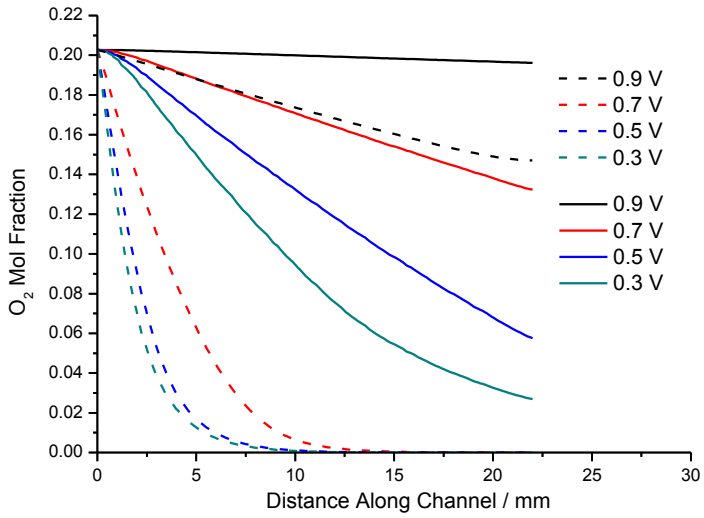

Figure 3.19: Oxygen Mole Fraction along the cell channel when the GDL permeability is 10^{-10} (solid lines) and 10^{-11} m^2 (dashed lines), respectively.

3.7 Heat Transfer and Flow Properties: A 3D comparison

3.7.1 Flow Distribution

The conventional GDL/FFP is difficult to compare with the integrated metallic foam design in 2D because of the complex nature of the flow pattern in the conventional FFP. It is common to use a complex meandering flow field design such as the single serpentine channel (Figure 3.20) as this is necessary to generate the pressure to expel liquid water from the cell. This means that a 3D model is required when considering heat transfer within the cell, as the fluid flow and the heat transfer need to be decoupled. As such, a 3D model was developed to aid in the comparison of the importance of the GDL thermal conductivity and to assess the gas input pressure that would be required. This model depicts the cathode side of the MEA including the electrode, GDL and flow field. Anode conditions are assumed to be constant. A

standard cooling plate design consisting of straight parallel channels, located on the backside of the flow field plate, was used in order to provide a heat sink for the heat generated from the cell reactions. The parameters used to study the flow velocity, flow pressure and the thermal distribution within the cell are outlined in Table 3.7.

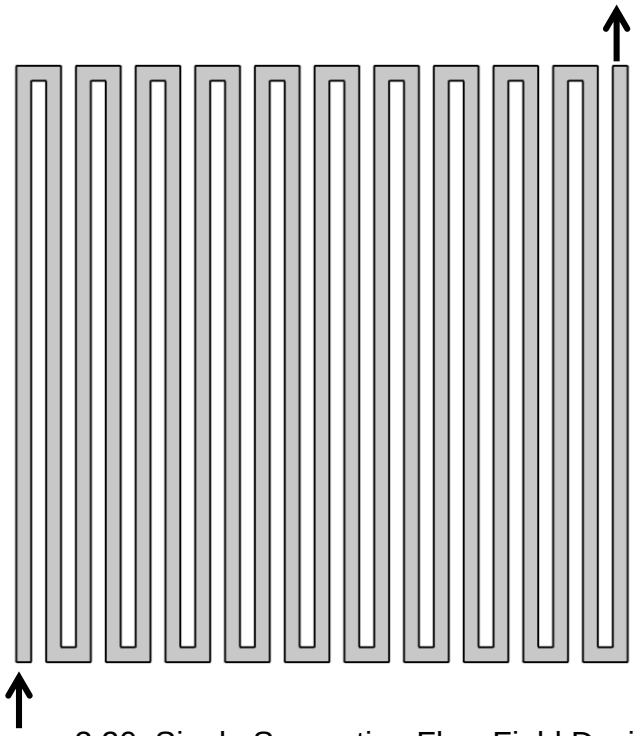

Figure 3.20: Single Serpentine Flow Field Design

Table 3.7: Parameters used to compare a conventional flow field/GDL and an integrated flow field

Parameter	**Value**
Average GDL Porosity, ε_{GDL}	50 %
Average GDL permeability, κ_{GDL}	8.9 x 10^{-12} m^2 [193]
Metallic Foam Porosity, ε_{foam}	80 % [199].
Metallic Foam Permeability, κ_{foam}	1.13 x 10^{-8} m^2 [190]
Cell Operating Potential, V_c	0.6 V
Current Density at Operating Potential	1 A cm^{-2}
Electrical Power, P_{elec}	9.6 W
Cell Efficiency	52 %

Parameter	Value
Heat Power, P_{heat}	8.6 W
Cathode Inlet Flow Rate, U_c	300 mL min^{-1}
Cooling Channel Inlet Pressure	1 x 10^{-5} bar
Cooling Channel Inlet Temperature	293 K

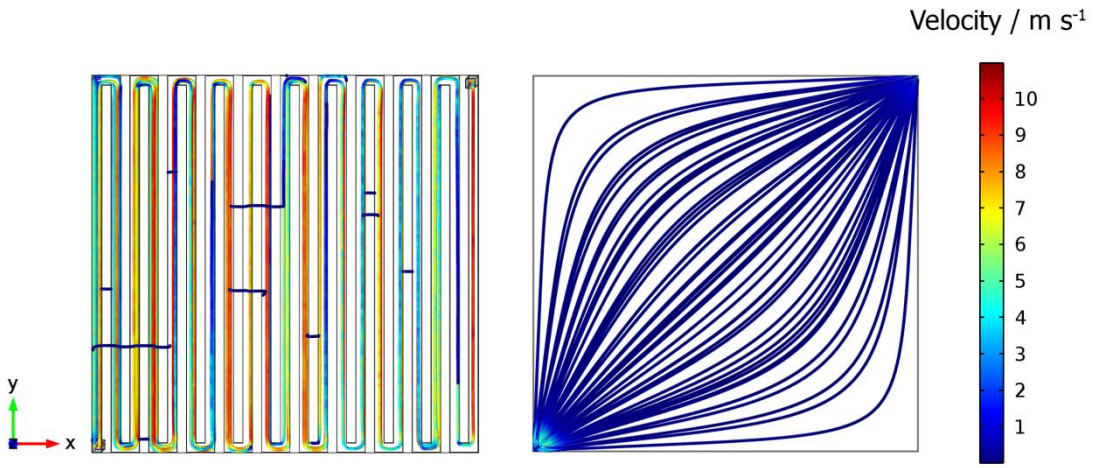

Figure 3.21: Velocity profiles for the cathodes in a conventional GDL/FFP (left) and an integrated GDL/FFP (right)

Figure 3.21 shows the flow through both a conventional GDL/FFP cell and an integrated GDL/flow field cell. As is expected, the flow is much faster in the conventional flow field but more variable than in the foam based GDL as the metallic foam has a much increased effective cross section. In the conventional flow field design, the streamlines show slow moving gas “jumping” from one flow field channel to the next via the GDL, thus generating the convective forces required to expel the water that is generated from the fuel cell reactions. The flow of gas within the integrated metallic foam cathode is more uniform and generally slower however as the high

pressure drops and fast moving gas are not required in the IT-PEFC, this is not a disadvantage. Furthermore, the diagonal flow cell design as shown in Figure 3.21 is not yet optimised and is only used for comparative purposes. As such, it is clear that the current design with a single input and output in the corners of the active area would most likely not evenly distribute oxygen to the catalyst layer. However, this could be solved through the optimisation of the gas manifold which would result in more uniformity of gas flow within the cell.

3.7.2 Pressure Distribution

The pressure drop across each flow field design is important to consider from a systems point of view as the required gas supply pressure will depend on the design chosen. It would be of advantage to have a smaller balance of plant as this will help to increase the overall system efficiency. In this case, a flow system whereby the pressure drop is smaller is advantageous as the blower/air pumps required can also be much smaller thus decreasing gas supply energy demand. In the case of a conventional PEFC, high gas pressures are required in order to force the fuel/air gas through the complex flow field designs. Furthermore, the required blower power can increase drastically when the temperature gradient is low as higher stoichiometries of cathode gas are required to provide the necessary cooling for the cell. In the case of the IT-PEFC, these problems can be reduced as the requirement for the complex flow field design is eliminated.

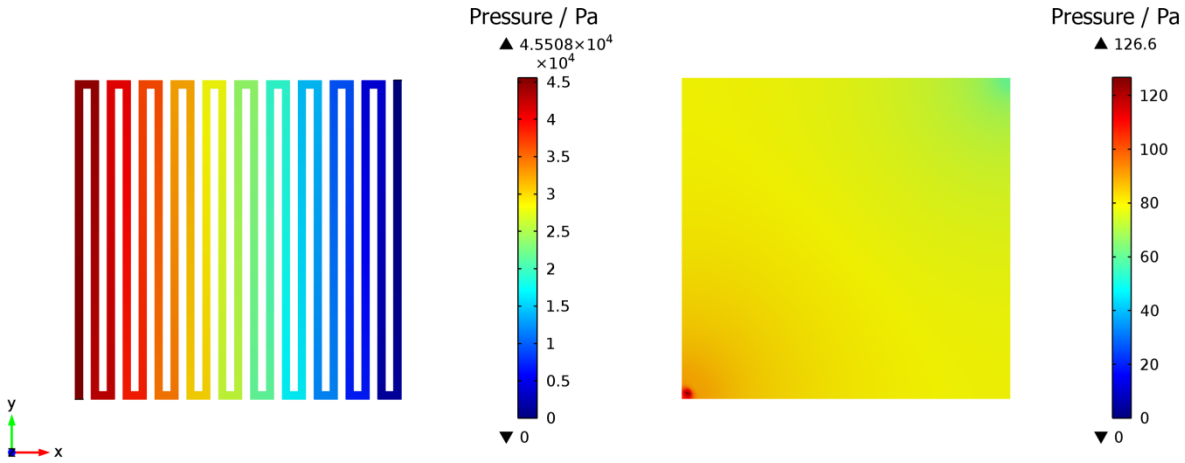

Figure 3.22: Pressure profiles for the single serpentine flow field (left) and an integrated GDL/flow field (right).

Figure 3.22 shows the pressure profiles for the conventional single serpentine flow field and the integrated metallic foam cathodes. The pressure drop across the flow field in the conventional flow field/GDL cell is worked out to be 4.5 x 10^4 Pa (0.45 bar) whereas the pressure drop in the integrated metallic foam cathode is worked out to be 125 Pa (1.25 x 10^{-3} bar). This represents a 360 fold decrease in the required pressure and therefore translates to a considerable decrease in the air supply blower power, whilst providing the same amount of oxygen.

3.7.3 Heat Transfer Properties

The thermal conductivity of the conventional GDL and the metallic foam were used to calculate the thermal removal efficiency of each GDL. One of the challenges of stack design is in how to manage the thermal aspect of the stack. As such, using materials with a high thermal conductivity will allow for the MEA to act as a more efficient heat exchanger thus allowing for more facile removal of heat from the stack.

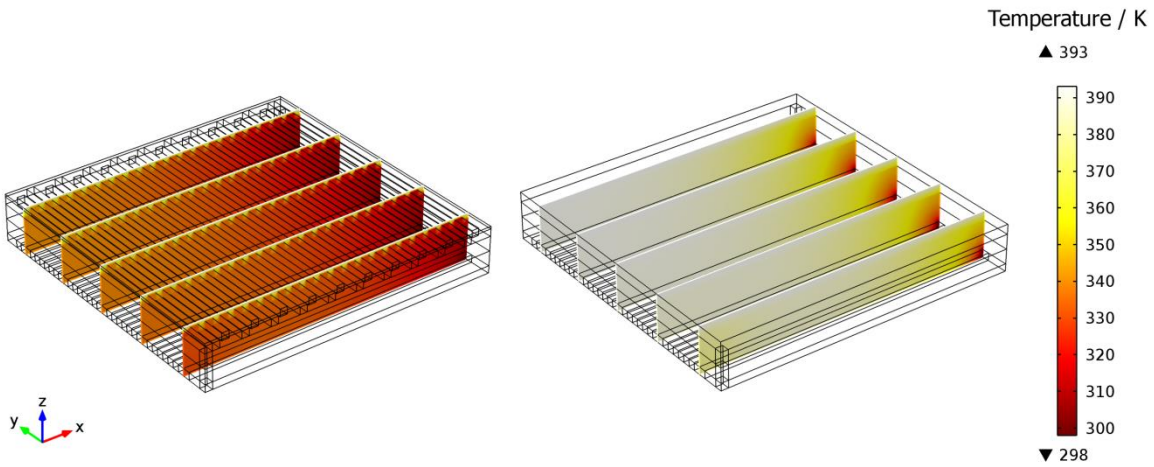

Figure 3.23: Temperature Isotherms showing the thermal profile of each cathode

Figure 3.23 shows the temperature profile of each cathode. It clearly demonstrates that the use of a metallic foam within the MEA will be beneficial for the removal of heat. The coolant air is heated up to the cell temperature after just 5 % along the coolant channel length, allowing this heat to be removed whereas the conventional GDL has a much lower thermal conductivity (0.3 W m^{-1} K^{-1} compared with 13 W m^{-1} K^{-1} for the metallic foam) which means that the thermal gradient is greater within the MEA. This may be damaging for the potential lifetime of the cell as hotspots are known to cause faster degradation. This poor thermal conductivity is offset by using higher stoichiometries of air in the cooling channels, or using a more efficient coolant fluid. However, both of these solutions mean more effort is required on the balance of plant side and thus the overall system efficiency will be lower.

3.8 Conclusions

IT-PEFCs operating at 120 ^{o}C offer many benefits due to their higher operating temperature, such as the elimination of liquid water within the cell and improved heat rejection. However, in order to fully realise these benefits, further improvement of cell components is required. For example, using a membrane material or a GDL that has been optimised for use in a conventional PEFC will not allow the full use of the advantages of the IT-PEFC. As such, theoretical studies are important for investigating which component material properties are vital to the performance of the cell, especially when considering the relative novelty of this field.

The membrane material and the GDL have both been investigated in this study. It was found that attempting to increase the membrane conductivity beyond that of 10 S m^{-1} would not bring about significant returns in terms of cell performance as other losses within the cell appear to then dominate performance.

The GDL is one of the less well understood components of the PEFC and the effect of the different material properties has not been thoroughly studied. Within this investigation, it was found that the porosity of the material can be optimised in order to maximise cell performance. A porosity between 35 and 55 % was found to be best for the cell at all operating voltages however a porosity of 40 % was found to be ideal for a cell's typical operating voltage (0.6-0.8 V). It was also found that the permeability is quite important to the cell performance but only when considering convective forces. Within a conventional GDL/FFP design, these convective forces would be found when gases are forced from one gas channel to another through the GDL, thus forcing water

to be removed from the cell. This is not necessary for an IT-PEFC, however, as water will be in the vapour phase and will be removed via passive diffusion effects.

The use of a metallic foam in place of the conventional GDL/FFP was considered as further element of design simplification in this analysis. The metallic foam offers many advantages that are synergistic with the IT-PEFC. The lack of liquid water means that high pressure air supply systems are not required and therefore the overall cost of the system can be reduced as the machining of the FFP is reduced as well as reduced power consumption in the balance of plant. The relatively high electrical conductivity of the metallic foam allows for a thicker foam which will aid in giving the MEA mechanical stability. Furthermore, the higher thermal conductivity of the metallic mesh means that the cell will act as a much more efficient heat exchanger when compared with a conventional GDL/FFP cell design. This will aid in simplifying stack design as the thermal management will be simpler. The only possible disadvantage with the metallic foam would be the possibility for metallic corrosion which could lead to increased degradation of other components such as the membrane or increasing contact resistance. However, special material coatings are being developed for metal BPPs which could also be applied to a metallic GDL and thus reduce this issue. The only drawback with this solution is that the coating may reduce the conductivity of the metallic GDL to some extent. However, considering the interest in coating technology, this barrier is being researched extensively.

CHAPTER 4

Establishing a Baseline: Nafion212 Based MEA at Intermediate Temperature Operation

"Ideas do not always come in a flash, but by diligent trial and error experiments that take time and thought"

Charles K. Kao, 2009

Chapter 4 Establishing a Baseline: Nafion212 Based MEA at Intermediate Temperature Operation

4.1 Introduction

Nafion based membrane electrode assemblies (MEAs) have been analysed extensively at low and high temperatures (sub 100 ^{o}C and above 120 ^{o}C). However, the effect of increasing the temperature into the intermediate temperature region (100-120 ^{o}C) has not been well studied. In order to understand how the different parameters of the gas diffusion layer (GDL) affects the cell performance, it is important to understand how temperature and relative humidity affect the Nafion membrane. Within the literature, intermediate temperature operation on a Nafion based MEA is only performed to compare with different membranes that are being tested [17,200–203]. As such, it was decided to study the effect of operation temperature on a Nafion based MEA so that; (i) a baseline could be established with commercial electrodes for testing GDLs and (ii) of humidity on cell performance could be studied.

4.2 Experimental

4.2.1 MEA Preparation

Membrane Electrode Assemblies (MEAs) were prepared from commercially available materials. Commercially available gas diffusion electrodes (GDEs) (Pt loading of 0.4 mg cm^{-2}, Sigracet 34BC, supplier: Johnson Matthey) were painted with a Nafion solution (10 wt% solution, supplier: Ion Power) such that the dry Nafion loading was

0.6 mg cm^{-2}. The electrodes were then dried in a vacuum oven for 15 hours. Following the drying procedure, the GDEs were placed on either side of the Nafion membrane (Nafion 212, supplier: Ion Power) and were hot pressed at 125 ^{o}C for 120 s under a pressure of 600 psi. The active area of all MEAs tested was 4 cm^2.

Scanning electron microscopy (SEM) was performed to determine the surface morphology of the electrodes and the membrane using a JEOL 6060.

4.2.2 Fuel Cell Testing

The MEA was tested using a Scribner 850e Fuel Cell Test Station. All tests were conducted using 1.8 bar back pressure, under a minimum flow control regime of 0.2 L min^{-1} H_2 and 0.5 L min^{-1} air. These flow rates were chosen as they would give a stoichiometry of 5 for both the anode and cathode at a current density of 1.5 A cm^{-2}. A range of operating conditions were chosen and are summarised in Table 4.1.

Table 4.1: Cell Operating Conditions

Operating Temperature / ^{o}C	**Relative Humidity / %**
80	25, 50, 75, 100
100	25, 50, 75, 100
120	25, 50, 75, 100

4.2.3 Impedance Spectroscopy

In-situ impedance spectroscopy was conducted using the impedance analyser from the Scribner 850e test stand. Impedance spectroscopy was recorded at current densities of 0.1, 0.5 and 1 A cm^{-2} at the respective operating temperature. In order to ascertain the fuel cell resistances, a frequency scan between 1 Hz and 10 kHz was used. The equivalent circuits [204] shown in Figure 4.1 were used to analyse the

different sources of resistance within the cell. In all of the cases, the charge transfer resistance is assumed to be for the cathodic oxygen reduction reaction (ORR) only as the resistance of anodic hydrogen oxidation reaction (HOR) is assumed to be negligible.

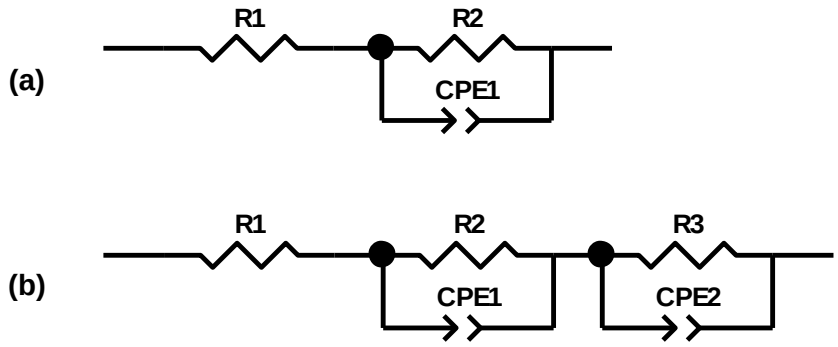

Figure 4.1: Equivalent Circuits used to describe the ohmic resistance and the charge transfer resistance for (a) 0.1 A cm^{-2}, (b) 1 A cm^{-2} and 1.5 A cm^{-2}, where R1 is the cell ohmic resistance, R2 is the charge transfer resistance, R3 is the mass transfer resistance, CPE1 is the constant phase element of the charge transfer resistance and CPE2 is the constant phase element for the mass transfer resistance.

4.3 Results and Discussion

4.3.1 Characterisation of the MEA

SEM was used to characterise the GDEs and the assembled MEA. The commercial GDE was first imaged prior to the application of the Nafion layer.

(a)

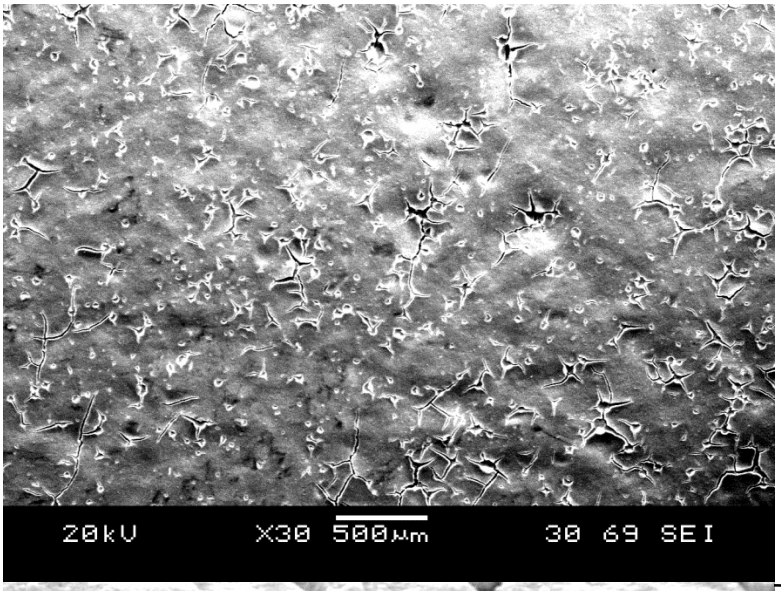

(b)

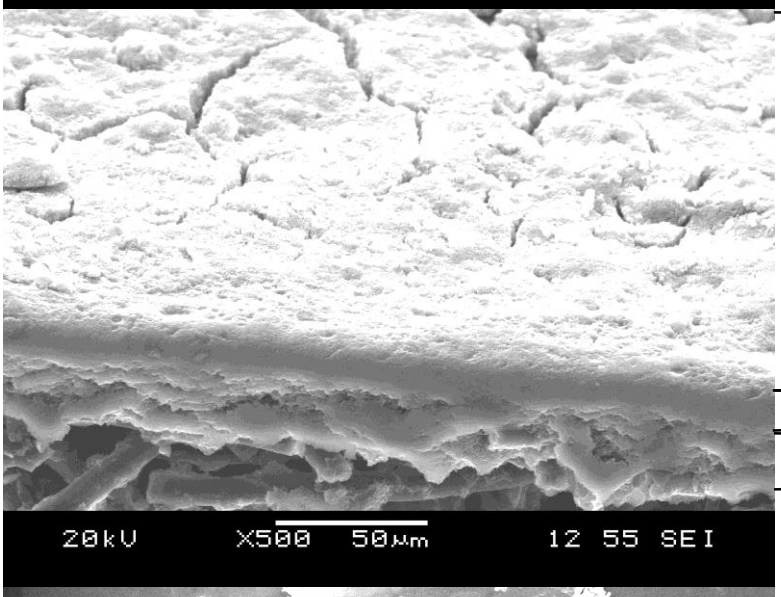

Catalyst Layer top side

Catalyst Layer side profile

MPL

(c)

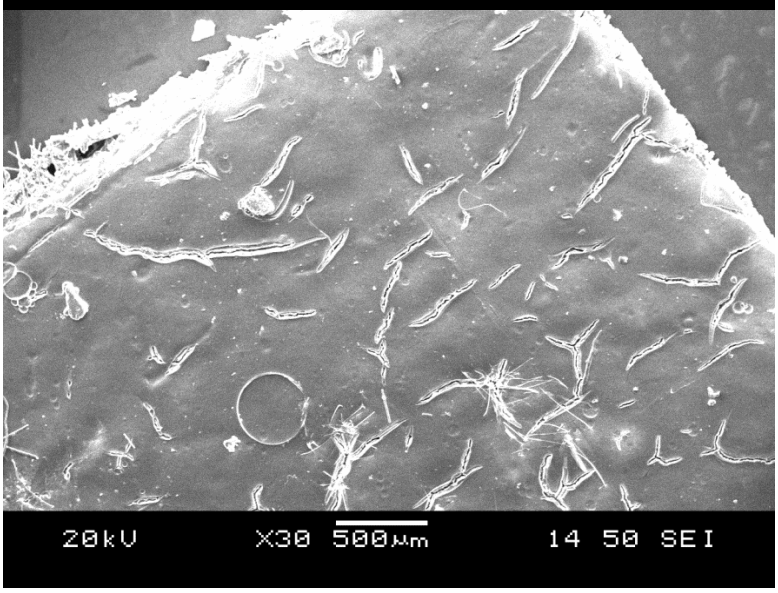

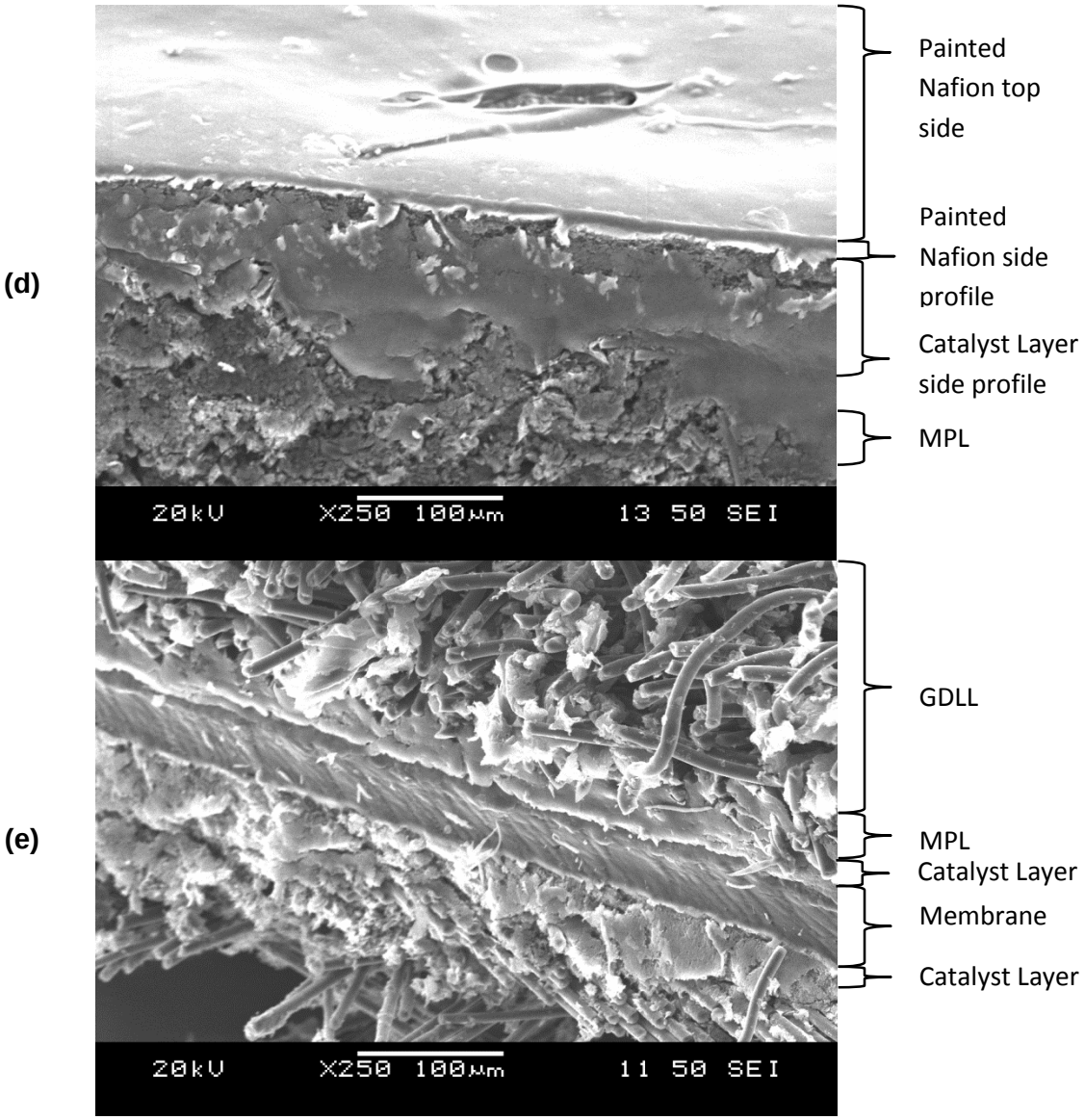

Figure 4.2: SEM images of (a) the commercial electrode (top side view), (b) the commercial electrode (cross section), (c) the commercial electrode post application of Nafion (top view), (d) the commercial electrode post application of Nafion (cross section) and (e) the assembled MEA.

Figure 4.2(a) shows the commercial GDE prior to the application of a Nafion layer. There appears to be a large number of small cracks in the catalyst layer which are most likely formed as the catalyst layer is drying and the catalyst ink solvents are evaporating. Currently, it is unknown the exact effect that these cracks have on the performance of the electrode but it is hypothesised that they aid in the removal of the

water generated. Figure 4.2(b) shows the cross section view of the commercial electrode. It can be seen that the average thickness of the catalyst layer is approximately 15 µm.

Before this electrode is used in producing an MEA, it is painted with a layer of Nafion. This is so that a better contact can be achieved between the catalyst layer and the Nafion membrane during the hot pressing step of manufacture. The electrode was then imaged after the Nafion layer was applied (Figure 4.2(c) and (d)). The layer appears to be much smoother after the Nafion ink is applied, with much fewer cracks. It is important to note that the layer is also very thin (approximately 10 µm). Figure 4.2(c) shows the assembled MEA post hot pressing. It can be seen that the thickness of the membrane does not change much post hot pressing as new Nafion 212 has a thickness of 50 µm and post hot pressing, the membrane thickness is still approximately 50 µm. The MEA was then conditioned by using a potentiostatic procedure whereby the MEA voltage was held at 0.6 V for 10 hours at high relative humidity.

4.3.2 Influence of Operating Temperature on Cell Performance

The influence of operating temperature on the cell performance was then tested. The following polarisation curves were obtained Figure 4.3.

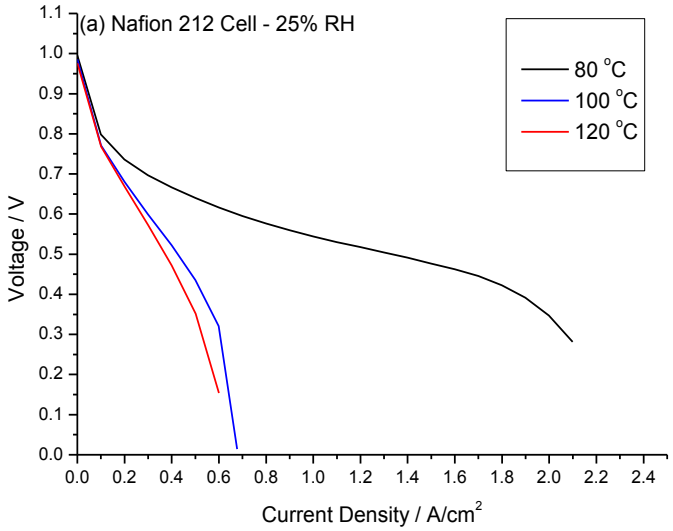
(a) Nafion 212 Cell - 25% RH
80 °C
100 °C
120 °C
Voltage / V
Current Density / A/cm2
1.1
1.0
0.9
0.8
0.7
0.6
0.5
0.4
0.3
0.2
0.1
0.0
0.0 0.2 0.4 0.6 0.8 1.0 1.2 1.4 1.6 1.8 2.0 2.2 2.4

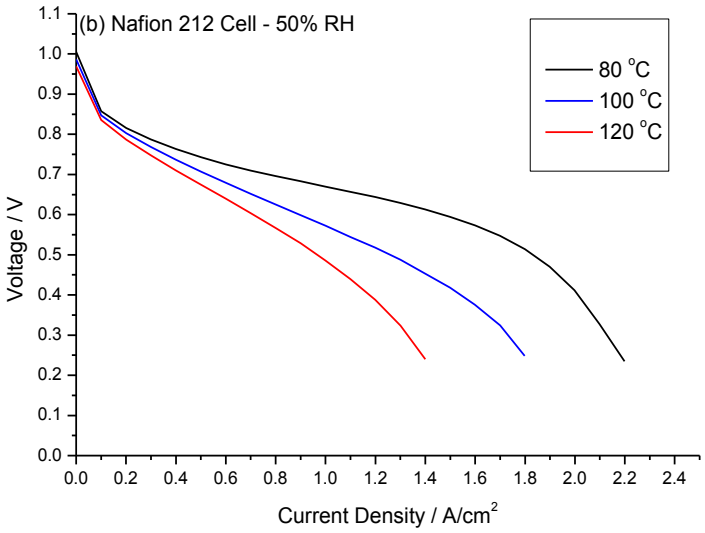
(b) Nafion 212 Cell - 50% RH
80 °C
100 °C
120 °C
Voltage / V
Current Density / A/cm2
1.1
1.0
0.9
0.8
0.7
0.6
0.5
0.4
0.3
0.2
0.1
0.0
0.0 0.2 0.4 0.6 0.8 1.0 1.2 1.4 1.6 1.8 2.0 2.2 2.4

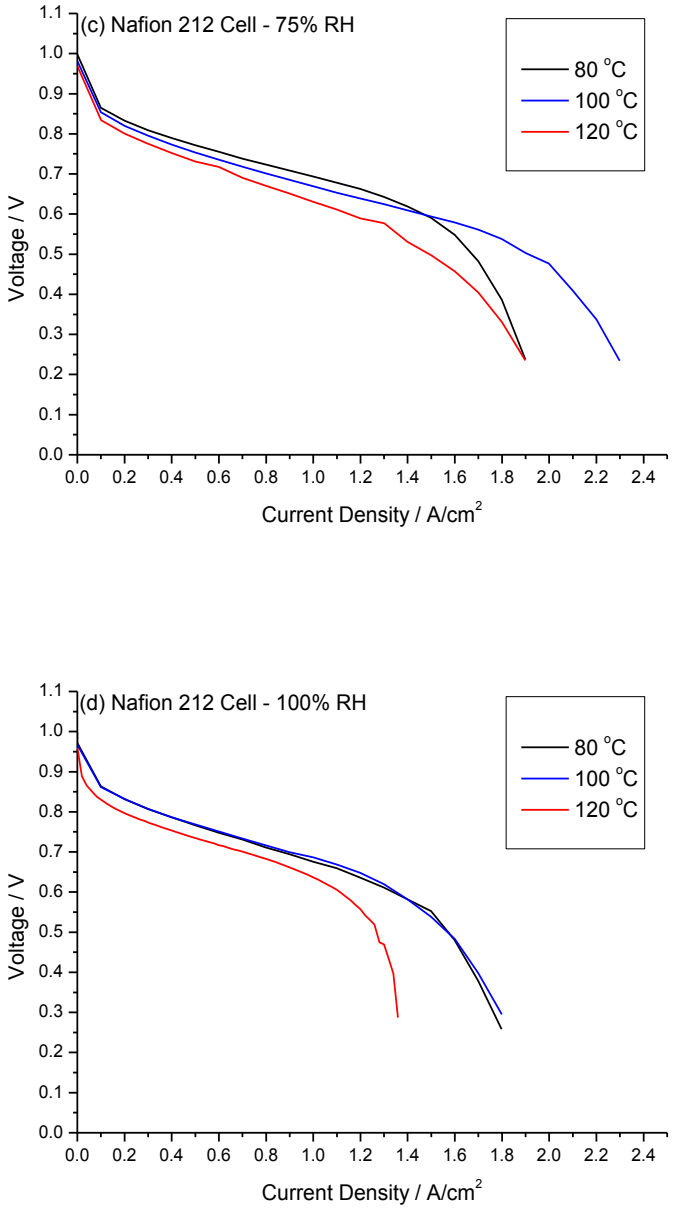

Figure 4.3: Cell performance as a function of temperature with the relative humidity remaining fixed; (a) 25% RH, (b) 50% RH, (c) 75% RH and (d) 100% RH

At 25 % RH the MEA performance decreases significantly as the cell temperature increases from 80 ºC to 100 ºC. However, the MEA performance does not decrease further as the cell temperature is increased from 100 ºC to 120 ºC. This trend is

representative of the membrane becoming dehydrated. This can be seen when comparing impedance spectra at these operating temperatures at 25 % RH. Equivalent circuit modelling was performed on the impedance data using the model and the results are shown in Figure 4.4(b).

At 50 % RH, the performance again deteriorates as the temperature increases. However, the absolute performance decrease isn't as large as it is at 25 % RH. The performance is higher at all temperatures which is due to the membrane having higher hydration. This hydration is somewhat aided by the increasing amount of product water which the membrane is able to hydrate itself with which results in an increased protonic conductivity.

75 % RH is a very interesting case because when testing at 100 ^{o}C the highest current density (2.3 A cm^{-2}) at 0.3 V was produced. This is of interest as the ohmic region of the polarisation curve shows poorer performance at 100 ^{o}C than at 80 ^{o}C which is expected as the membrane should be more dehydrated. However, the mass transport region of the polarisation curve shows higher performance which means that the maximum current density achieved by the cell is the highest at 100 ^{o}C. This is in line with the theory as above 100 ^{o}C, water should be mainly in the vapour phase and hence water removal is simplified. The performance drops when increasing to 120 ^{o}C in all aspects of the polarisation curve which is due to the membrane losing water at a faster rate than it is able to replenish the water from product of the fuel cell reaction and the incoming fuel streams.

At 100 % RH, the membrane conductivity does not change much at the different operating temperatures. The MEA performance is similar at these operating

temperatures, which indicates that the vaporisation of the water does not increase the rate of water removal which is most likely due to the high concentration of water at this high humidity.

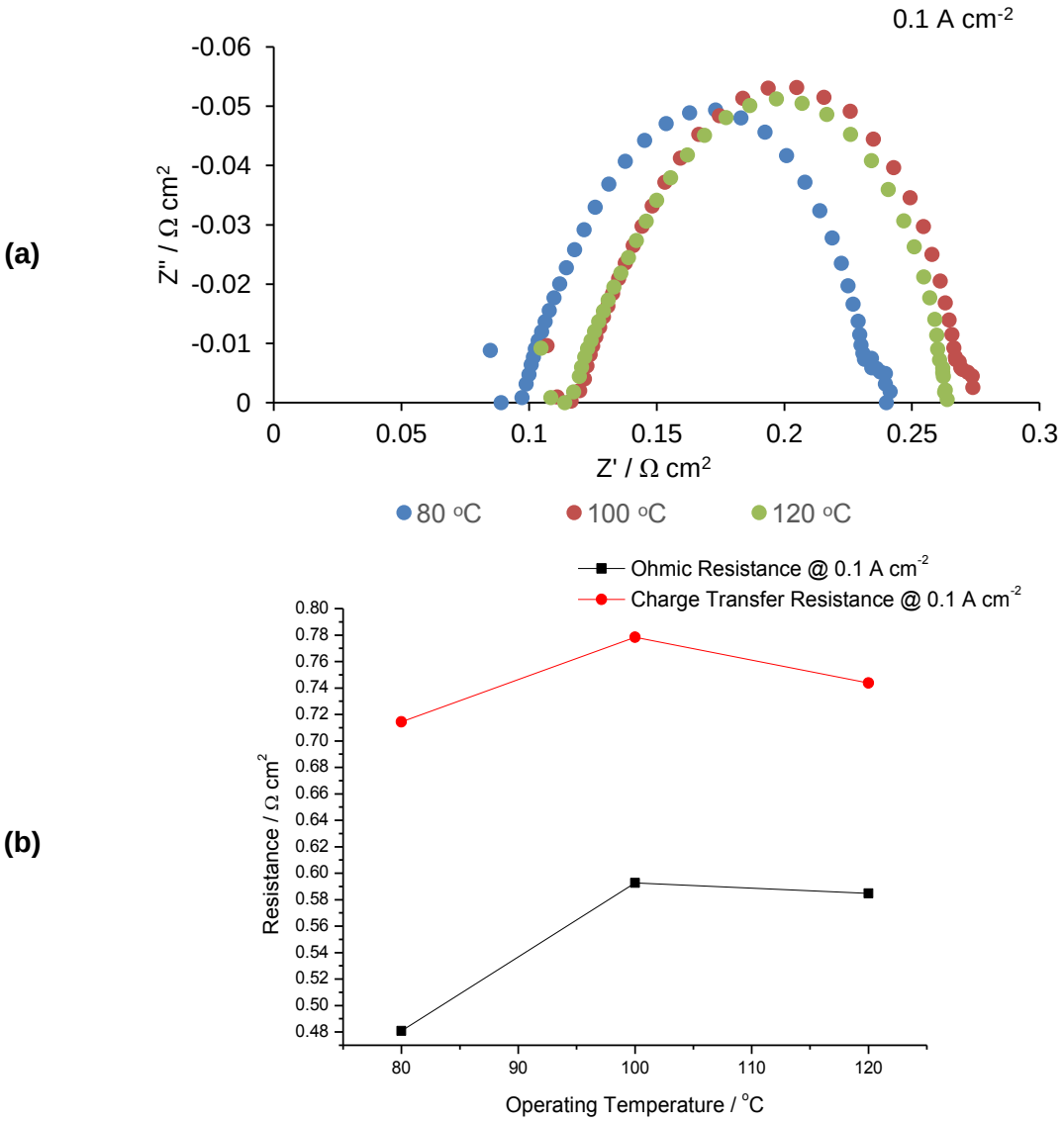

Figure 4.4: (a) Impedance Spectrum at 25 % RH and 0.1 A cm^{-2}, (b) Ohmic and Charge Transfer Resistance from equivalent circuit modelling

The above data shows that the high frequency intercept and therefore the ohmic resistance of the cell increases when the cell operating temperature is increased from

80 ^{o}C to 100^{o}C (480-592 mΩ cm^{2}) and then stays constant from 100 ^{o}C to 120 ^{o}C (592-584 mΩ cm^{2}). From the impedance data, the ORR charge transfer resistance does not change much between the operating temperatures with a total difference of 64 mΩ cm^{2}. This suggests that the biggest source of resistance within the cell as the temperature increases is the dehydration of the membrane however beyond 100 ^{o}C, the membrane cannot further dehydrate and thus the ohmic resistance does not change much (8 mΩ cm^{2}). Equivalent circuit modelling was then performed on the impedance data at higher relative humidities for 0.1 A cm^{-2}. The resistance values are shown in Figure 4.5.

(a)

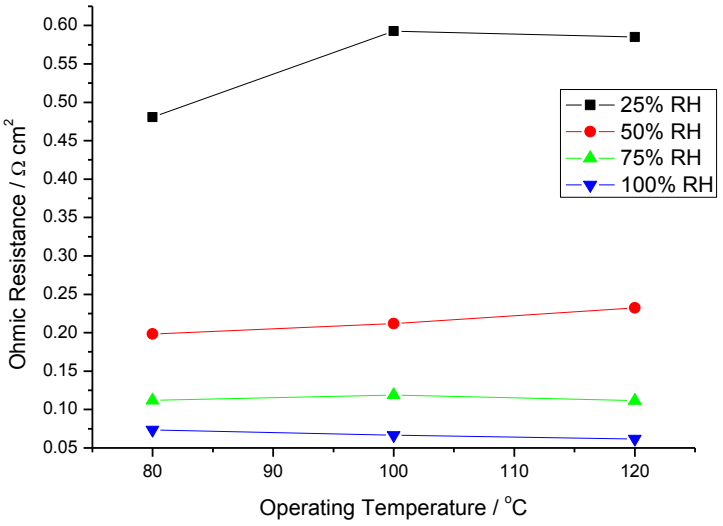

(b)

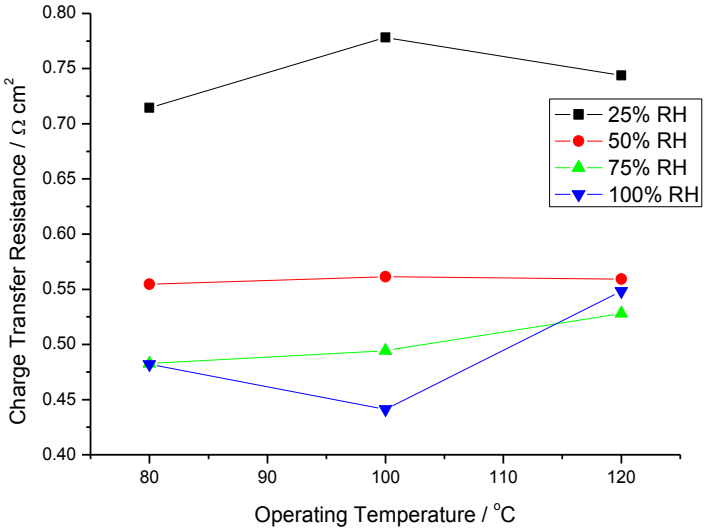

Figure 4.5: Resistance values for (a) ohmic resistance and (b) charge transfer resistance at 0.1 A cm^{-2}

From Figure 4.5(a), at higher relative humidities (75 % and 100 %), the ohmic resistance does not change significantly as the operating temperature is increased (1 mΩ cm^2 and 12 mΩ cm^2 respectively between 80-100 ^oC). However, at lower relative humidities (50 % and 25 %) the ohmic resistance increases with operating temperature which corresponds to the dehydration of the membrane and therefore a loss in protonic conductivity.

On the other hand, at 50-75 % RH the charge transfer resistance does not change much as the operating temperature is increased. This indicates that the operating temperature is having little effect on the ORR kinetics, and that the limiting factor on the ORR kinetics is related to the humidity level. However, the trend observed at 100 % RH is different. It appears that the ORR kinetics improve when the temperature increases from 80-100 ^oC. This indicates that the relative humidity is no longer a limiting factor in the ORR and as the temperature is increased, the kinetics improve.

However, as the temperature is increased further to 120 ^{o}C, the charge transfer resistance increases. This could be explained by the presence of too much water in the catalyst layer, which would slow down the ORR [205] through the blockage of active sites.

4.3.3 Influence of Relative Humidity on Cell Performance

The influence of relative humidity was then measured by fixing the cell operating temperature and obtaining the cell performance as a function of relative humidity (Figure 4.6)

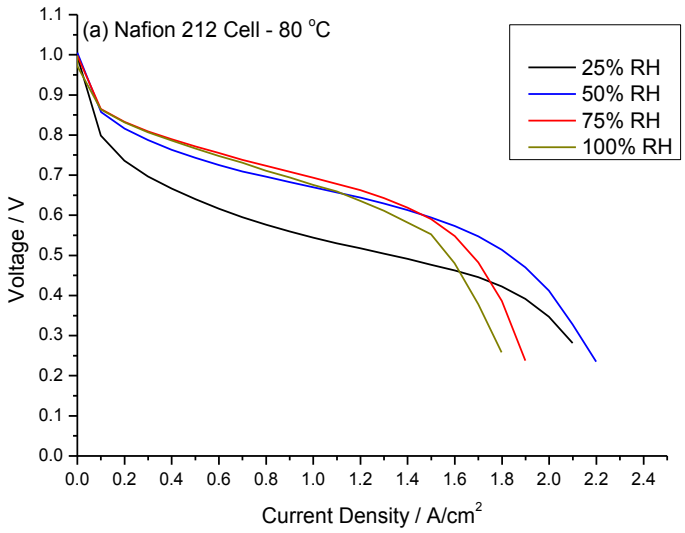

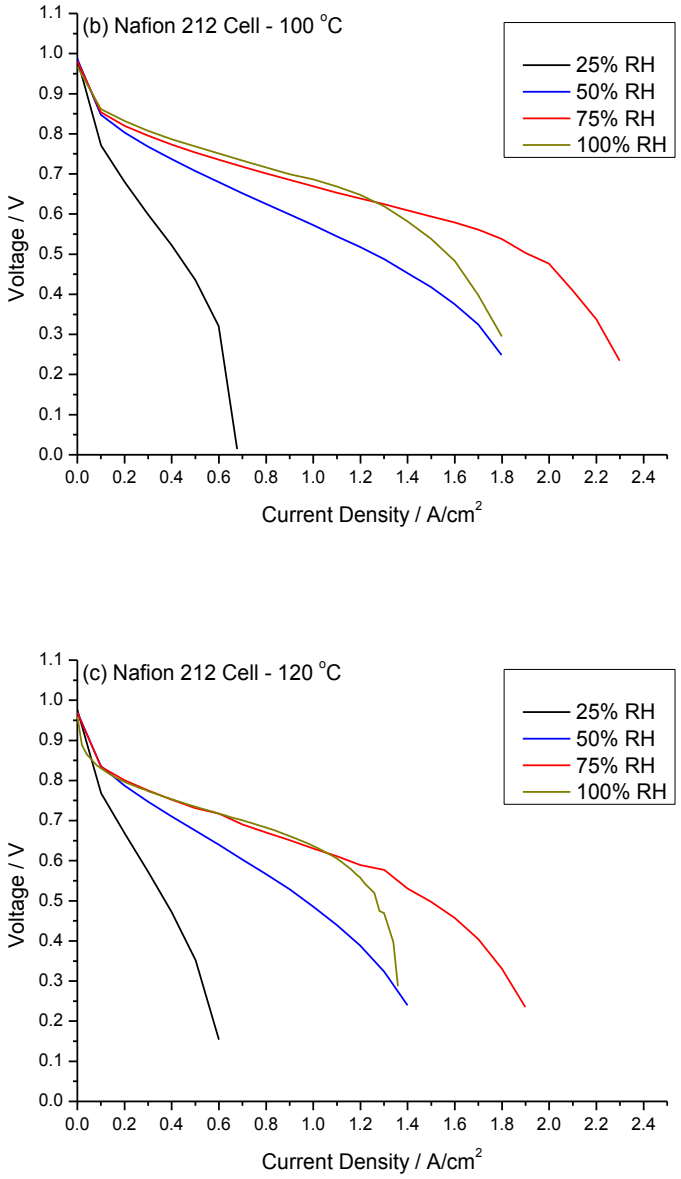

Figure 4.6: Cell performance as a function of relative with the operating temperature remaining fixed; (a) 80 ºC, (b) 100 ºC and (c) 120 ºC

The polarisation curves in Figure 4.6 show that, as expected, for each temperature, the performance is poorest at 25 % RH. As previously discussed, the membrane will have a low conductivity due to dehydration. At 80 ºC, the cell performance is highest when a relative humidity of 50 % is used, as the membrane is sufficiently hydrated by

water from the fuel streams and water generated from the fuel cell reaction. However, as the humidity is increased to 75 % and 100 %, the MEA performance decreases. This is not due to the MEA ohmic resistance, which doesn't change much, rather it is due to the mass transport limitations increasing. This is in line with the theory in that at higher relative humidities, there is a lot more water present in the electrodes and the rate at which water will be removed from the electrodes will decrease as less of a concentration gradient is present.

At 100 and 120 ^{o}C, the trend is slightly different in that the cell performance is higher when a relative humidity of 75 % is used. This is because the membrane is losing water at a faster rate than at lower temperatures, and thus a higher base supply of water is required from the fuel streams. As such, the ohmic resistance is significantly higher at 50 % RH than at 75 % RH after which the ohmic resistance doesn't decrease further. Mass transport limitations still dominate at 100 % RH for both 100 and 120 ^{o}C indicating that water removal is still a big problem. This is to be expected in because even though theoretically the water should exist in the vapour phase, the pressure in our test set up (1.8 bar back pressure, 2.8 absolute pressure) means that the boiling point of water is much higher (approximately 130 ^{o}C as calculated by the Antoine equation). However, within the MEA there are large temperature gradients, with the possibility of +10 ^{o}C at the catalyst layers at higher operating current densities thus the true phase of the water within the MEA is unknown. From the results shown at 100 % RH, it would appear that within the GDL and flow fields, the presence of liquid water causes mass transfer to still be a problem.

Impedance measurements were taken of the MEA at these different operating conditions and equivalent circuit modelling was used to confirm the trends observed from the polarisation curves (Figure 4.7).

(a)

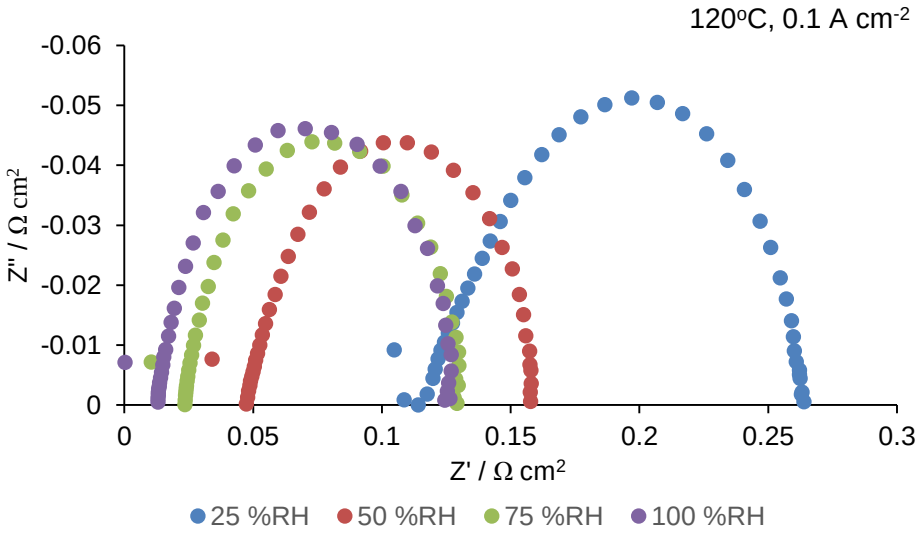

(b)

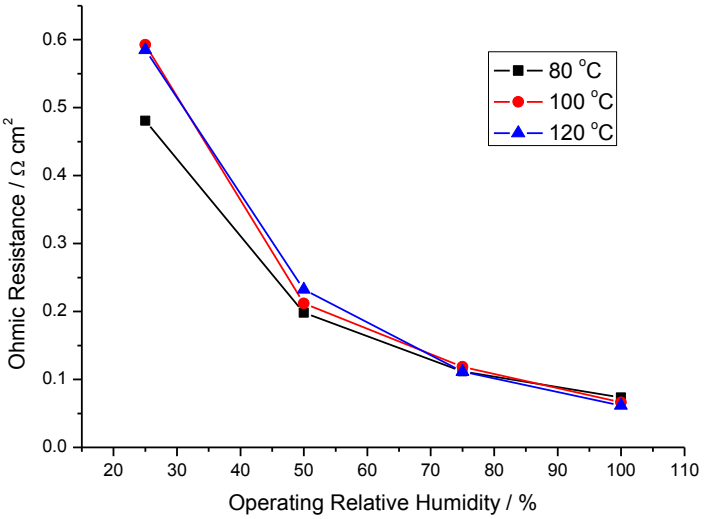

(c)

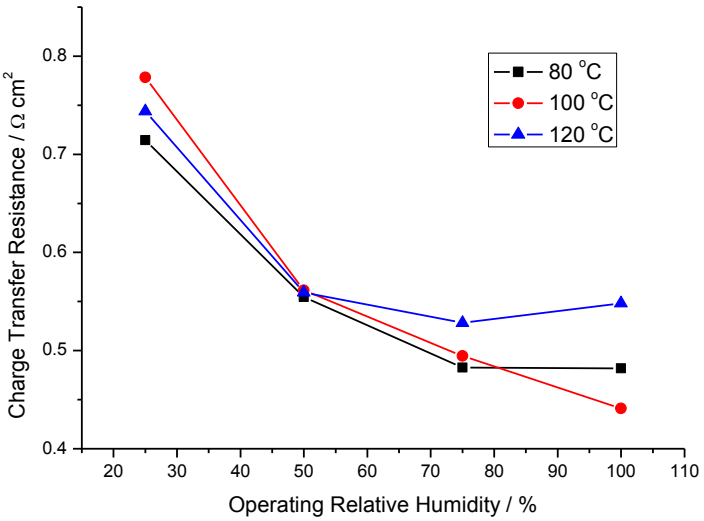

Figure 4.7: Impedance spectra at (a) 120 ºC at 0.1 A cm^{-2} and equivalent circuit modelling for both (b) Ohmic Resistance and (c) Charge Transfer Resistance.

From Figure 4.7(a), there are a few general trends which are listed below:

1. As expected, the Ohmic resistance decreases as the relative humidity increases. This is evidenced by the shifting of the high frequency intercept towards the origin (Figure 4.7 (b)).

2. As the relative humidity is decreased, the angle of the high frequency arc decreases, tending towards 45º. This is explained by the dehydration of the ionomer chains that are present in the catalyst layer causing mass transport resistance.

3. As the relative humidity decreases, an increase in the high frequency arc is observed (Figure 4.7 (c)). This is due to low water content in the catalyst layer which reduces the ORR kinetics [205,206].

More specifically, Figure 4.7 (c) shows that the charge transfer resistance increases when the cell is at 100 % RH at 80 ^{o}C and 120 ^{o}C, indicating that the ORR kinetics are slightly slower than at 75 % RH. This doesn't appear to be the case when operating at 100 ^{o}C. This maybe because the rate of water removal from the membrane is lower than at 120 ^{o}C meaning that there will be less water present in the catalyst layer. Theoretically, at both 100 and 120 ^{o}C (if the pressure is close to atmospheric pressure), the water should exist in the vapour phase and considering that the water in the fuel streams is the same, the rate of water removal from the electrodes should be the same (if not slightly faster at 120 ^{o}C due to the elevated temperature).Therefore, the apparent slowing of the ORR could be due to flooding of the electrode due to water being lost from the membrane at a faster rate [207]. This could in turn, affect the mechanism of the ORR, slowing down the reaction [205].

4.3.4 Optimisation of Cell Operating Parameters on the Tafel Slope and the Area Specific Resistance (ASR)

From the polarisation curves shown in sections 4.3.2 and 4.3.3, it is possible to optimise the operating parameters of the cell in order to maximise cell performance. This is useful if current MEA materials were to be used at intermediate temperature. However, this does not take into account the lifespan or durability of the cell. The Tafel slope was measured in the current density range of 10-100 mA cm^{-2}.

(a)

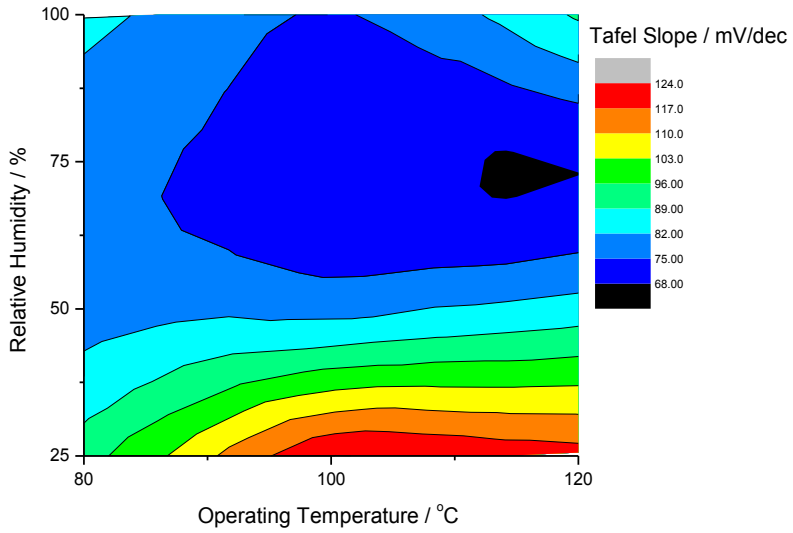

(b)

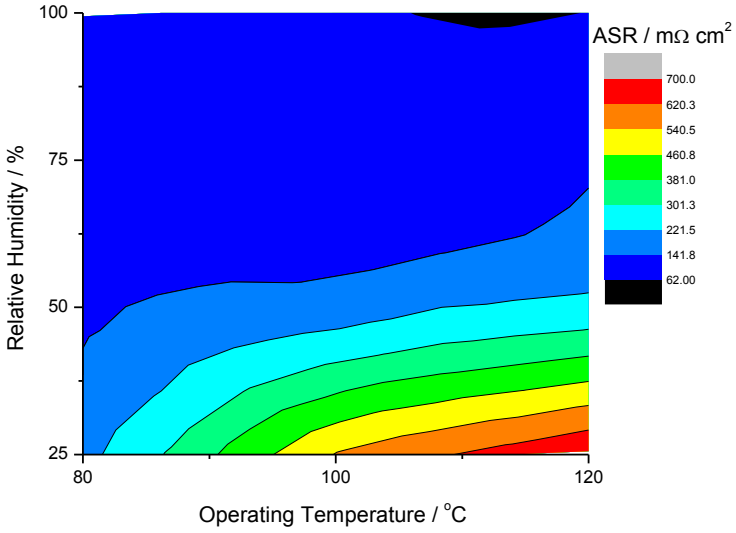

Figure 4.8: Contour plots showing (a) the Tafel Slope and (b) the Area Specific Resistance (ASR) as a function of both operating temperature and relative humidity.

From Figure 4.8(a), it can be seen that in order to have the smallest Tafel slope, and therefore best performing MEA, an operating condition of 117-120 ^{o}C between 74-75 % RH would be ideal. On the other hand, the lowest ASR can be achieved between 117-120 ^{o}C at 100 % RH. However, the ASR does not change much between 75 % and 100 % RH.

4.4 The Influence of Thermal Integrity on the Phase of Water

When working at intermediate temperature, thermal integrity of the fuel system is very important. A lack of enough thermal lagging on the fuel lines can lead to “cold spots” which can cause condensation of the water within the lines. This can lead to oscillations of the current as liquid water is pushed into the cell (Figure 4.9) Furthermore, this can also cause the relative humidity to be higher than expected.

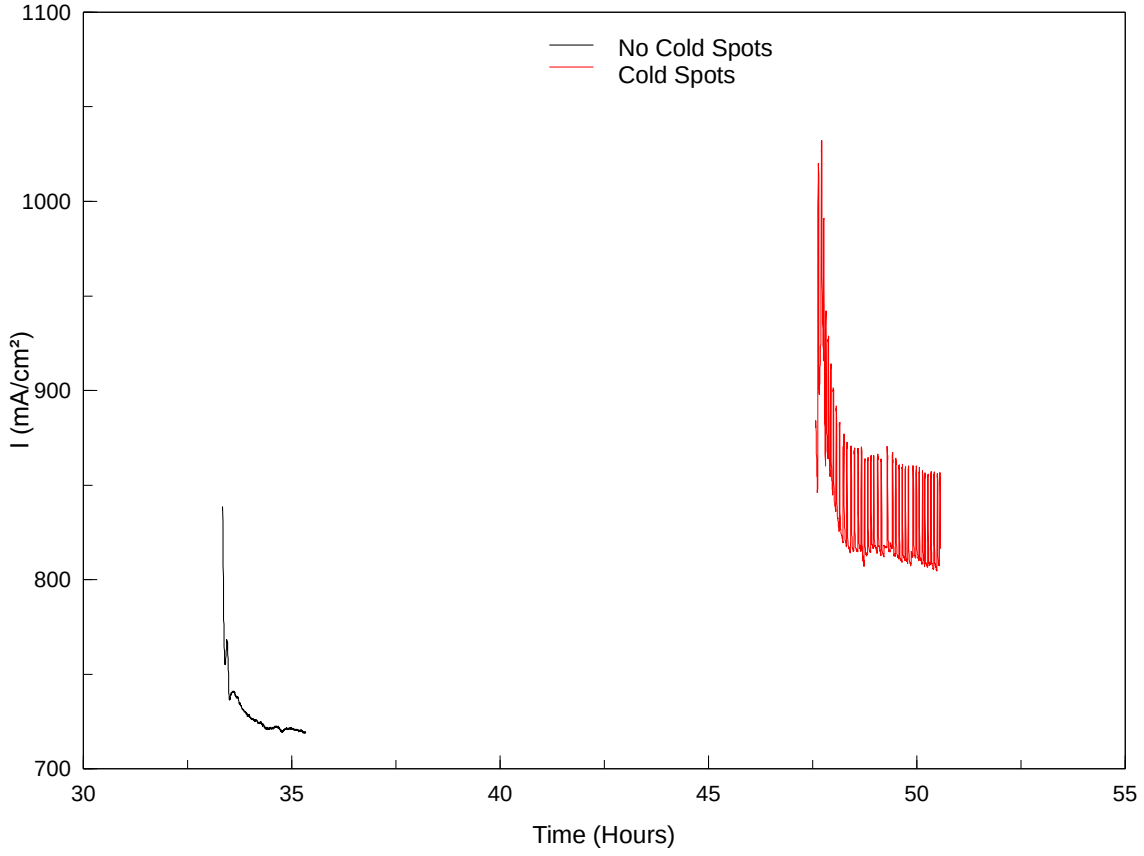

Figure 4.9: Constant voltage (0.6 V) measurements at 120 ºC, 75 % RH

The thermal integrity is a very important consideration at intermediate temperature as it has a big effect on the phase of the water within the fuel cell. In order to understand this trend, it is important to look at a phase diagram for water [208]. At the current

operating pressure of 1.8 bar, at both 80 ^{o}C and 100 ^{o}C, the water exists quite firmly in the liquid phase, even when considering that the temperature at the catalyst layers is most likely higher than that in the bipolar plates where temperature measurements are taken. However, at 120 ^{o}C, the water will be in a transition state between water and vapour with a higher amount of vapour present than at 100 ^{o}C. This means that if there are cold spots, the excess water can cause condensation within the cell at high relative humidities. The observed current oscillations are not good from a system design perspective as they can cause difficulty in the system management and thus should be avoided. However, current research into novel membranes within the field is aimed towards producing membranes that work well at low operating humidities and thus this should not be an issue for much longer in the future [5,209–211].

4.5 Conclusions

Studying commercially available Nafion membrane and commercially available electrodes at intermediate temperature is important so that the effects of the cell operating conditions on different parameters can be ascertained. In particular, it was found that decreasing the relative humidity significantly decreased the cell performance at all of the cell operating temperatures tested. The magnitude of the performance decrease became larger as the operating temperature increased. This is because at the low operating humidity, the Nafion membrane becomes dehydrated which causes a loss in the protonic conductivity thus significantly increasing the MEA Ohmic resistance. In turn, this low performance means that the fuel cell reaction cannot proceed at a fast enough rate for the generated water to sufficiently hydrate the

membrane. The lack of hydration in the catalyst layer also causes deprotonation of the ionomer chains, thus increasing the ohmic resistance.

It was found that increasing the relative humidity (50-75 %) increased the MEA performance. Initially, this is due to increasing hydration which decreases the Ohmic resistance within the cell. As the operating temperature is increased, the performance does not decrease as much as at low operating humidities, despite the higher rate of water loss due to evaporation. This is because the incoming water from the fuel streams is able to replenish the water in the membrane as well as slowing down the rate at which water is removed from the electrode. However, at low temperatures mass transport limitations within the electrodes increases at lower relative humidities (i.e. at 75 % RH, mass transport causes a decrease in maximum current density compared with 50 % RH). At higher operating temperatures (100-120 ^{o}C), mass transport limitations are less of an issue. This has been attributed to the vaporisation of the water within the cell which should not hinder the diffusion of oxygen through the electrode. Furthermore, it appears that there is in an increase in the ORR kinetics with the increasing humidity as is evidenced by the decrease in the Tafel slope and a reduction in the charge transfer resistance.

At the maximum relative humidity (100 %), flooding of the electrodes is a problem at all of the operating temperatures, however is worst at 120 ^{o}C. This excess water causes a slowing down of the ORR kinetics as evidenced by the increase in the Tafel slope and an increase of the charge transfer resistance.

The phase of the water within the cell was also found to be important to the MEA performance. This is especially apparent when the thermal integrity of the cell is

compromised as current oscillations are observed when constant voltage measurements are taken. The lack of thermal integrity causes condensation of water and excess water which is especially a problem when operating at intermediate temperature. However, a goal of membrane design within this field to have a membrane that works well at low humidities and therefore when such a material is produced this should not be too big of a problem.

Finally, it was found that the optimum conditions for an MEA constructed of commercially available Nafion 212, with commercially available GDEs was at 117-120 ^{o}C and at 75 % RH. However, this did not take into account the durability of these materials as they are designed for use at low temperatures.

CHAPTER 5

Understanding the Role of the Microporous Layer (MPL) in GDLs for MEAs at Intermediate Temperature

"I have yet to see any problem, however complicated, which, when you looked at it the right way, did not become still more complicated"

Paul Alderson, 1969

Chapter 5 Understanding the Role of the Microporous Layer (MPL) in GDLs for MEAs at Intermediate Temperature

5.1 Introduction

A conventional GDL may feature a microporous layer (MPL). The MPL is typically a mixture of hydrophobic agent and amorphous carbon black [11,74–78].

Current work reported in the literature has been conducted to understand the influence of the MPL on cells operating at low temperatures (sub 100 ^{o}C). The main function of the MPL is to increase the contact between the catalyst layer and the substrate layer of the GDL through the formation of a flat and uniform layer that does not let the catalyst layer fall “into” the GDL. Given the electrode is made of relatively fragile material, it can fracture under mechanical stress and the material can be distributed within the large pores of the GDL.

Furthermore, the MPL has been shown to enhance the water management properties of the GDL thus improving MEA performance. One of the key methods by which water is removed from the catalyst layer is by capillary driven flow, which arises from the pressure difference between the liquid phase and the vapour phase [93,94]. As the vapour pressure is assumed to not change at the conventional operating temperature of the PEFC, it is the liquid pressure which builds up between the catalyst layer and the MPL which acts as the driving force for the flow of water from the catalyst layer [75,87,95–97]. It is suspected that high liquid water pressure between the catalyst layer

and the MPL would reduce the cell performance through the reduction of active area of the catalyst particles. This is due to the amount of water within the catalyst layer blocking active sites. However, it was found that the oxygen diffusion rate within the GDL substrate dominated the polarisation curve in the mass transport resistance region [96]. The effect of different parameters of the GDL/MPL (e.g. the porosity, hydrophobicity, and thickness) have been investigated and reviewed for conventional MEAs [47,54,212] where it was found that the MEA performance could be improved through the modification of the microstructure.

This poses an interesting question for the effectiveness of the MPL at intermediate temperature. Theoretically, at intermediate temperature, the water should exist mainly in the vapour phase. Therefore, the state of the art theories on the effect by which the MPL works at conventional operating temperatures may be altered as the vapour pressure will also be changing in addition to the liquid pressure. This could potentially mean that the MPL is rendered ineffective at intermediate temperature from a water management point of view as the product water may not be removed by capillary forces. Therefore, it is important for the design of GDLs at intermediate temperature to analyse whether the MPL is still important for cell performance.

In this study, the influence of the MPL on cell performance is assessed by comparing MEAs with and without MPLs at both conventional operating temperatures and intermediate temperatures. A range of relative humidities are also used in order to assess the ability of the GDLs to manage the amount of water within the cell as well as the impact this has on cell performance. The influence of the phase change of water on the cell performance is also discussed.

5.2 Experimental

5.2.1 MEA Production and Testing

For the purpose of studying the influence that the MPL has on the fuel cell performance, the materials 25BA (without MPL) and 25BC (with MPL) (SGL, Sigracet) were chosen. This is because both of these GDLs share the same substrate structure and thus changes in electronic conductivity, density and the influence of the substrate structure can be considered negligible. The properties of these two GDLs are summarised in Table 5.1 (adapted from [193]).

Table 5.1: Key properties of 25BA and 25BC

Properties	**Gas Diffusion Layer**	
	25BA	**25BC**
Thickness / µm	190	235
Area Weight / g m^{-2}	40	86
Real Density / g cm^{-3}	1.941 $\pm$ 0.002	2.009 $\pm$ 0.007
Bulk Density / g cm^{-3}	0.21	0.34
Porosity / %	66.2	36.5
Tortuosity	1.45	2.92
Mean Pore Diameter / nm	1704	842
Permeability / m^2	4.54 x 10^{-11}	5.64 x 10^{-12}

Membrane electrode assembly (MEA) fabrication was carried out by using the method suggested by Kim et al. [213]. Catalyst inks were produced by ultrasonically mixing commercially available Pt/C catalyst (Tanaka Kikinzoku Kogyo, 45.9 wt % Pt/C), solvent (IPA) and Nafion solution (10 wt%, Ion power). This ink was then hand painted onto the GDL of interest (5 cm^2, SGL Sigracet) to produce the cathode gas diffusion

electrode (GDE). The active area of all MEAs was 5 cm^2 with a catalyst loading of 0.4 mg_{Pt} cm^{-2}.

The anode GDE was produced by painting a thin layer of Nafion solution (with a Nafion dry weight of 0.6 mg cm^{-2}, 5.8 µL cm^{-2} from a 10 wt% solution (ionpower)) onto commercial GDE (Johnson Matthey, Pt loading: 0.4 mg cm^{-2}, GDL: 34BC Sigracet). The anode GDE and the cathode GDE were then placed on either side of a Nafion 212 membrane (ion power) before being hot pressed at 125 ^oC for 120 s under a pressure of 600 psi. To ensure repeatability, 3 MEAs for each GDL were produced and tested. Nafion 212 was used as the materials developed within our group for use at intermediate temperature are Nafion variants.

The MEAs were then tested using a Scribner 850e Fuel Cell Test Station with EIS capabilities. All tests were conducted at 80, 100 and 120 ^oC and a back pressure of 1.8 bar (gauge pressure). The relative humidity (RH) at the cell inlet was varied between 25 % and 100 % RH. Constant flow rates of 0.2 L min^{-1} and 0.5 L min^{-1} were used to supply the anodic (hydrogen) and cathodic (air) gases respectively. All MEAs were preconditioned before testing by operating the cell at a constant potential (0.6V) for 10 hrs. A polarisation curve was obtained at each operating condition by current scanning between open circuit voltage and 0.3V.

The electrode surface morphology was characterised using both a Zeiss Axiovision optical microscope and a JEOL 6060 scanning electron microscope (SEM).

From the polarisation curves obtained, it was possible to derive values for the ohmic resistance, which will give information on the cell ohmic resistance, the Tafel slope, which will give information on the ORR kinetics, the maximum current density (defined

as the current density at 0.3 V) and the maximum power density produced by the different MEAs. This delivers information on how well each GDL is able to transport water from the cell as well as on the overall cell efficiency. The ohmic resistance was determined by using the inbuilt current interrupt analyser on the test stand. The Tafel slope was derived by applying the model developed by Srinivasan et al [201,214] which empirically describes the relationship between voltage and current density (Equation 5.1) [202,215–217].

$$E = E_0 - b\log(i) - Ri \qquad \text{Equation 5.1}$$

With

$$E_0 = E_r + b\log i_0 \qquad \text{Equation 5.2}$$

where E is the cell potential (V), i is the cell current density (A m-2) and R is the cell area specific resistance (Ω m2) and the two last terms ($b\log(i)$ and Ri) describe the activation loss and ohmic loss, respectively. E_r is the theoretical cell reversible potential (V), i_0 and b are the exchange current density (A m-2) and Tafel slope (V/decade) respectively.

5.2.2 Impedance Spectroscopy

In-situ impedance spectroscopy was conducted using the impedance analyser from the Scribner 850e test stand, directly connected to the electronic load. The impedance measurements were taken in galvanostatic mode using an AC signal amplitude equivalent to 10 % of the recorded current density (for example, at 0.1 A cm^{-2} a current amplitude of 0.01 A cm^{-2}). Impedance spectroscopy was recorded at current densities of 0.1, 0.5 and 1 A cm^{-2} at the respective operating temperature. In order to ascertain the fuel cell resistances, a frequency scan between 1 Hz and 10 kHz was used, acquiring 10 points per decade. The equivalent circuits [204] shown in Figure 5.1 were

used to analyse the different sources of resistance within the cell. Two different simple equivalent circuits are used to describe the different phenomena occurring at different polarisation curves. Figure 5.1(a) is used at low operating current densities to describe the ohmic and activation resistances. Figure 5.1(b) is used at intermediate current densities to describe the ohmic, activation and mass transport resistances. In all of the cases, the charge transfer resistance is assumed to be for the cathodic oxygen reduction reaction (ORR) only as the resistance of anodic hydrogen oxidation reaction (HOR) is assumed to be negligible [204].

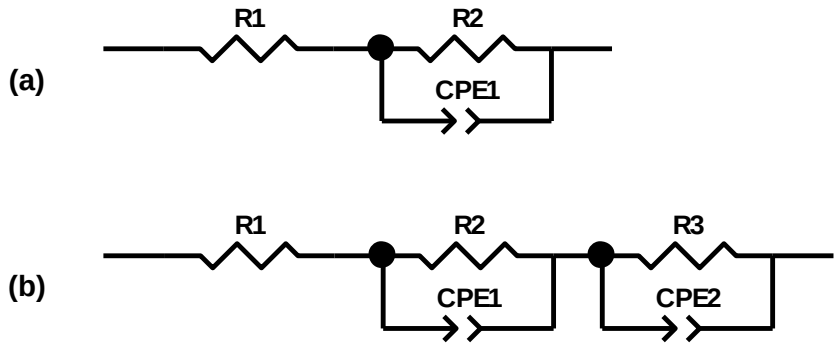

Figure 5.1: Equivalent Circuits used to describe the ohmic resistance and the charge transfer resistance for (a) 0.1 A cm^{-2}, (b) 0.5 A cm^{-2} and 1 A cm^{-2}, where R1 is the cell ohmic resistance, R2 is the charge transfer resistance, R3 is the mass transfer resistance, CPE1 is the constant phase element of the charge transfer resistance and CPE2 is the constant phase element for the mass transfer resistance [204].

5.3 Results and Discussion

5.3.1 Influence of Temperature MPL on the MEA Performance

MEAs constructed using both 25BC (with MPL) and 25BA (without MPL) as the cathode GDL were tested at various temperatures (80, 100 and 120 ^{o}C). The relative humidity was kept constant at 75 % in both the air and fuel flow in order to assess the

influence of temperature and MPL independently of the relative humidity. Polarisation curves from these tests are shown in Figure 5.2.

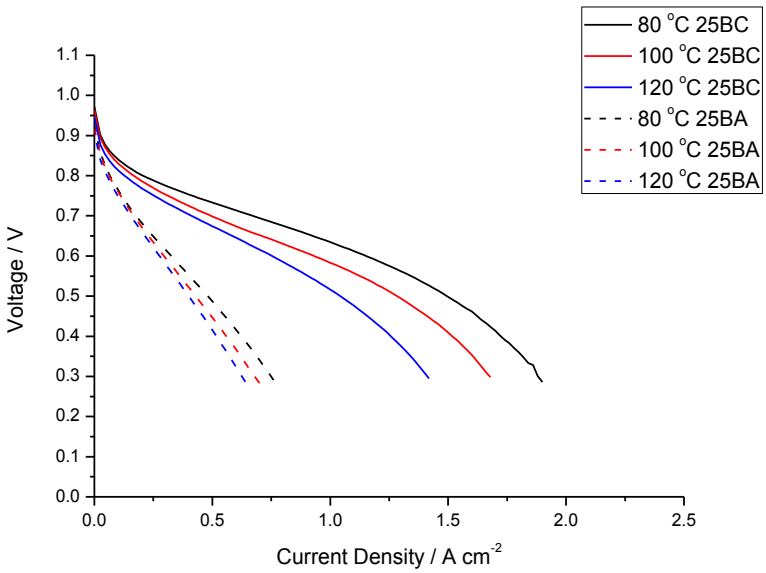

Figure 5.2: Polarisation Curves for the MEAs with 25BA (without MPL) and 25BC (with MPL) at 80 ^{o}C, 100 ^{o}C and 120 ^{o}C

From Figure 5.2, it can be seen that as the temperature increases, the MEA performance decreases. This is partly due to the dehydration of the Nafion based membrane which is not designed to operate at intermediate temperature. However, the MPL is also playing a role in the cell performance. The use of a GDL with MPL obviously leads to much improved MEA performance with lower ohmic resistance. In order to further understand the effects at play, both current interrupt measurements and impedance measurements were taken.

(a)

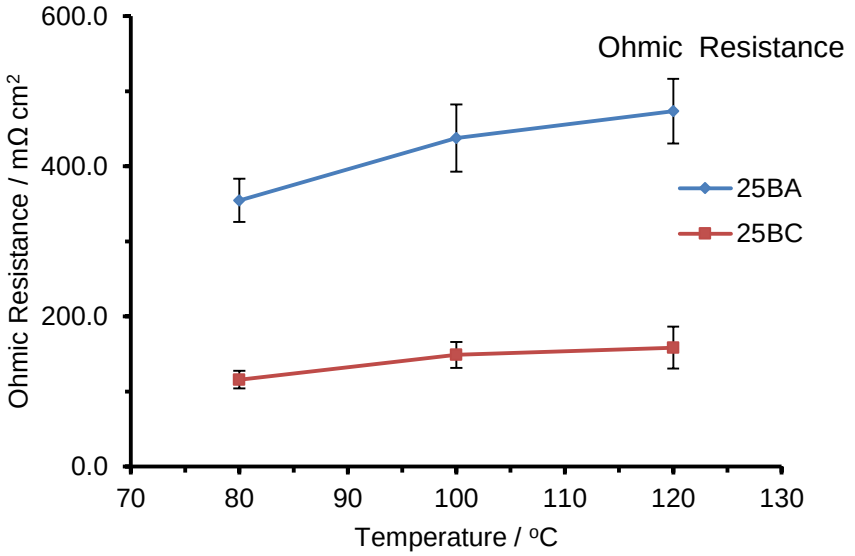
Ohmic Resistance
Ohmic Resistance / mΩ cm²
600.0
400.0
200.0
0.0
70
80
90
100
110
120
130
Temperature / °C
25BA
25BC

(b)

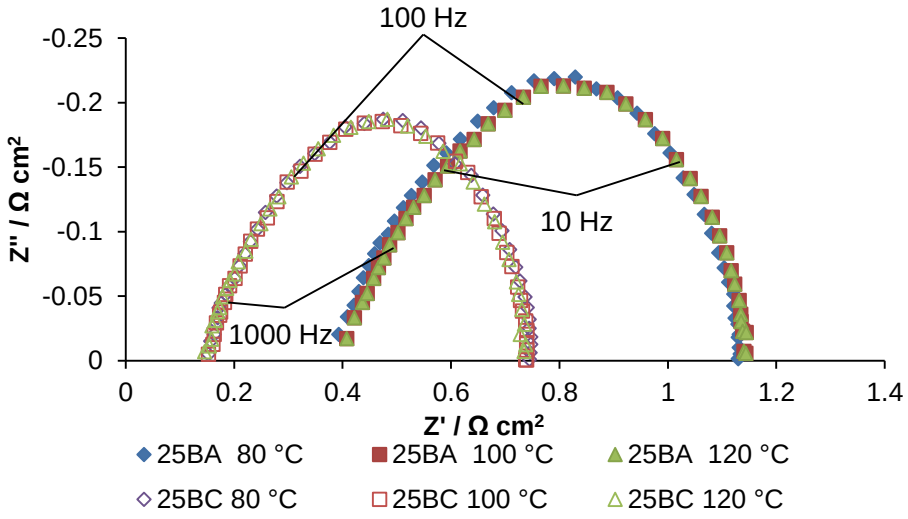
100 Hz
10 Hz
1000 Hz
Z'' / Ω cm²
-0.25
-0.2
-0.15
-0.1
-0.05
0
0
0.2
0.4
0.6
0.8
1
1.2
1.4
Z' / Ω cm²
25BA 80 °C
25BA 100 °C
25BA 120 °C
25BC 80 °C
25BC 100 °C
25BC 120 °C

(c)

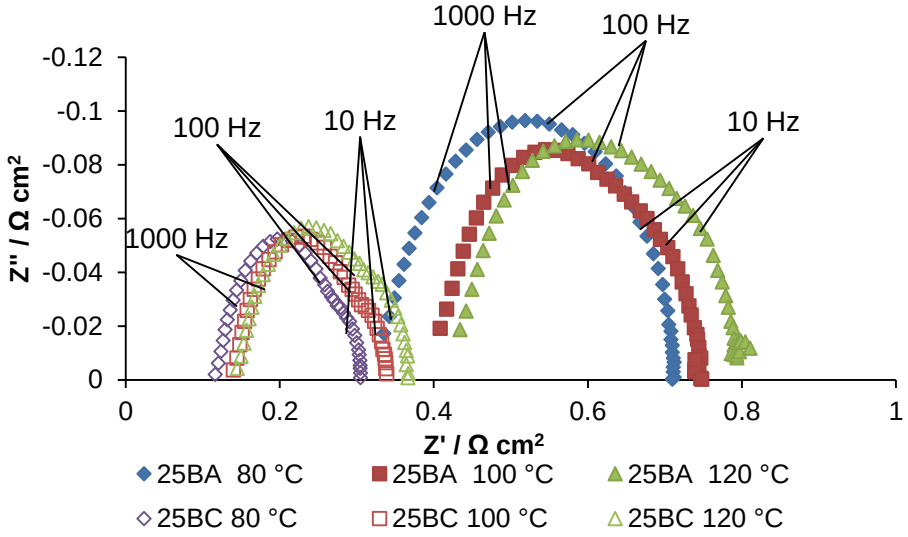
1000 Hz
100 Hz
100 Hz
10 Hz
10 Hz
1000 Hz
Z'' / Ω cm²
-0.12
-0.1
-0.08
-0.06
-0.04
-0.02
0
0
0.2
0.4
0.6
0.8
1
Z' / Ω cm²
25BA 80 °C
25BA 100 °C
25BA 120 °C
25BC 80 °C
25BC 100 °C
25BC 120 °C

(d)

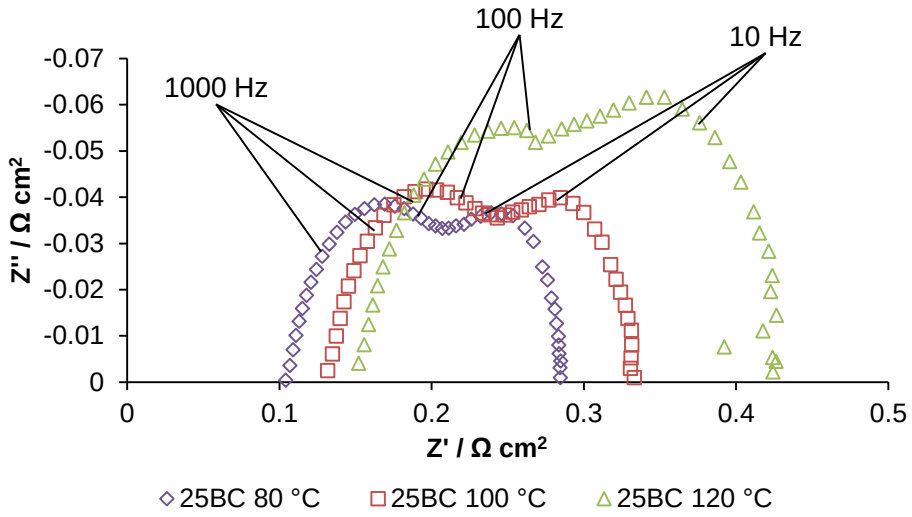

Figure 5.3: Characterisation for MEAs with 25BA (without MPL) and 25BC (with MPL) showing; (a) the MEA Ohmic Resistance measured by current interrupt, (b) impedance spectra at 0.1 A cm^{-2} , (c) impedance spectra at 0.5 A cm^{-2} and (d) impedance spectra at 1.0 A cm^{-2} for 25BC only.

Figure 5.3 (a) shows the MEA ohmic resistance as measured by the current interrupt method. From this data, it is apparent that at 75 % RH, the MEA ohmic resistance increases slightly with temperature. This is confirmed from Figure 5.3 (c), which shows an impedance spectrum taken at 0.5 A cm^{-2}, which is the same current density at which the current interrupt measurement is taken. However, when looking at how the ohmic resistance changes with respect to the operating current density, it appears that at 0.1 A cm^{-2} (Figure 5.3 (b)) there is little difference between the different operating temperatures. This difference increases as the current density increases (Figure 5.3 (d)), which shows a similar trend to that observed in Figure 5.3 (a), i.e. that the ohmic resistance decreases as the operating temperature decreases. This indicates that the cell current density will also play a role in state of hydration of the membrane. Further

information can be gained by looking at the impedance spectra with respect to the current density (Figure 5.4).

(a)

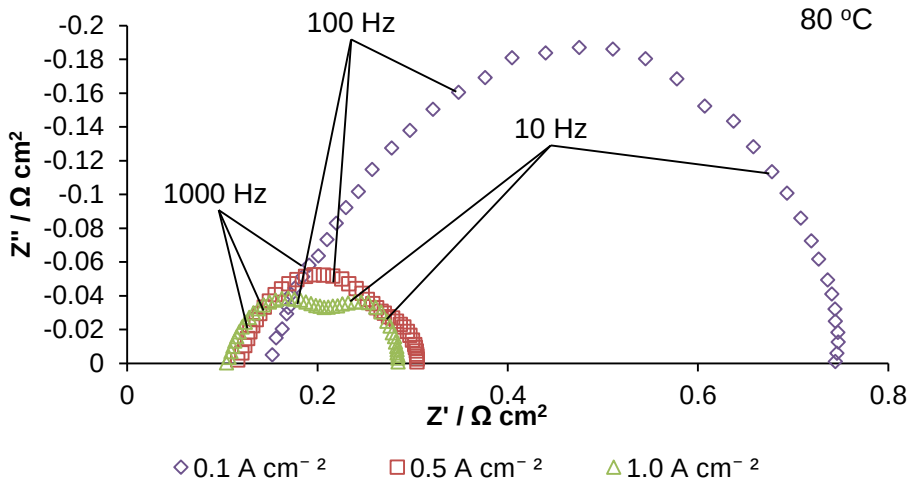

(b)

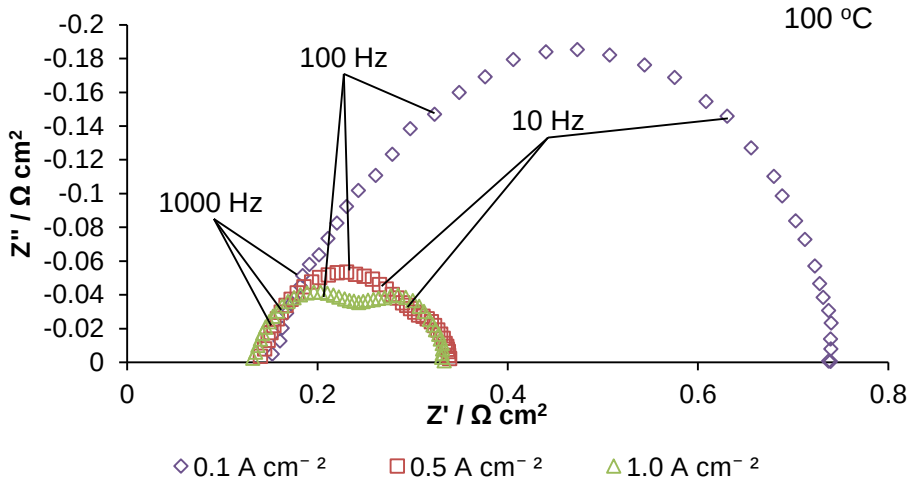

(c)

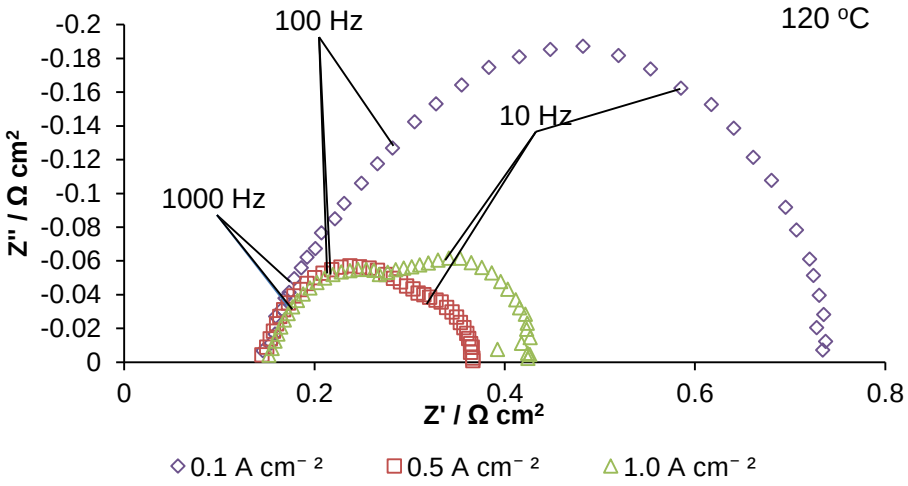
100 Hz
120 °C
10 Hz
1000 Hz
Z'' / Ω cm²
Z' / Ω cm²
-0.2
-0.18
-0.16
-0.14
-0.12
-0.1
-0.08
-0.06
-0.04
-0.02
0
0
0.2
0.4
0.6
0.8
0.1 A cm⁻ ²
0.5 A cm⁻ ²
1.0 A cm⁻ ²

(d)

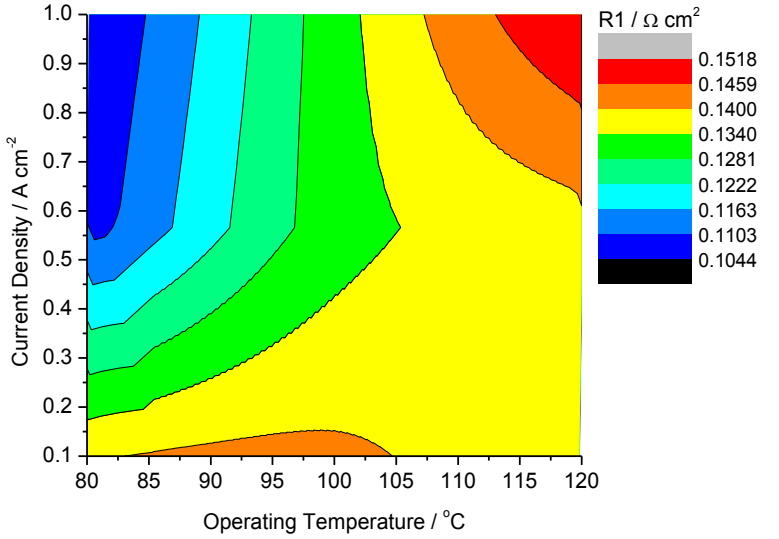
R1 / Ω cm²
0.1518
0.1459
0.1400
0.1340
0.1281
0.1222
0.1163
0.1103
0.1044
Current Density / A cm⁻²
Operating Temperature / °C
1.0
0.9
0.8
0.7
0.6
0.5
0.4
0.3
0.2
0.1
80
85
90
95
100
105
110
115
120

(e)

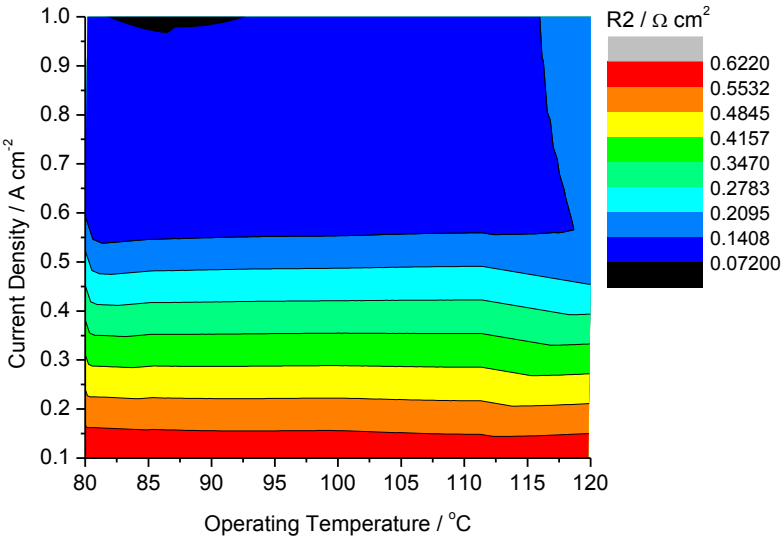
R2 / Ω cm²
0.6220
0.5532
0.4845
0.4157
0.3470
0.2783
0.2095
0.1408
0.07200
Current Density / A cm⁻²
Operating Temperature / °C
1.0
0.9
0.8
0.7
0.6
0.5
0.4
0.3
0.2
0.1
80
85
90
95
100
105
110
115
120

(f)

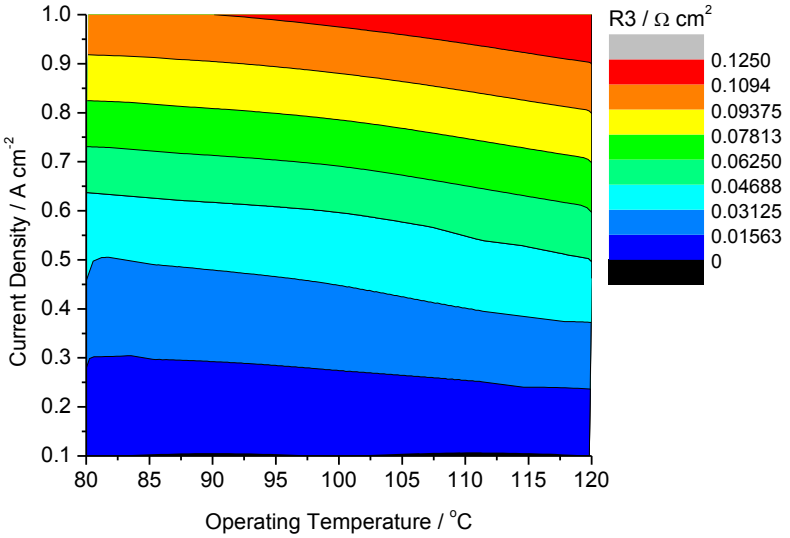

Figure 5.4: Impedance data for 25BC (with MPL) at 0.1, 0.5 and 1.0 A cm^{-2} for (a) 80 ^{o}C, (b) 100 ^{o}C, (c) 120 ^{o}C and equivalent circuit modelled data as a function of current density and operating temperature for (d) R1 (ohmic resistance), (e) R2 (charge transfer resistance) and (f) R3 (mass transport resistance)

Figure 5.4 (a-d) shows that the 25BC MEA ohmic resistance changes with current density and temperature. This effect is most pronounced at 80 ^{o}C, where the ohmic resistance decreases as the current density increases. However, at the higher operating temperatures of 100 and 120 ^{o}C, the ohmic resistance does not change as significantly as the current density. This effect can also be observed for the 25BA MEA in Figure 5.3 (c) where the ohmic resistance at 0.5 A cm^{-2} 80 ^{o}C is lower than at 100 or 120 ^{o}C. The reason for this decrease in ohmic resistance at 80 ^{o}C as the current density increases is that the water generated by the fuel cell reaction is hydrating the membrane and therefore increasing the cell performance. Furthermore, by this water being “taken up” by the membrane, the amount of water in the electrode is therefore reduced and the associated mass transport resistance is lower. However, in the case of the higher operating temperatures (100-120 ^{o}C) the MEA ohmic resistance is higher:

- This is because a majority of the water should exist in the vapour phase, therefore the membrane is unable to take up as much water to improve electrolyte conductivity.

- Furthermore, as the water exists in both the vapour phase (close to catalyst layers) and liquid phase (within the GDL and flow field) the main mechanism of water removal from the catalyst layer would be by diffusion and therefore in order to increase the rate at which water is removed, a greater diffusion gradient should exist. This is illustrated in Figure 5.4 (f) which shows the mass transport resistance as a function of operating temperature and current density.

- From Figure 5.4 (f), at low current densities, the mass transport resistance is negligible as expected. As the current density increases, the mass transfer resistance increases also. At the higher current densities, the operating temperature begins to play more of a role, which as previously described is due to the water existing in the vapour phase.

- Figure 5.4 (e) shows how the charge transfer resistance changes with both temperature and current density. As expected, the charge transfer resistance decreases as the current density increases. However, the operating temperature does not seem to have a significant effect on the charge transfer resistance.

Another major trend that is shown in Figure 5.2 and Figure 5.3 is that both the ohmic resistance and the mass transport resistance are greater for the 25BA MEA (without MPL) than the 25BC MEA (with MPL). From the figures shown, there are three contributing factors to the difference in the MEA ohmic resistances, namely;

I. Increased water retention by the MPL

II. Enhancement of the electrical properties of the GDL resulting in a decrease in the ohmic resistance of the MEA.

III. A more cohesive catalyst layer forming on the MPL surface resulting in an enhanced electrical contact between the catalyst layer and the GDL

In conventional PEFCs, GDLs with an MPL have been shown to better manage water transport resulting in an overall enhancement of cell performance [11,74–78]. The results obtained here indicate that this applies for both conventional operating temperatures and higher operating temperatures. The MPL reduces the amount of water saturation required to break through the GDL out to the flow field channel [49]. This results in much lower mass transfer resistance as the water does not accumulate at the GDL surface resulting in catalyst layer flooding or blockage of GDL pores. Thus the “effective porosity” of the GDL in the 25BC is higher than that of the 25BA.

Another aspect that should be taken into account is the intrusion of the catalyst layer into the GDL as this will affect the contact between the membrane and the catalyst layer and therefore will affect the ionic conductivity. For this purpose, both optical microscope and SEM images were used to compare the catalyst layers and the base GDLs.

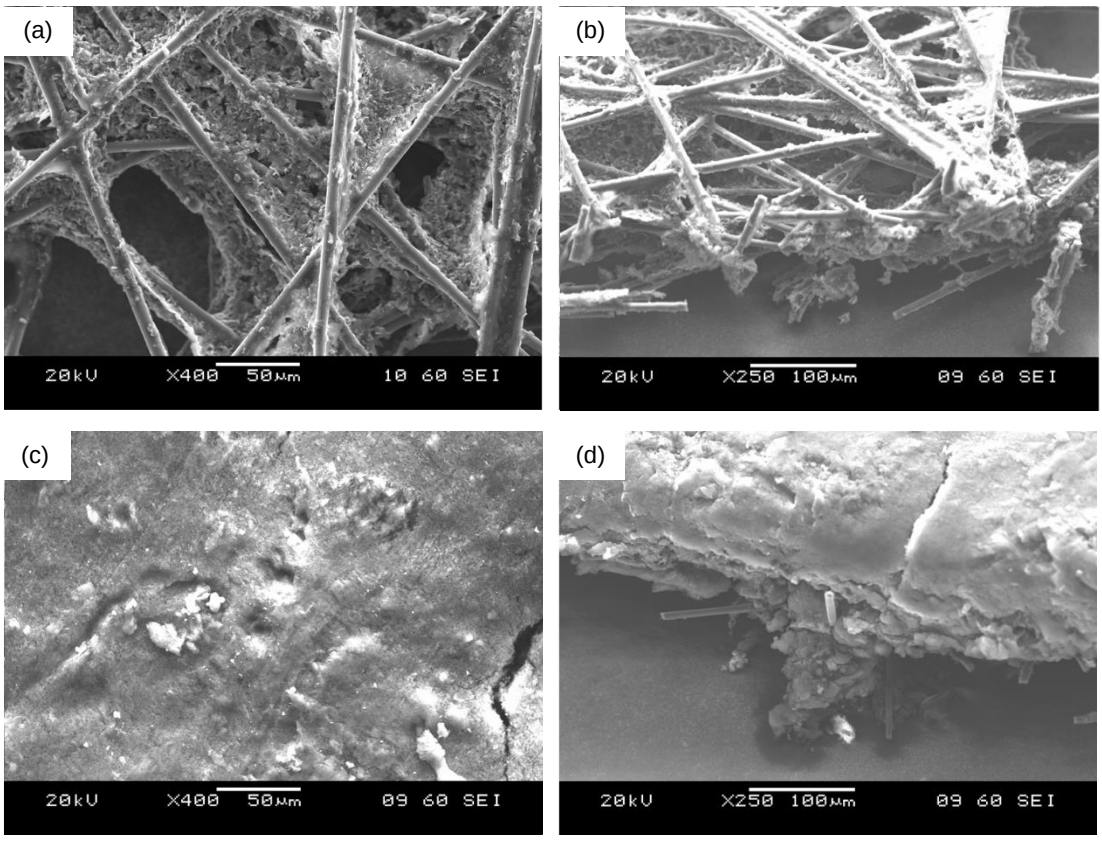

Figure 5.5: SEM images for 25BA (without MPL): (a) surface view, (b) cross section and 25BC (with MPL): (c) surface view of MPL (backing layer is same as 25BA and (d) cross section.

Figure 5.5 (a) and (c) show the difference in surface morphology for the 25BA and 25BC GDLs. Both of these GDLs share the same backing structure however it is possible to see that adding in the MPL will have a large impact on the catalyst layer when it is applied. From Figure 5.5(a) it can be seen that the pore sizes are much larger than those in (c). Figure 5.5(b) and (d) show side profile views of the GDLs. From these images, it becomes apparent that the 25BA has a much more exposed 3D structure compared with the 25BC where the MPL forms a cohesive smooth layer for electrode application. Images were then taken of the two GDLs with the catalyst layers applied.

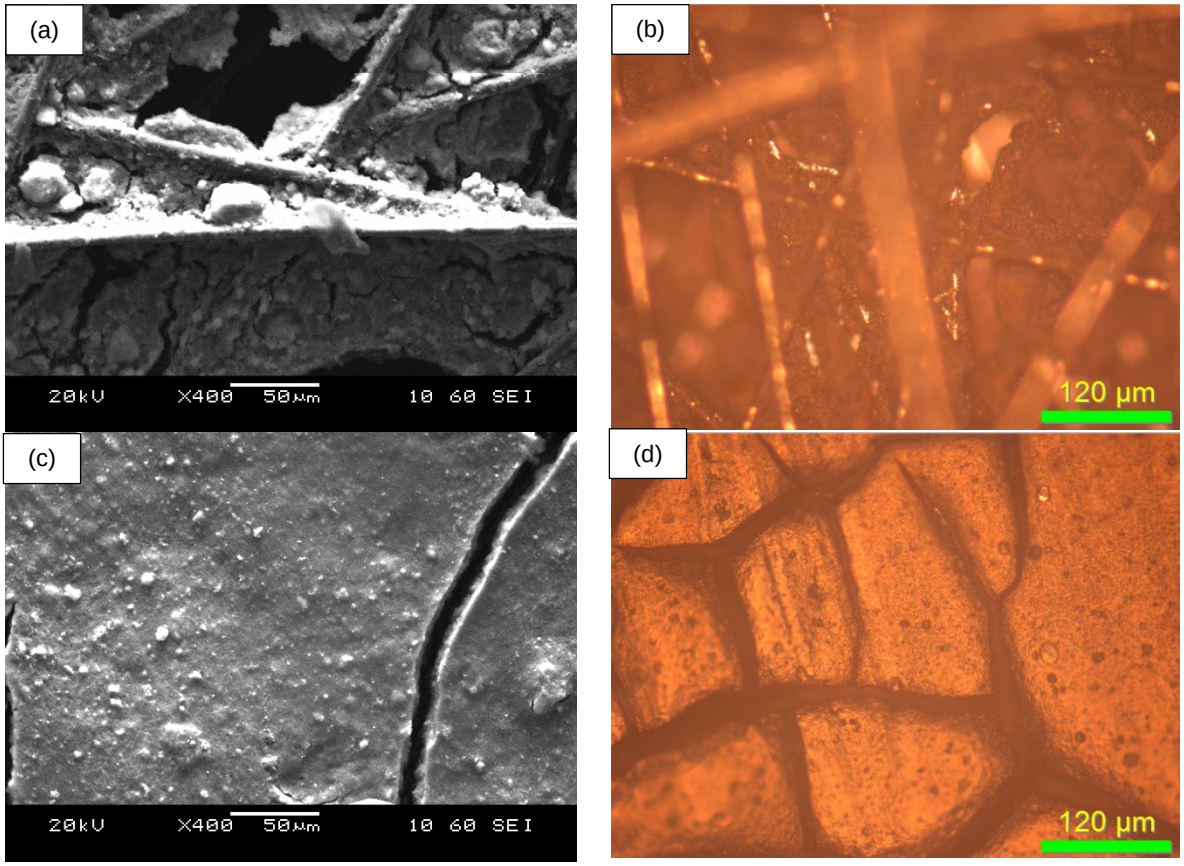

Figure 5.6: Images of catalyst layers on 25BA (without MPL) using an: (a) SEM, (b) Optical Microscope and 25BC (with MPL) using an: (c) SEM, (d) Optical Microscope.

From Figure 5.6 it is clear that the catalyst layer on the 25BC GDL is a lot more cohesive than the catalyst layer on the 25BA GDL. The 25BA electrode has hardly any surface area upon which to apply an electrode. This means that any excess ink will "fall into the holes" but will be rendered ineffective as it does not form a triple phase boundary. Therefore, this intrusion into the GDL results in a smaller effective surface area which means that the contact area with the membrane is small. Assuming that the SEM images (Figure 5.5 and Figure 5.6) are representative of the entire GDL surface, the calculated effective surface area for ink application of the 25BA is approximately 6 %. However, when comparing the polarisation curves, it is obvious

that the 25BA does not have 6 % the performance of the 25BC electrode. This is because the effective surface area will also comprise of the PTFE within the electrode. Furthermore, the effective surface area will increase when the electrode is compressed as more of the intruded catalyst layer will be in contact with the membrane. On the other, the MPL forms a more cohesive structure which means that the effective electrode area is much higher and therefore leads to better contact and better performance.

From the data shown, the following conclusions can be drawn;

I. The ohmic resistance increases with cell temperature which is due to the decreasing membrane hydration.

II. The electrode charge transfer resistance does not change significantly with operating temperature so the activity of the catalyst layer does not change with operating temperature.

III. The mass transfer resistance increases with operating temperature at high current densities. At high operating temperatures and current densities, the water will exist mostly in the liquid phase which results in an apparent increase in mass transport resistance with respect to operating temperature and relative humidity. This means that high operating relative humidities may not necessarily be best for intermediate temperature operation from a mass transport perspective and care must be taken to optimise the relative humidity and electrode design with respect to MEA requirements.

5.3.2 Influence of Relative Humidity and MPL on the MEA Performance

The influence of the relative humidity and the MPL on the MEA performance was assessed by testing the MEAs at 120 ^{o}C over a range of relative humidities. Results from the polarisation curves from these tests are shown in Figure 5.7.

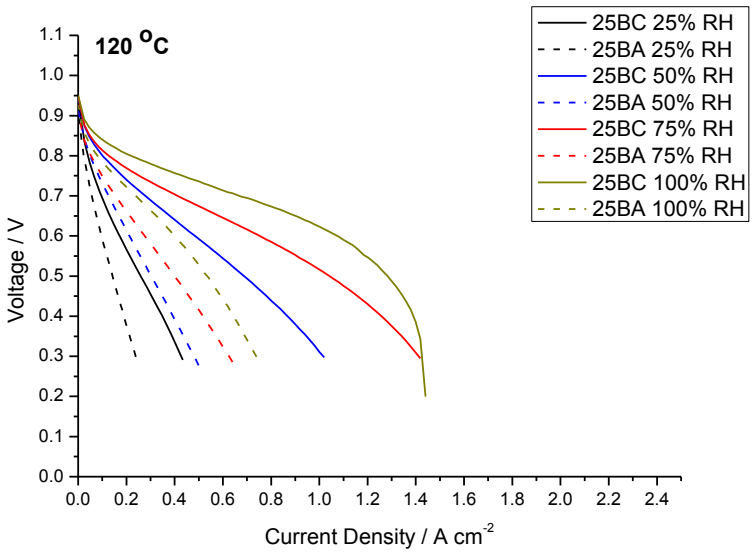

Figure 5.7: Polarisation Curves for the MEAs 25BA (without MPL) and 25BC (with MPL) at 120 ^{o}C

From Figure 5.7 several general trends can be seen. As the relative humidity is increased, the performance of the MEA increases. This is true for both the 25BA and 25BC electrodes. However, in the case of the 25BC electrode, when the relative humidity is increased to 100 %, a mass transfer limited current is reached. At higher relative humidities, the incoming air has a high partial pressure of water and thus as the current density increases, the air is unable to remove enough water to reduce the slowdown in the fuel cell reaction. This results in the flooding which is observed. This

limiting current effect isn't noticed in the 25BA electrode, which is most likely due to the smaller amount of water present within the electrode.

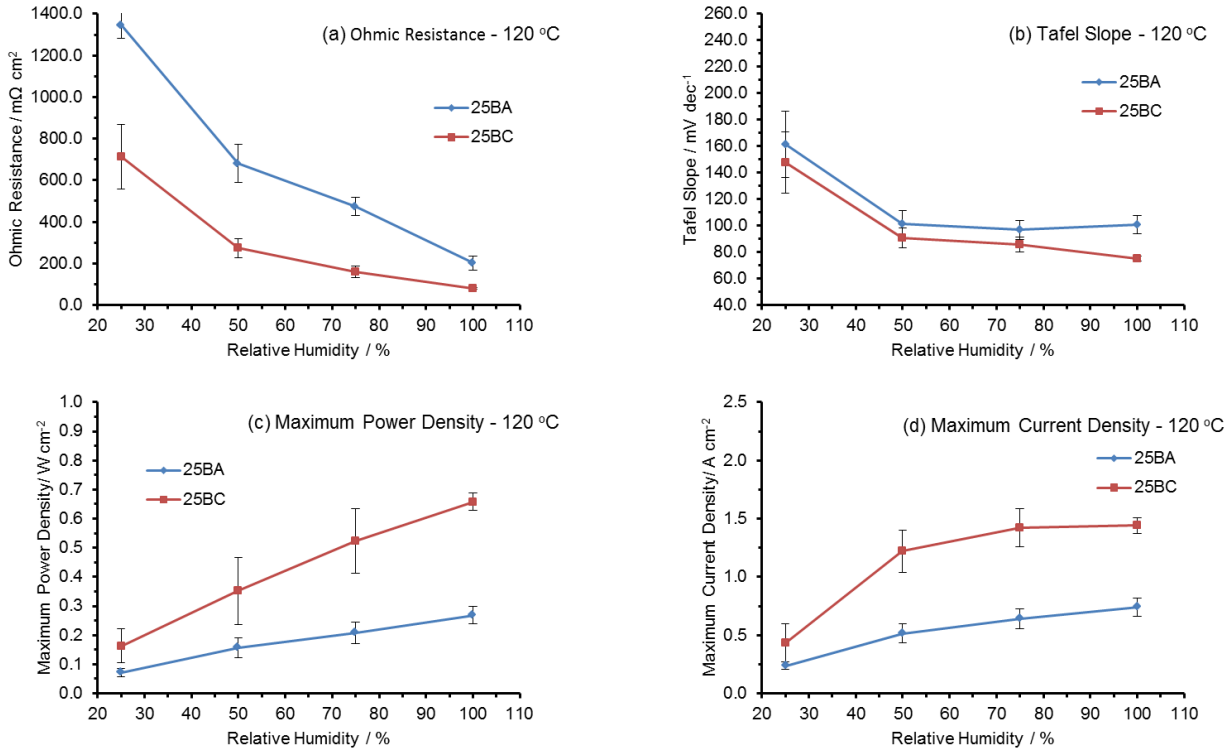

Figure 5.8: measurements for 25BA (without MPL) and 25BC (with MPL) for (a) ohmic resistance, (b) Tafel slope, (c) maximum power density and (d0 current density at 0.3 V

With regards to the ohmic resistance, Figure 5.8(a) shows that for both the electrode with the MPL and without the MPL, the ohmic resistance of the MEA decreases as the inlet humidity is increased. This is expected as in both cases, the membrane hydration increases thus increasing the membrane ionic conductivity. From Figure 5.8 (b), the Tafel slope also decreases as the relative humidity increases, indicating that the cathodic reaction kinetics increase as the inlet relative humidity increases from 25 % to 50 %. However, further increases in relative humidity do not decrease the Tafel slope significantly. In the case of maximum power density (Figure 5.8 (c)), values for

both electrodes increase as the inlet relative humidity increases, which is related to the increase in the membrane conductivity. On the other hand, the maximum current density (Figure 5.8 (d)) stops increasing beyond 75 % RH for the 25BC electrode as the limiting current is reached. The electrode without the MPL has a much lower maximum power density and current density at the higher relative humidities which is due to the GDL. Confirmation of this is seen when looking at the impedance data for the electrode at these different relative humidities (Figure 5.9).

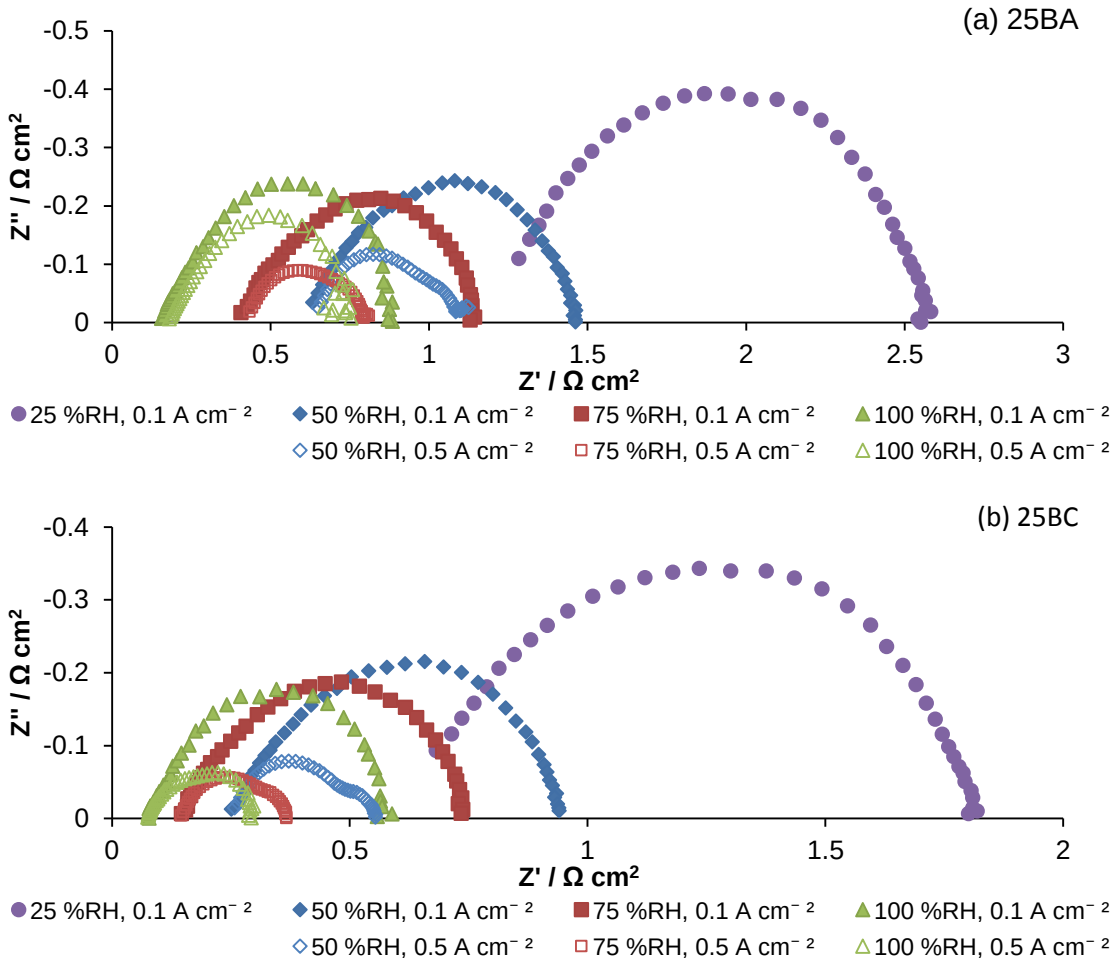

Figure 5.9: Impedance spectra for (a) 25BA at 0.1 A cm^{-2} and at 0.5 A cm^{-2}, and (c) 25BC at 0.1 A cm^{-2} and at 0.5 A cm^{-2}

Figure 5.9 (a) and (b) clearly show that the MEA ohmic resistance decreases as the relative humidity increases which is attributed to an increase in the electrolyte conductivity. Furthermore, in both cases at 0.1 A cm^{-2}, the charge transfer resistance is also decreasing as the relative humidity increases which indicates that the lack of hydration affects the rate at which the ORR can proceed. In the case of 25BA (without MPL), Figure 5.9 (a) shows that at 0.5 A cm^{-2}, the mass transport resistance (low frequency arc) within the electrode is increasing with relative humidity and this resistance dominates at the 100 % RH. Whilst the mass transport resistance also increases in Figure 5.9 (b) for 25BC at 0.5 A cm^{-2}, the magnitude of the increase is not as large. This indicates that the electrode with the MPL is better able to transport the product water from the electrode and better able to supply reactants to the active sites.

From the data shown it is possible to conclude the following:

I. As the inlet relative humidity increases, the MEA ohmic resistance decreases which is attributed to the hydration of the membrane.

II. The Tafel slope decreases as the inlet relative humidity increases from 25 % to 50 % however does not decrease further.

III. The GDL with the MPL is better able to remove product water from the electrode and supply the electrode with reactant gases. This means that the electrode with the MPL has a higher maximum current density and power density. However, there are mass transport limitations at higher relative humidities.

5.4 Conclusions

In this work, the influence of the MPL with respect to operating temperature and operating relative humidity has been studied extensively in order to ascertain its influence over MEA performance.

As the MEA operating temperature increased, the MEA ohmic resistance was found to also increase. This was attributed to the membrane becoming dehydrated as the temperature increased. It was also found that the electrode charge transfer resistance did not change significantly with the operating temperature. However, as expected, the charge transfer resistance reduces as the current density increases. The mass transport resistance was also found to increase as the operating temperature increased. It is difficult to confirm the precise phase of the water from within the electrode due to the pressure within the test set up (2.8 bar absolute pressure). The phase of the water likely causes the phase of the water to change from vapour to a liquid as the water is further removed from the higher temperature catalyst layer. As a result, mass transport still appears to be an issue. However, if closer to ambient pressure was used (1 bar), then it is expected that the phase of the water would remain in the vapour phase which should reduce the mass transport resistance at intermediate temperature.

It was also found that the presence of the MPL for IT-PEFC performance is important. The electrode containing the MPL saw a significant improvement in performance, in some cases as much as a 4 fold increase, over the electrode without the MPL. With respect to the quality of the catalyst layer produced, the electrode with the MPL had a much more cohesive catalyst layer than the electrode without the MPL such that the

catalyst layer “falls” into the pores of the electrode without the MPL due to the lower effective surface area for an electrode to be applied upon the GDL surface. This leads to an increase in the ohmic resistance as there is poorer contact between the catalyst layer and the membrane which can be confirmed via impedance spectroscopy. The MPL also aids in keeping the membrane hydrated at higher operating temperatures, helping to reduce the MEA ohmic resistance and improving the performance.

As the operating relative humidity increased, so did the MEA performance which is to be expected as the membrane became more hydrated thus reducing the MEA ohmic resistance. It was also found that the Tafel slope decreased as the relative humidity increased from 25 % to 50 % RH, however does not decrease significantly above 50 % RH. Finally, the electrode with the MPL was found to have a higher performance than the electrode without the MPL as the relative humidity was increased. This is because the MPL aids in the removal of the water from the electrode.

From this study, it was found that an ideal electrode material for use at IT-PEFC will contain an MPL. It was also found that if IT-PEFCs are to be seriously considered for widespread usage, novel membrane materials must be developed which are better able to retain the water and thus conductivity at intermediate temperature. However, with conventional membrane materials, which are not designed for IT-PEFC usage, the rate of water loss at intermediate operating temperatures is too high at lower operating relative humidities and thus the membrane water loss becomes the limiting factor to the advancement of the technology.

CHAPTER 6

Understanding the Role of Hydrophobic Treatment of the GDL using PTFE for MEAs at Intermediate Temperature

"A really good Hydrophobe has to be trained on dehydrated water from birth"

Terry Pratchett, 1983

Chapter 6 Understanding the Role of Hydrophobic Treatment of the GDL using PTFE for MEAs at Intermediate Temperature

6.1 Introduction

One aspect of the GDL that is very important to consider is it's propensity to retain water. This is particularly a problem at low temperature where liquid water is formed at the cathode. Liquid water is notorious for being adhesive due to the potential for hydrogen bonds to form with the substrate it is on. Therefore, control of the substrate hydrophobicity is of paramount importance. Hydrophobic treatment of the carbon paper or cloth is used to control the wettability in order to aid in the removal of the saturating water within the cathode [75,95]

The hydrophobicity is controlled using treatment with various agents. For example, Teflon® (Polytetrafluoroethylene PTFE) [11,112,113], fluorinated ethylene propylene (FEP) [114,115] and polyvinylidene fluoride (PVDF) [116]. Application of this hydrophobic treatment is done using all of the usual methods, for example, spray coating, dip coating, brushing etc. The trade-off for this control in the hydrophobicity is that the porosity is decreased, tortuosity is increased and the pore size is decreased which all reduce the ability for the GDL to transport reactants to the catalyst layer thus affecting mass transport.

Current work within the literature is focused on understanding the influence of the hydrophobic treatment on the performance of the MEA as well as optimising the

loading of the hydrophobic material within the GDL. It has been found in many studies that using hydrophobic treatment of the GDL aids in the removal of waste water and thus is preventing flooding of the cathode [75,95]. The reasons for this improvement are that the hydrophobic treatment changes the interfacial energy between the water droplets and the GDL. This means that water is less likely to saturate the GDL and is easier to remove from the pores, which in turn increases the rate of diffusion for the reactant gases. However, the aforementioned disadvantages of this process cause an increase in the mass transport limitations of the MEA. Thus a fine balance is required. To the authors' knowledge, no work has been done to investigate the influence of the hydrophobic treatment of the GDL at intermediate operating temperature. Indeed, due to the potential for the phase change of the water from a liquid to a vapour, it may be that treatment of the GDL is ineffectual to cell performance for an IT-PEFC.

In this study, the influence of hydrophobic treatment using Teflon on MEA performance is assessed by comparing MEAs with and without Teflon treatment at both conventional operating temperatures and intermediate temperatures. A range of relative humidities are also used in order to assess the ability of the GDLs to manage the amount of water within the cell as well as the impact this has on cell performance.

6.2 Experimental

6.2.1 MEA Production and Testing

For the purpose of studying the influence that teflonation has on the MEA performance, the materials P75 (without teflonation) and P75T (with teflonation) (Ballard) were chosen. This is because both of these GDLs share the same substrate structure and thus changes in electric conductivity, density and the influence of the substrate

structure can be considered negligible. The properties of these two GDLs are summarised in Table 6.1 (adapted from [193]).

Table 6.1: Key properties of P75 and P75T

Properties	**Gas Diffusion Layer**	
	P75	**P75T**
Thickness / µm	230	255
Area Weight / g m^{-2}	75	88
Real Density / g cm^{-3}	2.083 $\pm$ 0.005	2.087 $\pm$ 0.003
Bulk Density / g cm^{-3}	0.35	0.36
Porosity / %	62.4	59.9
Tortuosity	2.43	2.23
Mean Pore Diameter / nm	2074	1227
Permeability / m^2	1.11 x 10^{-11}	1.31 x 10^{-11}
Water Contact Angle / °	107 $\pm$ 7	113 $\pm$ 3

Membrane electrode assembly (MEA) fabrication was carried out by using the method suggested by Kim et al. [213]. Catalyst inks were produced by ultrasonically mixing commercially available Pt/C catalyst (Tanaka Kikinzoku Kogyo, 45.9 wt % Pt/C), solvent (IPA) and Nafion solution (10 wt%, Ion power). This ink was then hand painted onto the GDL of interest (5 cm^2, P75 and P75T, Ballard) to produce the cathode gas diffusion electrode (GDE). The active area of all MEAs was 5 cm^2 with a catalyst loading of 0.4 mg_{Pt} cm^{-2}.

The anode GDE was produced by painting a thin layer of Nafion solution (with a Nafion dry weight of 0.6 mg cm^{-2}, 5.8 µL cm^{-2} from a 10 wt% solution (ionpower)) onto commercial GDE (Johnson Matthey, Pt loading: 0.4 mg_{Pt} cm^{-2}, GDL: 34BC Sigracet). The anode GDE and the cathode GDE were then placed on either side of a Nafion 212 membrane (ion power) before being hot pressed at 125 ^oC for 120 s under a pressure

of 600 psi. To check for reproducibility, 3 MEAs for each GDL were produced and tested.

The MEA was then tested using a Scribner 850e Fuel Cell Test Station with EIS capabilities. All tests were conducted at 80, 100 and 120 ^{o}C and a back pressure of 1.8 bar. The relative humidity (RH) at the cell inlet was varied between 25 % and 100 % RH. Constant flow rates of 0.2 L min^{-1} and 0.5 L min^{-1} were used to supply the anodic (hydrogen) and cathodic (air) gases respectively. All MEAs were preconditioned before testing by operating the cell at a constant potential (0.6V) for 10 hrs. A polarisation curve was obtained at each operating condition by current scanning between open circuit voltage and 0.3V.

The electrode surface morphology was characterised using a JEOL 6060 scanning electron microscope (SEM).

From the polarisation curves obtained, it was possible to derive values for the ohmic resistance, which will give information on the cell ohmic resistance, the maximum current density (defined as the current density at 0.3 V) and the maximum power density produced by the different MEAs which give information on how well each GDL is able to transport water from the cell as well as the overall cell efficiency. The ohmic resistance was worked out by using the inbuilt current interrupt analyser on the test stand.

6.2.2 Impedance Spectroscopy

In-situ impedance spectroscopy was conducted using the impedance analyser from the Scribner 850e test stand. Impedance spectroscopy was recorded at current

densities of 0.1, 0.5 and 1 A cm^{-2} at the respective operating temperature. In order to ascertain the fuel cell resistances, a frequency scan between 1 Hz and 10 kHz was used. The equivalent circuits [204] shown in Figure 6.1 were used to analyse the different sources of resistance within the cell. In all of the cases, the charge transfer resistance is assumed to be for the cathodic oxygen reduction reaction (ORR) only as the resistance of anodic hydrogen oxidation reaction (HOR) is assumed to be negligible [204].

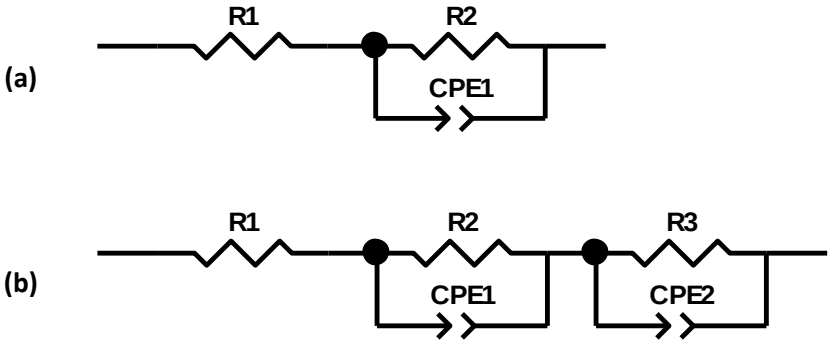

Figure 6.1: Equivalent Circuits used to describe the ohmic resistance and the charge transfer resistance for (a) 0.1 A cm^{-2}, (b) 0.5 A cm^{-2} and 1 A cm^{-2}, where R1 is the cell ohmic resistance, R2 is the charge transfer resistance, R3 is the mass transfer resistance, CPE1 is the constant phase element of the charge transfer resistance and CPE2 is the constant phase element for the mass transfer resistance [204].

6.3 Results and Discussion

6.3.1 Influence of Temperature and Hydrophobic Treatment on the MEA Performance

MEAs were constructed using P75 (without Teflonation) and P75T (with Teflonation) as the cathodic GDL over a range of temperatures (80, 100 and 120 ^{o}C) and with a constant relative humidity of 75 %. This was so that the influence of hydrophobic

treatment of the GDL on MEA performance at intermediate operating temperatures could be assessed.

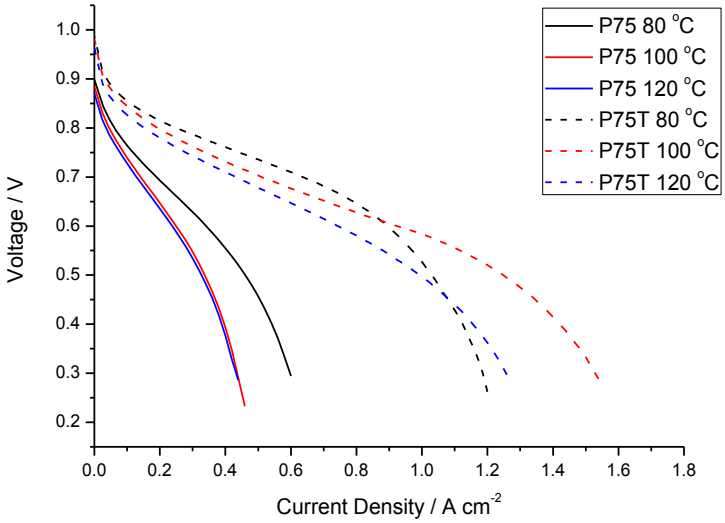

Figure 6.2: Polarisation curves for MEAs with P75 (without Teflonation) and P75T (with Teflonation) at 80 ºC, 100 ºC and 120 ºC; RH = 75%

From Figure 6.2 it is clear that P75T shows much higher performance than that of P75. Both the P75 and the P75T show a decrease in MEA performance as the operating temperature increases. This is primarily due to dehydration of the Nafion, which leads to an increase in the MEA ohmic resistance as the protonic conductivity of the membrane is reduced (Figure 6.3). However, this ohmic resistance does not increase significantly from 100 ºC to 120 ºC (Figure 6.2). This can be seen from the polarisation curves for P75 for 100 ºC and 120 ºC where there is little difference. Furthermore, as the ohmic resistance is very high, the performance of the MEA is such that the water generated from the fuel cell reaction is insufficient to keep the membrane hydrated. This can be seen when the ohmic resistance obtained using the current interruption is

plotted against the MEA current density (Figure 6.3(d)). For P75 at 80 ^{o}C, the ohmic resistance decreases as the current density increases until a current density of 0.5 A cm^{-2} is obtained at which point the ohmic resistance begins to increase again. This is indicative that the membrane begins to dry. However, when the operating temperature is increased for P75 to 100 and 120 ^{o}C, as the current density increases, the ohmic resistance increases which indicates that this is the dominating factor in limiting MEA performance.

On the other hand for P75T, the MEA ohmic resistance is relatively lower than that of the P75. This can be seen from Figure 6.3(a) and (b). As the operating temperature of the P75T is increased from 80 to 120 ^{o}C, the ohmic resistance initially increases before reaching a plateau. This is not immediately obvious when comparing the polarisation curves. When looking at how the ohmic resistance changes with the current density (Figure 6.3(d)), it is shown that at 80 ^{o}C, the ohmic resistance decreases as the current density increases until a plateau is reached. This indicates that the water generated from the fuel cell reaction is sufficient to fully hydrate the membrane and thus the main limitation to MEA performance is the mass transport resistance (Figure 6.3(e)). This mass transport resistance is alleviated at 100 ^{o}C where the product water will exist as a higher percentage in the vapour phase. This leads to a greater performance despite higher ohmic resistance due to the high operating temperature dehydrating the membrane. Indeed, the MEA performance is such that the water generated is sufficient to cause a reduction in the ohmic resistance as the current density increases, overcoming the dehydration due to increased operating temperature. However, this rate of water generation is insufficient to overcome the dehydration of the membrane at 120 ^{o}C, where the ohmic resistance increases with current density. In this case,

there is a combination of ohmic resistance increasing with current density, and the generated water, which should exist mainly in the vapour phase. However, as has been mentioned previously, the pressure (2.8 bar) means that the water may still exist within the liquid phase. This, coupled with the fast reaction kinetics at higher temperatures, means that more water is generated and thus there is more mass transport.

In general however, it can be concluded that the presence of Teflon within the GDL is beneficial to the performance of the MEA. At conventional operating temperatures, it is commonly accepted within the literature that the hydrophobic treatment reduces the adhesive effect of the water droplets to the pore walls within the GDL [75,95] by changing the interfacial energy between the water droplets and the GDL. This aids in the reduction of mass transport resistance when compared with a non-treated GDL. As the operating temperature increases, the presence of Teflon is still beneficial. This is because in our test set up, the high pressure means that water exists mainly in the liquid phase. The Teflon prevents the water from adhering to the pore surfaces. Water existing in the vapour phase closer to the catalyst sites (due to the temperature gradient which exists within the MEA) are also prevented form condensing as the water is moved through the GDL [118,120–123].

(a)

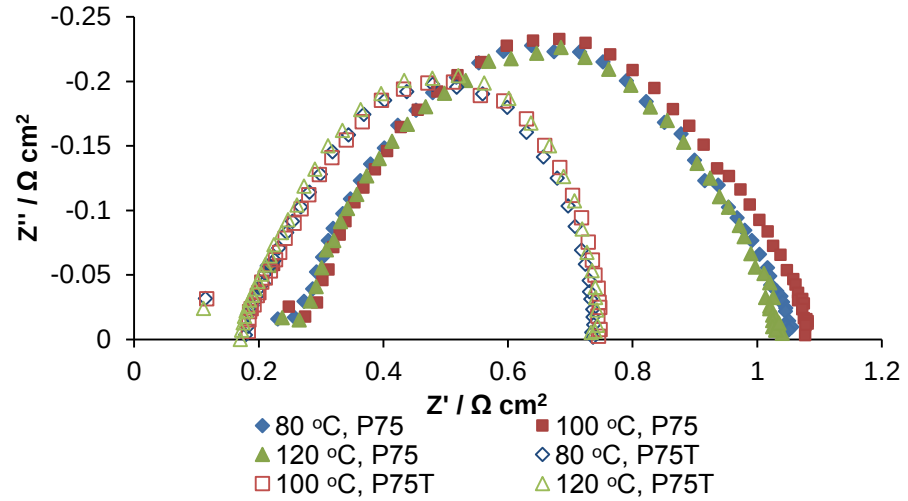
-0.25
-0.2
-0.15
-0.1
-0.05
0
Z'' / Ω cm²
0
0.2
0.4
0.6
0.8
1
1.2
Z' / Ω cm²
80 °C, P75
100 °C, P75
120 °C, P75
80 °C, P75T
100 °C, P75T
120 °C, P75T

(b)

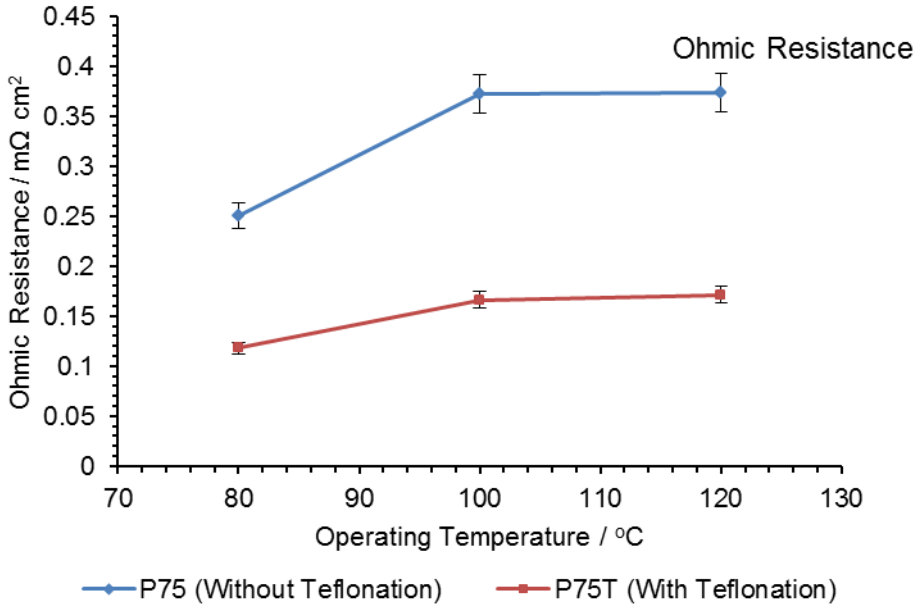
Ohmic Resistance
0.45
0.4
0.35
0.3
0.25
0.2
0.15
0.1
0.05
0
Ohmic Resistance / mΩ cm²
70
80
90
100
110
120
130
Operating Temperature / °C
P75 (Without Teflonation)
P75T (With Teflonation)

(c)

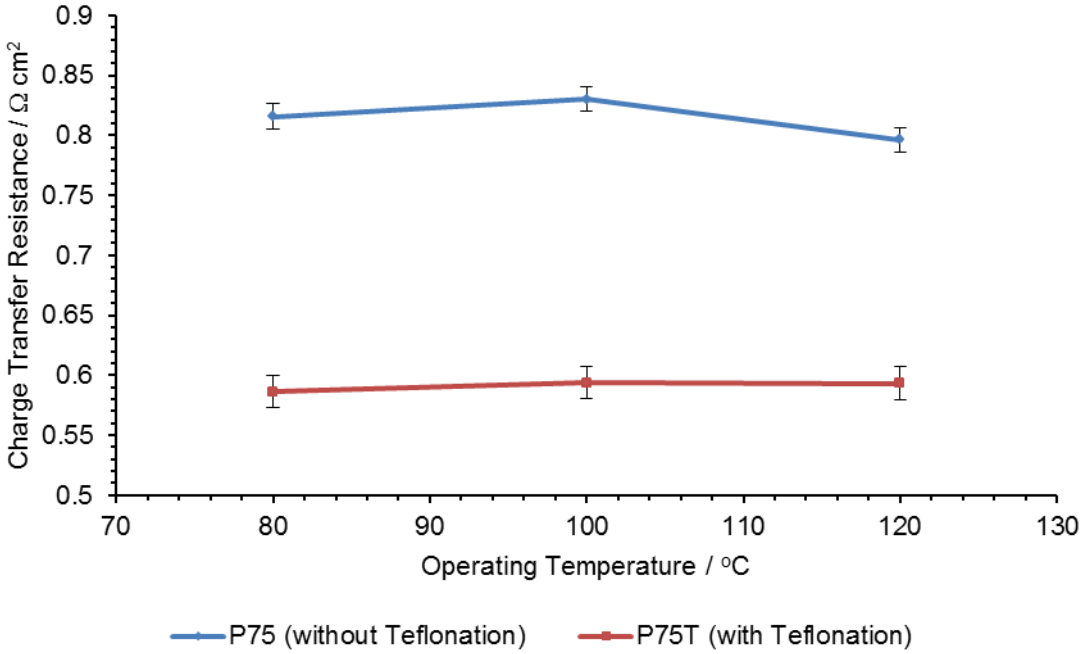
Charge Transfer Resistance / Ω cm2
0.9
0.85
0.8
0.75
0.7
0.65
0.6
0.55
0.5
70
80
90
100
110
120
130
Operating Temperature / oC
P75 (without Teflonation)
P75T (with Teflonation)

(d)

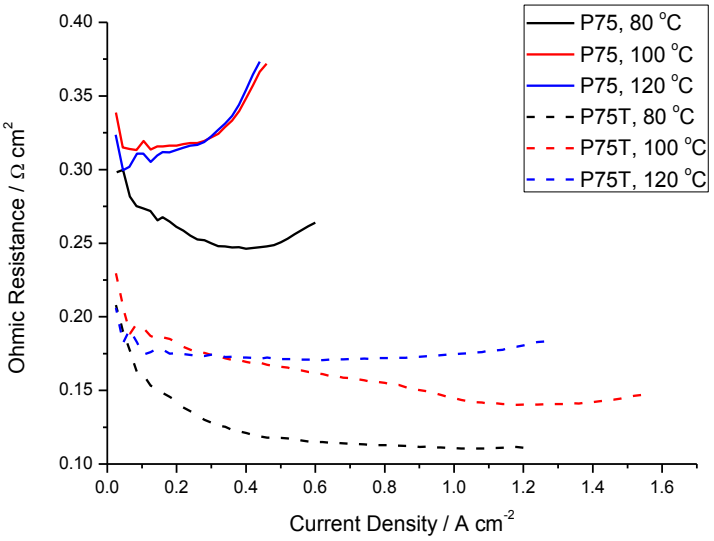
Ohmic Resistance / Ω cm2
0.40
0.35
0.30
0.25
0.20
0.15
0.10
0.0
0.2
0.4
0.6
0.8
1.0
1.2
1.4
1.6
Current Density / A cm-2
P75, 80 °C
P75, 100 °C
P75, 120 °C
P75T, 80 °C
P75T, 100 °C
P75T, 120 °C

(e)

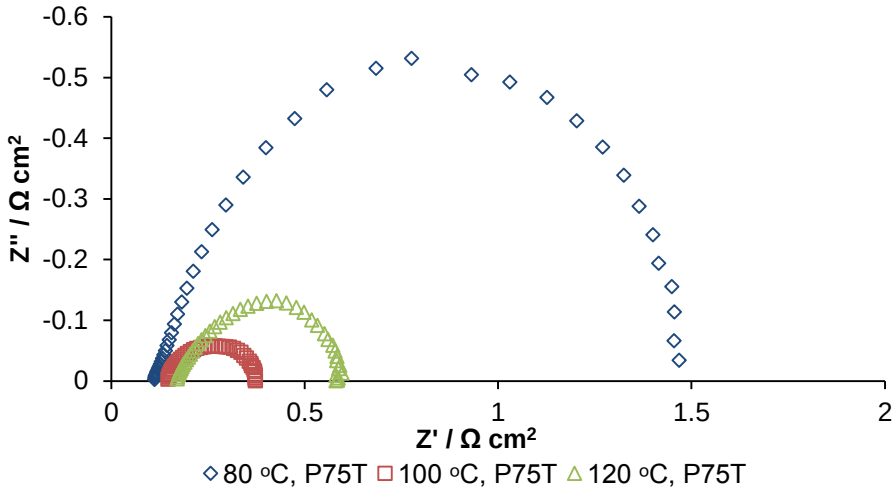

Figure 6.3: For P75 and P75T at 75%RH; (a) EIS at 0.1 A cm^{-2} from 80 °C to 120 °C, (b) Ohmic resistance with respect to the operating temperature, (c) the influence of the operating temperature on the charge transfer resistance, (d) Ohmic resistance with respect to the operating current density and (e) EIS at 1.0 A cm^{-2} from 80 °C to 120 °C.

6.3.2 Influence of Relative Humidity and Hydrophobic Treatment on the MEA Performance

The influence of the relative humidity and hydrophobic treatment on the MEA performance was then assessed by testing the MEAs at 120 °C over a range of relative humidities. The Polarisation curves are shown in Figure 6.4.

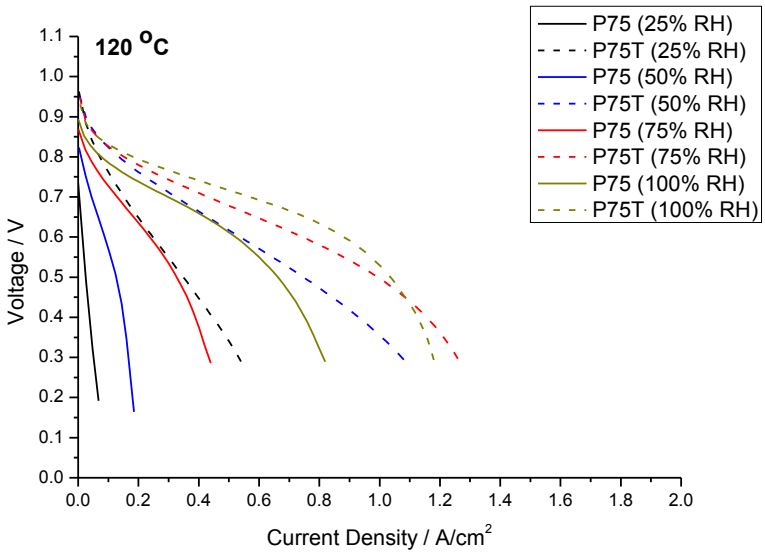

Figure 6.4: Polarisation curves for MEAs with P75 (without Teflonation) and P75T (with Teflonation) at 120 °C at different operating relative humidities

From Figure 6.4 several general trends can be observed. As in the previous case, the P75T MEAs with hydrophobic treatment performed significantly better than the P75 MEAs without this hydrophobic treatment. Furthermore, as the relative humidity increases, the MEA performance increases for all MEAs. This is mainly due to the membrane resistance which decreases as the relative humidity increases. This can be demonstrated using EIS, which shows how the ohmic resistance changes with relative humidity at 0.1 A cm^{-2} (Figure 6.5(a-c)). This is true for when both P75 and P75T are used as the GDL material. Furthermore, as the relative humidity increases, the charge transfer decreases. This is most likely a consequence of the ionomer within the catalyst layer becoming hydrated and therefore the resistance to the ORR decreasing. The change in ohmic resistance with respect to the current density is also shown (Figure 6.5(e-f)). This further reinforces that the ohmic resistance dominates overall MEA performance, which is mainly due to the membrane resistance.

When comparing the performance of the MEAs with respect to the GDL that is used, it is again clear that the P75T performs better than the P75 GDL at all relative humidities tested. At the low relative humidities, the superior performance of the P75T is most likely due to the Teflon preventing the build-up and saturation of the GDL with the waste water that is generated. At the higher relative humidities, there is a higher percentage of water existing in the liquid phase as the fuel streams become saturated, especially towards the exit of the cell. In this case, the presence of Teflon within the GDL prevents the water from sticking to the GDL walls which means that mass transport resistance is decreased. This water management aspect of the GDL can also be seen when comparing the change in ohmic resistance with respect to the current density. In Figure 6.5(e), the ohmic resistance of the cell is continuously increasing as the current density increases, indicating that this GDL is incapable of managing the water within the electrode to sufficiently keep the membrane hydrated. On the other hand, Figure 6.5 (f) shows the case of where the MEA ohmic resistance only changes significantly in the case of the 25% RH. This decrease in the ohmic resistance is most likely due to the membrane gaining conductivity from the water generated by the fuel cell reaction as the current density increases. In all of the other cases, the ohmic resistance does not change significantly as the current density increases.

(a)

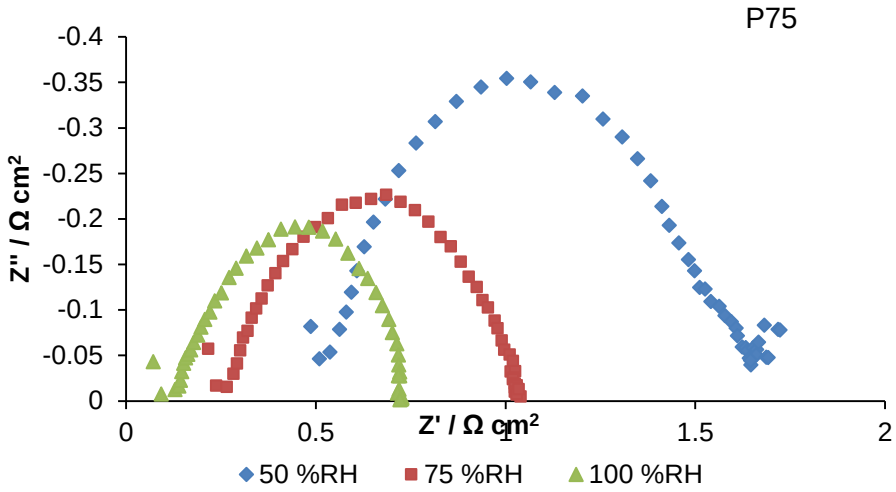
P75
Z'' / Ω cm²
-0.4
-0.35
-0.3
-0.25
-0.2
-0.15
-0.1
-0.05
0
0
0.5
1
1.5
2
Z' / Ω cm²
50 %RH
75 %RH
100 %RH

(b)

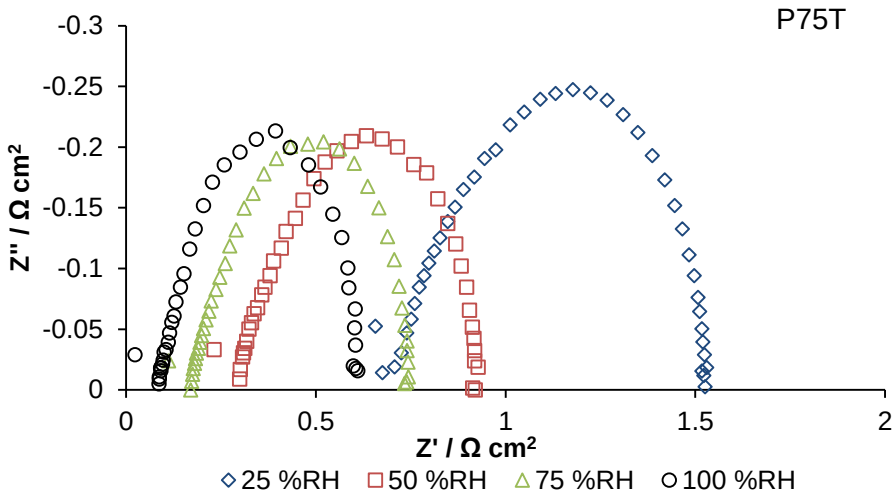
P75T
Z'' / Ω cm²
-0.3
-0.25
-0.2
-0.15
-0.1
-0.05
0
0
0.5
1
1.5
2
Z' / Ω cm²
25 %RH
50 %RH
75 %RH
100 %RH

(c)

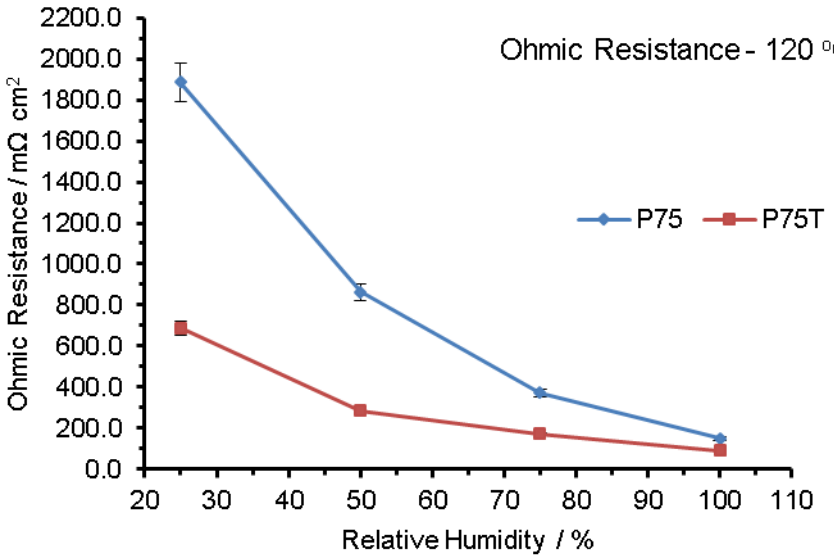
Ohmic Resistance - 120 °C
Ohmic Resistance / mΩ cm²
2200.0
2000.0
1800.0
1600.0
1400.0
1200.0
1000.0
800.0
600.0
400.0
200.0
0.0
20
30
40
50
60
70
80
90
100
110
Relative Humidity / %
P75
P75T

(d)

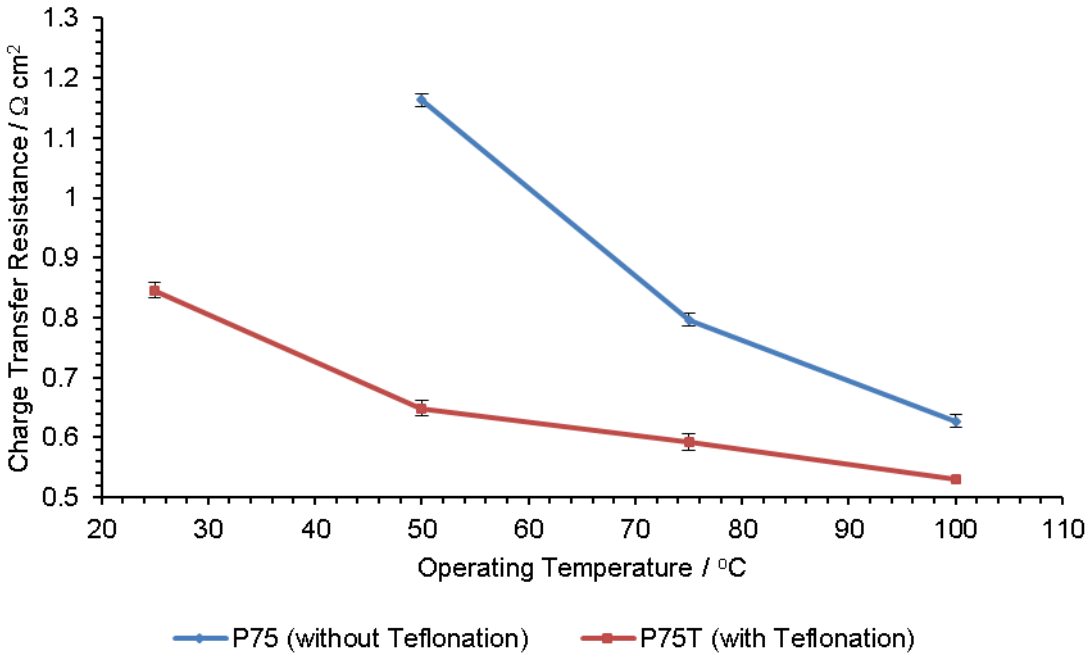
Charge Transfer Resistance / Ω cm2
1.3
1.2
1.1
1
0.9
0.8
0.7
0.6
0.5
20
30
40
50
60
70
80
90
100
110
Operating Temperature / 0C
P75 (without Teflonation)
P75T (with Teflonation)

(e)

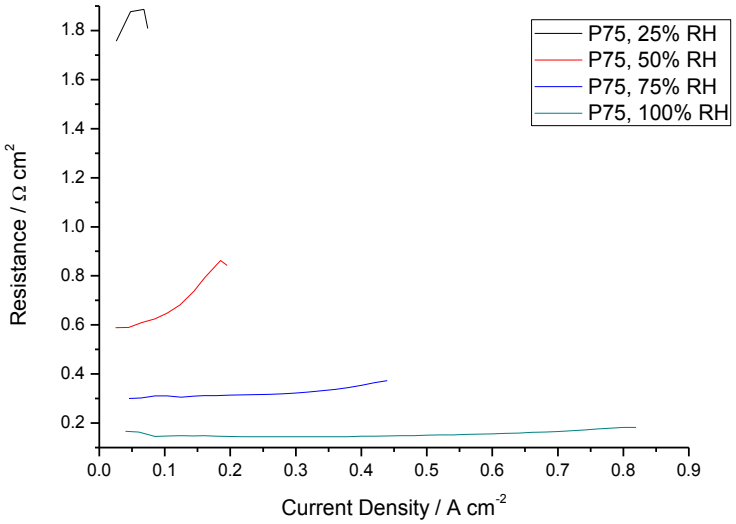
Resistance / Ω cm2
1.8
1.6
1.4
1.2
1.0
0.8
0.6
0.4
0.2
0.0
0.1
0.2
0.3
0.4
0.5
0.6
0.7
0.8
0.9
Current Density / A cm-2
P75, 25% RH
P75, 50% RH
P75, 75% RH
P75, 100% RH

(f)

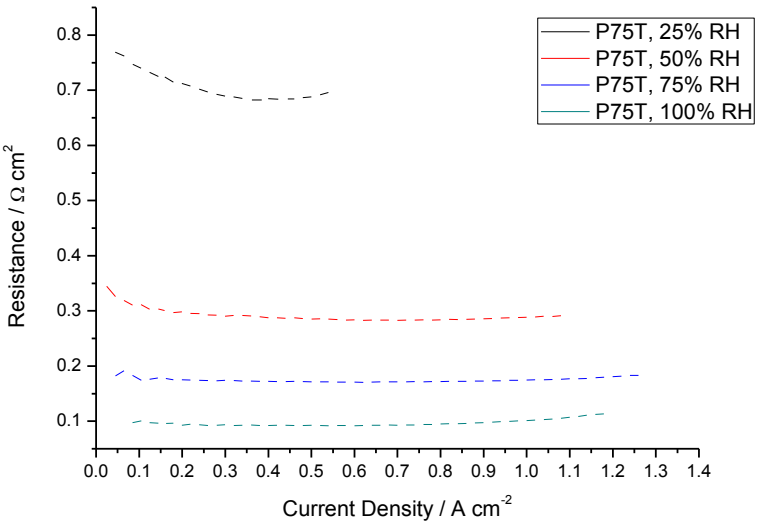

Figure 6.5: For P75 and P75T; (a-b) EIS at 0.1 A cm^{-2} from 25%RH to 100%RH at 120 ^{o}C, (c) Ohmic resistance with respect to the operating relative humidity, (d) the influence of the operating relative humidity on the charge transfer resistance and (e-f) Ohmic resistance with respect to the operating current density

6.4 Conclusions

In this work, the influence of Teflon treatment with respect to the operating temperature and operating relative humidity were studied using a combination of polarisation curves and EIS. This was done to inform whether Teflon treatment of the GDL is necessary when considering intermediate temperature operation.

As the operating temperature increased, the Teflon treatment of the GDL was found to be beneficial to MEA performance. At conventional operating temperatures, this is attributed to the hydrophobic treatment stopping the liquid water from sticking to the pore walls of the GDL as has been shown within the literature previously. As the operating temperature increases, there are competing effects at play, with the MEA ohmic resistance dominating the MEA performance as the membrane becomes more

dehydrated. Furthermore, due to the increased operating temperature, a high percentage of the product water should exist within the vapour phase close to the catalyst layer. It was found that at high temperature, the Teflon treated GDL gave superior performance to that of the GDL without hydrophobic treatment. This has been attributed to the Teflon preventing the water from adhering to the GDL pores as the water changes phase from vapour phase to liquid phase.

It was also found that the Teflon treated GDL showed better performance as the operating humidity was increased from 25% to 100% at 120 ^{o}C. In both cases the performance of the MEA increased, which has been attributed to a decrease in the MEA ohmic resistance due to the membrane remaining better hydrated with increasing operating humidity. However, the increase in performance when a Teflon treated electrode was used was greater than that of the non-Teflon treated GDL. At the lower relative humidities, this has been attributed to the Teflon treated GDLs' ability to keep product water within the membrane. At higher relative humidities, it is more likely that the air stream would become saturated with water vapour thus causing some water to condense out of the stream. In this case, as in the case of low temperature operation, the Teflon treated GDL prevents water from sticking within the pores, aiding in water removal.

From this study, it can be concluded that hydrophobic treatment of the GDL is necessary, even at intermediate temperature where the water should exist mostly in the vapour phase as the Teflon will prevent the water from adhering to the GDL pore surfaces as the water changes phase between vapour phase and liquid phase.

CHAPTER 7

Understanding the Role of GDL Thickness on MEA Performance at Intermediate Temperature

"Experimental confirmation of a prediction is merely a measurement. An experiment disproving a prediction is a discovery."

Enrico Fermi, n.d.

Chapter 7 Understanding the Role of GDL Thickness on MEA Performance at Intermediate Temperature

7.1 Introduction

The thickness of the GDL is one property which must be considered when designing a GDL for use at intermediate temperature. Current work within the literature has been conducted to understand the influence of GDL thickness with respect to low temperature operation [54,77,78,98]. It is commonly accepted that the thinner GDLs offer better mass transport characteristics, however suffer from water saturation and flooding. In contrast, the thicker GDLs are more resistant to flooding through saturation of the pores with water, however suffer from mass transport limitations due to the longer diffusion path length. Indeed, the thickness of the GDL was found to have a greater impact on the MEA performance than the PTFE content of the electrode. Another benefit of the thinner GDL is the lower electrical resistance compared with the thicker GDLs. However, no work has been conducted at intermediate temperature where the water should exist in the vapour phase. Therefore, the GDL thickness is important to consider as the change in phase of water should mean that water accumulation within the GDL should be reduced.

In this study, the influence of the GDL thickness on cell performance is assessed by comparing MEAs with the same structure and different thicknesses at both conventional operating temperatures and intermediate temperatures. A range of

relative humidities is also used in order to assess the ability of the GDLs to manage the amount of water within the cell as well as the impact this has on cell performance.

7.2 Experimental

7.2.1 MEA Testing

For the purpose of studying the influence that teflonation has on the MEA performance, the materials H-060, H-090 and H-120 (Toray) were chosen. This is because these GDLs share the same substrate structure and thus changes in electric conductivity, density and the influence of the substrate structure can be considered negligible. The properties of these GDLs are summarised in Table 7.1 (adapted from [193]).

Table 7.1: Key properties of H-060, H-090 and H-120

Properties	**Gas Diffusion Layer**		
	H-060	**H-090**	**H-120**
Thickness / µm	190	280	370
Real Density / g cm^{-3}	2.002 $\pm$ 0.003	2.019 $\pm$ 0.003	1.985 $\pm$ 0.004
Bulk Density / g cm^{-3}	0.44	0.44	0.45
Porosity / %	63.1	67.2	61.8
Tortuosity	2.76	2.55	2.51
Mean Pore Diameter / nm	2631	3324	1717
Permeability / m^2	6.15 x 10^{-12}	4.53 x 10^{-12}	3.90 x 10^{-12}
Water Contact Angle / º	129 $\pm$ 9	138 $\pm$ 8	121 $\pm$4

The membrane electrode assemblies (MEAs) consisted of commercial catalyst coated membranes (CCMs) (Johnson Matthey, Pt loading: 0.4 mg$_{Pt}$ cm^{-2}, membrane Nafion

212). Commercial Sigracet 34BC was used as the anodic GDL to ensure repeatability and reliability so that comparison between the cathodic GDLs. The produced MEAs were tested three times to ensure repeatability. The active area of all MEAs was 5 cm^2. For the cathode, three GDLs were used in this study; Toray H-060, H-090 and H-120.

The MEAs were then tested using a Scribner 850e Fuel Cell Test Station with EIS capabilities. All tests were conducted at 80, 100 and 120 ^oC and a back pressure of 1.8 bar. The relative humidity (RH) at the cell inlet was varied between 25 % and 100 % RH. Constant flow rates of 0.2 L min^{-1} and 0.5 L min^{-1} were used to supply the anodic (hydrogen) and cathodic (air) gases respectively. All MEAs were preconditioned before testing by operating the cell at a constant potential (0.6V) for 10 hrs. A polarisation curve was obtained at each operating condition by current scanning between open circuit voltage and 0.3V.

From the polarisation curves obtained, it was possible to derive values for the ohmic resistance, which will give information on the cell ohmic resistance, the maximum current density (defined as the current density at 0.3 V) and the maximum power density produced by the different MEAs which give information on how well each GDL is able to transport water from the cell as well as the overall cell efficiency. The ohmic resistance was worked out by using the inbuilt current interrupt analyser on the test stand.

7.2.2 Impedance Spectroscopy

In-situ impedance spectroscopy was conducted using the impedance analyser from the Scribner 850e test stand, directly connected to the electronic load. The impedance measurements were taken in galvanostatic mode using an AC signal amplitude

equivalent to 10% of the recorded current density (for example, at 0.1 A cm $^{-2}$ a current amplitude of 0.01 A cm $^{-2}$). Impedance spectroscopy was recorded at current densities of 0.1, 0.5 and 1 A cm^{-2} at the respective operating temperature. In order to ascertain the fuel cell resistances, a frequency scan between 1 Hz and 10 kHz was used, acquiring 10 points per decade. The equivalent circuits [204] shown in Figure 7.1 were used to analyse the different sources of resistance within the cell. In all of the cases, the charge transfer resistance is assumed to be for the cathodic oxygen reduction reaction (ORR) only as the resistance of anodic hydrogen oxidation reaction (HOR) is assumed to be negligible [204].

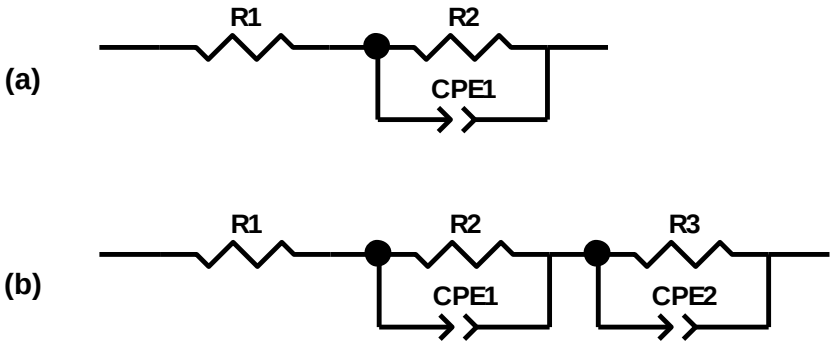

Figure 7.1: Equivalent Circuits used to describe the ohmic resistance and the charge transfer resistance for (a) 0.1 A cm^{-2} and 0.5 A cm^{-2}, and (b) 1 A cm^{-2} , where R1 is the cell ohmic resistance, R2 is the charge transfer resistance, R3 is the mass transfer resistance, CPE1 is the constant phase element of the charge transfer resistance and CPE2 is the constant phase element for the mass transfer resistance [204].

7.3 Results and Discussion

7.3.1 Influence of Temperature and GDL Thickness on the MEA Performance

The prepared MEAs were tested at three operating temperatures (80, 100 and 120 ^{o}C) to assess the influence of operating temperature and GDL thickness. The relative humidity for anode and cathode inlet was kept constant at 100 %.

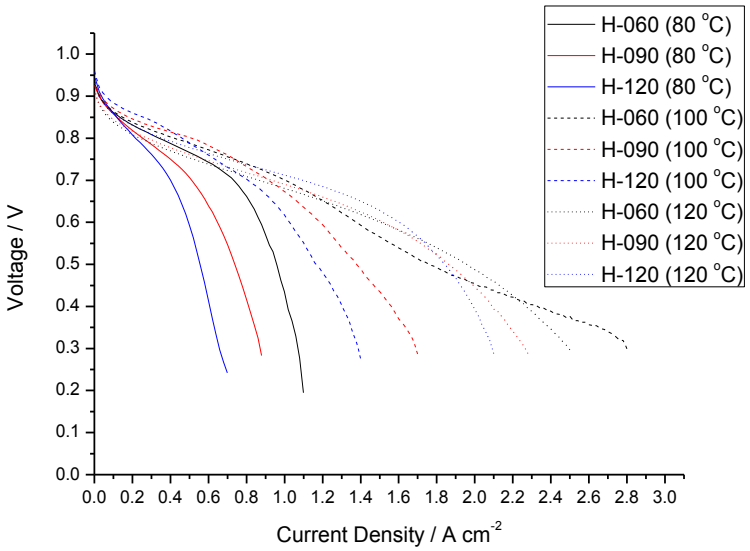

Figure 7.2: Polarisation Curves for the MEAs with H-060, H-090 and H-120 at 80 ^{o}C, 100 ^{o}C and 120 ^{o}C

When this data is compared to that of Figure 4.3 or other MEAs from the previous chapters, the performance is different. This is because the MEAs in this chapter are CCMs as opposed to CCS in previous chapters and therefore the MEA data presented here should be considered independent of the data presented in previous chapters. From Figure 7.2, it is clear that as the GDL becomes thicker, the MEA performance

decreases regardless of the operating temperature. This manifests in the mass transport resistance region of the polarisation curve. In order to better understand what different effects are influencing the polarisation curve, impedance spectroscopy and current interruption were used to obtain information about the different resistances within the cell (Figure 7.3). At all operating temperatures, the ohmic resistance is lowest when the H-120 is used as the cathodic GDL, followed by the H-090 and then the H-060 (Figure 7.3 (a)). This difference is most likely due to the increasing compression acting upon the GDL as the GDL thickness increases which results in better contact between the catalyst layer and the GDL as well as the between the GDL and the flow field plate. However, the difference in the ohmic resistance when H-060, H-090 and H-120 are used is smallest at 80 ^{o}C (ca.10 mΩ cm^{2}) and is largest at 120 ^{o}C (ca. 15 mΩ cm^{2}). This similarity in ohmic resistance is due to the high level of humidity of the reactant fuel streams which means that the Nafion membrane will remain well humidified and will have a high conductivity. Out of the GDLs, the H-120 GDL displays an ohmic resistance that is consistently the lowest at all temperatures, followed by the H-090, with the H-060 having the highest ohmic resistance. This is most likely due to the better electrical contact between the H-120 and the catalyst layer as the H-120 is thicker and has a higher level of compression which creates more contact points. This is followed by H-090 and then H-060.

Generally, the mass transfer resistance decreases significantly with operating temperature (Figure 7.3 (b) and (c)). From Figure 7.3 (b), even though there are single arcs within the EIS spectrum, this is solely due to mass transport with the charge transfer resistance arc being subsumed into the overall signal. Indeed, the highest mass transfer resistance at 100 and 120 ^{o}C is smaller than the lowest mass transfer

resistance at 80 ^{o}C. At 80 ^{o}C, the largest resistance is the mass transfer resistance, which is demonstrated in Figure 7.3 (b) and (c). The mass transfer resistance is largest for the H-120 GDL, followed by H-090 and H-060. This indicates that the mass transfer resistance increases with GDL thickness. As the operating temperature increases, at a current density of 0.5 A cm^{-2} (Figure 7.3 (c)), the mass transfer resistance does not change significantly between the three GDLs. This indicates that the increased operating temperature counteracts the mass transport limitations. This is most likely due to changing phase of water from primarily liquid to primarily vapour, which means that the water is no longer saturating the GDL. This can be further illustrated by (Figure 7.3 (d)) which shows the current density at low operating voltages (0.3 V). This current density can be related to the concentration losses occurring due to the oxygen diffusion limitation. Generally, as the temperature increases, the current density at 0.3 V increases as well. The H-060 always shows the highest current density, followed by the H-090 and the H-120. Generally, the performance at 120 ^{o}C is highest for all GDLs except the H-060. The H-060 shows the best performance at 100 ^{o}C, however this is quite similar to the current density at 120 ^{o}C.

(a)

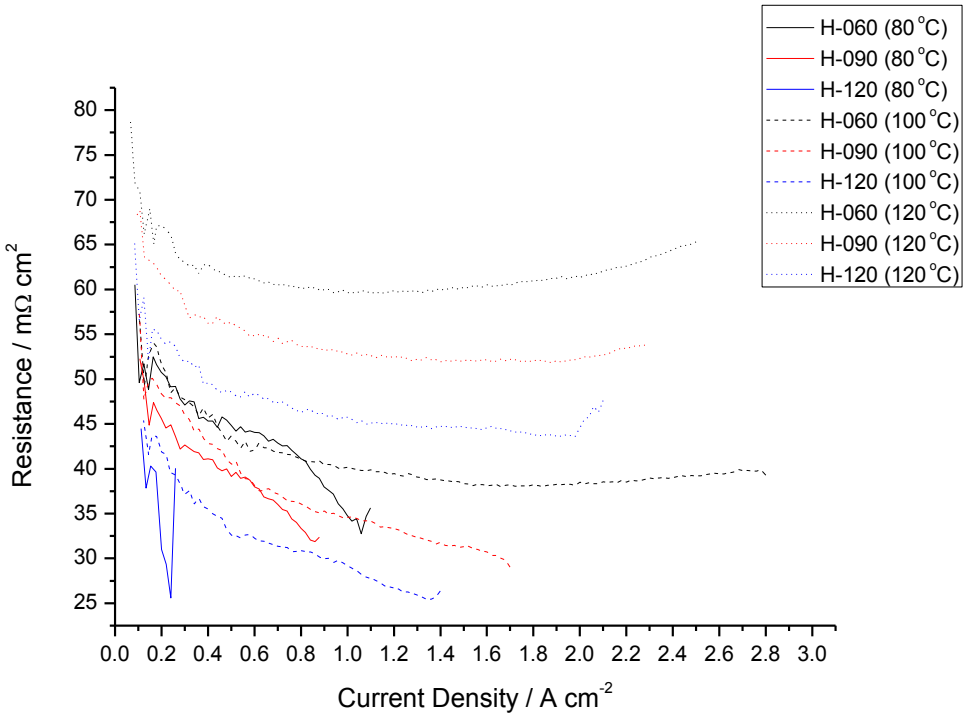
H-060 (80°C)
H-090 (80°C)
H-120 (80°C)
H-060 (100°C)
H-090 (100°C)
H-120 (100°C)
H-060 (120°C)
H-090 (120°C)
H-120 (120°C)
Resistance / mΩ cm2
Current Density / A cm-2

(b)

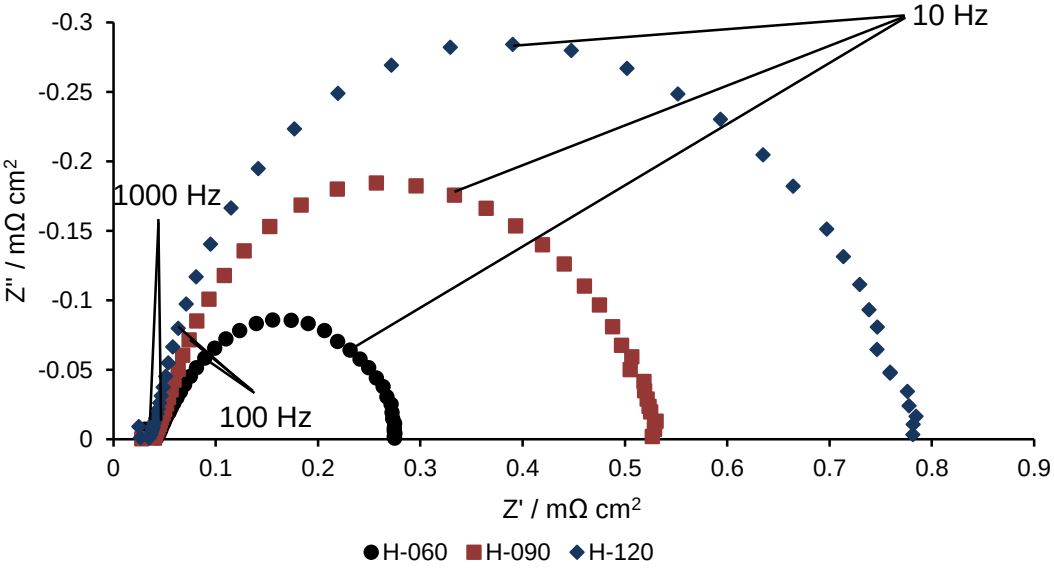
10 Hz
1000 Hz
100 Hz
Z'' / mΩ cm2
Z' / mΩ cm2
H-060
H-090
H-120

(c)

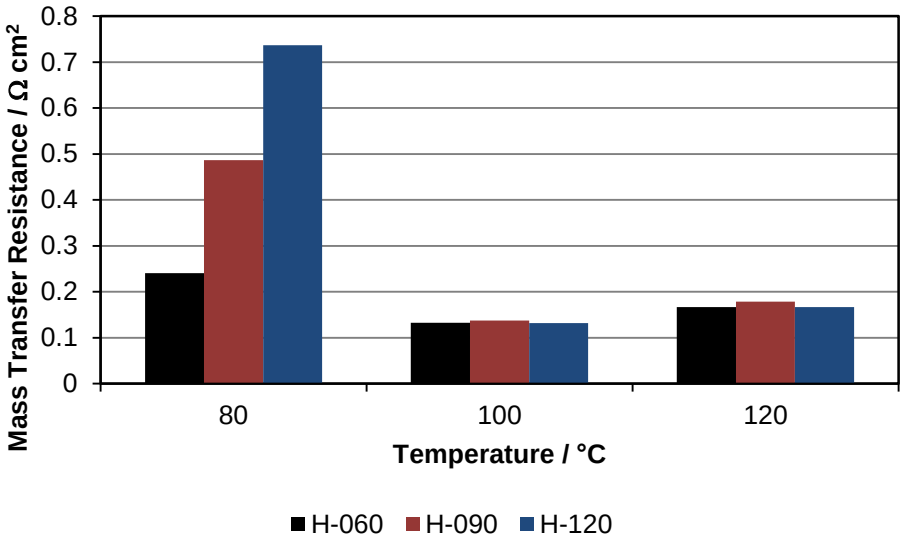

(d)

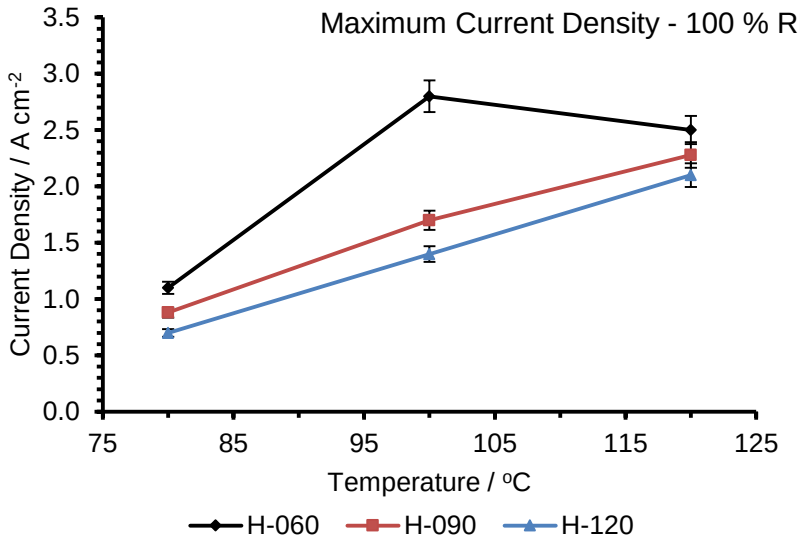

Figure 7.3: (a) ohmic resistance as measured by current interruption with respect to operating current density, (b) EIS for H-060, H-090 and H-120 at 80 ºC and 0.5 A cm^{-2}, (c) mass transfer resistance for H-060, H-090 and H-120 at 80 ºC, 100 ºC and 120 ºC at 0.5 A cm^{-2} and (d) measured current density at 0.3 V for H-060, H-090 and H-120 at 80 ºC, 100 ºC and 120 ºC.

7.3.2 Influence of Relative Humidity and GDL Thickness on the MEA Performance

The MEAs were then tested to assess the influence of relative humidity and GDL thickness on the MEA performance. This was done by keeping the operating temperature set at 120 ^{o}C whilst varying the operating relative humidity.

(a)

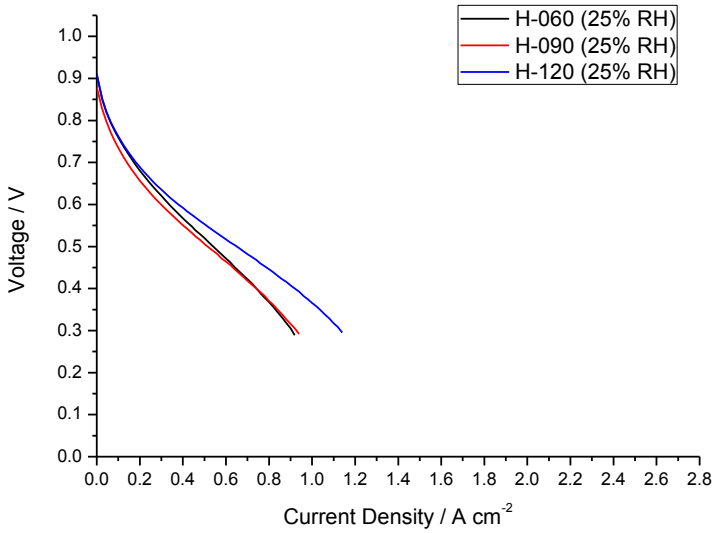

(b)

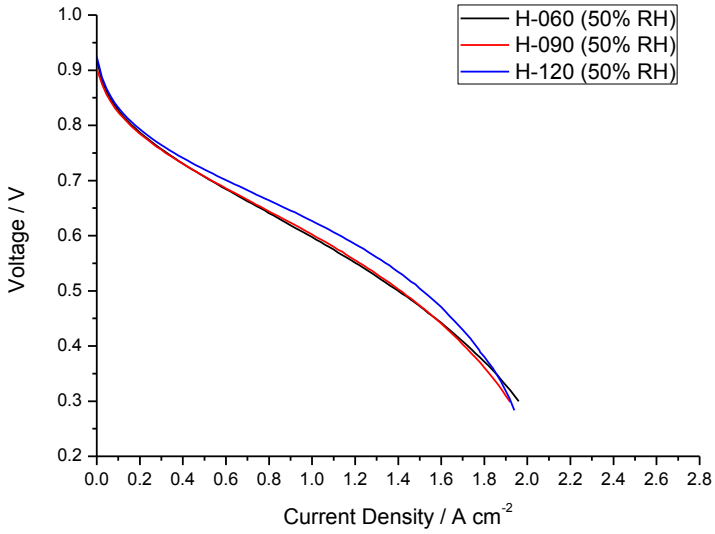

(c)

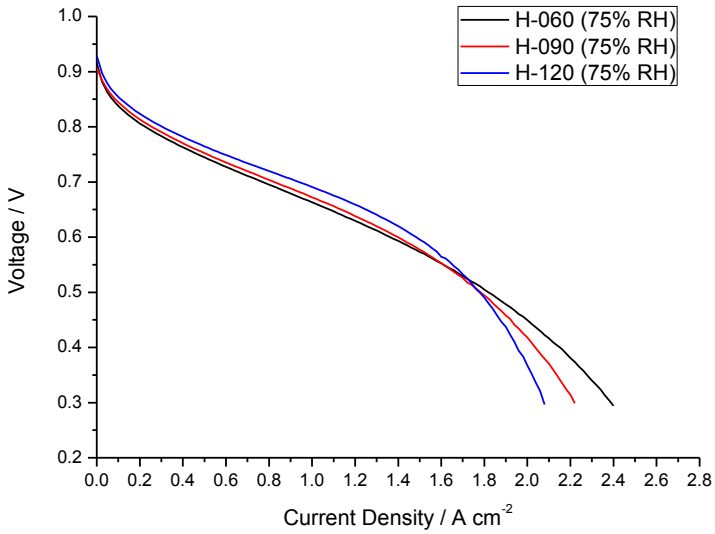

(d)

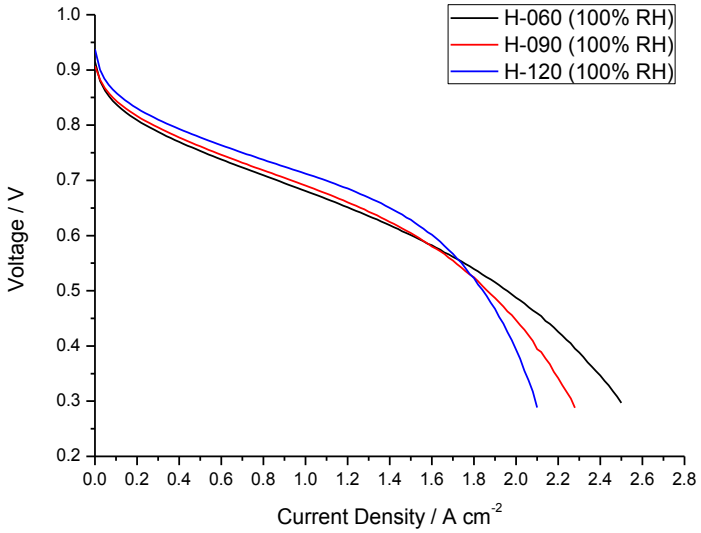

Figure 7.4: Polarisation Curves showing the performance of the H-060, H-090 and H-120 at (a) 25 % RH, (b) 50 % RH, (c) 75 % RH and (d) 100 % RH

Figure 7.4 generally shows that as the relative humidity increases, the performance of the MEA also increases. This is true regardless of the cathodic GDL used. This is primarily due to the hydration of the Nafion based membrane which directly affects the conductivity. Due to the high operating temperature, the membrane is constantly losing water which is alleviated by the water produced by the fuel cell reaction and the

incoming humidity from the fuel stream. At low relative humidities, the incoming water is insufficient to keep the membrane hydrated, thus the membrane ohmic resistance is the dominating resistance which limits MEA performance. At high relative humidities, there is enough water for the membrane to stay well hydrated and to reach high current densities. This can be seen from the ohmic resistance measurements in Figure 7.5 (a). Interestingly, it appears that the H-120 consistently has the lowest ohmic resistance out of the three GDLs tested (Figure 7.5(b)). This is especially true at low humidities (25% RH), which see the largest decrease in ohmic resistance with respect to current density. This indicates that the H-120 aids the membrane in the retention of water by reducing the rate of diffusion through the GDL in comparison to H-090 and H-060. This reduces the rate of diffusion of water vapour within the GDL, thus slowing down the loss of water from the membrane. This in turn reduces the loss of conductivity, indeed aiding the membrane significantly as the current density increases. This also explains why the H-120 GDL gives a better performance in the ohmic region of the polarisation curves (Figure 7.4). However, at higher relative humidities, this positive influence on the membrane conductivity becomes less noticeable (Figure 7.5(b)) as there is sufficient humidity present within the MEA to help keep the membrane hydrated. At these high humidities, the thinner GDLs show their advantage in the mass transport region of the polarisation curve. This increase in mass transfer resistance with the thickness of the GDL is related to the path length the reactants must take through the GDL. This is shown in Figure 7.5(c) and (d), where the H-120 GDL consistently has the highest mass transfer resistance as the relative humidity increases. Figure 7.5(d) also seems to indicate that as the relative humidity increases, the mass transport resistance seems to decrease. However, this is not the case. The data used for Figure

7.5(d) was obtained via impedance spectroscopy when the MEA was held at a current density of 1 A cm^{-2}. As can be seen from the polarisation curves (Figure 7.4), as the relative humidity increases, the MEA performance increases. This means that as the relative humidity increases, 1 A cm^{-2} corresponds to higher MEA voltages which means that the data for mass transfer resistance at this current density corresponds to the mass transfer resistance in the ohmic region of the polarisation curve.

(a)

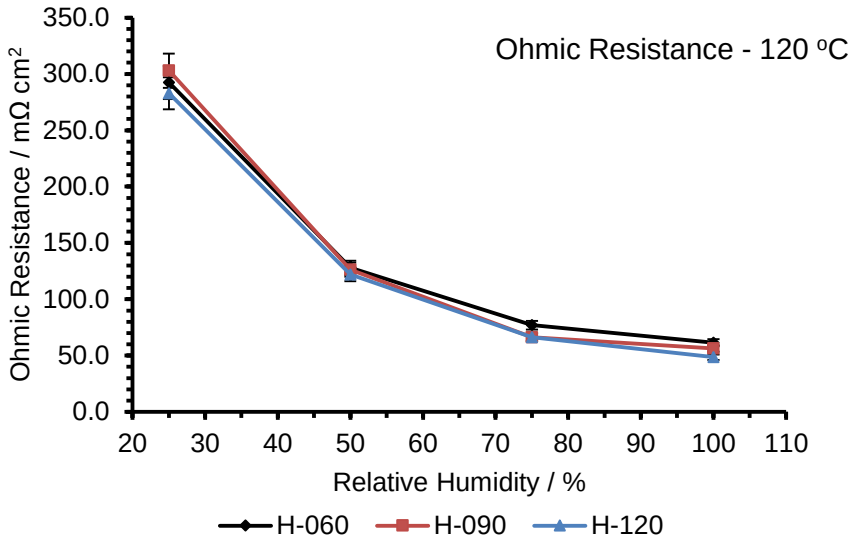

(b)

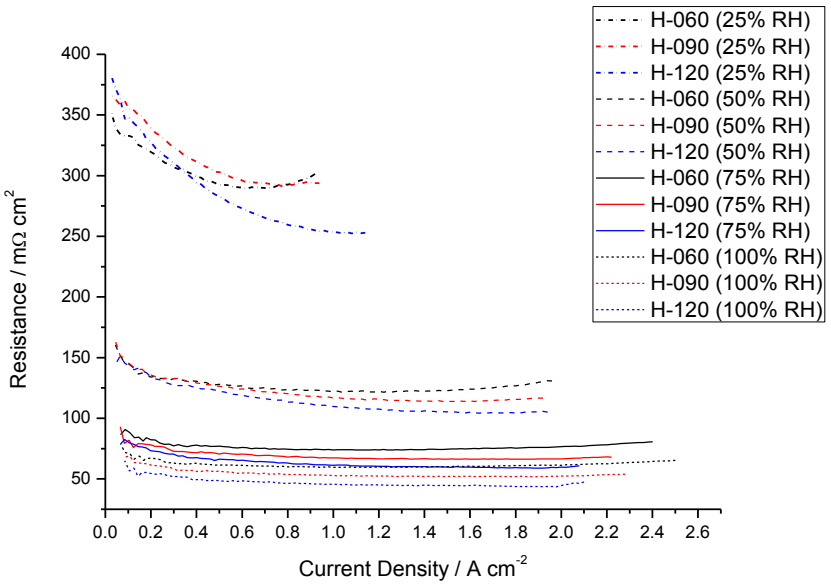

(c)

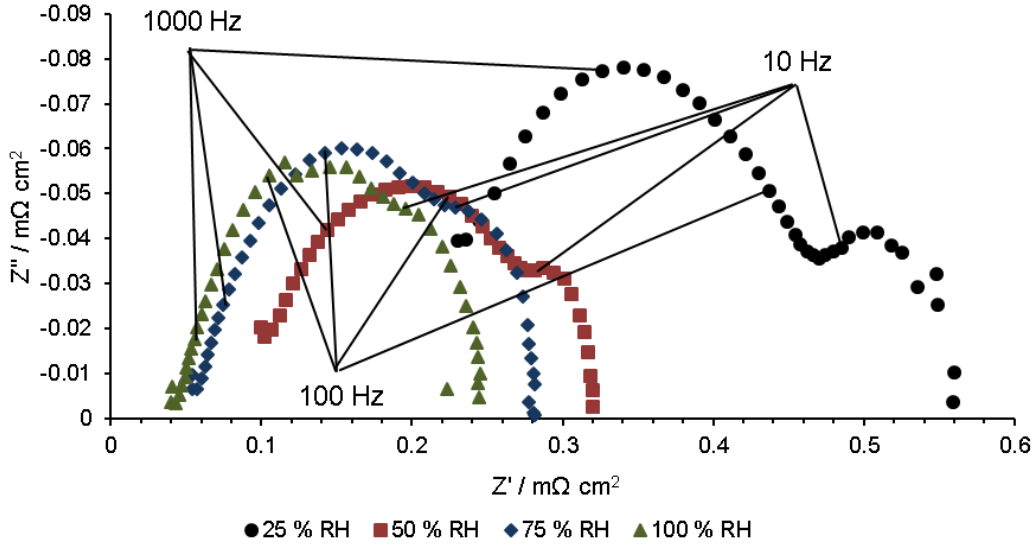

(d)

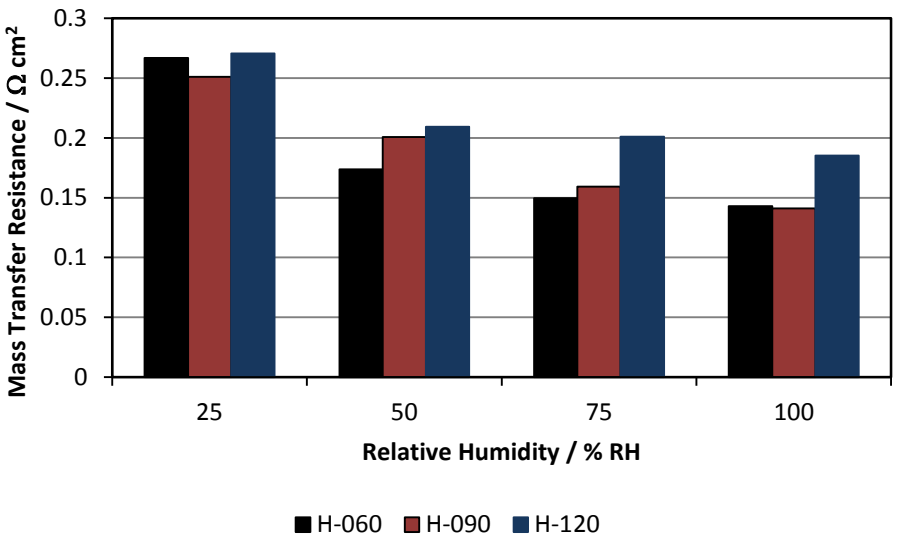

Figure 7.5: (a) Ohmic resistance of MEAs with H-060, H-090 and H-120 at 0.5 A cm $^{2-}$, (b) MEA ohmic resistance with respect to current density as measured by current interruption, (c) Impedance spectra for H-120 at 1 A cm^{-2} and (d) mass transfer resistance for H-060, H-090 and H-120 at 80 ^{o}C, 100 ^{o}C and 120 ^{o}C at 1.0 A cm^{-2}

7.4 Conclusions

In this study, the influence of the GDL thickness with respect to the operating temperature and the operating relative humidity has been studied. It was found that as the operating temperature increased, the performance of the MEAs increased. This was primarily attributed to the decrease in mass transfer resistance at intermediate temperature compared with conventional temperatures. However, this is in contrast with the MEA ohmic resistance, which increases with operating temperature. This is attributed to the dehydration of the Nafion membrane which results in a loss of conductivity despite the high operating temperature. It was also found that as the GDL increased in thickness, the mass transfer resistance increased, as would be expected.

The relative humidity was also varied at intermediate temperature to see what influence the GDL material has on the MEA performance. It was generally found that as the relative humidity increased, so did the MEA performance. This was attributed to the increase in membrane conductivity. However, there was a difference in performance depending on the GDL used. At low humidities, the H-120 showed better performance than H-090 or H-060. This increase in performance was found to be due to a decrease in the ohmic resistance which was attributed to the trapping of water within the GDL. This would slow the rate at which water is removed from the membrane. On the other hand, at higher relative humidities, the thicker H-120 was found to show worse performance. This was attributed to the increased mass transfer resistance, which overcomes the positive effect of lowering the ohmic resistance which H-120 possesses.

In summary, as the temperature and relative humidity are varied for the three GDL thicknesses, three effects superimpose:

i. Increase in performance with temperature

ii. More facile water transport at higher temperature

iii. Increased drying of the membrane at higher temperature

Whist the thicker GDL can prevent drying at low relative humidities, a thinner GDL is of advantage at high relative humidities.

Therefore, it can be concluded that the thickness of the GDL has an important impact on the performance of the MEA. Which thickness of GDL that is used at intermediate temperature will depend on the intended operating parameters for the MEA. For example, conventional MEA operating at intermediate temperature and at low current densities, it would be beneficial to use a thicker GDL as this will help mitigate the loss of conductivity in the membrane.

CHAPTER 8

Using Metallic Meshes as the GDL

"Not cost minimisation but added value maximisation"

Robert Steinberger-Wilckens, 2003

Chapter 8 Using Metallic Meshes as the GDL

8.1 Introduction

Metallic Gas Diffusion Layers (GDLs) offer an interesting prospect for use at intermediate temperature. The high thermal conductivity and the highly uniform structure in particular allow for greater elements of design to be used when considering the GDL. Very little research has been conducted into the use of metallic GDLs within PEFC MEAs, and no research for use at intermediate temperature. Materials such as stainless steel mesh [139], nickel mesh [61], titanium mesh [57–59,140–143], or Nickel-Chromium alloy foam [144] work well as a good diffusion facilitator for liquid fuel (i.e. in a direct methanol fuel cell) as well as in the cathode of the PEFC.

In this study, the first aspect that was considered is whether or not a metallic GDL will work at intermediate temperature as a GDL. Following this, the ohmic resistance and mass transport properties of the GDL were assessed and coated meshes were tested. A range of operating temperatures and relative humidities were used in order to assess the performance change with respect to temperature and ability of the metallic GDL to manage water. For comparison, a Toray H-090 was used as the conventional carbon GDL.

8.2 Experimental

8.2.1 MEA Testing

For the purpose of studying the metallic based GDLs, a stainless steel grade 304 mesh was used. The physical properties are outlined in Table 8.1 [193,218] and a picture of the mesh200 is included .

Table 8.1: Key properties of Mesh200 and H-090

Properties	**Gas Diffusion Layer**	
	Mesh200	**H-090**
Thickness / µm	50	280
Aperture / µm	77	-
Wire Diameter / µm	50	-
Real Density / g cm^{-3}	2.32	2.019 $\pm$ 0.003
Bulk Density / g cm^{-3}	-	0.44
Porosity / %	0.37	67.2
Tortuosity	-	2.55
Mean Pore Diameter / nm	99000	3324

Figure 8.1: Mesh200

The membrane electrode assemblies (MEAs) consisted of commercial catalyst coated membranes (CCMs) (Johnson Matthey, Pt loading: 0.4 mg_{Pt} cm^{-2}, membrane Nafion 212). This was to ensure repeatability and reliability so that comparison between the cathodic GDLs. Sigracet 34BC was used as the anodic GDL. The active area of all MEAs was 5 cm^2. For the cathode, two base GDLs were used in this study; Mesh200 and H-090.

The MEAs were then tested using a Scribner 850e Fuel Cell Test Station with EIS capabilities. All tests were conducted at 80, 100 and 120 ^oC and a back pressure of 1.8 bar. The relative humidity (RH) at the cell inlet was varied between 25 % and 100 % RH. Constant flow rates of 0.2 L min^{-1} and 0.5 L min^{-1} were used to supply the anodic (hydrogen) and cathodic (air) gases respectively. All MEAs were preconditioned before testing by operating the cell at a constant potential (0.6 V) for 10 hrs. A polarisation curve was obtained at each operating condition by current scanning between open circuit voltage and 0.3 V.

From the polarisation curves obtained, it was possible to derive values for the ohmic resistance, which will give information on the cell ohmic resistance, the Tafel slope, which will give information on the ORR kinetics, the maximum current density (defined as the current density at 0.3 V) and the maximum power density produced by the different MEAs which give information on how well each GDL is able to transport water from the cell as well as the overall cell efficiency. The ohmic resistance was calculated using the inbuilt current interrupt analyser on the test stand..

8.2.2 Interfacial Contact Resistance Measurement

5 cm^2 GDL samples were manually cut (both carbon and metal mesh) and placed between two plain POCO graphite (POCO AXF-5Q) plates (industry standard material often used as a reference material). The contact resistance was then measured at various clamping pressures. The clamping pressure was monitored using a controlled compression device (Zwick Roel Z030). The resistance was measured by the 4-wire Kelvin method using a BS407 precision Ohmmeter.

8.3 Results and Discussion

8.3.1 Performance of a Stainless Steel Mesh GDL

The initial test performed compared a single stainless steel mesh with the Toray H-090 in order to see if the stainless steel mesh would show any performance at intermediate temperature.

(a)

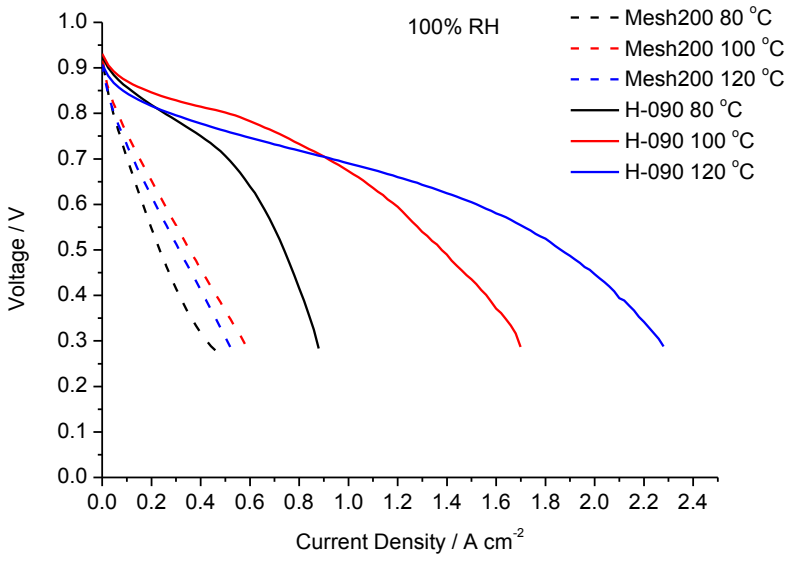

(b)

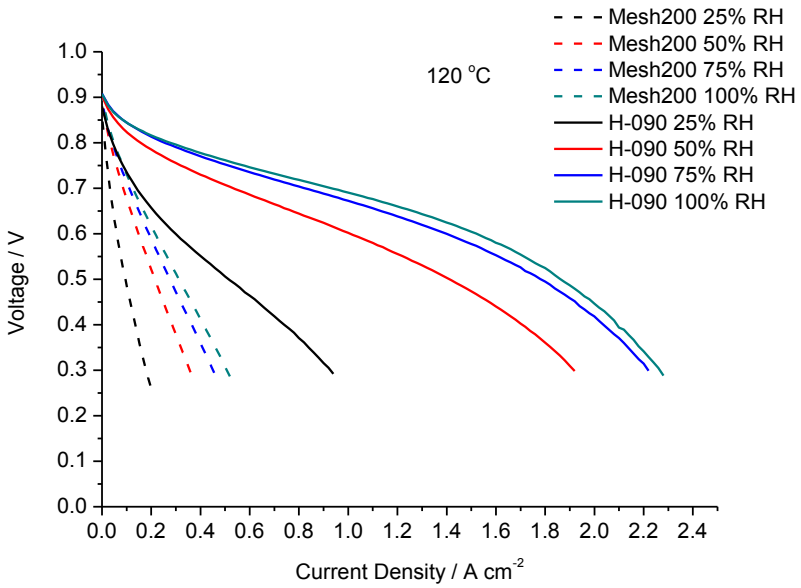

Figure 8.2: Polarisation Curves for the MEA with Mesh200 and H-090 as the cathode GDL; (a) at 80 ºC, 100 ºC and 120 ºC with a constant 100 % RH and (b) at 25 %RH, 50 %RH, 75 %RH and 100 %RH at a constant 120 ºC.

From Figure 8.2(a-b), it is clear that whilst the Mesh200 does give some performance, there is a large difference between the performance of the H-090 and the Mesh200. In the case of increasing the temperature whilst operating at a high relative humidity (Figure 8.2(a)), the performance of the Mesh200 MEA does not change significantly as the temperature. When compared with the performance change that is observed for the H-090 as the temperature is increased it's apparent that the ohmic resistance is restricting the MEA performance. This is also true when observing the polarisation curve change with respect to the relative humidity (Figure 8.2(b)). The Mesh200 MEA performance increases with the relative humidity, however this increase is minimal, especially when compared with the H-090. This domination of the ohmic resistance can be observed when looking at the ohmic resistance as obtained by the current interrupt method (Figure 8.3).

(a)

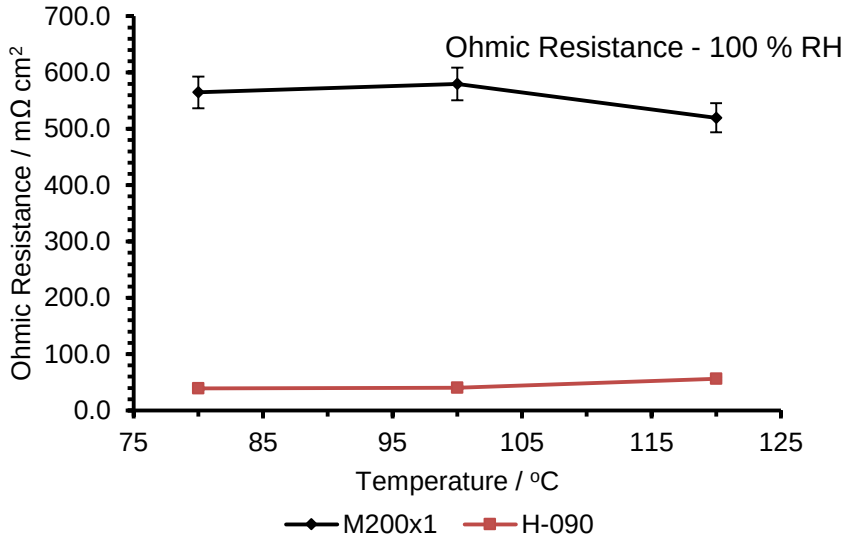
Ohmic Resistance - 100 % RH
Ohmic Resistance / mΩ cm²
700.0
600.0
500.0
400.0
300.0
200.0
100.0
0.0
75
85
95
105
115
125
Temperature / ºC
M200x1
H-090

(b)

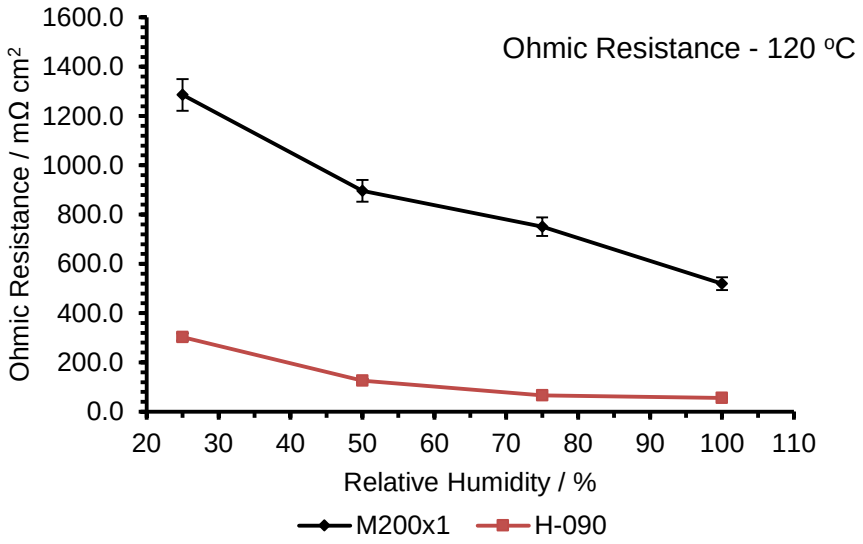
Ohmic Resistance - 120 ºC
Ohmic Resistance / mΩ cm²
1600.0
1400.0
1200.0
1000.0
800.0
600.0
400.0
200.0
0.0
20
30
40
50
60
70
80
90
100
110
Relative Humidity / %
M200x1
H-090

(c)

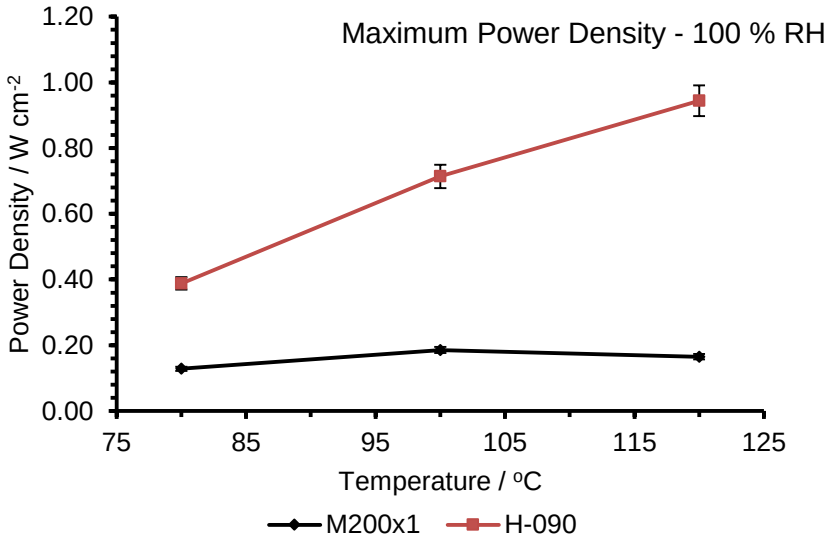
Maximum Power Density - 100 % RH
Power Density / W cm⁻²
1.20
1.00
0.80
0.60
0.40
0.20
0.00
75
85
95
105
115
125
Temperature / ºC
M200x1
H-090

(d)

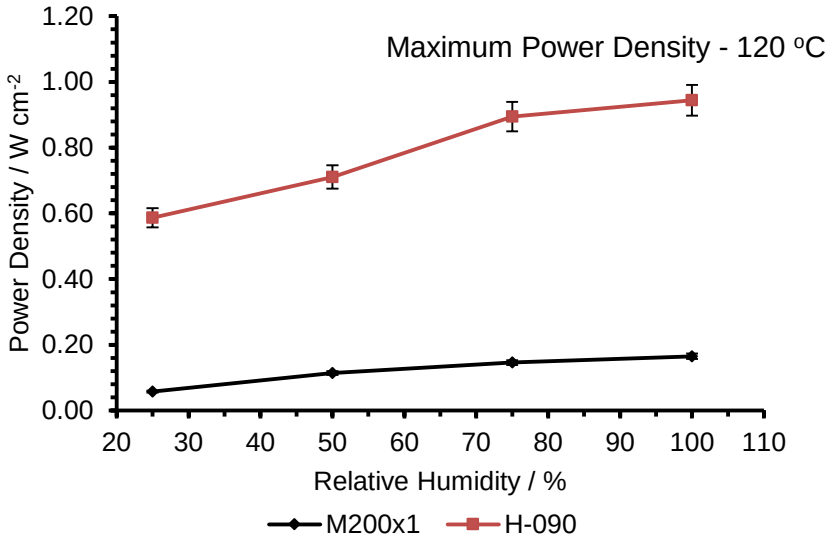

Figure 8.3: Ohmic resistance for the MEA with Mesh200 and H-090 as the cathode GDL; (a) at 80 °C, 100 °C and 120 °C with a constant 100 % RH, (b) at 25 %RH, 50 %RH, 75 %RH and 100 %RH at a constant 120 °C and the maximum power density at (c) at 80 °C, 100 °C and 120 °C with a constant 100 % RH, (d) at 25 %RH, 50 %RH, 75 %RH and 100 %RH at a constant 120 °C

From Figure 8.3(a) it can be seen that the MEA ohmic resistance does not change significantly as the cell temperature is increases. This is most likely because the high humidity means that the membrane conductivity cannot increase further and thus this indicates that there is another factor which is causing the high ohmic resistance. This can also be confirmed by looking at how the ohmic resistance changes with respect to the relative humidity Figure 8.3(b). The ohmic resistance decreases as the relative humidity increases, which is also observed for the H-090. However, the H-090 reaches a plateau at approximately 60 mΩ cm^2, whereas the Mesh200 MEA ohmic resistance only goes as low as approximately 600 mΩ cm^2. This is also reflected in the maximum power density that is recorded for both MEAs (Figure 8.3(c-d)). The Mesh200 MEA does not show a significant change in maximum power density as the temperature increases, which is in contrast with the H-090. As the relative humidity increases

(Figure 8.3(d)), the power density does increase slightly for the Mesh200 which is again due to the slight increase in the membrane conductivity.

There are two potential reasons for the high ohmic resistance of the stainless steel mesh:

I. There is not enough compression on the Mesh200 MEA to ensure good contact as the gasket used was 50 µm in thickness and the mesh is also 50 µm in thickness.

II. The stainless steel has a high Interfacial Contact Resistance (ICR).

In order to ascertain the reason for the high ohmic resistance it was decided to increase the Mesh200 thickness by layering multiple meshes and to also use ex-situ test methods to measure the ICR of the mesh.

8.3.2 Impact on MEA Performance of Layering Stainless Steel Mesh200

The Mesh200 was layered in order to assess the impact on MEA performance. Polarisation curves from this experiment are shown in Figure 8.4.

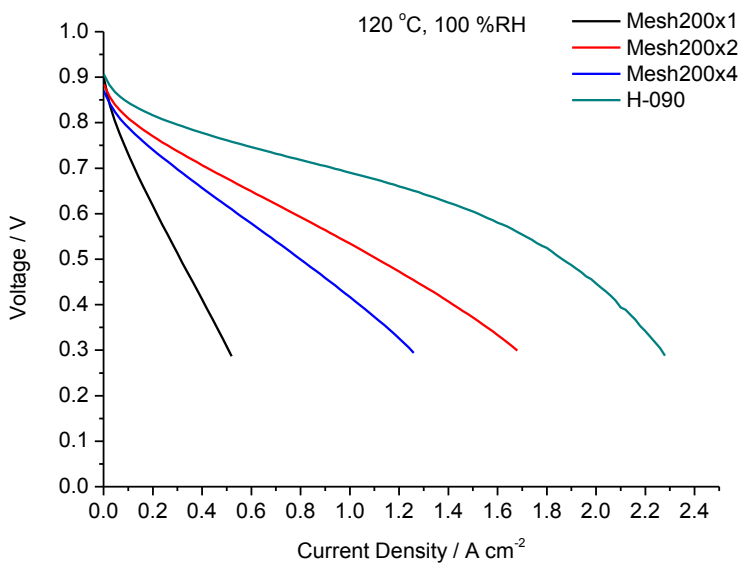

Figure 8.4: Polarisation Curves for Mesh200x1, Mesh200x2, Mesh200x4 and H-090 at 120 °C and 100 %RH

From Figure 8.4, it can be seen that layering the stainless steel meshes has a marked impact on the MEA performance. When the number of meshes is increased from one to two, there is a large increase in performance (a 240 % improvement at 0.3 V) which is most likely due to better contact between the MEA components from the effective compression. This is reflected in the ohmic resistance measurements of the MEAs (Figure 8.5(a)) which shows that the ohmic resistance decreases by approximately four times. However, when the number of meshes increases to four, the performance decreases. This is most likely because the number of contact points between the layers is increasing which overcomes the benefit that increased compression has on the MEA performance. This is again reflected in the ohmic resistance measurements (Figure 8.5(a)) which show that the resistance increases between 2 mesh layers and 4 mesh layers. Unfortunately, it was not possible to test 3 mesh layers as the Nafion membrane

would consistently fail. From the configurations tested, the dual layer Mesh200 gave the best performance.

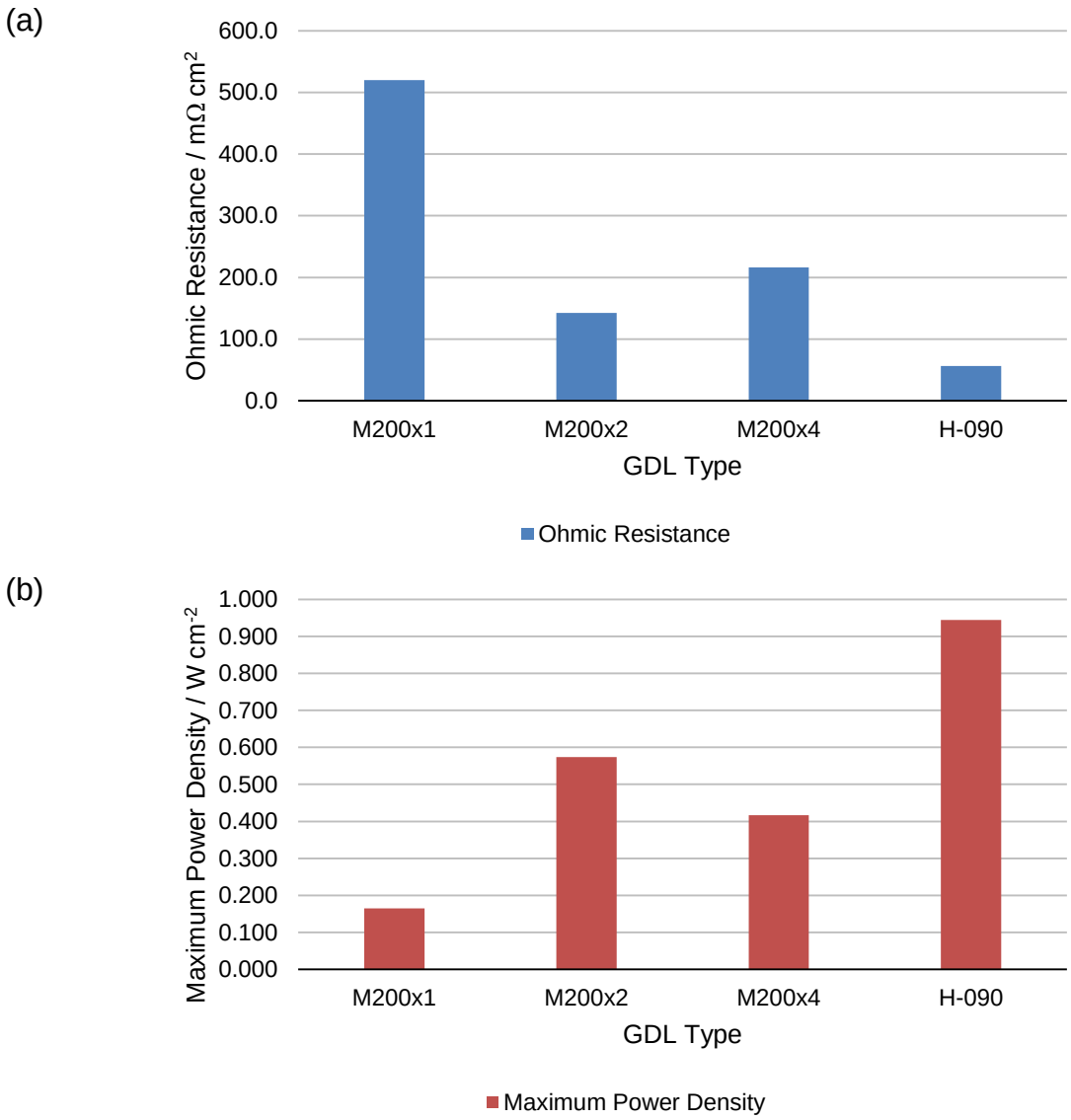

Figure 8.5: (a) ohmic resistance and (b) maximum power density for Mesh200x1, Mesh200x2, Mesh200x4 and H-090 at 120 ºC and 100 %RH

The Mesh200 was then compared with the H-090 at different relative humidities and temperatures (Figure 8.6).

(a)

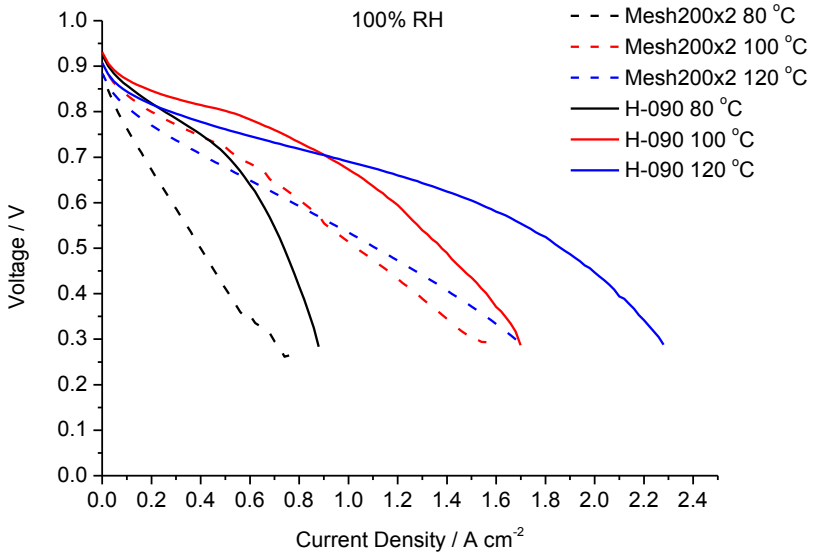

(b)

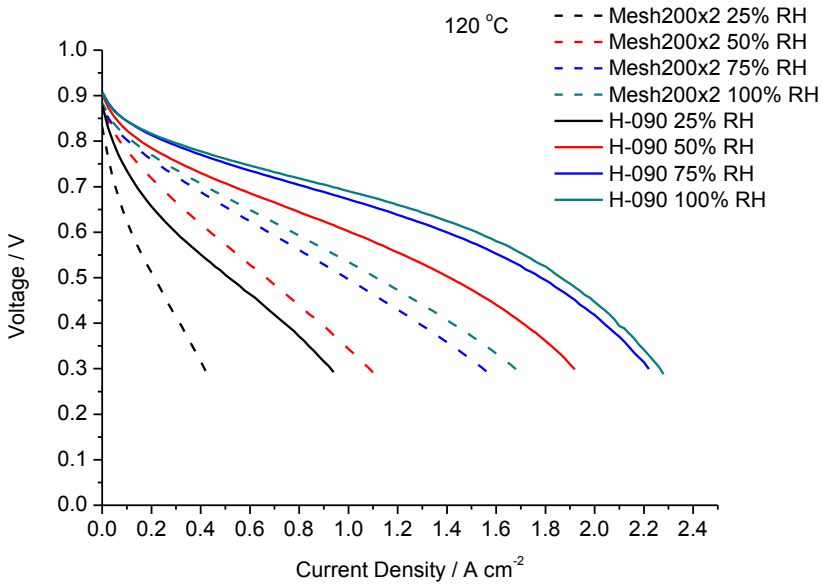

Figure 8.6: Polarisation curves for Mesh200x2 and H-090; (a) at 80 ºC, 100 ºC and 120 ºC with a constant 100 % RH and (b) at 25 %RH, 50 %RH, 75 %RH and 100 %RH at a constant 120 ºC.

The polarisation curves (Figure 8.6) show that the ohmic resistance no longer totally dominates the MEA performance. However, the ohmic resistance for the Mesh200x2 is still higher than that of the H-090 at all operating parameters (Figure 8.7). Indeed, similar trends for both the H-090 and the Mesh200 can be observed. When comparing

the performance at different operating temperatures, it is clear in both cases that the higher operating temperature gives the best MEA performance whereas at 80 ^{o}C, the performance is much reduced. When the relative humidity is changed at 120 ^{o}C, the MEA ohmic resistance decreases as the relative humidity increases for both H-090 and Mesh200x2. Indeed, in both cases, a plateau is reached which indicates that at 100 %RH, the membrane reaches a maximum conductivity/lowest resistance. However, the Mesh200x2 MEA still has a higher resistance which indicates that the stainless steel mesh has a high ICR which is limiting the MEA performance.

(a)

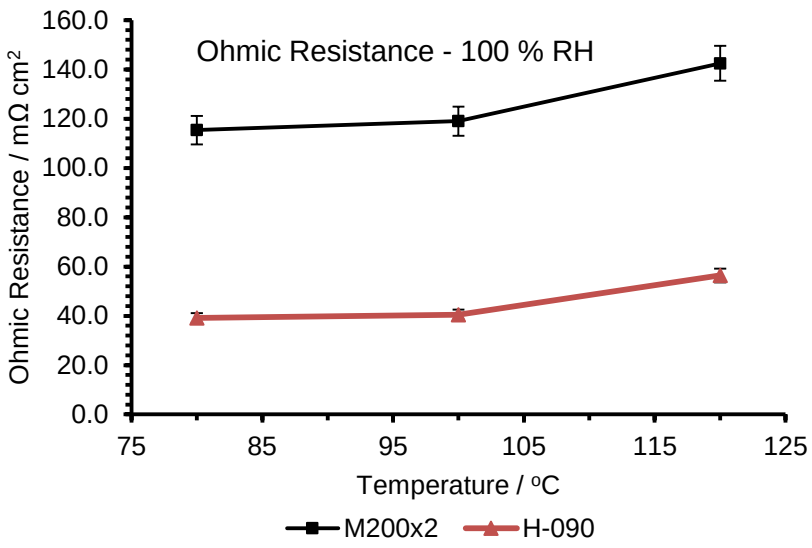

(b)

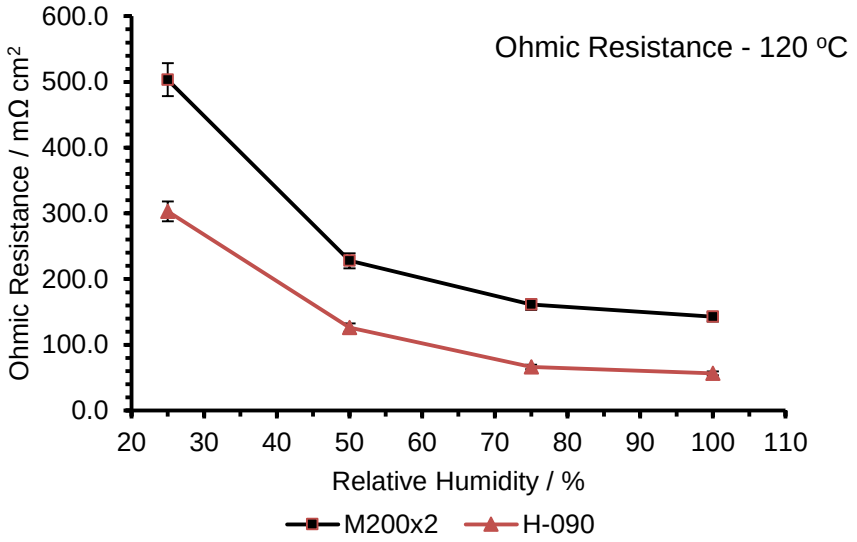

Figure 8.7: Ohmic resistance for the MEA with Mesh200 and H-090 as the cathode GDL; (a) at 80 ºC, 100 ºC and 120 ºC with a constant 100 % RH and (b) at 25 %RH, 50 %RH, 75 %RH and 100 %RH at a constant 120 ºC

8.3.3 Measuring the ICR of the GDLs

The tested GDLs were then characterised for their ICR using ex-situ characterisation techniques

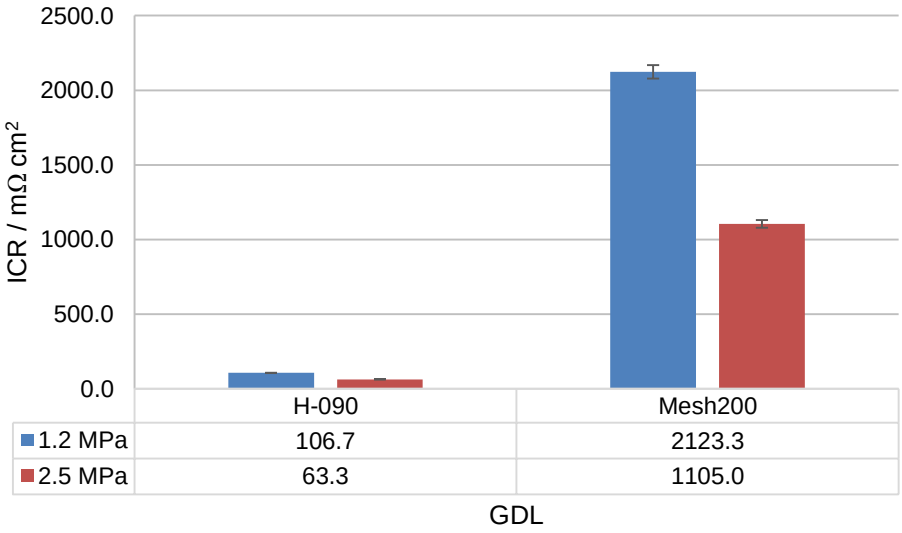

Figure 8.8: Interfacial Contact resistance for H-090 and Mesh200

From Figure 8.8, it can be seen that the stainless steel Mesh200 has an ICR which is 19 and 17 times larger than the H-090 at 1.2 and 2.5 MPa respectively. This confirms the in-situ results which show that the Mesh200 has a much higher ohmic resistance than the H-090 carbon GDL.

Based on this result, it was decided to use coated Mesh200. Specifically titanium and gold were used to compare with the base stainless steel Mesh200 and the H-090. Ex-situ ICR measurements were taken of these coated meshes (Figure 8.9).

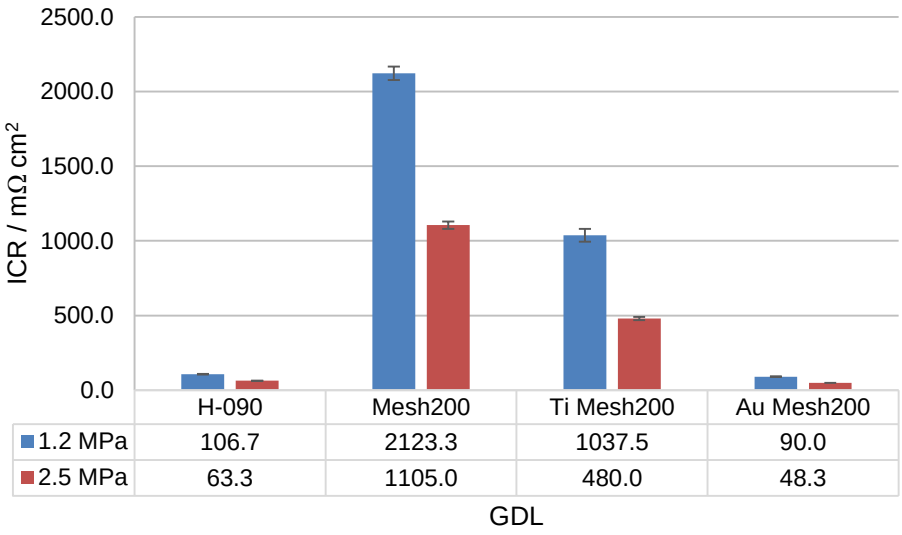

Figure 8.9: Interfacial Contact resistance for H-090, Mesh200, Ti Mesh200 and Au Mesh200

Figure 8.9 shows that the ICR of the stainless steel Mesh200 can be significantly reduced by coating the base mesh with another metal. As is expected, the gold coating shows the lowest ICR of all of the GDLs tested and the titanium coating shows half the ICR of the stainless steel mesh. This should mean that the in-situ ohmic resistance of the MEA should also be reduced. Based on these results, in-situ characterisation of the GDLs was carried out.

8.3.4 Using Titanium and Gold Coated Mesh200 as a GDL

A titanium coated and gold coated Mesh200 was then assessed and compared with an H-090. Polarisation curves were generated and are shown in Figure 8.10.

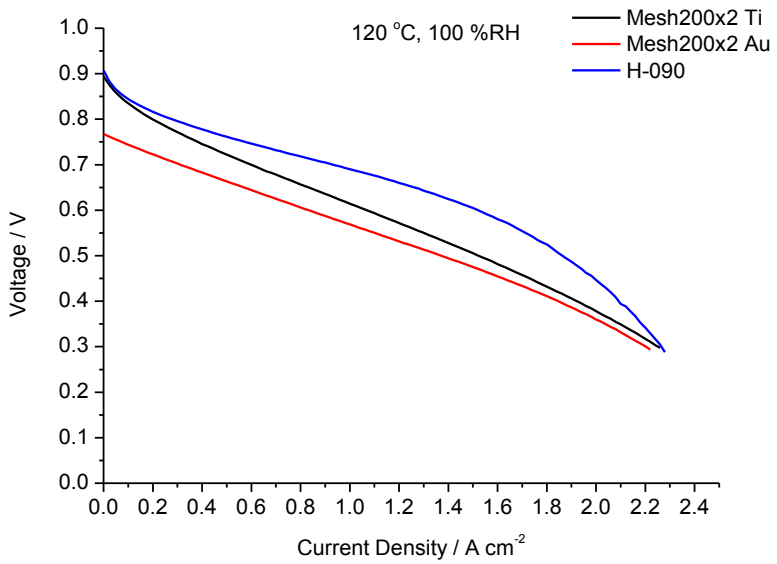

Figure 8.10: Polarisation curves for Ti Mesh200, Au Mesh200 and H-090

Figure 8.10 shows that the performance of the coated Mesh200 is now much closer to that of the H-090. The Ti Mesh200 in particular shows very good performance. Specifically, whilst there is almost double the amount of ohmic resistance compared with the H-090 (Figure 8.11(a)), there is little evidence of mass transport resistance. This indicates that the Mesh200 is better for MEA performance when considering mass transport. This is also shown in the maximum power density, where the Ti coated Mesh200 has a similar maximum power density to the H-090 (Figure 8.11(b)). In order to try and improve the MEA performance, the stainless steel Mesh200 was also coated in gold as gold is known to have a low ICR. Unfortunately, it was not possible to achieve a test with the Au Mesh200 where the membrane was not punctured. This explains

why the open circuit voltage is lower for the Au Mesh200 (0.75 V) compared with both the Ti Mesh200 and the H-090 (0.9 V). This ultimately led the Au Mesh200 to have a lower performance than either the Ti Mesh200 or the H-090, despite an ohmic resistance that was closer to the H-090. This also led to the Au Mesh200 displaying a lower maximum power density than either the H-090 or the Ti Mesh200.

(a)

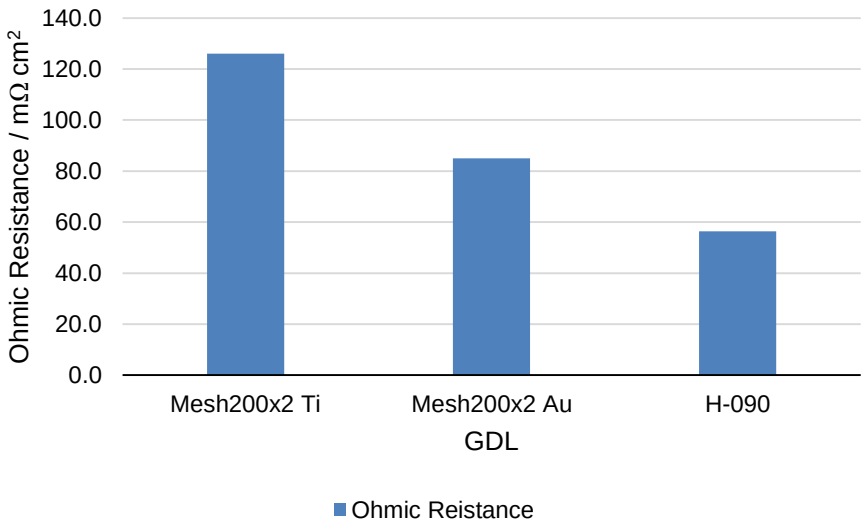

(b)

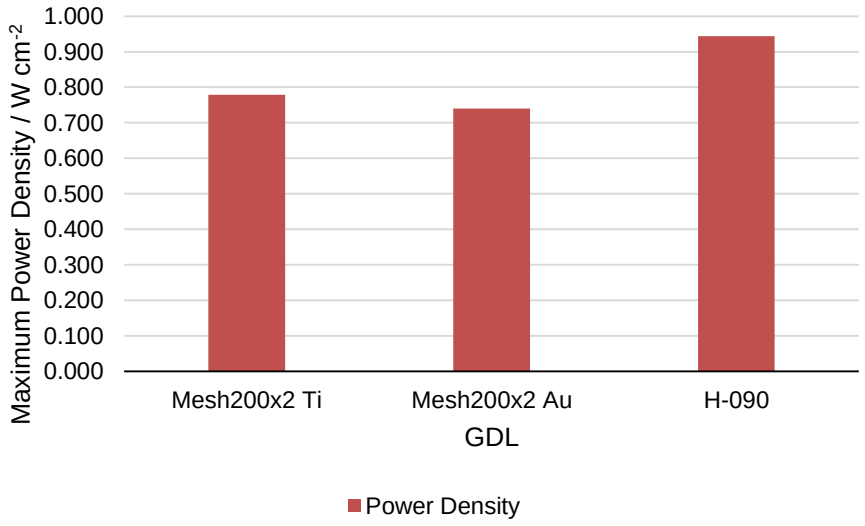

Figure 8.11: (a) Ohmic Resistance and (b) Maximum Power Density for Ti Mesh200, Au Mesh200 and H-090

The Ti Mesh200 and the H-090 were then compared at different operating temperatures and relative humidities (Figure 8.12).

(a)

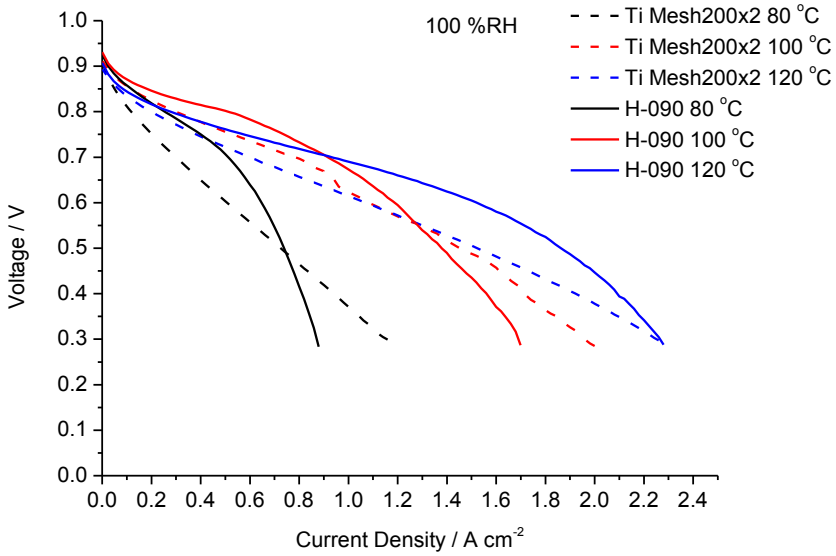

(b)

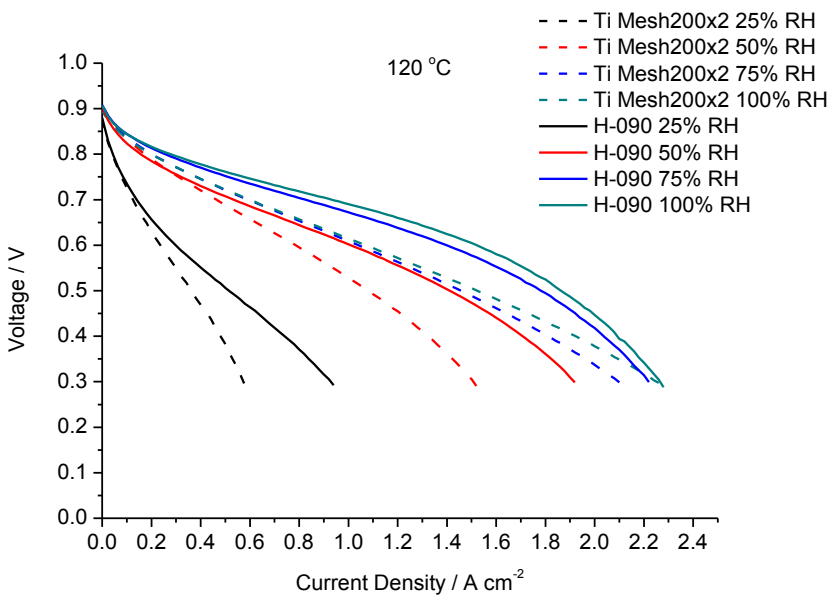

Figure 8.12: Polarisation curves for Ti Mesh200x2 and H-090; (a) at 80 ºC, 100 ºC and 120 ºC with a constant 100 % RH and (b) at 25 %RH, 50 %RH, 75 %RH and 100 %RH at a constant 120 ºC.

As previously established, the Ti coated Mesh200 shows a higher ohmic resistance than the H-090, which is true at all of the operating temperatures and relative humidities (Figure 8.12(a-b)). At 80 ºC and 100 ºC, the Ti coated Mesh200 shows better performance at higher current densities than the H-090 which indicates that the

Mesh200 is better at handling the water generated at these temperatures than the H-090. This is quite positive as it indicates that, providing the right coating is used and the ohmic resistance is lowered sufficiently, the stainless steel mesh should show a better performance than a conventional carbon GDL. However, at 120 ^{o}C the Ti Mesh200 shows a worse performance than the H-090, due to a greater ohmic resistance (Figure 8.13(a)). This is most likely due to the H-090 having a greater thickness than the Ti Mesh200. As has been shown in previous chapters, this greater thickness will aid the membrane by slowing the removal of water from the membrane, thus aiding in the maintenance of a high membrane conductivity compared with the Ti Mesh200. The high ICR of the Ti Mesh200 will also contribute to this poorer performance at 120 ^{o}C.

A similar trend is also observed when the relative humidity is changed at 120 ^{o}C (Figure 8.12) between the H-090 and Ti Mesh200. However, in this case, the Ti Mesh200 does not show a better performance at any operating parameter to the H-090. This is primarily due to the high ohmic resistance of the Ti Mesh200 as the overall MEA ohmic resistance shows the same trend as the H-090 (Figure 8.13(b)).

(a)

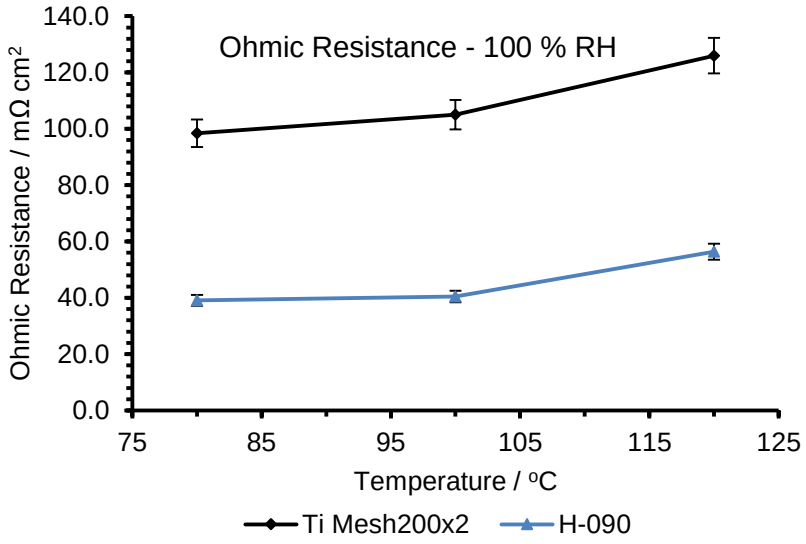

(b)

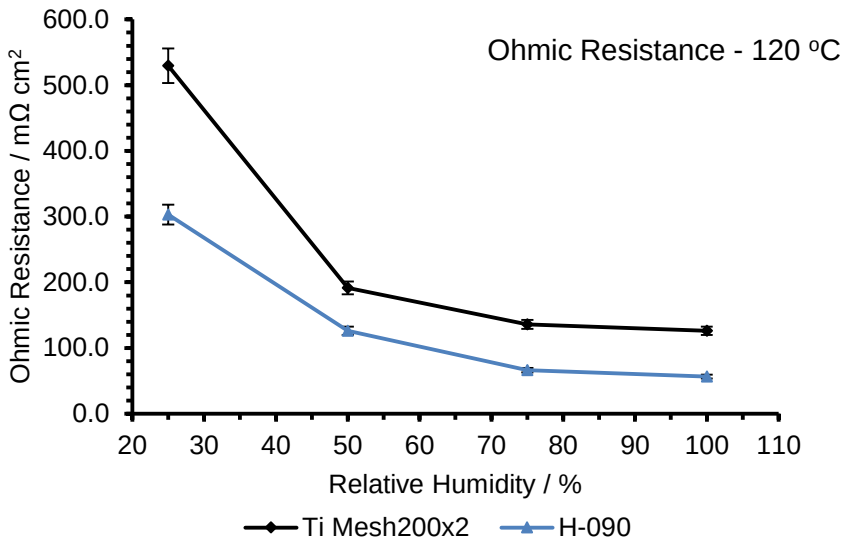

Figure 8.13: Ohmic resistance for the MEA with Ti Mesh200 and H-090 as the cathode GDL; (a) at 80 ºC, 100 ºC and 120 ºC with a constant 100 % RH and (b) at 25 %RH, 50 %RH, 75 %RH and 100 %RH at a constant 120 ºC

8.3.5 Mechanical Failure of the Nafion Membrane

From the tests carried out, the biggest challenge faced by the metallic meshes is their propensity to damage the Nafion membrane. This is observed in Figure 8.10 where the Au Mesh200 caused mechanical failure of the membrane multiple times. This often results in the formation of holes (e.g. Figure 8.14) in the membrane which causes a

severe loss in MEA performance. If metallic meshes are to be seriously considered for use in MEAs, this issue will need to be addressed.

Figure 8.14: Punctured Membrane

8.4 Conclusions

In this study, several experiments were carried out in order to:

I. Investigate if the stainless steel metallic mesh would work as a GDL at intermediate temperature

II. Investigate why the stainless steel metallic mesh gave a much poorer performance compared with a conventional carbon GDL.

III. Investigate if this poor performance could be improved

To that end, initially an MEA was constructed with a stainless steel Mesh200 as the cathode GDL. It was found that, whilst the GDL “worked”, the performance was very poor. This was attributed to the high ohmic resistance of the MEA. This ohmic resistance did not change significantly as the relative humidity increased and was thus attributed to either the ICR of the stainless steel or the low compression on the Mesh200 compared with the H-090. In order to verify this, the Mesh200 was then layered in order to increase the overall thickness. From this it was found that layering the Mesh200 twice was ideal as the MEA ohmic resistance was decreased by a factor of four.

Ex-situ ICR measurements were also carried out on the stainless steel Mesh200 and the H-090. It was found that the stainless steel Mesh200 had an ICR value that was almost 20 times higher than that of the H-090 which confirmed that the ICR also was a key factor in the poor MEA performance.

In order to attempt to improve performance, the stainless steel Mesh200 was coated with titanium and gold and these were then characterised for their ICR values. It was

found that the Ti coating halved the ICR value of the stainless steel whilst the Au coating showed a lower ICR than the H-090.

These coated meshes were then characterised in-situ where it was found that the Ti Mesh200 mesh gave much better performance compared with the uncoated Mesh200. At low temperatures, the Ti Mesh200 showed better performance than the H-090 in terms of the mass transport. However, at 120 ^{o}C the performance of the Ti Mesh200 was lower than the H-090. Overall the MEA ohmic resistance of the Ti Mesh200 still caused the MEA performance, which was in agreement with the ex-situ ICR tests. When the Au Mesh200 was tested, the MEA showed an ohmic resistance that was very similar to that of the H-090. However, it was not possible to get a set of data where the membrane was not punctured by the mesh which meant that the performance of the Au Mesh200 appeared to be worse than that of the H-090.

These results are not as expected when taking into consideration the simulation results (Chapter 3) which suggests that the metallic GDLs should show much greater performance than they actually do. This is mainly because the simulation does not take into account the ICR which appears to be the main limiting factor to good performance. However, if this barrier can be overcome, there exists great potential for using metallic GDLs.

In summary, the metallic meshes show great promise, especially at low temperatures for reducing mass transport limitations. However, a suitable coating would need to be found that possesses a low ICR. The biggest challenge faced when using a metallic mesh as a GDL is that there is a high chance of puncturing the Nafion membrane. This must be overcome if these cells are to be used in a commercial setting.

CHAPTER 9

SUMMARY

"To achieve greatness, one must be capable of original thought"

Scott Hardman, 2013

Chapter 9 Summary

9.1 Conclusions

The GDL is a relatively recent research area. A majority of the commercially available products currently being sold are often the offshoots of products from other sectors. The highly anisotropic nature of the GDL means that it is difficult to design a GDL for use within a certain application. This study has contributed to the understanding of some aspects of the GDL material properties with an aim to design a GDL that is suitable for use within an IT-PEFC.

GDL properties were split up into those that could be only studied using simulation (e.g. influence of GDL porosity and permeability) and those that could be studied experimentally (e.g. Influence of the microporous layer (MPL), influence of hydrophobic treatment and influence of GDL thickness). While it would be possible to experimentally assess the effects of GDL porosity and permeability, it is difficult to know what the in-situ porosity is independent as this will change with compression. Similarly, the permeability will change with compression. So in order to consider the design of a metallic GDL for intermediate temperature, simulation studies were chosen for certain parameters.

From the simulation study, it was found that the GDL porosity has significant influence on the mass transport properties of the GDL and that it was important to understand the operating voltages that the MEA would be working under. A porosity between 35 and 55 % was found to be best for the cell at all operating voltages however a porosity

of 40 % was found to be ideal for a cell's typical operating voltage (0.6-0.8 V). It was also found that the permeability is quite important to the cell performance but only when considering convective forces. Within a conventional GDL/FFP design, these convective forces would be found when gases are forced from one gas channel to another through the GDL, thus forcing water to be removed from the cell. This is not necessary for an IT-PEFC, however, as water will be in the vapour phase and will be removed via passive diffusion effects.

The use of a metallic based GDL was also studied in detail using simulation methods. It was found that, due to the high conductivity of the metallic materials, the ohmic resistance never dominated at high porosities. This means that mass transport limitations should be significantly reduced as it should be possible to use a highly porous metallic material as a GDL. Furthermore, the higher thermal conductivity of the metallic mesh means that the cell will act as a much more efficient heat exchanger when compared with a conventional GDL/FFP cell design. This will aid in simplifying stack design as the thermal management will be simpler.

Using experimental testing methods, the influence of the MPL, hydrophobic treatment and GDL thickness was also studied. However, prior to this, a baseline using Nafion 212 was established. It was found that decreasing the relative humidity significantly decreased the cell performance at all of the cell operating temperatures tested. The magnitude of the performance decrease became larger as the operating temperature increased. This is because at the low operating humidity, the Nafion membrane becomes dehydrated which causes a loss in the protonic conductivity thus significantly increasing the MEA Ohmic resistance. In turn, this low performance means that the fuel cell reaction cannot proceed at a fast enough rate for the generated water to

sufficiently hydrate the membrane. The lack of hydration in the catalyst layer also causes deprotonation of the ionomer chains. It was also found that at higher operating temperatures, the mass transport limitations became less of an issue, which is one of the main advantages of moving to higher temperature operation. Finally, it was found that the optimum conditions for an MEA constructed of commercially available Nafion 212, with commercially available GDEs was at 117-120 ^{o}C and at 75 % RH. However, this did not take into account the durability of these materials as they are designed for use at low temperatures.

In terms of the MPL, it was found that the MPL gave significant improvement into the performance of the MEA (as much as a fourfold increase in performance was measured). This is partially due to the MPL providing a cohesive layer and therefore a large effective surface area upon which the catalyst layer could be applied. However, when the catalyst layer was applied to the GDL without the MPL, the MEA had a much lower performance as the effective triple phase boundary was much smaller.

Hydrophobic treatment was also found to be an important factor. The treatment of the GDL using a hydrophobic polymer is commonly used for conventional operating temperatures. It was found that the hydrophobic treatment of the GDL aided in reducing the mass transport limitation at intermediate temperatures.

Next, the influence of the GDL thickness was tested. It was found that the GDL thickness has a larger impact on the GDL performance at intermediate temperature. This is especially the case when the relative humidity is varied. At low relative humidities, the thicker GDL gave better performance which was most likely due to the GDL slowing the rate at which water is removed from the MEA thus improving the

membrane conductivity. On the other hand, at high relative humidities, the performance increased as the GDL became thinner which is mainly due to the resistance to diffusion through the GDL from the flow field to the catalyst layer.

From this research, it was found that an ideal GDL for use at intermediate temperatures would have the following properties:

I. will have a MPL

II. will be treated with hydrophobic agents

III. will be thin if working with a high relative humidity or thick if working with a low relative humidity

These parameters apply to conventional carbon based materials as well as metallic based GDL.

The final part of this study was to experimentally explore the possibility of using metallic GDLs. From this study, it was found that using an uncoated stainless steel mesh would not produce good performance. This is mainly due to the high level of contact resistance on the steel. This was somewhat reduced as the compression on the cell was increased. In order to combat this, the stainless steel mesh was coated with titanium, which reduced the contact resistance of the stainless steel mesh. In this case, at conventional operating temperatures, the coated mesh showed better mass transport performance, which is most likely due to the thinness of the mesh. However, at intermediate temperature, the coated mesh showed a worse performance which was due to the ohmic resistance. This was due to the membrane drying out, which the coated mesh being too thin to significantly aid in retaining water for the membrane.

The main disadvantage observed from the use of metallic GDLs is propensity for the mesh to puncture the membrane. This led to significant reductions in the open circuit voltage and is an important aspect to consider.

9.2 Future Work

In terms of the development of GDLs for intermediate temperature usage, there are two main strands of work that require further investigation:

I. Further investigation into the water management at intermediate temperature through the use of in-situ neutron experiments. This will allow for visualisation of the water transport processes occurring within the MEA, which will provide validation of the theories about mass transport at intermediate temperature. Furthermore, this will allow for a better understanding of the role of the GDL at intermediate temperature in water management.

II. The continuation of investigation into the use of metallic materials as GDLs. The work presented in this thesis provides a basis for using metallic materials as GDLs at intermediate temperature with the simulation study showing valuable potential. However, further ex-situ and in-situ testing is required since the experimental results displayed some issues. For example, studying the impact of corrosion of a metallic GDL on MEA performance as well as how to apply an MPL or hydrophobic treatment to a metallic GDL.

REFERENCES

[1] C.F. Schoenbein, Philos. Mag. 14 (1839) 43.

[2] S.J. Peighambardoust, S. Rowshanzamir, M. Amjadi, Int. J. Hydrogen Energy 35 (2010) 9349.

[3] P.J. Hamilton, B.G. Pollet, Fuel Cells 10 (2010) 489.

[4] J. Zhang, Z. Xie, Y. Tang, C. Song, T. Navessin, Z. Shi, D. Song, H. Wang, D. Wilkinson, J. Power Sources 160 (2006) 872.

[5] A. Chandan, M. Hattenberger, A. El-kharouf, S. Du, A. Dhir, V. Self, B.G. Pollet, A. Ingram, W. Bujalski, J. Power Sources 231 (2013) 264.

[6] a El-kharouf, a Chandan, M. Hattenberger, B.G. Pollet, J. Energy Inst. 85 (2012) 188.

[7] A. Collier, H. Wang, X. Ziyuan, J. Zhang, D. Wilkinson, Int. J. Hydrogen Energy 31 (2006) 1838.

[8] V. Mehta, J.S. Cooper, J. Power Sources 114 (2003) 32.

[9] W. Schmittinger, A. Vahidi, J. Power Sources 180 (2008) 1.

[10] J. Lobato, P. Cañizares, M. a. Rodrigo, C. Ruiz-López, J.J. Linares, J. Appl. Electrochem. 38 (2008) 793.

[11] G.-G. Park, Y.-J. Sohn, T.-H. Yang, Y.-G. Yoon, W.-Y. Lee, C.-S. Kim, J. Power Sources 131 (2004) 182.

[12] X. Li, I. Sabir, Int. J. Hydrogen Energy 30 (2005) 359.

[13] Http://www.fuelcellmarkets.com/, (2010).

[14] www.fuelcelltoday.com, (2010).

[15] T. Tsukui, T. Shimizu, R. Doi, Y. Tsutsumi, (1985).

[16] Private Communication with Prof. Dr. Ferdinand Panik (University of Applied Science Esslingen, German), 2011, n.d.

[17] C. Wieser, Fuel Cells 4 (2004) 245.

[18] R. Devanathan, Energy Environ. Sci. 1 (2008) 101.

[19] a. Arvay, E. Yli-Rantala, C.-H. Liu, X.-H. Peng, P. Koski, L. Cindrella, P. Kauranen, P.M. Wilde, a. M. Kannan, J. Power Sources 213 (2012) 317.

[20] Y.-G. Chun, C.-S. Kim, D.-H. Peck, D.-R. Shin, J. Power Sources 71 (1998) 174.

[21] A. Therdthianwong, P. Saenwiset, S. Therdthianwong, Fuel 91 (2012) 192.

[22] B. Millington, S. Du, B.G. Pollet, J. Power Sources 196 (2011) 9013.

[23] R. Taccani, N. Zuliani, Int. J. Hydrogen Energy 36 (2011) 10282.

[24] J.A. Asensio, S. Borros, P. Gomez-Romero, J. Polym. Sci. Part A Polym. Chem. 40 (2002) 3703.

[25] M. Hogarth, X. Glipa, G. Britain, High Temperature Membranes for Solid Polymer Fuel Cells, Harwell Laboratory, Energy Technology Support Unit, Fuel Cells Programme, 2001.

[26] P. Costamagna, C. Yang, a. B. Bocarsly, S. Srinivasan, Electrochim. Acta 47 (2002) 1023.

[27] S. Reichman, a. Ulus, E. Peled, J. Electrochem. Soc. 154 (2007) B327.

[28] M. Rikukawa, K. Sanui, Prog. Polym. Sci. 25 (2000) 1463.

[29] C. Yang, P. Costamagna, S. Srinivasan, J. Benziger, a. B. Bocarsly, J. Power Sources 103 (2001) 1.

[30] Q. Li, R. He, J.O. Jensen, N.J. Bjerrum, Chem. Mater. 15 (2003) 4896.

[31] Q. Li, R. He, J.-A. Gao, J.O. Jensen, N.J. Bjerrum, J. Electrochem. Soc. 150 (2003) A1599.

[32] C. Pan, R. He, Q. Li, J.O. Jensen, N.J. Bjerrum, H.A. Hjulmand, A.B. Jensen, J. Power Sources 145 (2005) 392.

[33] M. Martinez, Y. Molmeret, L. Cointeaux, C. Iojoiu, J.-C. Leprêtre, N. El Kissi, P. Judeinstein, J.-Y. Sanchez, J. Power Sources 195 (2010) 5829.

[34] D. Villers, X. Jacques-Bédard, J.-P. Dodelet, J. Electrochem. Soc. 151 (2004) A1507.

[35] H.-S. Oh, J.-G. Oh, B. Roh, I. Hwang, H. Kim, Electrochem. Commun. 13 (2011) 879.

[36] S. Bose, T. Kuila, T.X.H. Nguyen, N.H. Kim, K. Lau, J.H. Lee, Prog. Polym. Sci. 36 (2011) 813.

[37] L. Avery, National Travel Survey, 2009.

[38] S.W. K.Foli, O. Gronwald, S. Haufe, S.Kiel, U. M ähr, D. Melzner, A. Reiche , F. Walter, Fuel Cell Semin. Hawaii (2006).

[39] J.O. Jensen, L.N. Cleemann, Q. Li, Platin. Met. Rev. 57 (2013) 173.

[40] F. Heser, P. Marx, T. Scholz, (2007).

[41] A. Huth, N. Simon, (2008).

[42] G.D. Hübner, A. Huth, C.D. Jacksch, (2008).

[43] G.D. Hübner, (2008).

[44] N. Ematschenko, S.D.I. Schmitz, T. Schwarz, (2009).

[45] M.D. Kahlich, E. Schießwohl, T. von Dr. Unwerth, (2009).

[46] W. Sun, B. a. Peppley, K. Karan, J. Power Sources 144 (2005) 42.

[47] S. Park, J.-W. Lee, B.N. Popov, Int. J. Hydrogen Energy 37 (2012) 5850.

[48] a Bayrakceken, S. Erkan, L. Turker, I. Eroglu, Int. J. Hydrogen Energy 33 (2008) 165.

[49] J.H. Nam, K.-J. Lee, G.-S. Hwang, C.-J. Kim, M. Kaviany, Int. J. Heat Mass Transf. 52 (2009) 2779.

[50] K. Karan, H. Atiyeh, A. Phoenix, E. Halliop, J. Pharoah, B. Peppley, Electrochem. Solid-State Lett. 10 (2007) B34.

[51] H.K. Atiyeh, K. Karan, B. Peppley, A. Phoenix, E. Halliop, J. Pharoah, J. Power Sources 170 (2007) 111.

[52] J.T. Gostick, M. a. Ioannidis, M.W. Fowler, M.D. Pritzker, Electrochem. Commun. 11 (2009) 576.

[53] D. Spernjak, J. Fairweather, R. Mukundan, T. Rockward, R.L. Borup, J. Power Sources 214 (2012) 386.

[54] G. Lin, T. Van Nguyen, J. Electrochem. Soc. 152 (2005) A1942.

[55] O.S. Burheim, J.G. Pharoah, H. Lampert, P.J.S. Vie, S. Kjelstrup, J. Fuel Cell Sci. Technol. 8 (2011) 021013.

[56] J.M. Morgan, R. Datta, J. Power Sources (2013).

[57] C. Lim, K. Scott, R.G. Allen, S. Roy, J. Appl. Electrochem. 34 (2004) 929.

[58] Z.-G. Shao, W.-F. Lin, F. Zhu, P. a. Christensen, H. Zhang, Fuel Cells 6 (2006) 326.

[59] Z.-G. Shao, F. Zhu, W.-F. Lin, P. a. Christensen, H. Zhang, B. Yi, J. Electrochem. Soc. 153 (2006) A1575.

[60] F.-Y. Zhang, S.G. Advani, A.K. Prasad, J. Power Sources 176 (2008) 293.

[61] P. Liu, G.Y. Ã, Q. Lai, (2009) 1.

[62] M.F. Mathias, J. Roth, J. Fleming, W. Lehnert, in:, Handb. Fuel Cells, John Wiley & Sons, Ltd, 2010.

[63] T. Ko, Y. Liao, C. Liu, Energy & Fuels 22 (2008) 4092.

[64] Y.-K. Liao, T.-H. Ko, C.-H. Liu, Energy & Fuels 22 (2008) 3351.

[65] C.-H. Liu, T.-H. Ko, E.-C. Chang, H.-D. Lyu, Y.-K. Liao, J. Power Sources 180 (2008) 276.

[66] M.S. Yazici, J. Power Sources 166 (2007) 424.

[67] T.R. Ralph, G.A. Hards, J.E. Keating, S.A. Campbell, D.P. Wilkinson, M. Davis, J. St-Pierre, M.C. Johnson, J. Electrochem. Soc. 144 (1997) 3845.

[68] T. Frey, M. Linardi, Electrochim. Acta 50 (2004) 99.

[69] Y. Wang, C.-Y. Wang, K.S. Chen, Electrochim. Acta 52 (2007) 3965.

[70] V.P. Schulz, J. Becker, A. Wiegmann, P.P. Mukherjee, C.-Y. Wang, J. Electrochem. Soc. 154 (2007) B419.

[71] D. Gerteisen, T. Heilmann, C. Ziegler, J. Power Sources 177 (2008) 348.

[72] D. Gerteisen, C. Sadeler, J. Power Sources 195 (2010) 5252.

[73] S. Park, B.N. Popov, Fuel 90 (2011) 436.

[74] S. Park, J.-W. Lee, B.N. Popov, J. Power Sources 163 (2006) 357.

[75] U. Pasaogullari, C.-Y. Wang, Electrochim. Acta 49 (2004) 4359.

[76] M.S. WILSON, J.A. VALERIO, S. GOTTJBFELD, Electrochim. Acta 40 (1995) 355.

[77] V.A. Paganin, E.A. Ticianelli, E.R. Gonzalez, J. Appl. Electrochem. 26 (1996) 297.

[78] L. Giorgi, E. Antolini, A. Pozio, E. Passalacqua, Electrochim. Acta 43 (1998) 3675.

[79] F. Lufrano, E. Passalacqua, G. Squadrito, A. Patti, L. Giorgi, J. Appl. Electrochem. 29 (1999) 445.

[80] E. Passalacqua, G. Squadrito, F. Lufrano, A. Patti, L. Giorgi, J. Appl. Electrochem. 31 (2001) 449.

[81] E. Antolini, R.R. Passos, E.A. Ticianelli, J. Appl. Electrochem. 32 (2002) 383.

[82] Z. Qi, A. Kaufman, J. Power Sources 109 (2002) 38.

[83] C.S. Kong, D.-Y. Kim, H.-K. Lee, Y.-G. Shul, T.-H. Lee, J. Power Sources 108 (2002) 185.

[84] J. Chen, T. Matsuura, M. Hori, J. Power Sources 131 (2004) 155.

[85] J.H. Nam, M. Kaviany, Int. J. Heat Mass Transf. 46 (2003) 4595.

[86] U. Pasaogullari, C.-Y. Wang, K.S. Chen, J. Electrochem. Soc. 152 (2005) A1574.

[87] A.Z. Weber, J. Newman, J. Electrochem. Soc. 152 (2005) A677.

[88] M. V. Williams, E. Begg, L. Bonville, H.R. Kunz, J.M. Fenton, J. Electrochem. Soc. 151 (2004) A1173.

[89] L.R. Jordan, A.K. Shukla, T. Behrsing, N.R. Avery, B.C. Muddle, M. Forsyth, J. Appl. Electrochem. 30 (2000) 641.

[90] E. Antolini, R.. Passos, E.. Ticianelli, J. Power Sources 109 (2002) 477.

[91] T. Kitahara, T. Konomi, H. Nakajima, J. Power Sources 195 (2010) 2202.

[92] S. Park, B.N. Popov, Electrochim. Acta 54 (2009) 3473.

[93] A.Z. Weber, J. Newman, Modeling Transport in Polymer-Electrolyte Fuel Cells., 2004.

[94] C.-Y. Wang, Chem. Rev. 104 (2004) 4727.

[95] A.Z. Weber, R.M. Darling, J. Newman, J. Electrochem. Soc. 151 (2004) A1715.

[96] U. Pasaogullari, C.Y. Wang, J. Electrochem. Soc. 151 (2004) A399.

[97] C.Y. Wang, P. Cheng, Int. J. Heat Mass Transf. 39 (1996) 3607.

[98] L.. Jordan, A.. Shukla, T. Behrsing, N.. Avery, B.. Muddle, M. Forsyth, J. Power Sources 86 (2000) 250.

[99] H. Gharibi, M. Javaheri, R.A. Mirzaie, Int. J. Hydrogen Energy 35 (2010) 9241.

[100] M. Hunsom, P. Piumsomboon, K. Pruksathorn, N. Tantavichet, S. Endoo, K. Charutavai, K. Poochinda, Renew. Energy 36 (2011) 369.

[101] L. Cindrella, a. M. Kannan, Fuel Cells 10 (2010) 563.

[102] P. Gallo Stampino, L. Omati, C. Cristiani, G. Dotelli, Fuel Cells 10 (2010) 270.

[103] S. Park, J.-W. Lee, B.N. Popov, J. Power Sources 177 (2008) 457.

[104] Y. Hiramitsu, H. Sato, M. Hori, J. Power Sources 195 (2010) 5543.

[105] H.-K. Lee, J.-H. Park, D.-Y. Kim, T.-H. Lee, J. Power Sources 131 (2004) 200.

[106] E.C. Kumbur, K.V. Sharp, M.M. Mench, J. Power Sources 168 (2007) 356.

[107] A. Fischer, J. Jindra, H. Wendt, J. Appl. Electrochem. 28 (1998) 277.

[108] Y. Song, Y. Wei, H. Xu, M. Williams, Y. Liu, L.J. Bonville, H. Russell Kunz, J.M. Fenton, J. Power Sources 141 (2005) 250.

[109] D. You, Y. Lee, H. Cho, J.-H. Kim, C. Pak, G. Lee, K.-Y. Park, J.-Y. Park, Int. J. Hydrogen Energy 36 (2011) 5096.

[110] J. ZHAO, X. HE, L. WANG, J. TIAN, C. WAN, C. JIANG, Int. J. Hydrogen Energy 32 (2007) 380.

[111] J.H. Chun, K.T. Park, D.H. Jo, J.Y. Lee, S.G. Kim, E.S. Lee, J.-Y. Jyoung, S.H. Kim, Int. J. Hydrogen Energy 35 (2010) 11148.

[112] J. Ahn, R. Holze, J. Appl. Electrochem. 22 (1992) 1167.

[113] D. Bevers, R. Rogers, M. von Bradke, J. Power Sources 63 (1996) 193.

[114] P. Staiti, Z. Poltarzewski, V. Alderucci, G. Maggio, N. Giordano, A. Fasulo, J. Appl. Electrochem. 22 (1992) 663.

[115] C. Lim, C.Y. Wang, Electrochim. Acta 49 (2004) 4149.

[116] I. Cabasso, Y. Yuan, X. Xu, (1998).

[117] M. Prasanna, H.Y. Ha, E.A. Cho, S.-A. Hong, I.-H. Oh, J. Power Sources 131 (2004) 147.

[118] J. Benziger, J. Nehlsen, D. Blackwell, T. Brennan, J. Itescu, J. Memb. Sci. 261 (2005) 98.

[119] S. Park, B.N. Popov, Fuel 88 (2009) 2068.

[120] A. Turhan, S. Kim, M. Hatzell, M.M. Mench, Electrochim. Acta 55 (2010) 2734.

[121] A.Z. Weber, J. Newman, J. Electrochem. Soc. 153 (2006) A2205.

[122] S. Kim, M.M. Mench, J. Electrochem. Soc. 156 (2009) B353.

[123] S.F. Burlatsky, V. V Atrazhev, M. Gummalla, D.A. Condit, F. Liu, J. Power Sources 190 (2009) 485.

[124] K.T. Cho, M.M. Mench, J. Power Sources 195 (2010) 6748.

[125] M. Khandelwal, M.M. Mench, J. Power Sources 195 (2010) 6549.

[126] K.T. Cho, M.M. Mench, Int. J. Hydrogen Energy 35 (2010) 12329.

[127] J.F. Lin, J. Wertz, R. Ahmad, M. Thommes, A.M. Kannan, Electrochim. Acta 55 (2010) 2746.

[128] L. Cindrella, A.M. Kannan, R. Ahmad, M. Thommes, Int. J. Hydrogen Energy 34 (2009) 6377.

[129] Y. Wang, S. Al Shakhshir, X. Li, Appl. Energy 88 (2011) 2168.

[130] R. Ranjan, W.J. Brittain, Macromolecules 40 (2007) 6217.

[131] J.W. Kim, L.U. Kim, C.K. Kim, Biomacromolecules 8 (2007) 215.

[132] J. Giner, C. Hunter, J. Electrochem. Soc. 116 (1969) 1124.

[133] T.E. Springer, I.D. Raistrick, J. Electrochem. Soc. 136 (1989) 1594.

[134] M.L. Perry, J. Newman, E.J. Cairns, J. Electrochem. Soc. 145 (1998) 5.

[135] F. Jaouen, G. Lindbergh, J. Electrochem. Soc. 150 (2003) A1699.

[136] R. Schweiss, M. Steeb, P.M. Wilde, Fuel Cells 10 (2010) 1176.

[137] C. Hartnig, I. Manke, R. Kuhn, N. Kardjilov, J. Banhart, W. Lehnert, Appl. Phys. Lett. 92 (2008) 134106.

[138] M. Ahn, Y.-H. Cho, Y.-H. Cho, J. Kim, N. Jung, Y.-E. Sung, Electrochim. Acta 56 (2011) 2450.

[139] a Oedegaard, C. Hebling, a Schmitz, S. Møller-Holst, R. Tunold, J. Power Sources 127 (2004) 187.

[140] E.H. Yu, K. Scott, Electrochem. Commun. 6 (2004) 361.

[141] C.-C. Yang, S.-J. Chiu, C.-T. Lin, J. Power Sources 177 (2008) 40.

[142] Z.-G. Shao, W.-F. Lin, F. Zhu, P.A. Christensen, H. Zhang, B. Yi, J. Power Sources 160 (2006) 1003.

[143] Z.-G. Shao, W.-F. Lin, F. Zhu, P.A. Christensen, H. Zhang, B. Yi, J. Power Sources 160 (2006) 1003.

[144] R. Chen, T.S. Zhao, Electrochem. Commun. 9 (2007) 718.

[145] U. Wittstadt, E. Wagner, T. Jungmann, J. Power Sources 145 (2005) 555.

[146] T. Ioroi, T. Oku, K. Yasuda, N. Kumagai, Y. Miyazaki, J. Power Sources 124 (2003) 385.

[147] K. Fushinobu, D. Takahashi, K. Okazaki, J. Power Sources 158 (2006) 1240.

[148] R. a. Antunes, M.C.L. Oliveira, G. Ett, V. Ett, Int. J. Hydrogen Energy 35 (2010) 3632.

[149] Y. Wang, D.O. Northwood, Electrochim. Acta 52 (2007) 6793.

[150] K. Feng, G. Wu, Z. Li, X. Cai, P.K. Chu, Int. J. Hydrogen Energy 36 (2011) 13032.

[151] A. Pozio, R.F. Silva, M. De Francesco, L. Giorgi, Electrochim. Acta 48 (2003) 1543.

[152] J. Wind, R. Späh, W. Kaiser, G. Böhm, J. Power Sources 105 (2002) 256.

[153] C.-Y. Chung, S.-K. Chen, P.-J. Chiu, M.-H. Chang, T.-T. Hung, T.-H. Ko, J. Power Sources 176 (2008) 276.

[154] E.A. Cho, U.-S. Jeon, S.-A. Hong, I.-H. Oh, S.-G. Kang, J. Power Sources 142 (2005) 177.

[155] S. JOSEPH, J. MCCLURE, R. CHIANELLI, P. PICH, P. SEBASTIAN, Int. J. Hydrogen Energy 30 (2005) 1339.

[156] Y. Wang, D.O. Northwood, J. Power Sources 165 (2007) 293.

[157] S.-J. Lee, C.-H. Huang, Y.-P. Chen, J. Mater. Process. Technol. 140 (2003) 688.

[158] T.E. Springer, T.A. Zawodzinski, S. Gottesfeld, J. Electrochem. Soc. 138 (1991) 2334.

[159] T.E. Springer, M.S. Wilson, S. Gottesfeld, J. Electrochem. Soc. 140 (1993) 3513.

[160] D.M. Bernardi, M.W. Verbrugge, AIChE J. 37 (1991) 1151.

[161] D.M. Bernardi, M.W. Verbrugge, J. Electrochem. Soc. 139 (1992) 2477.

[162] D. Song, Q. Wang, Z.-S. Liu, C. Huang, J. Power Sources 159 (2006) 928.

[163] L. You, H. Liu, Int. J. Heat Mass Transf. 45 (2002) 2277.

[164] K. Jiao, X. Li, Prog. Energy Combust. Sci. 37 (2011) 221.

[165] P.T. Nguyen, T. Berning, N. Djilali, J. Power Sources 130 (2004) 149.

[166] T. V Nguyen, R.E. White, J. Electrochem. Soc. 140 (1993) 2178.

[167] A. Rowe, X. Li, J. Power Sources 102 (2001) 82.

[168] A. Kazim, H.T. Liu, P. Forges, (1999) 1409.

[169] D. Cheddie, N. Munroe, Energy Convers. Manag. 47 (2006) 1490.

[170] D. Cheddie, N. Munroe, J. Power Sources 156 (2006) 414.

[171] D. Cheddie, N. Munroe, Int. J. Hydrogen Energy 32 (2007) 832.

[172] T. Sousa, M. Mamlouk, K. Scott, Chem. Eng. Sci. 65 (2010) 2513.

[173] S.J. Andreasen, S.K. Kær, J. Fuel Cell Sci. Technol. 6 (2009) 41006.

[174] A.P. Sasmito, E. Birgersson, A.S. Mujumdar, Int. J. Hydrogen Energy 36 (2011) 12991.

[175] C. Bonnet, S. Didierjean, N. Guillet, S. Besse, T. Colinart, P. Carré, J. Power Sources 182 (2008) 441.

[176] P. Chang, J. Stpierre, J. Stumper, B. Wetton, J. Power Sources 162 (2006) 340.

[177] J.J. Baschuk, X. Li, J. Power Sources 142 (2005) 134.

[178] a. a. Kulikovsky, H.-F. Oetjen, C. Wannek, Fuel Cells 10 (2010) 363.

[179] O. Shamardina, A. Chertovich, A.A. Kulikovsky, a. R. Khokhlov, Int. J. Hydrogen Energy 35 (2010) 9954.

[180] X. Cheng, J. Zhang, Y. Tang, C. Song, J. Shen, D. Song, J. Zhang, J. Power Sources 167 (2007) 25.

[181] A. Kumar, R.G. Reddy, J. Power Sources 155 (2006) 264.

[182] Y. FERNG, A. SU, Int. J. Hydrogen Energy 32 (2007) 4466.

[183] T. Henriques, B. César, P.J.C. Branco, Appl. Energy 87 (2010) 1400.

[184] S. Dutta, S. Shimpalee, J.W. Van Zee, Int. J. Heat Mass Transf. 44 (2001) 2029.

[185] G.H. Guvelioglu, H.G. Stenger, J. Power Sources 147 (2005) 95.

[186] M. Le Bars, M.G. Worster, J. Fluid Mech. 550 (2006) 149.

[187] K. Jiao, X. Li, Fuel Cells 10 (2010) 351.

[188] H. Ju, H. Meng, C.-Y. Wang, Int. J. Heat Mass Transf. 48 (2005) 1303.

[189] J. Ramousse, S. Didierjean, O. Lottin, D. Maillet, Int. J. Therm. Sci. 47 (2008) 1.

[190] V. Paserin, S. Marcuson, J. Shu, D.S. Wilkinson, (2003) 1.

[191] E.U. Ubong, Z. Shi, X. Wang, J. Electrochem. Soc. 156 (2009) B1276.

[192] M. Hattenberger, S. Sharma, A. Chandan, W. Bujalski, V. Self, J. Richmond, in:, Eur. Fuel Cell Forum 2013, 2013.

[193] A. El-kharouf, T.J. Mason, D.J.L. Brett, B.G. Pollet, J. Power Sources 218 (2012) 393.

[194] S.G. Kandlikar, Z. Lu, T.Y. Lin, D. Cooke, M. Daino, J. Power Sources 194 (2009) 328.

[195] W. Zhou, Y. Tang, R. Song, L. Jiang, K.S. Hui, K.N. Hui, Mater. Des. 37 (2012) 161.

[196] M.J. V Goldschmidt, J.A.M. Kuipers, W.P.M. Van Swaaij, 56 (2001).

[197] H. Yakabe, M. Hishinuma, M. Uratani, Y. Matsuzaki, I. Yasuda, J. Power Sources 86 (2000) 423.

[198] J.G. Pharoah, J. Power Sources 144 (2005) 77.

[199] S. Miwa, S.T. Revankar, Transp. Porous Media 80 (2009) 269.

[200] a. Saccà, I. Gatto, a. Carbone, R. Pedicini, E. Passalacqua, J. Power Sources 163 (2006) 47.

[201] A. Parthasarathy, C.R. Martin, S. Srinivasa, J. Electrochem. Soc. 138 (1991) 916.

[202] C. Yang, J. Memb. Sci. 237 (2004) 145.

[203] M. Schuster, T. Rager, a. Noda, K.D. Kreuer, J. Maier, Fuel Cells 5 (2005) 355.

[204] G. Dotelli, L. Omati, P. Gallo Stampino, P. Grassini, D. Brivio, J. Power Sources 196 (2011) 8955.

[205] H. Xu, Y. Song, H.R. Kunz, J.M. Fenton, J. Electrochem. Soc. 152 (2005) A1828.

[206] F.A. Uribe, T.E. Springer, S. Gottesfeld, J. Electrochem. Soc. 139 (1992) 765.

[207] P.W. Majsztrik, M.B. Satterfield, A.B. Bocarsly, J.B. Benziger, J. Memb. Sci. 301 (2007) 93.

[208] (2014) https://www.wolframalpha.com/input/?i=water+phase+.

[209] V. Antonucci, A. Di Blasi, V. Baglio, R. Ornelas, F. Matteucci, J. Ledesma-Garcia, L.G. Arriaga, A.S. Aricò, Electrochim. Acta 53 (2008) 7350.

[210] C. Wannek, B. Kohnen, H.-F. Oetjen, H. Lippert, J. Mergel, Fuel Cells 8 (2008) 87.

[211] I. Honma, O. Nishikawa, T. Sugimoto, S. Nomura, H. Nakajima, Fuel Cells (2002) 52.

[212] L. Cindrella, a. M. Kannan, J.F. Lin, K. Saminathan, Y. Ho, C.W. Lin, J. Wertz, J. Power Sources 194 (2009) 146.

[213] J.-H. Wee, K.-Y. Lee, S.H. Kim, J. Power Sources 165 (2007) 667.

[214] S. Srinivasan, E.A. Ticianelli, C.R. Derouin, A. Redondo, J. Power Sources 22 (1988) 359.

[215] a. Kianimanesh, Q. Yang, S.S. Park, D. Xue, T. Freiheit, Fuel Cells 13 (2013) 1005.

[216] A.L. Ong, D.K. Whelligan, M.L. Fox, J.R. Varcoe, Phys. Chem. Chem. Phys. 15 (2013) 18992.

[217] G. Samjeské, S. Nagamatsu, S. Takao, K. Nagasawa, Y. Imaizumi, O. Sekizawa, T. Yamamoto, Y. Uemura, T. Uruga, Y. Iwasawa, Phys. Chem. Chem. Phys. 15 (2013) 17208.

[218] T.M. Company, Mesh Co. (2014) http://www.themeshcompany.com/products/Fine.